Charles University in Prague
Faculty of Science
Department of Biochemistry

António José Ribeiro Pombinho, MSc.

High-throughput screening for the discovery of small molecules modulating cell fate

Ph.D. thesis

Supervisor: RNDr. Petr Bartůněk, CSc.

Institute of Molecular Genetics
Academy of Sciences of the Czech Republic
Department of Cell Differentiation

Prague, 2014

Declaration:

I hereby declare that I worked independently, under the supervision of RNDr. Petr Bartůněk, CSc, and used only the literature cited. This work or a substantial portion of it has not been submitted to obtain the same or another academic degree.

Prague, July 2014

António José Ribeiro Pombinho

Acknowledgments

Abstrakt

Objevy sloučenin ovlivňujících buněčnou proliferaci, diferenciaci a smrt mohou vést nejen ke vzniku nových léčiv sloužících k léčbě či prevenci onemocnění, ale lze je také využít ke studiu molekulárních drah zapojených v těchto procesech. Pro testování tisíců těchto malých molekul v buněčných esejích je nezbytná přístrojová automatizace a miniaturizace.

V této práci jsou popsány postupy testování s vysokou propustností (HTS). Jako hlavní předměty studia byly vybrány dráhy hypoxie a Wnt zapojené v růstu kmenových a nádorových buněk, diferenciace hematopoetických, neurálních a mesenchymálních kmenových buněk, a dráha TRAIL vedoucí k selektivní likvidaci nádorových buněk. Tímto postupem bylo možné testovat efekt malých molekul v eukaryotických buňkách a jednobuněčných organismech, jak je ilustrováno na příkladu hledání sloučenin účinkujících proti parazitickým prvokům rodu *Leishmania*.

Několik sloučenin se ukázalo být aktivními modulátory osudu buňky. Jednalo se především o monensin, který inhibuje dráhu Wnt a zabraňuje růstu nádorů v myším modelu kolorektálního karcinomu, hemoharringtonine, který ve spolupráci s proteinem TRAIL indukuje smrt rakovinných buněk implantovaných do imunodeficientní myši, a diphenyleneiodonium chlorid, jenž zabíjí Leishmanie v buňkách. Žádná z těchto látek není v terapeutické oblasti toxická pro zdravé buňky nebo organismy. Pro studium buněčné diferenciace neposkytuje jednokrokový homogenní test dostatek informací, je tedy třeba využít tzv. high-content screenu, což je vícekroková a víceparametrová verze HTS.

Abstract

The discovery of chemical compounds able to modify the way cells proliferate, differentiate or die can lead not only to the formulation of new drugs for disease treatment or prevention but also to their use as biological probes in the study of the molecular pathways involved in these processes. In order to test thousands of these small molecules in cellular assays, instrument automation and assay miniaturization are necessary.

In this thesis, applications of high-throughput screening (HTS) procedures are described. The Hypoxia and Wnt pathways involved in stem and cancer cell proliferation; the differentiation of hematopoietic, neural and mesenchymal stem cells; and the TRAIL pathway leading to selective cancer cells death were the main subjects chosen. With this approach, it was possible to test the effect of small molecules in eukaryotic cells and in unicellular organisms as exemplified by the search of compounds leading to the death of the *Leishmania* protozoan parasite.

Several chemical compounds were identified as active in modulating cell fate. Of note were: monensin, which inhibits the Wnt pathway and prevents the growth of tumors in a mouse model of colorectal cancer; homoharringtonine, which, only in combination with TRAIL, induces the death of cancer cells implanted in immunodeficient mice; and diphenyleneiodonium chloride which kills intracellular *Leishmania*. None of these compounds display toxicity to healthy cells or organisms within the therapeutic window. To be able to study cell differentiation, homogeneous assays do not provide sufficient information and high-content screening, a multistep and multiparameter version of HTS, is required.

Table of Contents

1- Introduction

The use of chemical compounds for medical applications has been described throughout history. In traditional medicine, crude preparations from plants, fungi or insects were used. It was only at the beginning of the 19th century that the active compound (active ingredient) present in such preparations began to be isolated and identified. These secondary metabolites usually have large and complex chemical structures and existing synthesis methods are not advanced enough to produce them *in vitro*. However, in the last decades of the 20th century, chemists developed combinatorial chemistry, allowing for the synthesis of thousands of small molecules in a single process. At the same time, biologists discovered that cells react to extracellular signaling molecules through a biochemical chain of events known as signal transduction. In each cell, a complex network of signaling pathways responds to the microenvironment to modulate its fate. Extracellular stimuli induce conformational changes in receptors localized in the membrane, cytoplasm or nucleus of the cell. Receptor activation ultimately results in activation or repression of protein synthesis, either by directly binding to regulatory regions in the deoxyribonucleic acid (DNA) or by initiating a cascade of signaling molecules that transduce the signal until it reaches the promoter of target genes. These signals alter cell metabolism, gene expression or morphology. Consequently, a correct interpretation of the chemical cues in the surroundings and an adequate response are the basis for normal cellular activities such as homeostasis, development or immunity. Errors in the information processing are the cause of diseases such as cancer or autoimmunity. Therefore, small molecules can be used as probes for interrogating biological systems and as tools for regulating biological processes.

1.1- Chemical Genetics

Chemical genetics is a research approach that uses small molecules to study the way proteins and signal transduction pathways work. It is used to identify which proteins regulate different biological processes, to understand in molecular detail how proteins perform their biological functions and to identify small molecules that may be of medical value.

In order to test the millions of compounds that pharmaceutical companies have in their chemical libraries, special automated instrumentation is needed together with assay miniaturization and data processing. High-throughput screening (HTS), as a scientific method, is at the core of the drug discovery process and requires a collaboration of expertise between the fields of Biology, Chemistry, Informatics and Engineering. Previously performed only at

large pharmaceutical and biotechnology companies, HTS procedures are nowadays also established in academic laboratories. These academic procedures are usually more directed to the discovery of molecular tools rather than the development of new drugs. Although with usually much smaller compound libraries, academic laboratories may have the unique advantages of their compounds resulting from collaborations with academic chemists and also that the targets of their screens do not necessarily need to be financially relevant as opposed to the profit-driven companies.

Most HTS readouts rely on homogeneous assays based on "mix and read" detection reagents, without the need for cell washing or media replacement. High-Content Screening (HCS) is a variation of HTS where the result of a screening procedure is multiparametric. It relies mainly on the detection of fluorescent proteins, antibodies or dyes in cells. Therefore, it requires specific instruments for data acquisition, most frequently an automated fluorescent microscope or a flow cytometer, and specific software for data analysis. Although more complex to establish than regular HTS, the amount of information obtained from a single procedure makes HCS an attractive approach for screening laboratories.

1.2- Cell fate

Development of all mammals begins when a spermatozoid fertilizes an egg and creates a single-cell zygote. This fertilized egg is totipotent, meaning that it has the potential to form an entire organism. After few days and several cycles of cell division a fairly complex structure, the blastocyst, with three distinct cell lineages is formed. The blastocyst consists of the trophectoderm that will supply signaling sources to pattern the embryo before gastrulation and will form the placenta, an organ responsible for embryo attachment to the uterus as well as for nutrient and waste exchange; the primitive endoderm that will provide patterning signals and will contribute to the yolk sac; and the epiblast lineage that will give rise to all cells of the organism[1]. However, cells from the epiblast lineage cannot form the placenta and are therefore considered to be pluripotent and are designated as embryonic stem cells (ESC). What defines a stem cell is its ability to undergo both symmetric divisions (self-renewal, ability to go through numerous cycles of cell division while still maintaining its undifferentiated state) and asymmetric divisions (produces one stem cell and one differentiating cell able to become any other cell type in the organism). In adults, differentiated and more committed tissue-specific stem cells can be found that are considered to be multipotent. Examples of these adult stem cells are: hematopoietic stem cells that can give rise to all cells from the blood system; neural stem cells can be differentiated into

neuronal and glia cells; and mesenchymal stem cells that can differentiate into adipocytes, osteoblasts and muscle cells among others. It was recently shown that, at least *in vitro*, differentiation from stem cells into somatic cells does not follow unidirectionally but it can be reverted through overexpression of several transcription factors. These reprogrammed somatic cells share the properties of embryonic stem cells and were named induced pluripotent stem cells[2]. Oncogenic transformation frequently involves *de novo* acquisition of developmental programs, analogous to cellular reprogramming, and yields cells with unlimited self-renewal potential, a feature shared with ESC[3]. Finally, all cells must die, either in a controlled process mediated by an intracellular program or through an uncontrolled process known as necrosis, caused by external factors such as infection or trauma. While programmed cell death (e.g. apoptosis) is usually beneficial to the organism and naturally occurring in the separation of digits[4] or in the development of the neural system[5], necrosis results in the loss of cell membrane integrity and in an uncontrolled release of products of cell death into the intracellular space. The accumulation of necrotic cell debris can be life-threatening and surgical removal of the necrotic tissue may be the only treatment option.

1.3- Cell self-renewal

Several cellular signaling pathways are known to control the proliferation and differentiation status of embryonic and adult stem cells. Among an intricate network of interconnected pathways whose balance decides the fate of the cell, the most prominent for controlling the cells self-renewal ability are the Wnt[6], Notch[7], Sonic Hedgehog[8], TGF-β[9], FGF[10] and the Hypoxia[11] pathways. The self-renewal feature and the signaling pathways controlling it in stem cells are shared with cancer cells. Therefore, compounds promoting the expansion of cells in an undifferentiated state or somatic cell reprogramming can be important for use in regenerative medicine. On the other hand, aberrant activation of the pathways promoting the expansion of undifferentiated cells may result in uncontrolled cell proliferation and cause cancer and teratomas[12]. For that reason, small molecules inhibiting the self-renewal of these malignant cells can be useful in cancer therapy.

1.3.1- The Wnt pathway

The Wnt pathway is an evolutionarily conserved signaling mechanism that evolved in metazoans. The Wnt highly conserved family is composed of 19 proteins divided in 12 subfamilies in humans and play a crucial role in organism patterning throughout the animal kingdom[13]. The *Drosophila* Wingless gene, homolog of Wnt1, controls segment polarity

3

during larval development[14] and injection of mouse Wnt1 messenger ribonucleic acid (mRNA) into early frog embryos caused a duplication of the body axis in *Xenopus*[15].

Wnts are secreted proteins that, in the canonical pathway (Fig. 1A), interact with target cells through induction of a heterodimeric receptor complex, consisting of a Frizzled (Fz) and a low-density lipoprotein receptor (LRP) 5/6 protein. The ten mammalian Fz proteins are seven-transmembrane receptors and have large extracellular N-terminal cysteine-rich domains that provide a primary platform for Wnt binding. A single Wnt can bind multiple Fz proteins and vice versa[16]. Fzs cooperate with a single-pass transmembrane molecule of the LRP family known as LRP5/6 in vertebrates[17]. The formation of this dimeric receptor leads to phosphorylation of the cytoplasmatic tail of LRP5/6 by at least two separate kinases, glycogen synthase kinase (GSK) and casein kinase (CK)[18]. Recently, MAPKs have also been implicated in LRP5/6 phosphorylation[19]. A crucial step in the Wnt signaling is binding of Axin to phosphorylated LRP6[20]. At the same time, the cytoplasmic part of Fz interacts with disheveled (DVL), facilitating the interaction between the LRP tail and Axin[21]. If these interactions do not happen (in the absence of Wnt), Axin could serve as scaffold for the interaction with β-catenin, the tumor suppressor protein adenomatous polyposis coli (APC)[22] and two constitutively active serine-threonine kinases (CK1α/δ and GSK3α/β), forming the β-catenin destruction complex. CK1 and GSK3 phosphorylate Axin-bound β-catenin, marking the later for recognition by the β-transducin repeat-containing protein (βTrCP), part of an E3 ubiquitin ligase complex. CK1 phosphorylation of β-catenin at Serine 45 is the priming event for sequential phosphorylations of Serine 33 and 37 and Threonine 41 by GSK3[23]. As a consequence, β-catenin is ubiquitinated and targeted for rapid destruction by the proteasome[24], preventing activation of β-catenin target genes in the nucleus. Upon receptor activation by Wnt ligands, Axin is recruited to the phosphorylated tail of LRP.

Although all previously proposed models either assume a physical dissociation of the β-catenin destruction complex or an interference with β-catenin phosphorylation, leading to stabilization of β-catenin[25], recent data showed that, through Axin relocalization, the Wnt signal leads to stabilization of the destruction complex while inhibiting the β-catenin ubiquitination that normally occurs within the complex. Subsequently, the complex becomes saturated by the phosphorylated form of β-catenin, leading newly synthesized β-catenin to accumulate and translocate to the nucleus to activate target genes[26] (Fig. 1B).
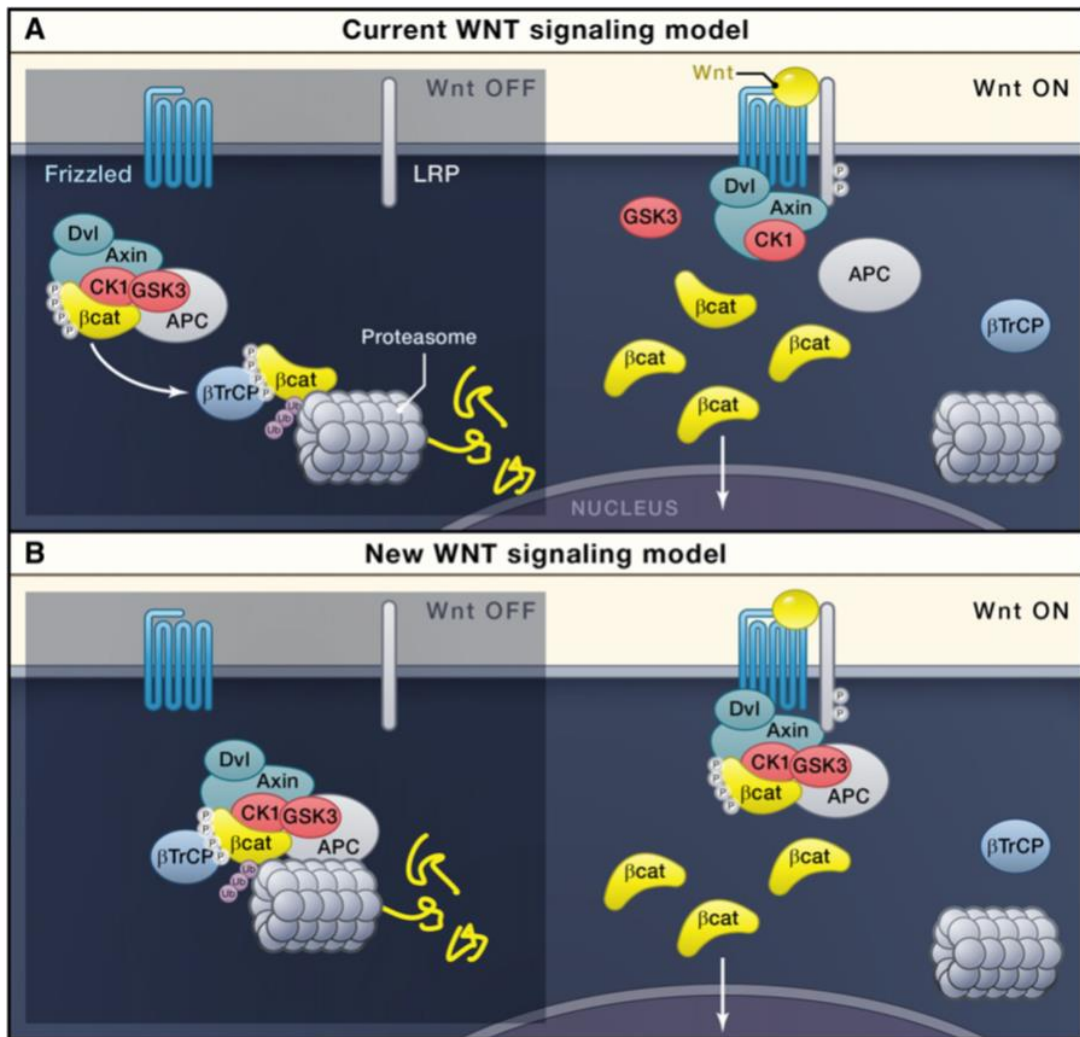
Figure 1: Current (A) and new (B) Wnt signaling models[27].

Upon Wnt pathway activation, β-catenin accumulates in the cytoplasm and then enters the nucleus, where it engages DNA-bound T cell factor (TCF)/ lymphoid enhancer-binding factor (LEF) transcription factors. Although the precise mechanism is not fully described, β-catenin might translocate to the nucleus through microtubule asymmetry and active transport[28]. When the Wnt pathway is not active, Groucho transcriptional repressors interact with TCF/LEF, preventing gene transcription[29,30]. When the pathway is active, β-catenin binds TCF/LEF, replacing Groucho. Genetic assays have revealed a daunting number and diverse nature of collaborating protein cofactors[31] regulating the gene expression upon β-catenin binding to TCF/LEF (Fig. 2). A comprehensive list of Wnt target genes can be found at "The Wnt Homepage"[32].
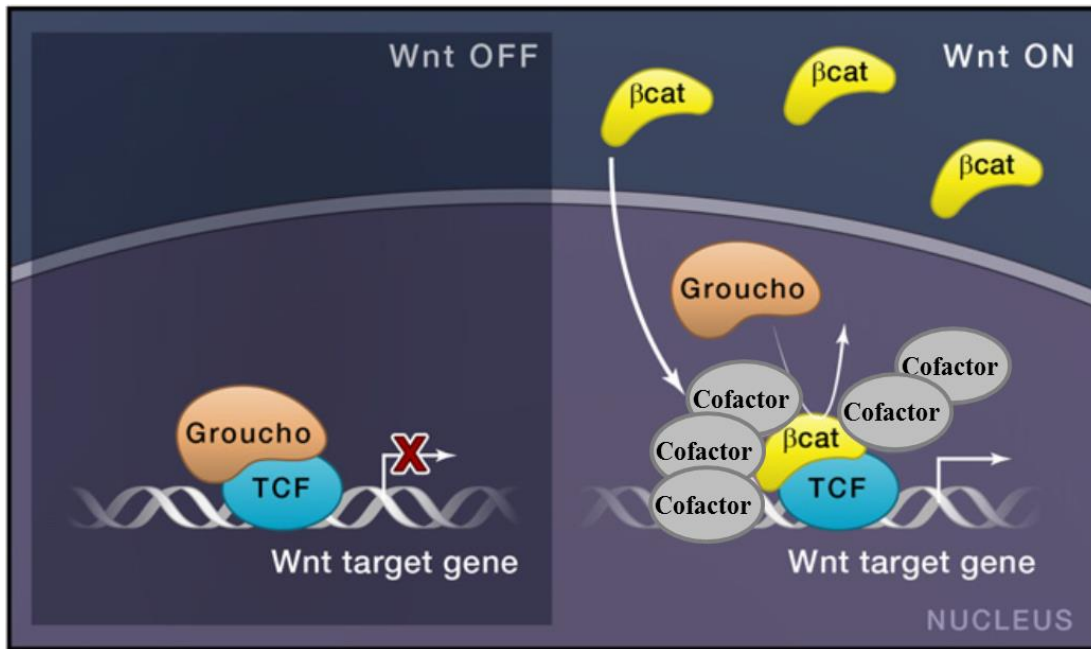
Figure 2: β-catenin signaling in the nucleus[27].

β‑Catenin is the most prominent member of the Armadillo repeat protein superfamily, featuring a central stretch of 12 imperfect Armadillo repeats[33,34], indispensable for binding to TCF[35]. As described above, CK1 and GSK3 phosphorylate β-catenin at its N-terminal region, whereas most collaborating protein cofactors bind its C-terminal region[31] (Fig. 3). The C-terminal transactivation domain of β-catenin was also shown to be necessary and sufficient for signaling by the LEF-1/β-catenin complex[36].
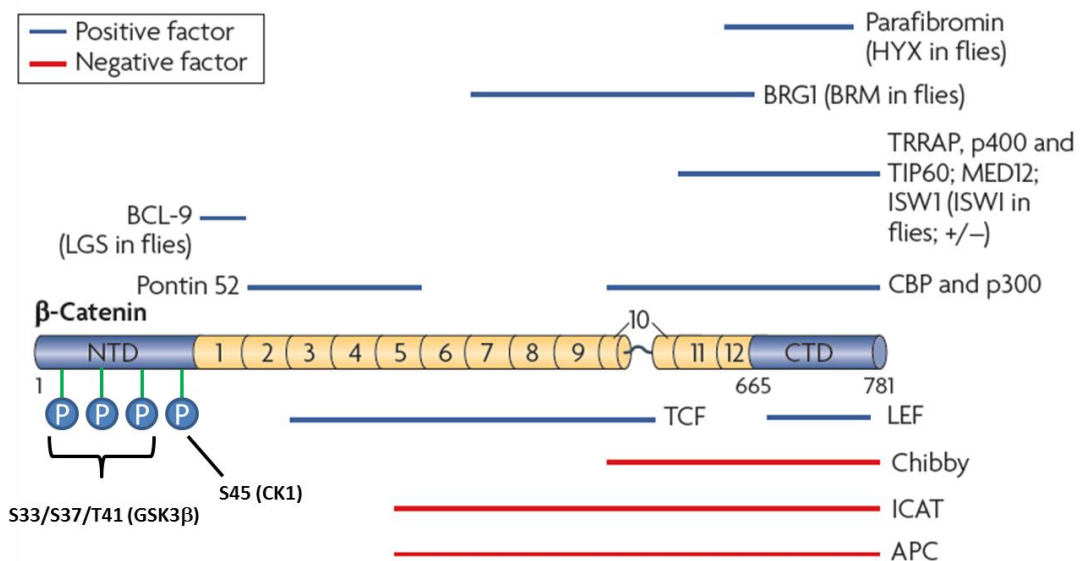
Figure 3: β-catenin structure and interactions[31].

The requirement of Wnt signaling for the maintenance of cell stemness has drawn particular interest. Although the mechanisms are not fully understood, it was shown that mutations in mouse TCF lead to loss of intestinal stem cells[37] and that addition of Wnt overcome the difficulty of expanding stem cells in a self-renewing state[38]. It is therefore not surprising that Wnt pathway mutations are frequently observed in cancer, most notably of tissues that normally depend on Wnt for self-renewal or repair. In colorectal cancer, one of the most common and lethal types of cancer, mutations in APC is present in vast majority, while all the others have mutations in the β-catenin gene[39]. Other examples where cancer is dependent on β-catenin signaling are cutaneous carcinomas[40] and leukemia[41]. As a result, extensive research efforts at targeting the Wnt pathway with small molecules are ongoing. Table 1 presents a list of published compounds with inhibitory effect on the Wnt pathway, together with the molecular target.

Downstream of DVL, the Wnt pathway diverges into at least two other branches apart from the canonical Wnt. These β-catenin-independent branches are the planar cell polarity (PCP) pathway[42] and the Wnt/calcium pathway. The PCP pathway controls the orthogonal polarity of cells within an epithelium[43], the convergent extension movements during gastrulation[44] and the orientation of cochlear cells in the inner ear[45]. Upon Wnt stimulation, activated Fz signals to DVL, which, in turn, activates the Ras homolog gene family, member A (RhoA) and Rac (small guanidine triphosphatases) leading to c-Jun N-terminal kinase (JNK) activation. Both the actin cytoskeleton and microtubules are likely to be affected by activation of the PCP pathway resulting in cell and tissue polarity and dendritogenesis[46]. The Wnt/calcium pathway induces ventral but antagonizes dorsal cell fates in early Xenopus laevis embryos[47]. It also regulates cell movements during gastrulation[48] and heart development[49]. Binding of Wnt to Fz receptors leads to through DVL to induce calcium influx and consequent activation of protein kinase C (PKC) and calcium/calmodulin dependent protein kinase II (CaMKII)/nuclear factor of activated T cells (NF-AT) to regulate the expression of genes controlling cell fate and movement[50] (Fig. 4). It has been described that the canonical pathway modulates intracellular calcium[51] and that NF-AT represses canonical Wnt signaling via its interaction with DVL[52], highlighting the interplay between β-catenin-dependent and -independent Wnt signaling. Furthermore, the calcium ionophores spiperone, ionomycin and thapsigargin were shown to inhibit the Wnt canonical pathway[53].

Table 1: Small molecules inhibitors of the Wnt pathway.

Compound	Target
IWP2	Porcupine[54]
Niclosamide	Fz[55]
NCS668036	DVL[56]
Pyrvinium	CK1[57]
XAV939	Tankyrase 1/2[58]
IWR-1	Tankyrase 1/2[54]
JW55	Tankyrase 1/2[59]
WIKI4	Tankyrase 2[60]
2,4-diamino-quinazoline	β-catenin/TCF[61]
PKF115-584	β-catenin/TCF[62]
Quercetin	β-catenin/TCF[63]
AV-65	β-catenin/TCF[64]
Aspirin	β-catenin/TCF[65]
Indomethacin	β-catenin/TCF[65]
FH535	β-catenin/TCF [66]
ICG-001	β-catenin/CBP[67]
Salinomycin	LRP6[68]
Silibinin	LRP6[69]
Harmine	PPARγ[70]

The specificity and efficacy of the compounds inhibiting the Wnt pathway need to be established and clinical trials have not yet been initiated. Only one small molecule inhibitor of GSK3-β, and therefore agonist of the Wnt pathway, is now in phase I clinical trials for treating Alzheimer's disease[71]. Moreover, our understanding of the pathway is incomplete, leaving room for the discovery of more components and druggable targets.
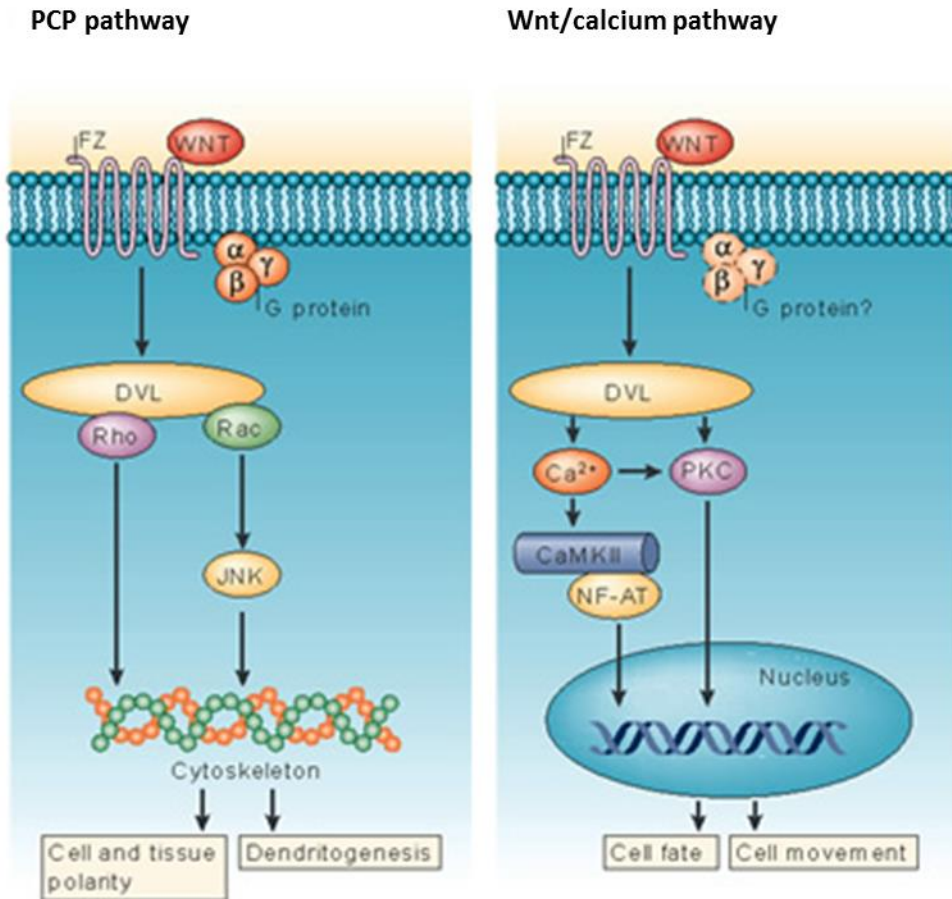
Figure 4: β-catenin-independent Wnt signaling pathways[46].

1.3.2- The Hypoxia pathway

Over the course of evolution, aerobic organisms have developed sophisticated systems for responding to alterations in oxygen concentration, as oxygen acts as a final electron acceptor in oxidative phosphorylation for energy (adenosine triphosphate, ATP) production. Oxygen availability regulates many physiological and pathophysiological processes, including embryonic development, adaptation to high altitudes, wound healing, and inflammation, as well as contributing to the pathophysiology of cancer and ischemic diseases such as infarction and stroke[72]. Proper cellular response to changes in oxygen tension during normal development or pathological processes is ultimately regulated by the transcription factor hypoxia-inducible factor (HIF)[73]. HIF plays a central role in the adaptive regulation of energy metabolism by triggering a switch from mitochondrial oxidative phosphorylation to anaerobic glycolysis in hypoxic conditions. HIF also reduces oxygen consumption in mitochondria by inhibiting conversion of pyruvate to acetyl CoA, suppressing mitochondrial biogenesis and activating autophagy of mitochondria concomitantly with reduction in reactive oxygen species production[74]. The HIF proteins belong to the bHLH-PAS (basic helix loop

9

helix-Per/ARNT/Sim) family of proteins and consist of three O^2-regulated α-subunits, HIF-1α, HIF-2α, and HIF-3α (Fig. 5A), and a constitutively expressed β-subunit of the Aryl hydrocarbon nuclear translocator family (Arnt, Fig. 5B). The HIF-α subunits are structurally homologous, containing an N-terminal bHLH domain that mediates DNA binding and specificity. The HLH and PAS domains mediate heterodimerization with the transcriptional partner Arnt[75].
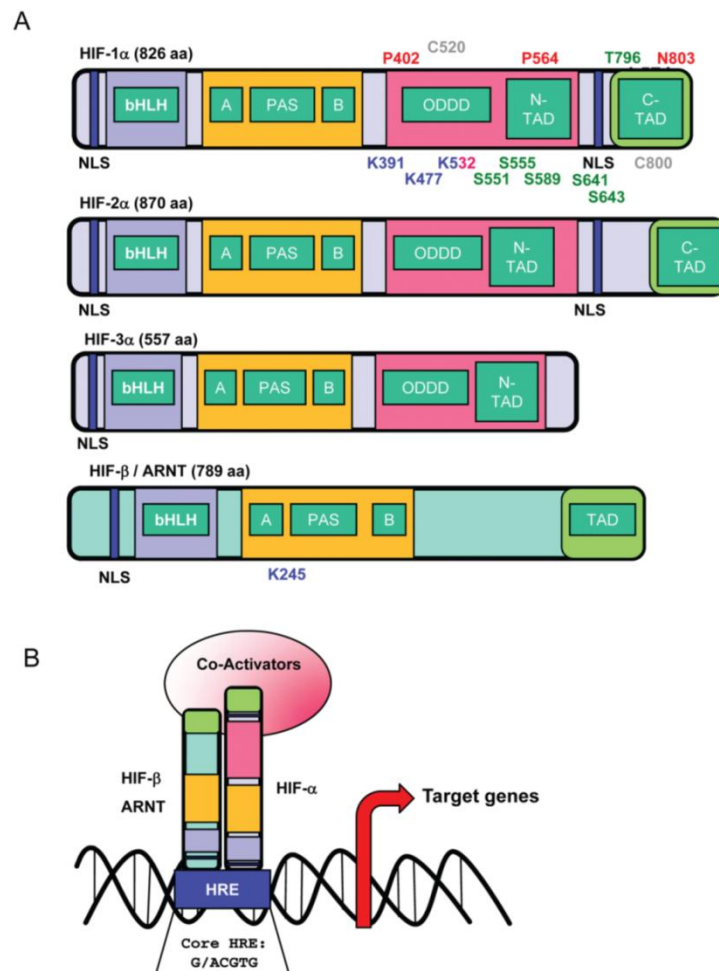
Figure 5: A) HIFs are heterodimers composed of 2 subunits: one α (HIF-1α, HIF-2α, HIF-3α) and one β (HIF-β/ARNT). B) Active HIF complex binds specific hypoxia-responsive elements (HRE, consensus sequence: G/ACGTG) in the promoters of target genes[75].

Under normal oxygen tension (Fig. 6A), HIFα is subject to oxygen-dependent prolyl hydroxylation by prolyl-hydroxylases (PHDs)[76], which allows for substrate recognition and ubiquitylation by the von Hippel-Lindau tumor suppressor protein (pVHL) and its associated ubiquitin–ligase complex. In addition to oxygen, PHDs require Fe^{2+}, 2-oxoglutarate, and ascorbate for prolyl-hydroxylase activity[77]. In contrast, the enzymatic function of PHDs has been reported to be inhibited by nitric oxide, several metabolic intermediates of the tricarboxylic acid (TCA) cycle such as succinate and fumarate as well as reactive oxygen

species (ROS)[78], which are in turn negatively modulated by the mitochondrial deacetylase sirtuin-3 (SIRT3)[79]. Polyubiquitylated HIFα is then degraded by the 26S proteasome[80]. Binding of the HIFα coactivator p300/Creb-binding protein (CBP) is inhibited by asparaginyl hydroxylation by factor inhibiting HIF (FIH)[81]. HIFα is upregulated at the mRNA level by mammalian target of rapamycin (mTOR)[82] and signal transducer and activator of transcription 3 (STAT3)[83], while sirtuin-6 (SIRT6) negatively regulates HIFα protein levels[84].

When oxygen levels fall below 5% (Fig. 6B), prolyl hydroxylation is abrogated, allowing HIFα to escape recognition by the pVHL ubiquitin–ligase complex and accumulate in the nucleus where it associates with nuclear HIFβ[85]. The heterodimer binds to a core consensus sequence at the promoters of HIF-responsive genes, the hypoxia responsive element (HRE), and initiates transcription upon binding to the coactivators p300/CBP[86] and pyruvate kinase isoform M2 (PKM2)[87]. The interaction between HIFα and p300 may be regulated by a variety of factors that sterically impede binding or add/remove post-translational modifications to influence the transcriptional activity of HIFα.
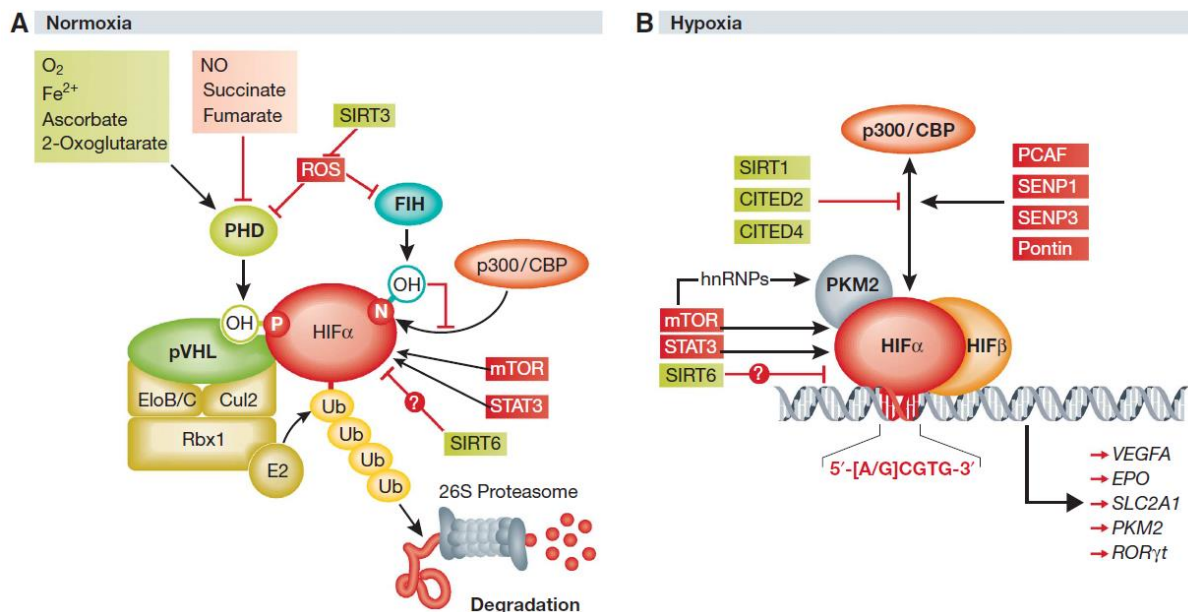
Figure 6: The HIF signaling pathway[73].

Rapidly growing tissues must coordinate growth with oxygen delivery. Furthermore, mammalian development occurs in the relatively O_2 poor uterine environment, with O_2 concentrations of $\leq 3\%$. After the primary vascular plexus is formed, endothelial cells form new capillaries primarily by sprouting angiogenesis. VEGF, considered a master regulator of angiogenesis, causes endothelial cells to detach from the parent vessel and migrate into the

neighboring stroma. Hypoxia is the principal regulator of VEGF expression, as it is a direct transcriptional target of both HIF-1α[88] and HIF-2α[89].

The ability to induce and regulate angiogenesis and vascular remodeling in a directed manner could represent a major advance in the treatment of ischemic vascular diseases. However, angiogenesis is also critical for tumor progression as tumor cell growth frequently outstrips the supply of O_2 and nutrients. HTS efforts have been conducted in order to discover small molecules inhibiting PHDs for treating ischemia (Table 2) or inhibiting HIFα for cancer treatment (Table 3).

Table 2: Small molecules inhibitors of PHDs.

Dimethyloxalylglycine	Mimics 2-oxoglutarate[109]
N-Oxalyl-D-phenylalanine	Mimics 2-oxoglutarate[110]
Deferoxamine	Fe^{2+} chelator[111]
Hydralazine	Fe^{2+} chelator[112]
Ethyl 3,4- dihydroxybenzoate	Blocks active site, Fe^{2+} chelator[113]
FG-0041	Fe^{2+} chelator[114]
Ciclopiroxolamine	Fe^{2+} chelator[115]
FG-4497	Blocks active site[116]
TM 6008	Blocks active site[117]
TM 6089	Blocks active site[117]
L-Mimosine	Blocks active site, Fe^{2+} chelator[118]
Dealanylalahopcin analogues	Block active site, Fe^{2+} chelator[119]
8-Hydroxyquinolines	Block active site, Fe^{2+} chelator[120]
Pyrazolopyridines	Block active site, Fe^{2+} chelator[121]

Some HIFα inhibitors are now marketed drugs for cancer treatment (CCI-779, topotecan, 2-methoxyestradiol, FK228, Bortezomib and Amphotericin B), but there are no FDA approved PHD inhibitors to date.

Table 3: Small molecules inhibitors of HIF-1α.

Compound	Target	Mechanism of HIF-1α inhibition
Wortmannin	PI3K	HIF-1α translation[90]
LY294002	PI3K	HIF-1α translation[90]
CCI-779	mTOR	HIF-1α translation[91]
Topotecan	Topo I	HIF-1α translation[92]
2-methoxyestradiol	Microtubule	HIF-1α translation[93]
Geldanamycin	Proteasome	HIF-1α degradation[94]
Radicicol	Hsp90	HIF-1α degradation[95]
SCH66336	Farnesyltransferase	HIF-1α degradation[96]
Apigenin	Hsp90	HIF-1α degradation[97]
LAQ824	HDAC	HIF-1α degradation[98]
FK228	HDAC	HIF-1α degradation[99]
Trichostatin A	HDAC	HIF-1α degradation[100]
YC-1	FIH	HIF-1α degradation /transcriptional activity[101]
PX-478	Unknown	HIF-1α degradation /transcriptional activity[102]
PX-12	Thioredoxin-1	HIF-1α degradation /transcriptional activity[103]
Pleurotin	Thioredoxin-1	HIF-1α degradation /transcriptional activity[103]
AJM290	Thioredoxin-1	HIF-1α degradation /transcriptional activity/ DNA binding[104]
AW464	Thioredoxin-1	HIF-1α degradation /transcriptional activity/ DNA binding[104]
Echinomycin	HRE	DNA binding[105]
Chetomin	p300	Transcriptional activity[106]
Bortezomib	Proteasome	Transcriptional activity[107]
Amphotericin B	FIH-1	Transcriptional activity[108]

1.4- Cell differentiation

Embryonic stem cells (ESC) are cells that have the potential to differentiate into any cell type of the organism. However, the ethical questions raised about the source of these cells hampered the dynamics of research of stem cells, especially their use in clinics. The discovery that, through forced expression of defined transcription factors, somatic cells could be reprogrammed to pluripotency, opened new perspectives in stem cell research without ethical issues and with the possibility for personalized medicine, without the risk of immune rejection[2]. However, the low efficiency and reproducibility of the reprogramming, along with the need for interfering with the cell DNA, usually through the use of viral vectors, emphasizes the absolute necessity of a thorough characterization of these induced pluripotent stem cells before any clinical application should be considered[122]. The use of multipotent progenitor cells (cells with ESC self-renewal ability but already primed to a certain lineage) could help circumvent the issues with the pluripotent cells described before. Examples of multipotent progenitor cells are the hematopoietic, neural and mesenchymal stem cells. The promotion of the differentiation of one lineage from a progenitor by chemical compounds could be very useful for conventional pharmaceutical therapies[123].

1.4.1- Neural Stem Cells

Neural stem cells (NSC) can be defined operationally as cells that can continuously self-renew and have the potential to generate intermediate and mature cells of both glial and neuronal lineages[124]. Neurons are the functional components of the central nervous system (CNS) and are responsible for information processing and transmission; astrocytes and oligodendrocytes are known as 'glia' and play supporting roles that are essential for the proper neuronal function[125] (Fig. 8). NSC are usually isolated either from mice embryos whole brain or from a region of the fetal or adult brain that had been demonstrated to contain dividing cells in vivo (e.g. subventricular zone or hippocampus[126]). The dissected tissue is enzymatically digested and cells can be clonally expanded in cell culture plates either as suspension neurospheres or as a cell monolayer[127] in the presence of the mitogens epidermal growth factor (EGF) and/or fibroblast growth factor (FGF)[128]. The stemness of the isolated NSC is then proven after differentiation into the three terminally differentiated cell types and immunostaining with specific antibodies. Furthermore, NSC can be again implanted into the brain of a mouse and, surprisingly, the range of the surviving cell types that these grafted, expanded, nervous system stem cell populations can differentiate into is greater than that anticipated. Moreover, the fate of the grafted cells appears to be dictated by the local

environment rather than the intrinsic properties of the cells themselves. This means that NSC can be isolated from different parts of brain through different procedures, expanded *in vitro* under different conditions, but the cell type into which they differentiate upon grafting is specific for the target region[129].
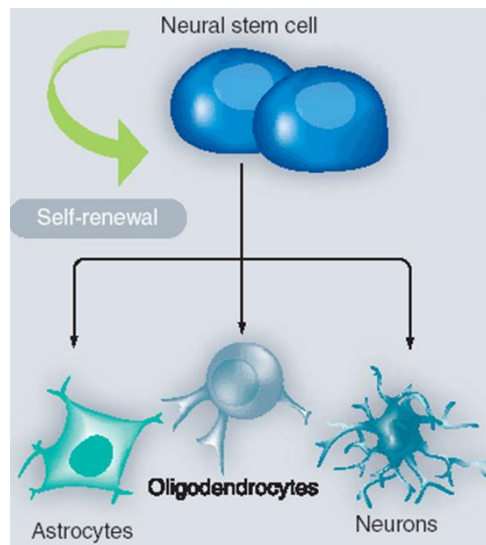
Figure 7: Neural stem cell differentiation (adapted from[130]).

Regardless of the type of neurological disease, all symptoms result from the significant loss of neurons or glial cells in the nervous system. Due to the limitations of pharmacological and other current therapeutic strategies, stem cell therapies have emerged as promising options for treating many incurable neurologic diseases such as Parkinson's disease, Huntington's disease and amyotrophic lateral sclerosis[131].

1.4.2- Mesenchymal Stem Cells

Mesenchymal stem cells (MSC) are an attractive cell source for application in regenerative medicine due to their excellent proliferation and differentiation capacities. Human MSC are a unique population of readily accessible pluripotent cells capable of differentiation into cells of the mesodermal lineage, such as bone, fat and cartilage cells, but they also have endodermic and neuroectodermic transdifferentiation potential[132,133,134] (Fig. 9). Although having been isolated from almost every type of connective tissue[135], MSC have mainly been characterized after isolation from the bone marrow. Although MSC surface markers have been extensively characterized, no specific marker has so far been identified. They are thus defined by their multilineage differentiation capacity[136].
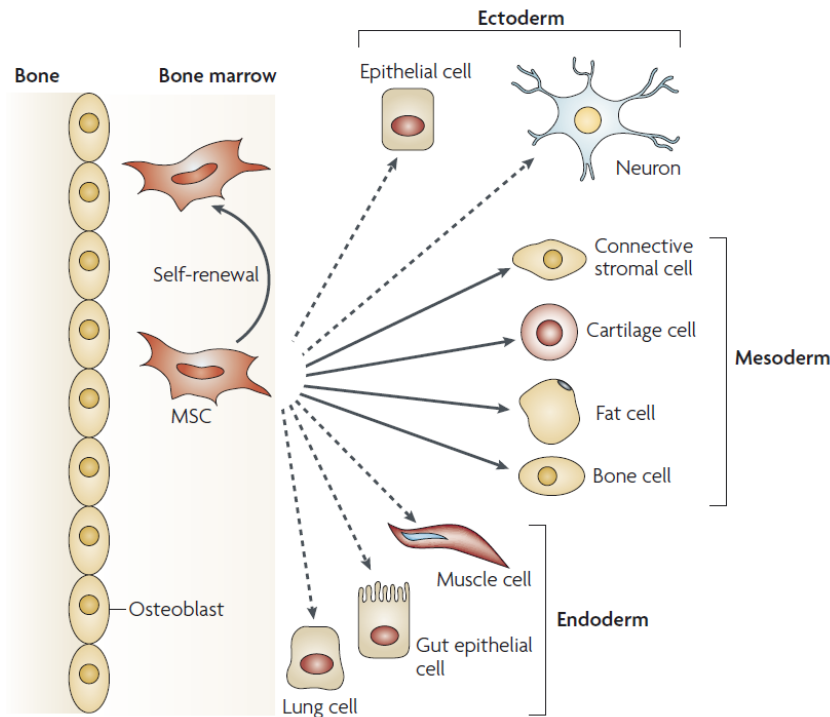
Figure 8: The multipotentiality of MSC[134].

Bone marrow MSC have been successfully transplanted in children with osteogenesis imperfecta, a genetic disorder resulting in the abnormal production of collagen type I[137].

1.4.3- Hematopoietic Stem Cells

Blood is one of the most highly regenerative tissues, with approximately 10^{12} cells arising daily in adult human bone marrow (BM). In 1909, the observation of a wide variety of cellular morphologies corresponding to cells of various blood lineages and stages of differentiation lead to the postulation that hematopoiesis is organized as a cellular hierarchy derived from a common precursor, a hematopoietic stem cell (HSC)[138]. A major obstacle to studying HSC biology is that these cells are extremely rare. Only 1 in 10^6 cells in human BM is a transplantable HSC[139], requiring purification from the bulk of differentiated cells. HSC undergo a stepwise differentiation procedure until becoming the functional terminally differentiated cells (Fig. 7). The different steps are characterized by changes in expression of membrane protein markers termed complexes of differentiation (CD).
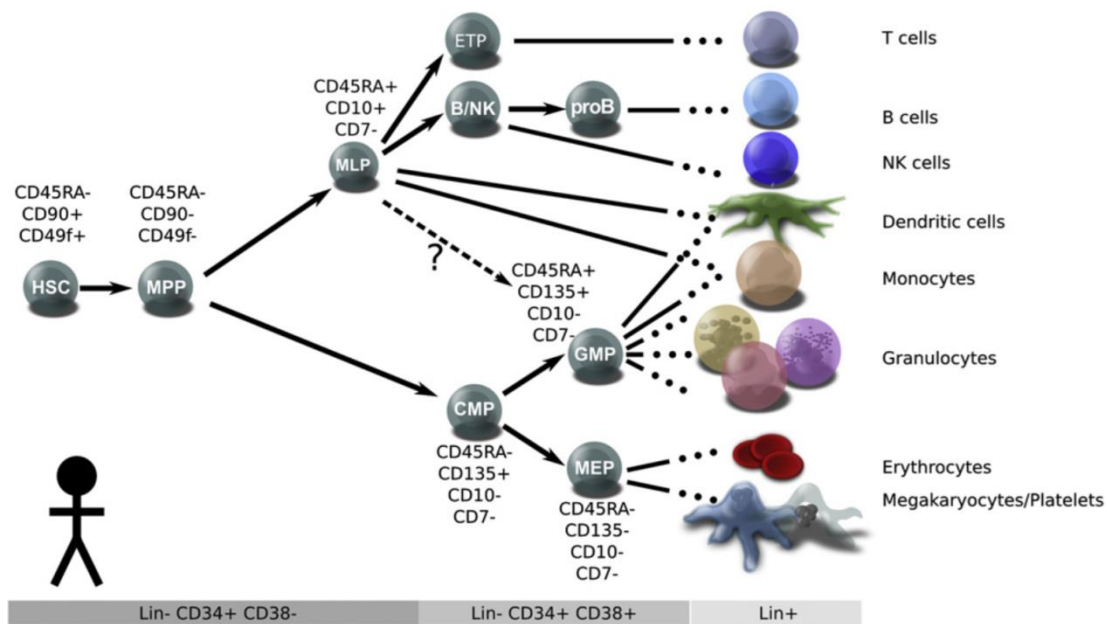
Figure 9: Model of lineage determination in human hematopoiesis[140].

Blood cells can be divided into the myeloid and lymphoid lineages. T, B and natural killer (NK) cells arise from a multilymphoid progenitor (MLP) and are long-lived cells involved in the immune system. Myeloid cells are specialized cells that require rapid replenishment from progenitors. The common myeloid progenitors (CMP) can give rise to megakaryocyte/erythrocyte progenitors (MEP) and to granulocyte/monocyte progenitors (GMP) and subsequently to the terminally differentiated cells. Unlike myelopoiesis, which can be studied in conventional colony-forming units (CFU) assays, known cytokines are insufficient to generate human B and T cells from HSC *in vitro*, complicating analysis of early human lymphoid development.

In the field of molecular-targeted therapy, hematological malignancies are the front-runners for drug development[141]. Among the successful stories of small molecules and antibodies for treatment of these diseases, imatinib is of special note for the treatment of chronic myeloid leukemia (CML) as it was the very first molecular-targeted drug to be developed successfully[142]. On the other hand, numerous conditions lead to the depletion of specific blood lineages, either as a direct result of bone marrow failure or as a consequence of leukemia, viral infection or aggressive treatments including radiation and chemotherapy. The ability to generate sufficient quantities of differentiated, functional cells to replenish the deficient compartment has long been a focus of regenerative medicine. So far, HTS efforts have uncovered Euphohelioscopin A (a PKC activator capable of inducing macrophage differentiation)[143] and SR1 (an aryl hydrocarbon receptor antagonists that promotes the

expansion of HSC)[144]. Another screen revealed that compounds enhancing prostaglandin E2 synthesis (such as linoleic acid) increased HSC numbers, and those that block prostaglandin synthesis (such as the cyclooxygenase 2 inhibitors celecoxib and indomethacin) decreased stem cell numbers[145]. Therefore, there is a need to find new compounds inducing HSC proliferation and controlled differentiation in order to achieve the large number of specialized cells required for transplantation.

1.5- Cell death

It is common knowledge that there is a need for treatments with a selective killing effect of harmful cells or microorganisms but without affecting the healthy cells of the patient.

In cancer, traditional chemical, radiation or hyperthermia therapy act by targeting rapidly dividing cells, one of the main properties of cancer cells. There are however important normal, non-tumor cells within the organism with rapid division cycles. Examples are the cells from the bone marrow and hair follicles and, the application of the above mentioned therapies, results in impaired immune system and hair loss, well known side effects in patients undergoing cancer therapy. Recently, targeted therapy with small molecules or monoclonal antibodies has shown the promise of specific cytotoxicity to cancer cells. So far, there are few cancer types that can be treated with the aim to cure the patient or, more often, to prolong life or reduce symptoms, relying on a combination of several of the available treatments.

In the treatment of infectious diseases, the use of antibiotics has been generally beneficial for public health. Despite the increased number of antibiotic resistant microorganisms, very few new antibiotics have been marketed in the last 40 years. This reduces the efficiency of antibiotic treatments and poses a serious health problem worldwide.

It is clear that there is the need for continuously searching for new agents with higher efficacy to aid in the ongoing fight against cancer and infectious diseases. This could involve the discovery of chemical compounds aiming at specific targets and inducing controlled cell death, avoiding the appearance of necrotic lesions. Traditionally based in morphological observations (where cell death may occur through apoptosis, autophagy or necrosis), it has recently become clear that apparently similar cell death morphotypes most often hide a great degree of functional, biochemical and immunological heterogeneity. In 2012, in an attempt to provide a uniform criteria based in biochemical methods, the Nomenclature Committee on Cell Death proposed the classifications of cell death presented in Table 4[146].

Table 4: Functional classification of regulated cell death modes[146].

	Main biochemical features	Caspase dependence
Anoikis	Downregulation of EGFR Inhibition of ERK1 signaling Lack of β1-integrin engagement Overexpression of BIM Caspase-3 (-6,-7) activation	++
Autophagic cell death	MAP1LC3 lipidation SQSTM1 degradation	−−
Caspase-dependent intrinsic apoptosis	MOMP Irreversible $\Delta\psi_m$ dissipation	++
Caspase-independent intrinsic apoptosis	Release of IMS proteins Respiratory chain inhibition	−−
Cornification	Activation of transglutaminases Caspase-14 activation	+
Entosis	RHO activation ROCK1 activation	−−
Extrinsic apoptosis by death receptors	Death receptor signaling Caspase-8 (-10) activation BID cleavage and MOMP (in type II cells) Caspase-3 (-6,-7) activation	++
Extrinsic apoptosis by dependence receptors	Dependence receptor signaling PP2A activation DAPK1 activation Caspase-9 activation Caspase-3 (-6,-7) activation	++
Mitotic catastrophe	Caspase-2 activation (in some instances) TP53 or TP73 activation (in some instances) Mitotic arrest	−−
Necroptosis	Death receptor signaling Caspase inhibition RIP1 and/or RIP3 activation	−−
Netosis	Caspase inhibition NADPH oxidase activation NET release (in some instances)	−−
Parthanatos	PARP1-mediated PAR accumulation Irreversible $\Delta\psi_m$ dissipation ATP and NADH depletion PAR binding to AIF and AIF nuclear translocation	−−
Pyroptosis	Caspase-1 activation Caspase-7 activation Secretion of IL-1β and IL-18	++

1.5.1- The TRAIL pathway

Apoptosis is a controlled biologic process resulting in cell death and can be initiated by two distinct, but interconnected, molecular signaling pathways. The first is the intrinsic pathway, which typically responds to severe DNA damage, hypoxia, or other cell stresses (such as that caused by chemotherapy or radiotherapy). The intrinsic pathway is largely mediated and controlled by interactions of pro-apoptotic and anti-apoptotic members of the B-

cell leukemia/lymphoma 2 (Bcl-2) protein family that can cause release of apoptosis-inducing factors from mitochondria[147]. The second is the extrinsic pathway, which induces apoptosis through an active process mediated by cell surface death receptors that transmit apoptotic signals when ligand-activated. These death receptors are members of the tumor necrosis factor (TNF) receptor superfamily and their ligands belong to the TNF family of cytokines[148], among which is the TNF-related Apoptosis-Inducing Ligand (TRAIL)[149].

TRAIL importance to cancer research is based in two unique characteristics that are not present in other members of the TNF family of cytokines: 1) it induces apoptosis in a variety of cancer cell lines while leaving normal cells unaffected[150] and 2) TRAIL mRNA is expressed in a wide range of tissues (including peripheral blood lymphocytes, spleen, thymus, prostate, ovary, small intestine, colon and placenta), while the expression of other TNF family members is tightly regulated and often only transient[149].

In humans, four membrane-bound receptors for TRAIL have been identified. Two of them signal for apoptosis: death receptors 4 and 5 (DR4[151] and DR5[152]). The other two, decoy receptors 1 and 2 (DcR1[152] and DcR2[153]) miss the intracellular domain and have a truncated death domain respectively and do not signal for apoptosis. A fifth, non-membrane-bound TRAIL receptor, decoy receptor 3 (DcR3), was identified as osteoprotegerin[154] (Fig. 10). Osteoprotegerin is a secreted TNF receptor homologue that inhibits osteoclastogenesis and increases bone density. However, a mouse model of TRAIL knock-out showed no effect on bone biology[155]. Decoy receptors have been proposed to be competitive inhibitors to regulate TRAIL-induced apoptosis[156].

The TRAIL pathway leading to apoptosis starts with TRAIL forming a central homotrimer around which three receptor molecules (DR4 or DR5) bind[157], leading to the rapid formation of the intracellular multiprotein death-inducing signaling complex (DISC), which, in addition to the ligand/receptor cluster, is composed of the adapter protein Fas-associated death domain (FADD) and the initiator pro-caspases-8 (Fig. 11). The anti-apoptotic protein FLIP can also be recruited to the DISC to replace caspase 8 and form an inactive complex[158]. Pro-caspase 8 is cleaved and activated at the DISC, and can then cleave multiple intracellular substrates (such as the downstream effector caspases 3, 6 and 7)[159]. Active caspase 8 can also cleave the pro-apoptotic Bcl-2 protein Bid, thus engaging the intrinsic pathway[160]. In some cells, activated caspase 8 is sufficient to trigger apoptosis (type I cells), while other cells require activation of the intrinsic pathway to amplify the apoptotic signal (type II cells)[161].
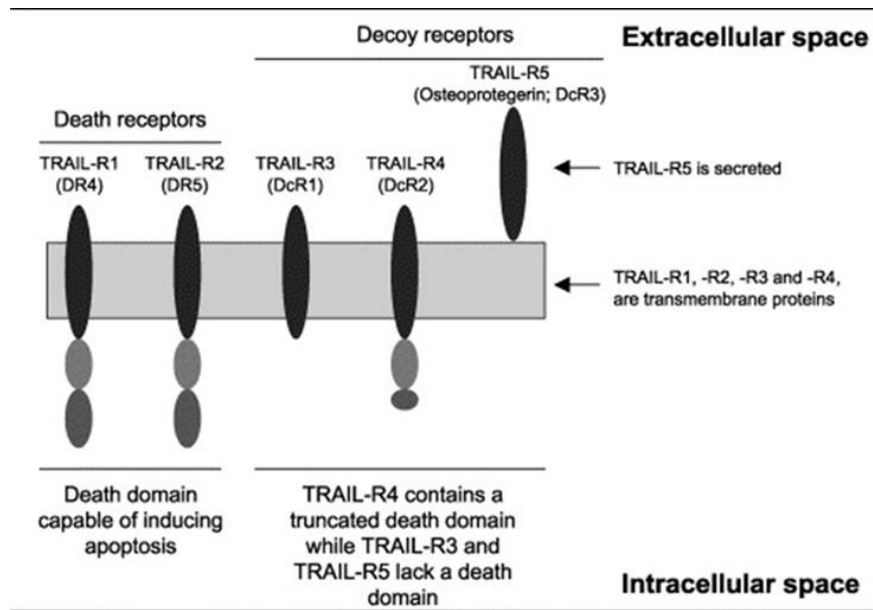
Figure 10: Human TRAIL receptors[162].
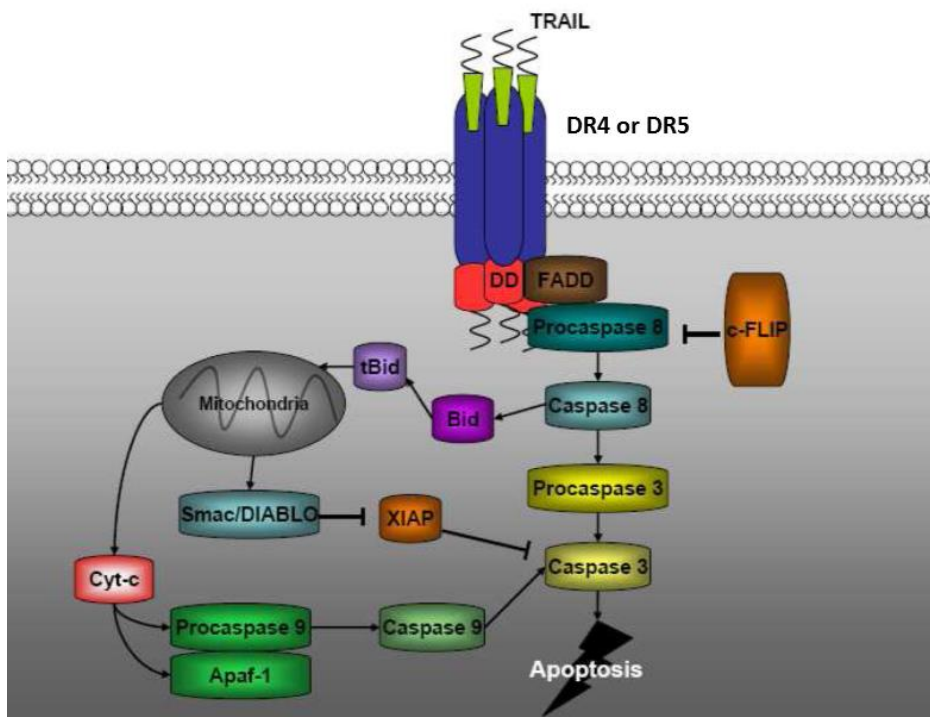
Figure 11: The TRAIL signaling pathway[163].

Once the intrinsic pathway is triggered, the integrity of the mitochondrial membrane is lost, resulting in second mitochondria-derived activator of caspases/direct inhibitor of apoptosis protein binding protein with low isoelectric point (Smac/ DIABLO) release, which acts as a natural inhibitor of X-linked inhibitor of apoptosis protein (XIAP)[164,165], which in turn directly inhibits both effector and initiator caspases[166]. In addition, cytochrome c escapes

from the mitochondria, allowing it to bind to apoptotic peptidase activating factor 1 (apaf-1) and caspase 9 to form the apoptosome[167].

Although a promise for cancer treatment, clinical trials using TRAIL or monoclonal antibodies for the death receptors (mapatumab for DR4[168] and lexatumumab[169], tigatuzumab[170] and conatumumab[171] for DR5) failed to provide satisfactory results. This was due to the fact that many primary cancer cells are resistant to TRAIL treatment. Several mechanisms leading to TRAIL resistance have been proposed:

- DcR1 overexpression[172].
- DcR2 overexpression[173].
- DR4 and DR5 correlation[174].
- DR4 and DR5 gene mutations[175].
- Cell-cycle sensitivity[176].
- Galectin overexpression[177]
- O-glycosylation deficiency[178].
- cFLIP overexpression[179].
- XIAP overexpression[180].
- Bcl-2 overexpression[181].
- Mcl-1 overexpression[182].

- Of special note is a study where acute leukemia primary cells showed TRAIL-induced activation of NF-kB signaling resulting in enhanced survival and proliferation of these resistant cells[183].

It is clear that there is a need to sensitize resistant cancer cells to TRAIL for this therapy to be successful and a combination with tested anti-tumor drugs seems to be the preferred choice. Compounds shown to sensitize resistant cancer cells to TRAIL-induced apoptosis are listed in Table 5, together with the proposed mechanism to overcome this resistance.

Table 5: Small molecules sensitizers of resistant cancer cells to TRAIL-induced apoptosis.

Simvastatin	G_1 arrest[176]
Nimbolide	up-regulation of DR4 and 5, p53, and Bax[184]
Wogonin	down-regulation of c-FLIP and up-regulation of DR5[185]
Bortezomib	proteasome inhibition[186]
Casticin	up-regulation of DR5[187]
Daunorubicin	downregulation of Mcl-1[188]
Amurensin G	up-regulation of c-Myc and DR5 surface expression and down-regulation of c-FLIP and Mcl-1[189]
Thiazolide	Bim activation[190]
Verticillin A	upregulation of BNIP3[191]
Bufotalin	activation of Bid- and STAT1-dependent pathways[192]
2-Methoxy-5-Amino-N-Hydroxybenzamide	up-regulation of c-Myc and DR5 surface expression and down-regulation of c-FLIP and Mcl-1[189]
Lanatoside C	Induction of necrosis[193]
4,5-dimethoxy-2-nitrobenzaldehyde	up-regulation of c-Myc and DR5[194]
Cycloartenyl ferulate	up-regulation of DR4 and DR5[195]
Honokiol	inhibition of c-FLIP[196]
Triptolide	up-regulation of DR5[197]
2-bromo-12,13-dihydro-5Hindolo[2,3-a]pyrrolo[3,4-c]carbazole-5,7(6H)-dione	down-regulation of Survivin Expression[198]
15-Deoxy-Delta(12,14)-prostaglandin J(2)	up-regulation of DR5[199]
Sodium butyrate	up-regulation of DR5[200]
Resveratrol	down-regulation of Survivin Expression[201]
Sorafenib	down-regulation of c-FLIP and Mcl-1[202]
Suberic bishydroxamate	multiple stages in the apoptotic pathway[203]
Indole-3-carbinol	up-regulation of DR4 and DR5[204]
Ouabain	down-regulation of Mcl-1[205]
Camptothecin	up-regulation of DR4 and/or DR5[206]
Thapsigargin	up-regulation of DR5[207]

1.5.2- Leishmaniasis

Leishmaniasis is a life-threatening disease caused by the vector-borne protozoan *Leishmania*. There are about 21 *Leishmania* species known to infect humans and approximately 30 species of sand flies (Phlebotomus species in Africa, South Europe and South Asia; Lutzomyia species in Central and South America) known to be vectors of the disease[208]. *Leishmania*'s life cycle can be divided in two stages: amastigotes in vertebrate hosts and promastigotes in the fly vector[209]. The infection occurs when a female sand fly takes a blood meal, injecting motile *Leishmania* promastigotes into the skin of mammals. Then, macrophages phagocyte the promastigotes that transform into non-motile amastigotes and multiply. If a female sand fly bites an infected animal, it will ingest infected macrophages that are then digested, releasing the amastigotes that transform back into promastigotes. These promastigotes divide in the midgut, migrate into the fly's proboscis and are ready to infect another host (Fig. 12).
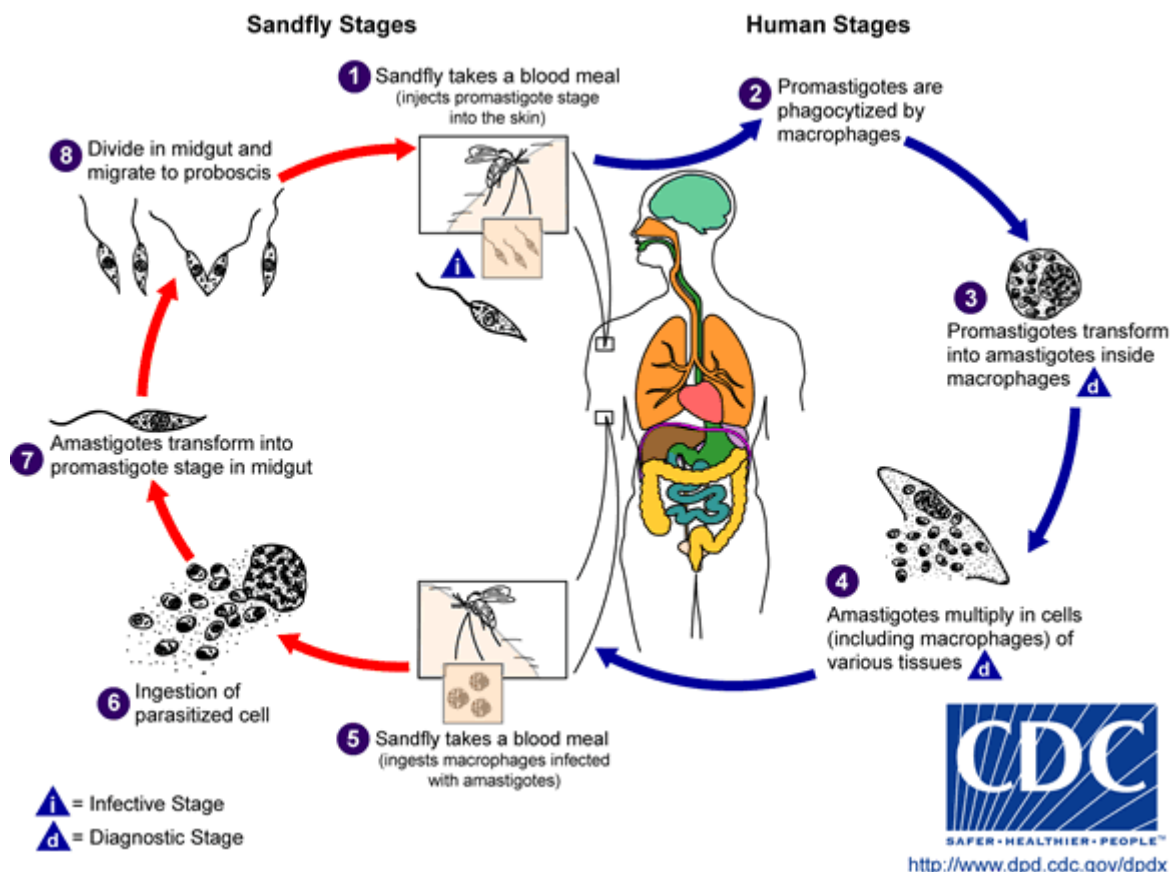

Figure 12: *Leishmania* life cycle.

Leishmania infection can cause three different types of disease with increasing degree of severity: CL- cutaneous leishmaniasis, localized or diffused in the skin; ML- mucocutaneous

leishmaniasis in the mucosa; VL- visceral leishmaniasis (also known as kala-azar or black fever), metastatic spread of infection to the spleen and liver. While CL and ML result in scars and disfiguration, VL is estimated to cause around 50.000 deaths per year in the areas of tropics and subtropics, including southern Europe, from the rain forests in the Americas to the deserts in Asia[210]. It is estimated that there are about 1.5 million new cases of CL and 500.000 new cases of VL each year, to a total of a 12 million people presently infected worldwide[211]. It is also estimated that approximately 350 million people are at risk in 88 countries where the disease is considered endemic. Because more than 90% of human leishmaniasis occurs in under-developed countries, it is one of the most neglected diseases[212]. The disease is nowadays spreading because of risk factors that include climate changes, population movements, long-distance tourism and trade[213].

Prevention of leishmaniasis through exposure to infected flies or vaccination with virulent live parasites has been attempted with very poor results, mainly due to the occurrence of uncontrollable lesions. There are, however, new attempts to create a different type of vaccine using virulence attenuated or dead *Leishmania*, *Leishmania* fractions or defined proteins or even fly saliva[214].

First-line drugs used to treat both visceral and cutaneous leishmaniasis are pentavalent antimonials (sodium stibogluconate and meglumine antimoniate), amphothericin B and pentamidine. Among others, drugs currently undergoing clinical trials are: miltefosine, paromomycin, sitamaquine, imiquimod and the azoles ketoconazole, fluconazole and itraconazole (Table 6; Fig. 13).

The pentavalent antimonials sodium stibogluconate and meglumine antimoniate have been the first-line treatment for leishmaniasis for more than 70 years. They are prodrugs, which are converted by glutathione system to biologically active trivalent forms (Sb_V to Sb_{III})[215]. This active form inhibits *Leishmania*'s glucose catabolism via glycolytic enzymes and fatty acid beta-oxidation[216], type I DNA topoisomerase[217], and trypanothione reductase[218]. Pentavalent antimonials used to be very effective against all types of leishmaniasis but the parasites acquired resistance followed by increased *in vivo* survival ability[219]. This resistance was attributed to the high expression of host and parasite gamma-glutamylcysteine synthetase[220]. Pentavalent antimonials have poor oral absorption and are given via intramuscular or intravenous injections, 20 mg/kg/day for 28 days[221]. Adverse side effects of the treatment include nausea and vomiting, arthralgia, hepatitis, pancreatitis and cardiac dysrhythmias[222].

Table 6: Current drugs used for the treatment of leishmaniasis[223].

Visceral leishmaniasis

First line drugs	Sodium stibogluconate (Pentostam, SSG); meglumine antimoniate (Glucantime)
	Amphotericin B (Fungizone)
	Liposomal amphotericin B (AmBisome)
	Pentamidine
Clinical trials	Miltefosine (oral, Phase IV; registered in India)
	Paromomycin (Phase III)
	Sitamaqine (oral, Phase II)
	Other amphotericin B formulations

Cutaneous leishmaniasis:

First line drugs	Sodium stibogluconate (Pentostam); meglumine antimoniate (Glucantime)
	Amphotericin B (Fungizone)
	Pentamidine
	Paromomycin (topical formulations with methylbenzethonium chloride or urea)
Clinical trials	Miltefosine (oral, Phase III, registered in Colombia)
	Paromomycin (topical formulation with gentamicin and surfactants, Phase II)
	Imiquimod (topical immunomodulator, Phase II)
	Also anti-fungal azoles – ketoconazole, fluconazole, itraconazole

Amphotericin B is an antifungal macrolide antibiotic isolated from *Streptomyces nodosus* and its antileishmanial activity was first shown in the early 1960s and has an excellent leishmanicidal activity[224]. The selective toxicity of amphotericin B appears to be the result of the capacity to form aqueous pores by binding more strongly to ergosterol, the principal *Leishmania* sterol, than cholesterol, the primary sterol counterpart in mammalian cells. The formation of aqueous pores causes the plasma membrane to become non-selectively leaky to K+ ions and essential metabolites, eventually leading to cell death[225]. Due to its toxicity, amphotericin B needs to be administered by slow infusion (1 mg/kg/day for 20 days). Adverse effects from this treatment could be fever with rigor and chills, thrombophlebitis and occasional serious toxicities like myocarditis, severe hypokalemia, renal dysfunction and even death. The development of lipid formulations of amphotericin B helped to reduce its side effects but they can be 10 times more expensive[224].

Pentamidine is an aromatic diamidine, competitive inhibitor of arginine transport and its leishmanicidal activity is possibly mediated via its influence on polyamine biosynthesis and the mitochondrial membrane potential[226]. Probably due to its extensive use as a prophylactic since 1940, the efficacy of pentamidine decreased drastically in the treatment of leishmaniasis. Also, the severe side effects, including nephrotoxicity, cardiotoxicity and

diabetes mellitus-like state[227], resulted in a recommendation of WHO to use pentamidine "only when no other options are available"[228].
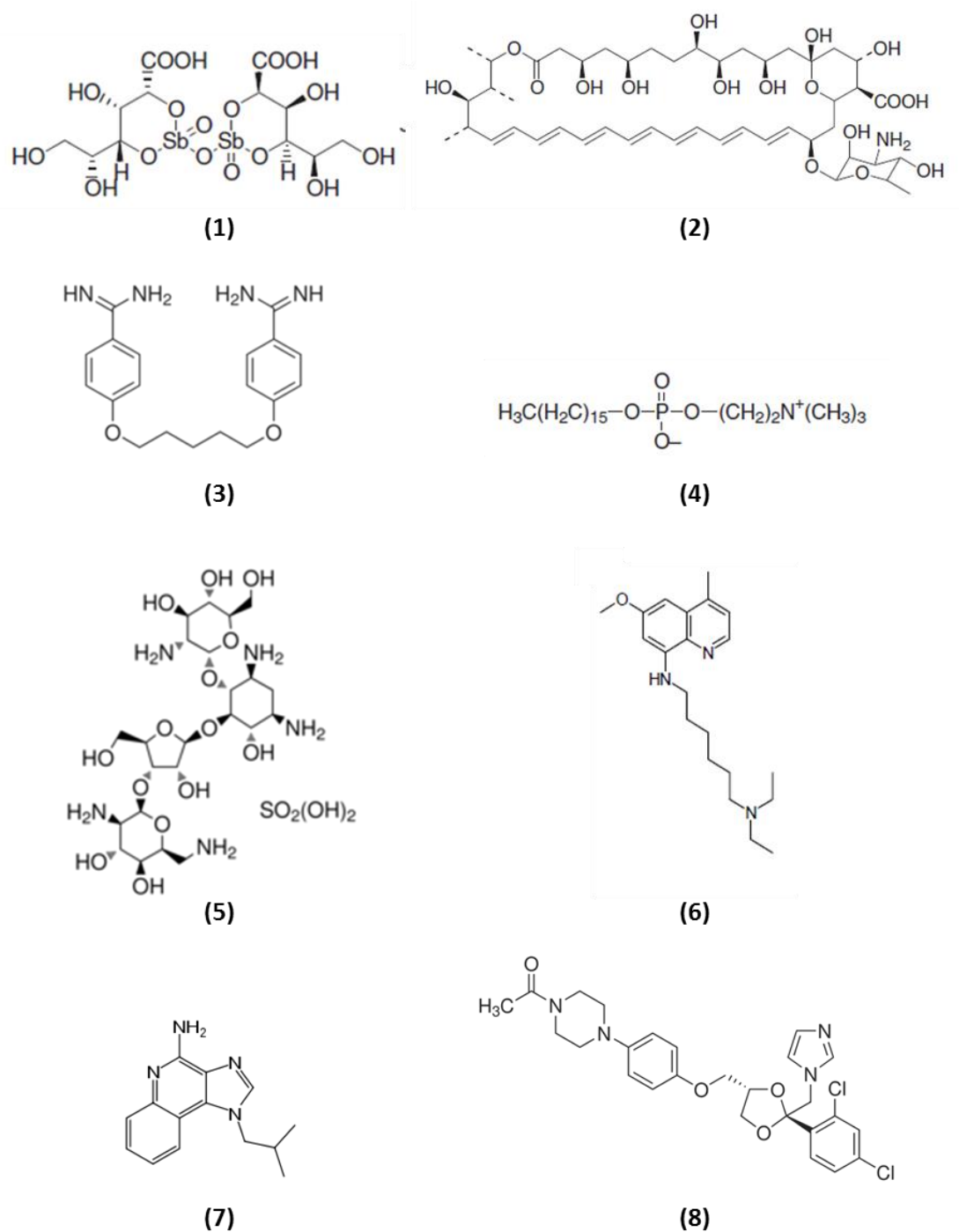
Figure 13: Chemical structures of anti-*Leishmania* drugs: (1) sodium stibogluconate, (2) amphotericin B, (3) pentamidine, (4) miltefosine, (5) paromomycin, (6) sitamaquine, (7) imiquimod, (8) ketoconazole.

Paromomycin is an aminoglycoside obtained from cultures of *Streptomyces rimosus*. It is hypothesized that paromomycin binds to leishmanial membrane glycocalyx, is internalized by endocytosis and induces a drop of mitochondrial dehydrogenases activities leading to

transcription and translation inhibition. It also induces alterations in the uptake of macromolecular precursors resulting in decreased membrane fluidity[229]. Although developed in the 1960s as an anti-leishmanial agent, the interest in manufacturing this drug has been intermittent[224], maybe due to its different efficacy depending on geographical region or *Leishmania* species or even maybe due to its cheap price. Despite efforts to create a parenteral formulation for VL, paromomycin is nowadays used in a number of countries to treat CL[214].

Some of the alternative drugs currently in clinical trials for treating leishmaniasis are: miltefosine, an alkylphospholipid derivative shown to inhibit cytochrome c oxidase[230] and acyl coenzyme A acyltransferase[231]; sitamaquine that inhibits succinate dehydrogenase in the respiratory chain[232]; imiquimod that activates macrophages by inducing the production of cytokines and nitric oxide in macrophages; and the azoles (itraconazole, ketokonazole and fluconazole) that inhibit 14-α-demethylation of lanosterol to ergosterol during cell wall synthesis and promote membrane permeability of *Leishmania*[222].

Treatment of leishmaniasis relies in drugs that were developed more than 50 years ago. The spreading of the disease and the limitations of the drugs used (strong adverse side-effects, resistance acquired by the parasite, strain and geographic region specificity and expensive treatments and difficult to apply), make clear the need for discovering new chemical substances with a leishmanicidal effect.

2- Aims of the study

The objective of the study was not only to develop technology that will allow us to perform phenotype-based assays in HTS mode but also to identify small molecules that affect processes of self-renewal, differentiation or cell death. The main specific tasks required to accomplish such goals were:

. Compound management.
. Development of assays for HTS and HCS.
. Perform screenings.
. Hit confirmation and validation.
. Study mechanisms of action.

3- Materials and methods

3.1- Instrumentation

In a first phase, the following stand-alone instruments were used for screening and hit confirmation:

- JANUS Automated Workstation (PerkinElmer) - liquid handler able to simultaneously transfer 96 samples, either through the use of tips or pintool (V&P Scientific).

- EnVision Multilabel Plate Reader (PerkinElmer) - allows fast measurement of absorbance, luminescence and several fluorescence technologies in 96, 384 and 1536-well plates.

- Multidrop combi (Thermo) - liquid dispenser suitable for 96, 384 and 1536-well plates.

- ALPS 50 V Microplate Heat Sealer (Thermo) - for sealing compound plates.

- HEPA class 100 (Thermo) - CO_2 incubator for cell culture.

- CASY TTC (Roche) - cell counter.

- Titramax 100 (Heidolph) - plate shaker.

- Z4MPlus (Zebra) - barcode printer for microplates.

- Quick Scan 6000 (PSC) - barcode handheld laser scanner.

For the second phase, an automated station was used that included following instruments:

- 6-axis VP series (Denso) - robotic arm feeding the plates to the different instruments in the system.

- JANUS Automated Workstation (PerkinElmer) - liquid handler able to simultaneously transfer 384 samples, either through the use of tips or pintool (V&P Scientific).

- Echo 520 (Labcyte) - acoustic liquid transfer from 384- to 1536-well source microplates into 96- to 3456-well destination microplates.

- EnVision Multilabel Plate Reader (PerkinElmer) - a version of the stand-alone reader with an ultra-sensitive luminescence module.

- Operetta (PerkinElmer) - high content imaging microscope. It is a xenon lamp-based microscope, able to automatically image fluorescence and brightfield from microscopy slides up to 384-well plates. It also allows confocal imaging.

- Multidrop combi (Thermo) - the same as in the stand-alone setup.

- ELX405 WASHER (Biotek) - aspirates and dispenses reagents into 96- and 384-well plates.

- PlateLoc Thermal Microplate Sealer (Agilent) - microplate sealer.

- Storex 110 IC (Liconic) - CO_2 incubator for cell culture with capacity for 110 microplates.

- Storex 110 HR (Liconic) - CO_2 incubator for cell culture, with temperature control down to 4°C with capacity for 110 microplates.

- PLATE::LIFT (PerkinElmer) - on-deck storage with capacity for 244 microplates, without random access.

- MTP Rack (PerkinElmer) - on-deck storage with capacity for 14 microplates, with random access.

- Teleshake 70 (Variomag) - plate shaker.

- VSpin (Velocity11) - microplate centrifuge.

- Barcode Reader (PerkinElmer) - reads barcodes in microplates.

- Lidding station (PerkinElmer) - station with 4 positions for removing and replacing lids in microplates.

3.2- Chemical compounds

The screening collection was built from the following libraries:

- Library of Pharmacologically Active Compounds (LOPAC1280, Sigma-Aldrich) - 1280 compounds.

- Prestwick Chemical Library (Prestwick Chemical) - 1120 compounds.

- NIH Clinical Trial Collection (NIH, USA) - 446 compounds.

- DIVERSet (Chembridge) - 10000 compounds.

- RE&D (Apigenex) - 4844 compounds.

- Steroid library (IOCB, Czech Republic) - 2332 compounds.

Other chemical compounds were purchased from Sigma-Aldrich unless stated otherwise.

3.3- Compound management

For long-term storage, compounds were placed in 96-deep well polypropylene plates (Costar), leaving the last column empty. Compounds were then repositioned in 384-well polypropylene plates (Costar), at a final concentration of 1 mM, resulting in empty last two columns for addition of assay controls. This reformatting was performed using tips in the

Janus liquid handler, transferring (and diluting if necessary) compounds from four 96-well plates (mother plates) into one 384-well plate (daughter plate) and a final volume of 25 µl. For each reformatting step, 5 daughter plates were created.

Some compounds are present in more than one of the LOPAC1280, Prestwick Chemical Library and NIH Clinical Trial Collection libraries. Thirty of these repeated compounds from the LOPAC1280 were removed during reformatting so that these libraries would fit in eight daughter plates - the library of bioactive compounds.

All compound plates were then sealed and barcoded. For storage, all compound plates were placed inside custom made inert gas (nitrogen) containers in a -20°C room. In a second stage, compounds were stored at -20°C, under the inert gas, in automated ASM freezers (Hamilton).

3.4- Cell and *Leishmania* culture

HEK293, U2OS, RKO, HT29, SW480, COLO320, LS147T, HCT116, CCD 841 and HEPG2 cells were maintained in growth medium consisting of Dulbecco's modified Eagle medium supplemented with 10% fetal bovine serum (FBS), 1% penicillin/streptomycin and 2 mM L-Glutamine (Gibco), in cell culture dishes (TTP) at 37°C and 5% CO_2. At approximately 80% confluency, the cells were passaged. For that, they were washed with 6 ml phosphate buffered saline (PBS) and 1 ml trypsin/EDTA (Gibco) was added. After all cells detached from the plate they were collected in growth medium and centrifuged for 5 minutes at 1000 rpm. The resulting pellet was diluted and plated into new 10 cm dishes.

NS5 cells[128] were grown adherent in gelatin-coated plates in a 1/1 mixture of DMEM/F12 and Neurobasal media supplemented with N2, B27 and 2 mM L-glutamine, 25 µg/ml bovine serum albumin, 12.5 µg/ml insulin, 50 µg/ml apo-transferrin, 10 ng/ml FGF-2 and 10 ng/ml EGF (Gibco), at 37°C and 5% CO_2. These cells were passaged similarly to the immortalized cells with the exception of using half the trypsin concentration.

MSC were isolated from Wistar rats' bone marrow and adipose tissue. The bone marrow from femurs was flushed in DMEM growth medium using a syringe and needle and MSC were collected from the interphase after Ficoll-Hypaque solution (density 1.073, Biochrom) centrifugation for 10 minutes at 2500 rpm. Adipose tissue from the inguinal area was cut into small pieces and incubated overnight at 4°C in 0.1% collagenase A (Roche) in DMEM growth medium. The digested tissue was disrupted by shaking and repeated pipetting. MSC from bone marrow and adipose tissue were washed and plated in cell culture dishes in DMEM

growth medium at 37°C and 5% CO_2. After 24 hours, the medium was replaced and the adherent cells were routinely passaged.

HSC were obtained from human umbilical cord blood collected during the night (collected from healthy human donors after their informed consent). The blood was diluted 1 to 4 in DMEM and after centrifugation with Ficoll-Hypaque solution the cells from the interphase were collected and used for CD34+ cells isolation or for erythroid progenitors expansion. CD34+ cells were isolated using the CD34 MicroBead Kit (Miltenyi). Erythroid progenitors were expanded by cultivating the cells from the interphase in StemSpan SFEM (STEMCELL Technologies) medium supplemented with Erythropoietin (2 U/mL), Stem Cell Factor (100 ng/mL) and Dexamethasone (10 μM), with daily partial medium change and cell number readjustment to 3 x 10^6 cells/ml.

Intraperitoneal macrophages were obtained from 10-16 weeks old BALB/c female mice 4 days after injection of 1 ml of 3% thioglycollate. The peritoneal exudate cells were harvested and plated in DMEM growth medium at 37°C and 5% CO2.

Wild type and green fluorescent protein (GFP)-transfected *Leishmania* major LV 561 (MHOM/IL/67/LRC-L137 JERICHO II) were stored in the overlay with 10% dimethyl sulfoxide in liquid nitrogen as subculture 0. Parasites were recovered and routinely cultured for 7 days at 23°C in saline-neopeptone-blood-9 (SNB-9) medium[233]. Solid phase and overlay for SNB-9 were prepared from BactoTM Agar, BactoTM Neopeptone (Dickinson and Company), NaCl and defibrinated rabbit blood (Bioveta). The overlay was supplemented with 50 μg/ml gentamicine. For promastigote growth inhibition assay, subculture 2 of L. major was cultivated in Schneider's Insect Medium supplemented with 50 μg/ml gentamicine, 63.7 μg/ml penicillin G potassium salt, 100 μg/ml streptomycin sulfate salt, 2% human urine and 10% heat-inactivated FBS.

Cell fixation and transfection were performed with 4% paraformaldehyde and polyethylenimine respectively, using standard protocols.

3.4- High-Thoughput Screening

The day before compound addition, cells were plated in solid white or black 384-well plates (Corning) for luminescent or fluorescent assays, respectively, using the Multidrop liquid dispenser. Compounds were transferred via pintool to a final concentration of 1 μM. In the stand-alone equipment setup, the assay controls were added to the last two columns manually using a 16-channel pipette. This was the case of the Wnt modulators, the TRAIL sensitizers and the *Leishmania* killers screens. For the Hypoxia screen, the automated system

was used and the assay controls were added using the Echo acoustic liquid transfer. The plates were gently shaken for 30 seconds and incubated for the assay-dependent time and culture conditions. The detection reagents were then added using the Multidrop liquid dispenser and the results measured by the EnVision plate reader.

3.5- Cell viability, Cytotoxicity and Caspase activation assays

Cell viability and cytotoxicity have a fluorescent readout and cells were plated into black 384-well plates (Corning), while Caspase activation has a luminescent readout and cells were plated into white 384-well plates (Corning). Cytotoxicity and Caspase activation were measured 4 h after compound addition using the CytoTox-ONE homogeneous membrane integrity assay (Promega) and the Caspase-Glo 3/7 assay (Promega), respectively. Cell viability was measured using the CellTiter-Blue cell viability assay (Promega) 48 h after compound addition. All assays readouts were obtained with the EnVision plate reader.

3.6- Differentiation assays

For astrocytic differentiation, NS5 cells were cultivated without FGF and EGF in the presence of 1% FBS for 4 days in gelatin coated plates. For neuronal differentiation, cells were cultivated in laminin/poly-L-ornithine coated plates for one week without EGF and then for another week without FGF and EGF. For oligodendrocytic differentiation, NS5 cells were cultivated in laminin/poly-L-ornithine coated plates without EGF, with 10 ng/ml platelet-derived growth factor (PDGF) and 10 μM forskolin for 4 days. Then cells were incubated 4 more days without EGF, with 200 μM ascorbic acid and 30 ng/ml triiodothyronine.

For osteoblastic differentiation, MSC were cultivated for two weeks in DMEM growth medium supplemented with 50 μg/ml ascorbic acid and 10 mM β-glycerophosphate with medium change twice per week. For adipocytic differentiation, MSC are cultivated for one week in DMEM growth medium supplemented with 0.5 mM isobutylmethylxanthine, 1 μM dexamethasone and 10 μg/ml bovine insulin. Extracellular matrix mineralization and lipid droplets were detected by alizarin red and oil red O staining respectively, using standard protocols.

CD34$^+$ cells isolated from human umbilical cord blood were plated in clear 384-well plates (Nunc) at a density of 2500 cells/well in StemSpan SFEM medium (STEMCELL) with 100 ng/ml stem cell factor and 40 ng/ml insulin growth factor-1. Cells were incubated at 37°C and 5% CO_2 in the presence of compounds for 5 days.

34

3.7- Flow cytometry

Suspension cells were transferred to a V-bottom polypropylene 384-well plate (Corning) using a 16-channel pipette, centrifuged at 1500 rpm for 5 minutes and washed 3 times in 25 µl PBS with 0.1% BSA. Then, 5 µl of multiplexed mouse anti-human monoclonal antibodies with a fluorophore directly conjugated were added to each well and incubated for 1 hour at 4°C. For the primary screen, 7 antibodies (BioLegend) were multiplexed (Table 7), while for the hit confirmation five groups of 4 and one group of 3 antibodies (Exbio) were multiplexed (Table 8). The wells were washed three times and the final cell pellet was resuspended in 50 µl PBS with 0.1% BSA and 0.5 µg/ml propidium iodide. Samples were immediately assayed by flow cytometry using an LSRII flow cytometer equipped with a HT Loader and data acquisition was performed using BD FACSDiva software (BD Biosciences). Data analysis was performed with the FlowJo software.

Table 7: Antibodies used in flow cytometry for the primary screen.

	Target protein	Conjugated fluorophore	Dilution factor	Target cell lineage
Primary screen	CD2	PE/Cy7	200	T-Cells
	CD11b	PB	80	Monocytes
	CD15	PerCP	40	Granulocytes
	CD19	A700	160	B-Cells
	CD34	A647	80	HSC
	CD41	PE	160	Platelets
	CD235a	FITC	640	Erythrocytes

Abbreviations :
CD- Complex of differentiation
HSC- Hematopoietic Stem Cells
FITC- Fluorescein isothiocyanate
PE- Phycoerythrin
APC- Allophycocyanin
A488- Alexa fluor 488
PB- Pacific Blue
PerCP- Peridinin Chlorophyll Protein
A700- Alexa fluor 700
A647- Alexa fluor 647

Table 8: Antibodies used in flow cytometry for hit confirmation.

		Target protein	Conjugated fluorophore	Dilution factor	Target cell lineage
Hit confirmation	Group 1	CD34	FITC	80	HSC
		CD117	PE	80	HSC
		CD133	APC	40	HSC
	Group 2	CD2	PE	80	T-Cells
		CD3	APC	80	T-Cells
		CD4	A488	200	T-Cells
		CD8	PB	200	T-Cells
	Group 3	CD19	PE	40	B-Cells
		CD22	FITC	80	B-Cells
		CD27	PB	200	B-Cells
		CD29	APC	80	B-Cells
	Group 4	CD11b	FITC	80	Monocytes
		CD14	APC	80	Monocytes
		CD177	PB	200	Granulocytes
		CD203c	PE	80	Granulocytes
	Group 5	CD15	APC	80	Granulocytes
		CD16	FITC	80	Granulocytes
		CD33	PB	200	Granulocytes
		CD66acde	PE	80	Granulocytes
	Group 6	CD41	PB	200	Platelets
		CD42b	PE	80	Platelets
		CD71	APC	80	Erythrocytes
		CD235a	FITC	80	Erythrocytes

3.8- RNA extraction and quantitative RT-PCR

Cells were plated in 12-well plates and allowed to attach overnight. Compounds were then added to the cell culture medium and after 16 hours total ribonucleic acid (RNA) was extracted using the Trizol reagent (Invitrogen). Random-primed complementary

deoxyribonucleic acid (cDNA) was prepared in a 20 µl reaction from 1 µg of total RNA using Superscript II RNAseH− reverse transcriptase (Invitrogen) and two percent of the resulting cDNA was used for one quantitative reverse transcription polymerase chain reaction (RT-PCR) reaction. PCR reactions were run using the LightCycler 480 Real-Time PCR System (Roche). Typically, a 5 µl reaction mixture contained 2.5 µl of LightCycler 480 SYBR Green I Master mix (Roche), 0.5 µl of primers (final concentration 0.5 µM) and cDNA diluted in 2 µl of deionized water. Crossing-threshold (CT) values were calculated by LightCycler® 480 Software (Roche) using the second-derivative maximum algorithm. The specificity of each PCR product was analyzed using the in-built melting curve analysis tool for each DNA product identified. Primers for the following human genes were used (first primer is derived from the plus and the second primer from the minus DNA strand): VEGF, 5'-CACATAGGAGAGATGAGC-3', 5'-CCGCCTCGGCTTGTCACA-3'; β-Actin, 5'-GATCTGGCACCACACCTTCT-3', 5'-GGGGTGTTGAAGGTCTCAAA-3'.

3.9- Immunostaining and Western Blot

Cells were plated in 6-well plates and allowed to attach overnight. Compounds were then added to the cell culture medium and incubated for 24 hours. For immunostaining, cells were washed with PBS and fixed with 4% paraformaldehyde overnight at 4°C, washed again with PBS and blocked for 1 hour with 3%BSA/PBS/Tween20 0.1%. Then, primary antibody was added in PBS/Tween20 0.1% (PBST) overnight at 4°C and after three washes with PBST, the secondary fluorescent antibody was added for 1 hour at room temperature. After three more washes with PBST, 1 µg/ml DAPI was added for 5 minutes and finally the cells were washed three times with water. For western blot, cells were washed and scrapped in 1 ml of PBS. After centrifugation (1000 rpm, 5 min), the pellet was dissolved in 100 µl of lysis buffer: 1M Tris pH 6.8, 2% SDS, 10% glycerol and 5% (v/v) β-mercaptoethanol. After two rounds of sonication for 10 seconds, 5 µl of each sample were heated at 95°C for 5 min, the proteins separated by SDS-polyacrylamide gel electrophoresis and transferred to a Protran nitrocellulose blotting membrane (Whatman). Membranes were block in 5% low-fat milk in TBS-T (Tris-Buffered Saline with Tween 20) and incubated overnight at 4°C with primary antibodies diluted in 1% low-fat milk in TBS-T. After three washes with TBS-T, the membranes were incubated for 1 hour at room temperature with horseradish peroxidase-conjugated secondary antibodies (Table 9) diluted in 1% low-fat milk in TBS-T. After three more washes with TBS-T, the protein-antibody complexes were visualized by the ECL

Western Blotting Substrate (Pierce) and the chemiluminescent signal was developed on Medical X-Ray Films (AGFA Healthcare).

Table 9: Antibodies used in immunostaining and Western blot.

| Primary antibodies			
Source	**Reactivity**	**Protein**	**Vendor**
mouse	human	HIF-1α	BD Biosciences
rabbit	human	Hydroxy-HIF-1α (Pro564)	Cell Signaling
rabbit	human	Actin	Sigma-Aldrich
mouse	mouse	GFAP	R&D Systems
mouse	mouse	O4	R&D Systems
mouse	mouse	b-III tubulin	R&D Systems
rabbit	human	P53BP1	Santa Cruz Biotechnology
mouse	human	γH2AX	Millipore
Secondary antibodies			
Source	**Reactivity**	**Protein**	**Vendor**
donkey	rabbit	IgG, HRP-linked	GE Healthcare
horse	mouse	IgG, HRP-linked	Cell Signaling
goat	mouse	IgG, Alexa Fluor 488-linked	Life Technologies
goat	rabbit	IgG, Alexa Fluor 488-linked	Life Technologies
goat	mouse	IgG, Alexa Fluor 568-linked	Life Technologies

4- Results and discussion

4.1- Pathways involved in cell self-renewal

Reporter-based cellular assays were applied for the discovery of small molecules modulating pathways involved in cell self-renewal and that can be used for stem cell biology (agonists and synergists) or for cancer therapy (antagonists). In the first example, a stable cell line harboring the Super TOPFLASH luciferase reporter[234] was used to uncover the role of monensin as a specific Wnt pathway inhibitor. In this reporter, luciferase is driven by 7 LEF/TCF consensus binding sites, determined experimentally to produce low background and high induction upon activation when transfected into HEK293 cells. This robust cell line was then used for more complex pathways analysis such as target discovery and combinatorial approach. In the second example, the Hypoxia pathway, cells transiently transfected with the hypoxia responsive element were used. Although not as robust as stably transfected cells, they were suitable for the identification of two new compounds activators of the hypoxia pathway.

4.1.1- Small molecules modulators of the Wnt pathway

Assay development was performed using the luciferase reporter cell line SuperTOPFLASH HEK293 (STF) cells[234]. These cells have a very low basal luciferase activity and a great luminescence dynamic range when stimulated with Wnt3a (Fig. 14). Increasing the concentration of supernatant from cells producing Wnt3a resulted in increased activation of the pathway up to a 1/200 dilution; with more concentrated Wnt3a, there is a drop in luminescence that most probably is associated with cell toxicity. It was then decided to perform the screen with 2500 STF cells plated per well, with no Wnt3a for agonist mode and with addition of 1/400 dilution of Wnt3a for antagonist/synergist mode. This concentration of Wnt3a was chosen to offer the possibility of detecting pathway antagonists, but not saturating the cell's response for allowing detection of synergists.
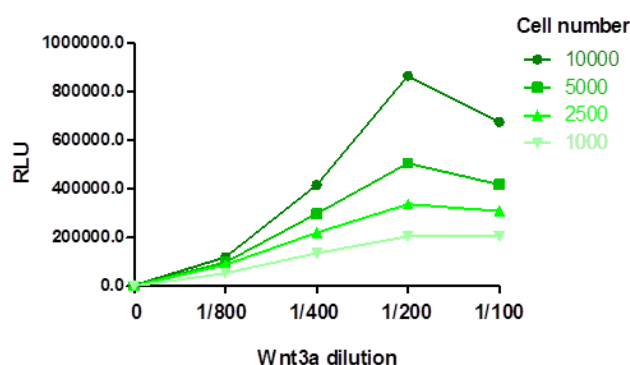

Figure 14: Assay development. Different number of STF cells were incubated with different amounts of Wnt3a for 24 hours before luminescence was recorded.

Approximately 23500 small molecules were screened for their ability to modulate the Wnt pathway in agonist mode, or in synergist/antagonist mode where compounds were co-incubated with recombinant Wnt3a (Fig. 15).
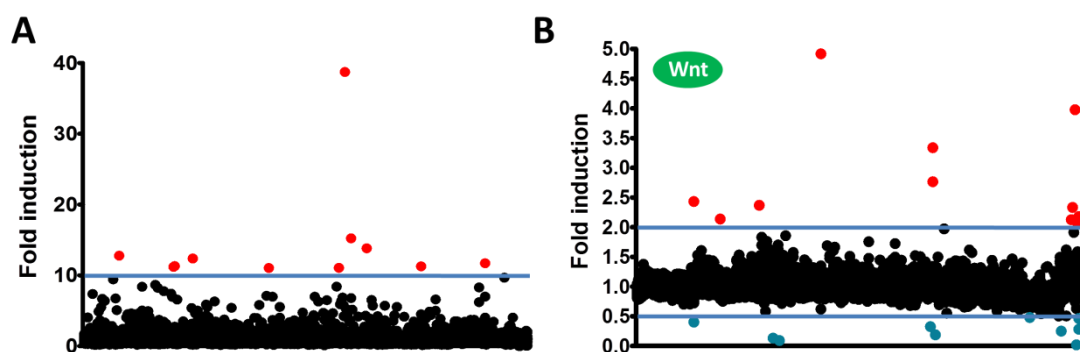

Figure 15: Primary screen. STF cells were incubated with compounds (A) or with compounds in the presence of 1/400 Wnt3a (B) for 24 hours before luminescence was recorded.

Primary hits were confirmed by testing them in dose-response and duplicates. The most potent agonists confirmed were GSK3β inhibitors and were responsible for a very robust activation of the pathway (Fig. 16). GSK3β is a Ser/Thr kinase constitutively active in cells[235] and is inactivated in response to cellular signals. Of the many diverse substrates, some of the key molecules mediating GSK3β functions in regulation of several cellular processes are glycogen synthase, tau protein and beta catenin. Given the multiple processes regulated by GSK3, it is not surprising that GSK3 has been implicated in various diseases such as diabetes, cancer, bipolar disorder and Alzheimer's to name a few, and GSK inhibitors are being actively developed as drugs for the treatment of the various disorders[236].
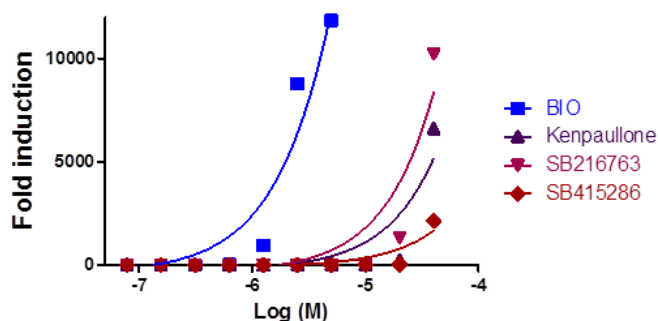

Figure 16: STF cells were incubated with different GSK3β inhibitors for 24 hours before luminescence was recorded.

Four new agonists were uncovered in the screen, confirmed by dose-response and validated after repurchasing (3 commercially available compounds) or after re-synthesizing (1 compound from RE&D library, CCG3048). Three of these new agonists, including the RE&D compound, have maximum induction between 100 and 200 fold (Fig. 17 left), while the remaining one is around 10 (Fig. 17 right).
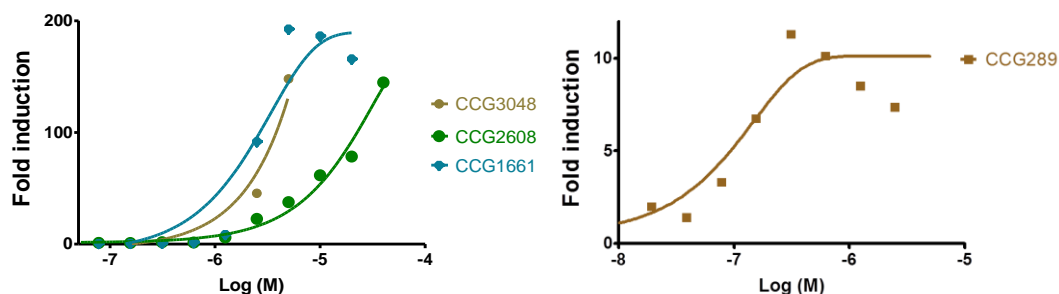

Figure 17: Luminescence measurement of compound activity after 24 hours incubation in STF cells. The graphs have different Y axis scale for better visualization due to the different potency of the compounds.

There were also two compounds with no effect on STF cells alone but that increased the Wnt3a activation of the pathway by approximately ten fold (Fig. 18). One of these small molecules was present in the NIH and the other in RE&D library, and both appear to be pure synergists of the Wnt signaling pathway.
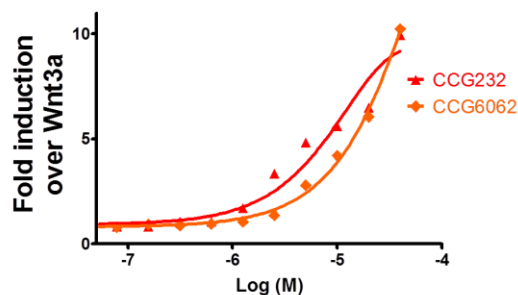
Figure 18: Luminescence measurement of compound activity after 24 hours co-incubation with Wnt3a in STF cells.

When the primary screen was performed in the presence of Wnt3a, previously identified inhibitors of the Wnt pathway, thapsigargin and harmine, were scored as hits and then confirmed in dose-response. However, for its novelty, the most interesting Wnt inhibitor found was monensin (Fig. 19). This antibiotic was approved by the US Food and Drug Administration for use in veterinary practice as a coccidiostat in poultry and growth-promoting agent in cattle. All ADME (absorption, distribution, metabolism and excretion) properties of monensin are known, making the repurposing of this drug easier. Despite some prevailing uncertainties about the detailed inhibitory mechanism, our data imply that monensin might be used as an anticancer drug, especially as a chemopreventive agent for reduction of neoplastic growth in individuals suffering from the familial adenomatous polyposis syndrome (Publication I).
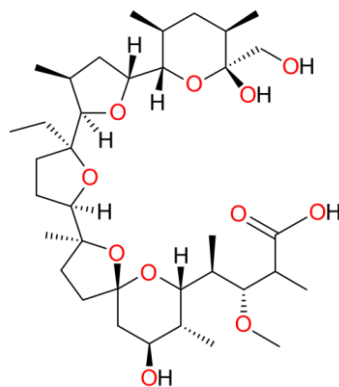
**Figure 19:** Chemical structure of monensin.

40

Six more compounds were identified as antagonists of the Wnt pathway (Fig. 20 left). All of them were more potent in inhibiting the Wnt3a activation of the pathway than the commercially available inhibitor (βCat inh, FH535[66]) without affecting cell viability (data not shown). One of newly identified inhibitors was present in the NIH collection; another in the LOPAC and four other belonged to the RE&D library. From these four, two were luciferase inhibitors (Fig. 20 right) and consequently false positives in all screens where luminescence is the readout. From the other two RE&D compounds, Wnt pathway antagonists and not luciferase inhibitors, one is under characterization and already showed promising *in vivo* activity.
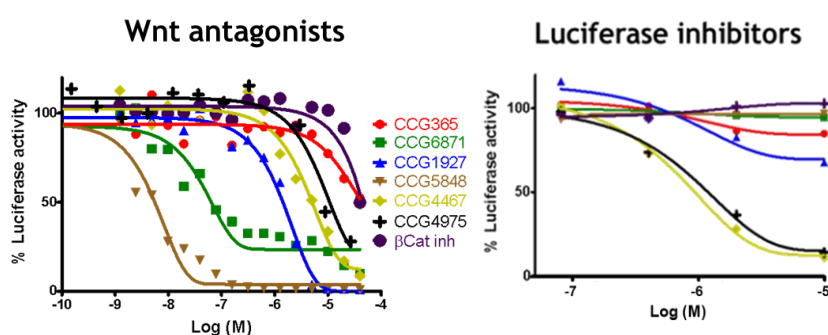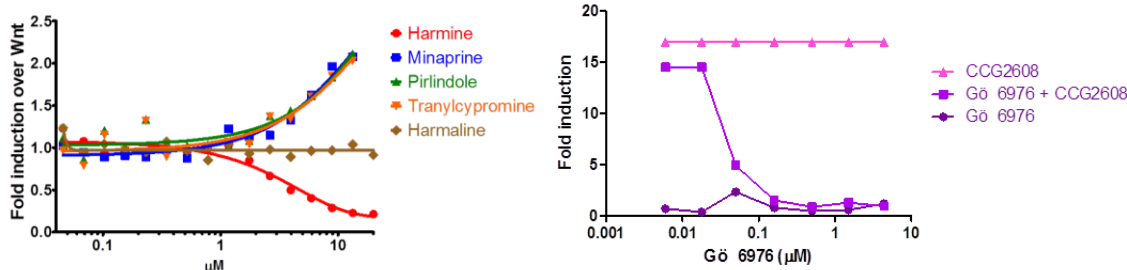

Figure 20: Luminescence measurement of compound activity after 24 hours incubation. (Left) Compounds were co-incubated with 1/400 Wnt3a in STF cells. (Right) HEK293 cells were transfected with a constitutive luciferase producing vector and then incubated with compounds.

A chemical genetics approach may help in the characterization of the mechanism of action of an active compound. When STF cells were treated with inhibitors of the Wnt pathway in the presence of BIO (Fig. 21), three of the compounds exhibited similar or even stronger inhibition of the BIO than of the Wnt3a activation of the pathway. This may indicate that the targets for these compounds are positioned downstream of GSK3β. The fourth compound failed to inhibit the BIO activation of the pathway which can indicate a GSK3β upstream target or even an extracellular aggregation with Wnt3a preventing it to bind the receptor and therefore inhibiting its activity.
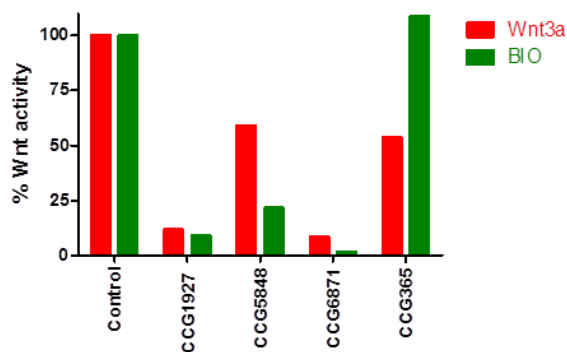
Figure 21: Luminescence measurement of compound activity after 24 hours co-incubation of Wnt inhibitors with Wnt3a or BIO in STF cells.
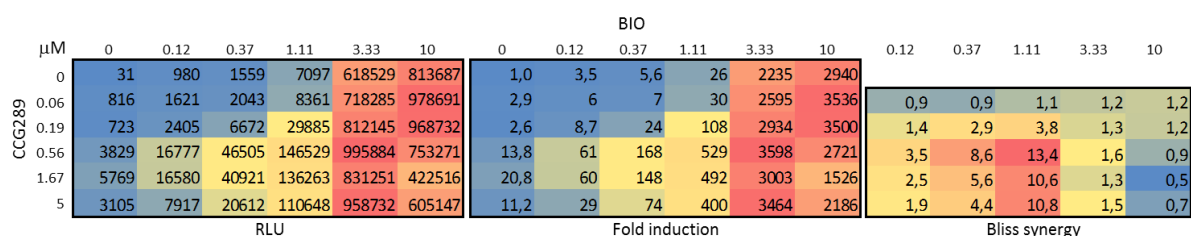
Again, using a chemical genetics approach, the molecular target may be identified, especially if there is some previous knowledge of the compound activity. Harmine has been classified as a monoamine oxidase inhibitor but other inhibitors of the same enzyme failed to inhibit the Wnt3a activation of the Wnt pathway (Fig. 22 left). Harmaline, the most structurally similar compound to harmine failed to inhibit the pathway whereas the others even behaved as weak synergists of Wnt3a. In another example, compound CCG2608 was reported to be a PKC activator and co-incubation with a PKC inhibitor abolished its activation of the Wnt pathway (Fig. 22 right). This proves that compound CCG2608 activates the Wnt pathway through activation of PKC.

Figure 22: Luminescence measurement of compound activity after 24 hours co-incubation of monoamine oxidase inhibitors with Wnt3a (left) or a fixed dose of compound CCG2608 with increasing doses of the PKC inhibitor GÖ 6976 (right) in STF cells.

Another possibility is the use of Chemical Genetics in the discovery of molecular targets is the combinatorial approach. Employing this approach, co-incubation of compounds hitting different targets in the pathway should result in a synergistic response. Having enough compounds and targets, patterns can be obtained that would allow to discover the target of an unknown compound through the synergy landscape. Moreover, the combination might allow decreasing the concentration of compounds while increasing the effect on the pathway, thus reducing the possible cytotoxic effects of individual compounds. The compounds were co-

incubated in a pairwise combination matrix as the example shown in Figure 23. The raw values or relative luminescence units (RLU) were recalculated to fold induction using the formula "fold induction=RLUsample/RLUcontrol". Then, to calculate the synergism between two compounds the formula "Synergy=COMBI(a,b)/SUM(a,b)" was applied, where COMBI is the actual fold induction induced by the compounds co-incubation, SUM is the theoretical sum of individual fold inductions and a,b are the two compounds tested. This formula is an adaptation from the Bliss independence equation where the interpretation is as follows: Synergy<1 implies antagonistic effect of the compounds; Synergy=1 implies simple additivism; and Synergy>1 implies synergistic effect. In this example, 1.11 μM BIO combined with 0.56 μM CCG289 results in a synergy of 13.4, the highest for the range of concentrations tested.

				BIO														
μM	0	0.12	0.37	1.11	3.33	10	0	0.12	0.37	1.11	3.33	10	0.12	0.37	1.11	3.33	10
0	31	980	1559	7097	618529	813687	1,0	3,5	5,6	26	2235	2940					
0.06	816	1621	2043	8361	718285	978691	2,9	6	7	30	2595	3536	0,9	0,9	1,1	1,2	1,2
0.19	723	2405	6672	29885	812145	968732	2,6	8,7	24	108	2934	3500	1,4	2,9	3,8	1,3	1,2
0.56	3829	16777	46505	146529	995884	753271	13,8	61	168	529	3598	2721	3,5	8,6	13,4	1,6	0,9
1.67	5769	16580	40921	136263	831251	422516	20,8	60	148	492	3003	1526	2,5	5,6	10,6	1,3	0,5
5	3105	7917	20612	110648	958732	605147	11,2	29	74	400	3464	2186	1,9	4,4	10,8	1,5	0,7
			RLU						Fold induction						Bliss synergy		

(CCG289 labels the left vertical axis)

Figure 23: Luminescence measurement of compound activity after 24 hours co-incubation of BIO with CCG289.

After the combination is performed with all pairs, a synergistic landscape can be designed (Fig. 24). The pairwise combination of all agonists revealed BIO as a central node where all the synergies converge, demonstrating the importance of GSK3β as a central regulator of the pathway. It also revealed the huge synergistic effect between compound CCG2608 and BIO, a PKC inhibitor and a GSK3β inhibitor, respectively. Perhaps the most interesting synergy was detected between compound CCG3048 and compounds CCG1661 and CCG289, indicating a unique role for the first and probably a similar activity for the other two in modulating the pathway.
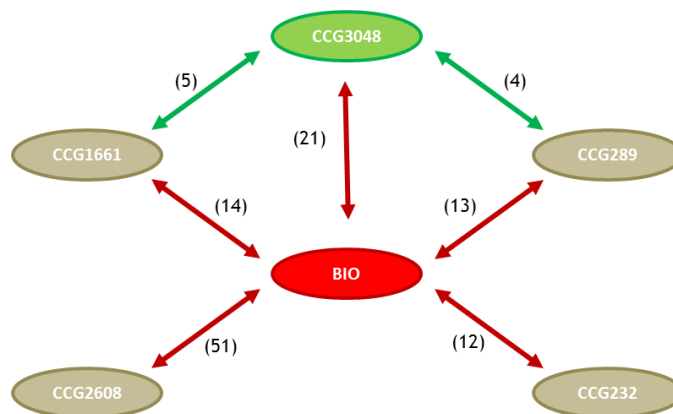
Figure 24: Synergistic landscape between Wnt pathway agonists. Values in brackets indicate the Bliss synergy between the compounds connected by the arrows.

The same combinatorial approach can be applied for antagonists of the pathway, but care must be taken in differentiating antagonism of the pathway and cytotoxicity that could also result in decrease of the luminescence measured. After having enough compounds modulating enough targets in the pathway, a pipeline can be created with the combinatorial approach that will allow determining the target of a new Wnt modulator through its position in the synergistic landscape.

4.1.2- Small molecules modulators of the Hypoxia pathway

A screening procedure was performed to discover new modulators of the Hypoxia pathway using U2OS cells transiently transfected with a pGL4 plasmid (Promega) containing 4 copies of the hypoxia responsive element (HRE), from the erythropoietin promoter, upstream the luciferase reporter gene. For the assay development, cells were transfected via polyethylenimine, the agonist deferoxamine was used as a hypoxia inducer and the luminescence was recorded 24 hours later (Fig. 25 left). For the antagonist mode, cells were co-incubated with the approximate EC_{50} of deferoxamine (100 μM) and the antagonist YC-1 (Fig. 25, right).
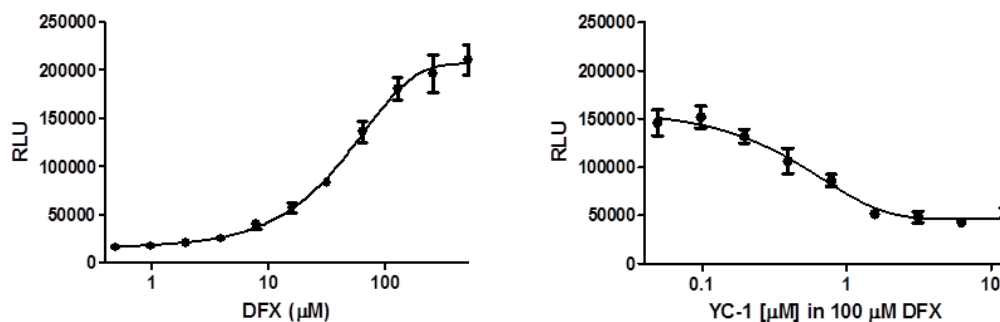
Figure 25: Luminescence measurement of compound activity after 24 hours incubation of deferoxamine (DFX, left) or co-incubation of YC-1 with 100 μM deferoxamine (right) in U2OS cells transiently transfected with the HRE-Luc plasmid.

The screen was then performed with the 10000 compounds from the Chembridge collection in agonist mode and in antagonist mode using 100 μM DFX as pathway activator. Two new compounds with different scaffolds, CCG20240 and CCG25177, were confirmed to activate the HRE in a dose-dependent manner (Fig. 26).
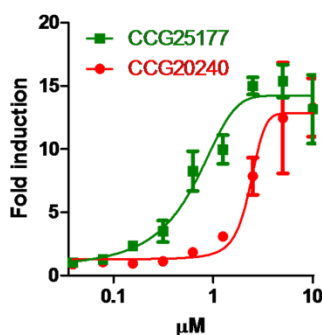

Figure 26: Hypoxia agonist screen validation. U2OS cells transiently transfected with the HRE-Luc plasmid were incubated with compounds and luminescence was measured 24 hours later.

In the antagonist screen, two compounds (CCG27915 and 19851) were found to inhibit the activation of the hypoxia pathway by deferoxamine without any cytotoxicity (Fig. 27 top). However, in a counterscreen, it was shown that they are luciferase inhibitors (Fig. 27 bottom) and not worth following the studies.
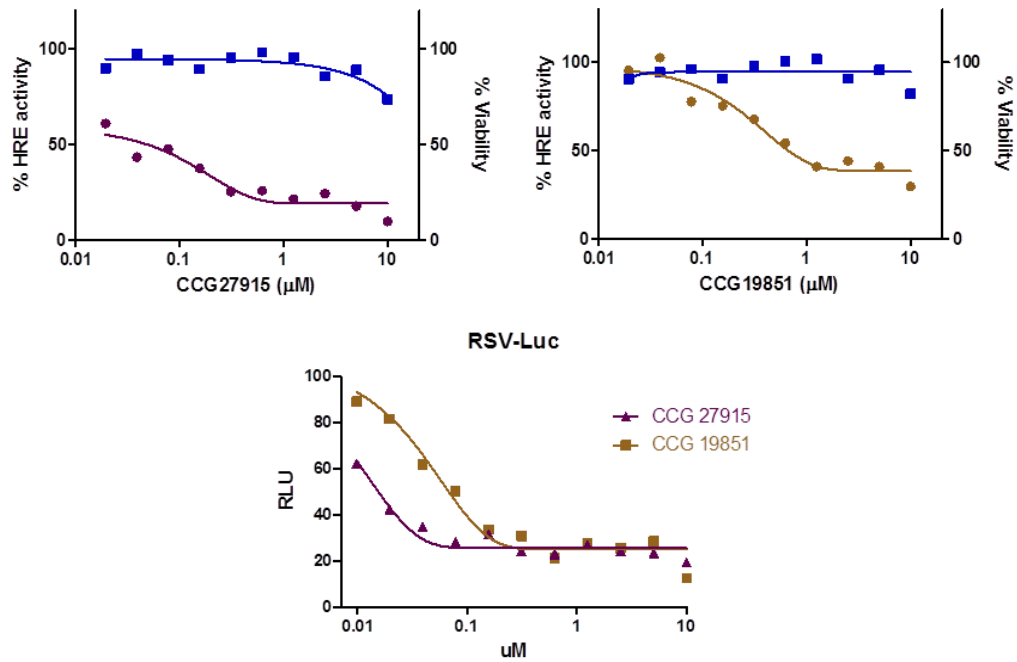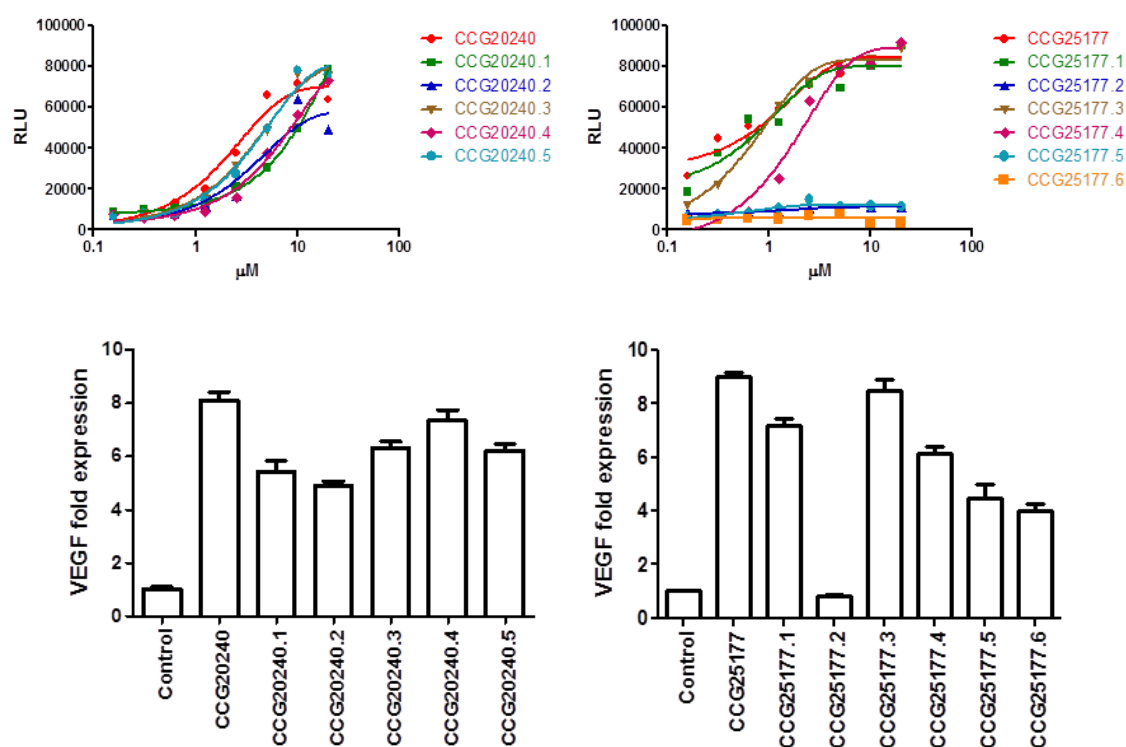
Figure 27: Hypoxia antagonist screen validation. (Top) U2OS cells transiently transfected with the HRE-Luc plasmid were incubated with compounds in the presence of 100 μM deferoxamine for 24 hours. (Bottom) U2OS cells transiently transfected with a luciferase producing constitutive vector and then incubated with compounds for 24 hours.

The next step in the validation of the pathway activators was to test if VEGF expression in U2OS cells would increase after incubation with the compounds. Indeed, quantitative real-time PCR showed that CCG20240 and CCG25177 induced a 6-8 fold up-regulation of VEGF mRNA production (Fig. 28), which was comparable to the effect of the positive control deferoxamine.
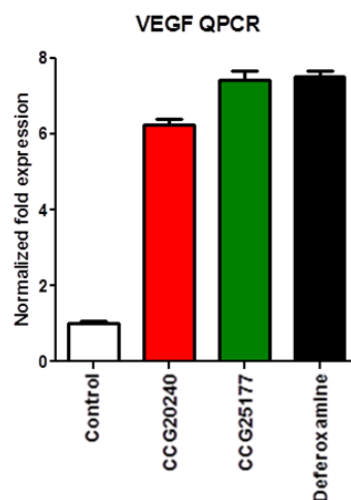
Figure 28: qRT-PCR with RNA extracted from U2OS untreated or treated for 24 hours with 10 μM CCG20240 and CCG25177 and 100 μM deferoxamine. Actin was used as housekeeping gene control.

The next validation step was to test the activity of structurally similar compounds. For this purpose, the similarity search engine provided at Chembridge website (http://www.hit2lead.com/) was used. In their collection there were 5 compounds with higher than 95% similarity to CCG20240 (named here as CCG20240.1 to CCG20240.5) and 6 to CCG25177 (CCG25177.1 to CCG25177.6). These similar compounds were purchased and tested for their ability to activate both the HRE-Luc plasmid (Fig. 29 top) and the expression of VEGF (Fig. 29 bottom). All compounds analogs of CCG20240 behaved similarly both in the reporter assay and in the RT-PCR readout. For CCG25177, there were three analogs displaying no activation of the HRE but only compound CCG25177.2 also showed no increase in VEGF gene expression. Compounds CCG25177.5 and CCG25177.6, although inactive in the reporter assay, were able to induce the expression of VEGF mRNA.

Figure 29: (Top) Luminescence measurement of U2OS cells transiently transfected with the HRE-Luc plasmid were incubated with 10 μM compounds for 24 hours. (Bottom) RT-PCR with RNA extracted from U2OS cells untreated or treated for 24 hours with compounds. Actin was used as housekeeping gene control.

The activity of the compounds in the hypoxia pathway was then evaluated by testing the presence of HIF-1α protein (Fig. 30). Western blot showed that all analogs of CCG20240 were able to induce the production or stabilization of HIF-1α protein as they were able to induce VEGF expression and to activate the HRE-Luc reporter. Analogs of CCG25177 behaved in a different way. Compound CCG25177 and its analogs 1, 3 and 4 showed activity

in the three assays. Compound CCG25177.2 displayed no activity in any of the three assays. Compound CCG25177.5 was not able to activate the HRE-Luc reporter but induced VEGF gene expression and accumulation of HIF-1α protein. Compound CCG25177.6 induced VEGF gene expression but not the activation of the HRE-Luc reporter or the accumulation of HIF-1α protein. These results may suggest that compounds CCG20240 and CCG25177 exert their effect on the hypoxia pathway through different mechanisms. While for the CCG20240 small modifications in its structure imply no change in its activity, for CCG25177 it may result in partial activity or in a totally inactive compound.
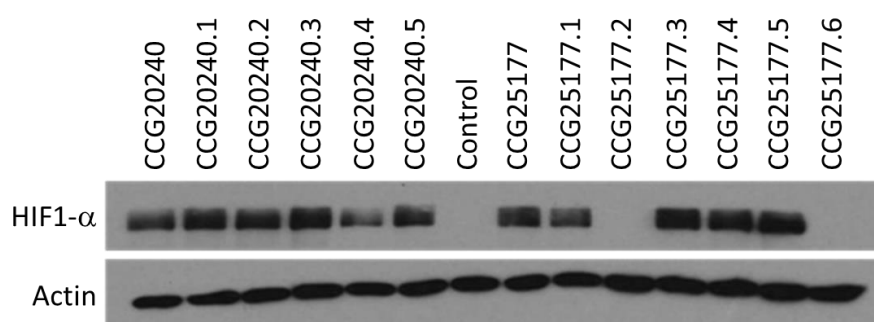
Figure 30: Extracts of HepG2 cells incubated with 10 μM compounds for 24 hours were immunoblotted with anti-HIF-1α and anti-actin antibodies.

In the hypoxia pathway, if HIF-1α is not hydroxylated, it escapes ubiquitylation and degradation in the proteasome and accumulates in the nucleus to activate the expression of target genes. Upon treatment with compounds, immunostaining revealed co-localization of HIF-1α with Hoechst, a DNA fluorescent dye, indicating the accumulation of HIF-1α in the nucleus (Fig 31).
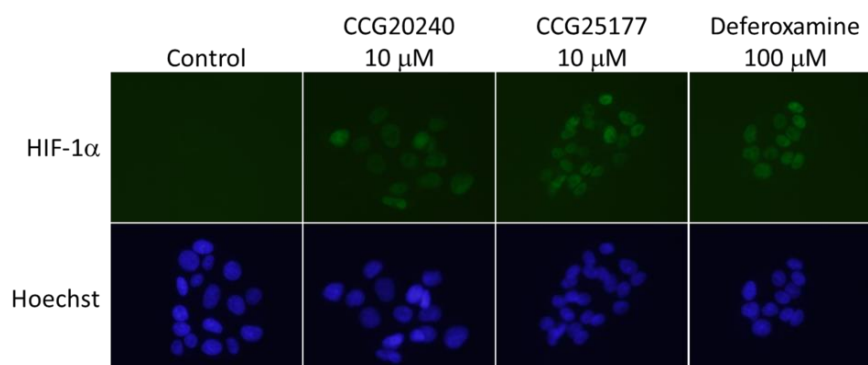
Figure 31: HepG2 cells were incubated with 10 μM CCG20240 and or 100 μM deferoxamine for 24 hours and immunostained with anti-HIF1α antibody. Cell nucleus was stained with Hoechst.

In order to determine their mechanism of action, it was hypothesized that CCG20240 and CCG25177 could prevent HIF-1α hydroxylation. Cell extracts of cultures treated with the compounds were immunoblotted with a hydroxyl-HIF-1α antibody that detects endogenous levels of HIF-1α only when hydroxylated by PHDs at Proline 564. For this, cells were co-treated with MG132, a proteasome inhibitor that would induce the increase of ubiquitylated and hydroxylated HIF-1α in normoxic conditions. Treatment with CCG20240, CCG25177 and, to a lesser extent, deferoxamine inhibited the hydroxylation of HIF-1α (Fig. 32).
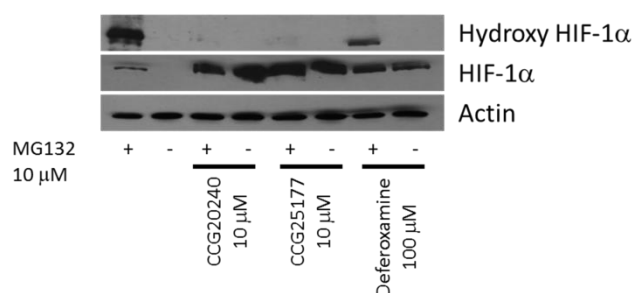

Figure 32: Extracts of HepG2 cells incubated with compounds alone or co-incubated with MG132 for 5 hours were immunoblotted with anti-hydroxy HIF-1α, anti-HIF1α and anti-actin antibodies.

The absence of hydroxylation indicates that the compounds are stabilizing HIF-1α through inhibition of PHDs. Besides oxygen, PHDs require iron for their activation. Co-treatment with ferric citrate, a source of iron, abolished the HIF-1α stabilization in response to CCG20240 and CCG25177 as well as to deferoxamine, previously identified as an iron chelator (Fig. 33). Hence, CCG20240 and CCG25177 are inhibiting PHDs by blocking their access to iron either by chelating it or through binding to the iron site in the PHDs (Fig. 34).
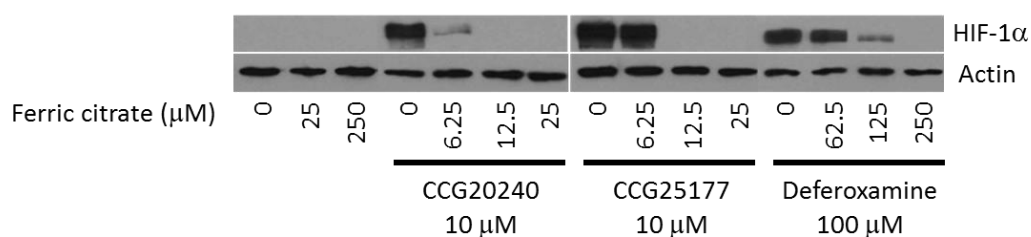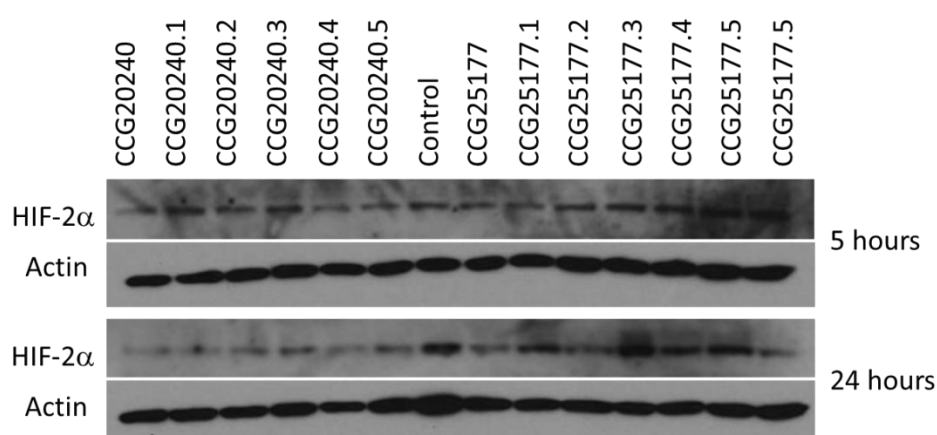

Figure 33: Extracts of HepG2 cells incubated with compounds alone or co-incubated with ferric citrate for 24 hours were immunoblotted with anti-hydroxy HIF-1α and anti-actin antibodies.
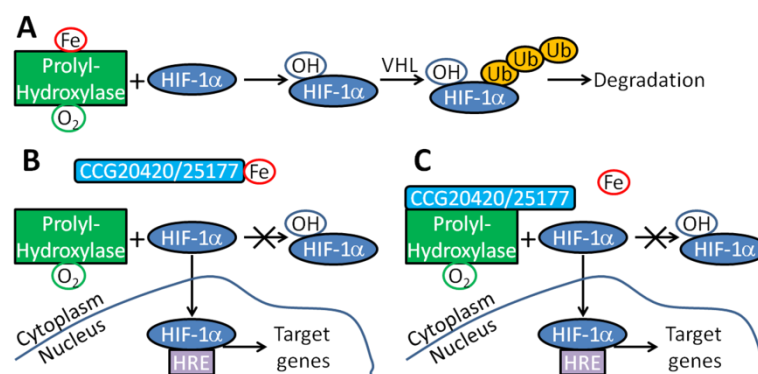
Figure 34: Model of activity of compounds CCG20240 and CCG25177. In normoxic conditions (A) HIF-1α protein is hydroxylated by a prolyl-hydroxylase which signals for ubiquitination by the VHL complex and consequent degradation by the proteasome. When either of the compounds is present, it blocks the access of the hydroxylase to iron either by chelating it (B) or through binding to the hydroxylase itself (C). HIF-1α can then translocate to the nucleus, bind the HRE and induce the expression of target genes.

To further identify the precise action of CCG20240 and CCG25177, several approaches are being studied: incubation of the compounds with iron followed by mass spectrometry may prove that the compounds are chelating free iron; biochemical assay using recombinant PHDs may prove that the compounds are inhibiting specific isoforms of PHDs; HIF-1α knockdown may abolish the induction of compounds of HRE activity or VEGF gene expression indicating specificity for this HIF isoform. As a first approach, the effect of compounds on HIF-2α was tested (Fig. 35). Neither CCG20240 and CCG25177, nor their analogs were able to induce the accumulation of HIF-2α protein in HEPG2 cells, which may indicate some level of specificity for these compounds. This result should however be replicated at least in different cell lines.


Figure 35: Extracts of HepG2 cells incubated with compounds for 5 hours or for 24 hours were immunoblotted with anti-HIF-2α and anti-actin antibodies.

To conclude, for the characterization of CCG20240 and CCG25177, an *in vivo* disease model of activity would be desirable. In diabetes, VEGF production is impaired through high

glucose-induced methylglyoxal modification of the coactivator p300, which attenuates association of p300 with HIF-1 and prevents HIF-1-mediated gene transactivation[237]. This results in impaired wound healing[238] and collateral vessel formation in the heart[239]. It is planned to start in the near future for the treatment of a diabetes mouse model and score for the accelerated wound healing upon compound treatment.

4.2- Cell differentiation

For the screening of compounds influencing cell differentiation, current homogeneous assays are not robust enough. Differentiation implies changes of cell phenotype and the methods to analyze these changes go far beyond the simple "mix and read" methods that define a homogeneous assay. Also, the instruments necessary for detecting changes in phenotype have sometimes to provide single-cell information of multiple parameters. The technology is therefore termed High-Content Screening (HCS). To better exemplify the type of readouts obtained, our first efforts for an HCS procedure will be briefly described. The goal was to find small molecules with the ability to modulate mechanisms controlling DNA repair in human cells. Two proteins involved in this process were stained with primary antibodies (mouse and rabbit), with secondary antibodies coupled with different fluorophores (Alexa 488 and Alexa 568) and with DAPI, a fluorescent dye that binds DNA, used to stain the nucleus. The proteins are relocalized to DNA repair foci when cells are subjected to X-ray irradiation that cause DNA breaks (Fig. 36).
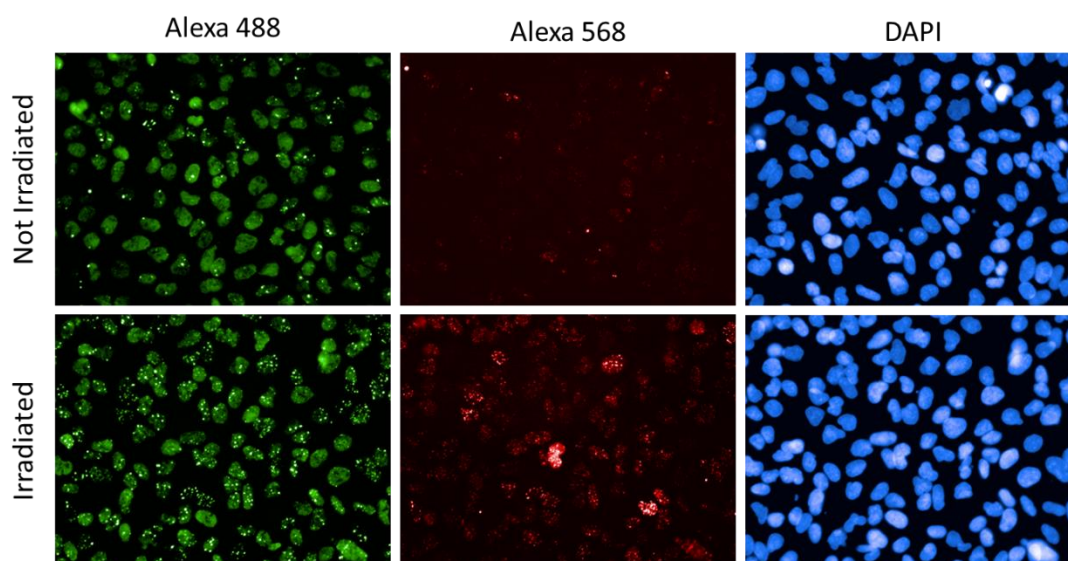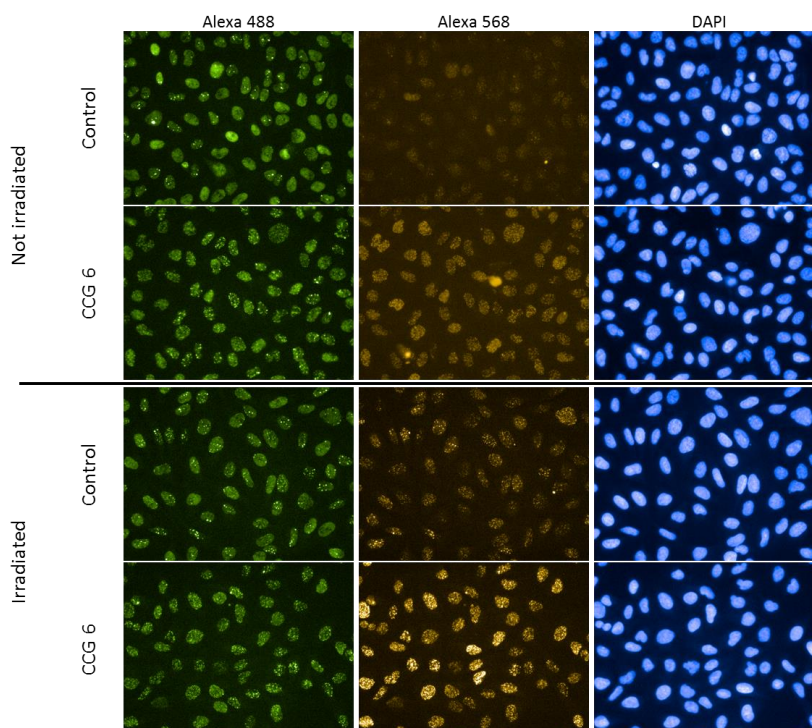

Figure 36: Automated fluorescent microscope images of not irradiated and X-ray irradiated cells, after antibody staining. DAPI was used to stain cell nucleus.

In this assay, the important parameters for analysis were nuclear fluorescence intensity and foci number, fluorescence intensity and size. Assay development indicated that a 40x objective and 8 fields/well in 384-well plates provide reproducible data. So far, the library of bioactive compounds was screened in irradiated cells in parallel with control not irradiated cells. Not surprisingly, several compounds induced DNA breaks and consequent activation of the repair machinery. One of such compounds, CCG 6, was able to increase several of the parameters for both proteins observable through quantification (Fig. 37) and by visual inspection (Fig. 38).
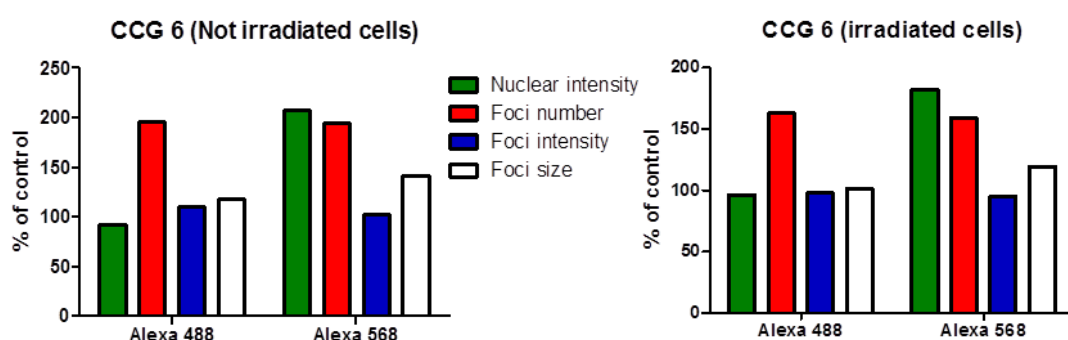
Figure 37: HCS parameters analyzed for the effect of compound CCG 6 on two proteins, represented by the respective fluorophores-conjugated secondary antibodies, on not irradiated and on X-ray irradiated cells.


Figure 38: Automated fluorescent microscope images showing the effect of compound CCG 6 on two proteins, represented by the respective fluorophores-conjugated secondary antibodies, on not irradiated and on X-ray irradiated cells.

Efforts are currently underway to automate the assay and to validate the primary screen hits.

For the discovery of small molecules modulating the differentiation of progenitor cells, high-content screenings using neural, mesenchymal and hematopoietic stem cells were planned.

Neural stem cells (NSC) have the potential to differentiate into astrocytes, oligodendrocytes and neurons under specific culture conditions. The mouse NSC-like cell line NS5[128], able to be propagated indefinitely in adherent conditions, was used due to their ability to differentiate into all three lineages. After differentiation, these cells were immunostained with antibodies that recognize specific markers of each lineage: GFAP for astrocytes, BIII-tubulin for neurons and O4 for oligodendrocytes (Fig. 39).
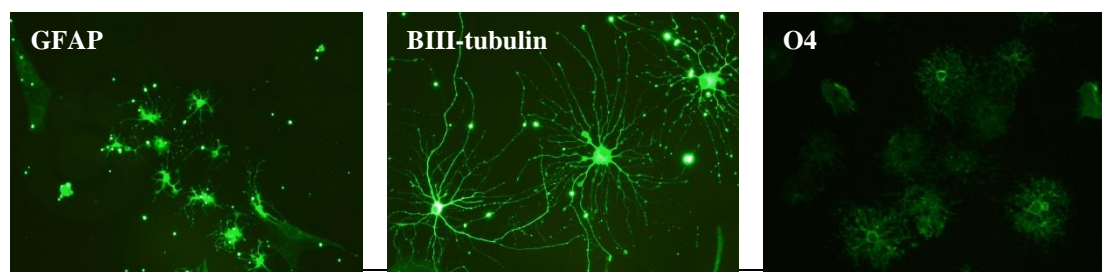
Figure 39: Differentiation of NS5 cells into astrocytes (left), neurons (middle) and oligodendrocytes (right), identified by immunostaining with the respective antibodies coupled to GFP.

One approach to create an assay suitable for discovery of compounds able to induce specific differentiation of NSC could be the stable transfection of the progenitor cells with plasmids containing different fluorophores (reporter proteins) under the control of the lineage specific marker genes.

Mesenchymal stem cells (MSC) can be obtained from bone marrow or from fat tissue. After a couple of passages, the cell culture presents a uniform phenotype and cells can be differentiated. Typically, MSC undergo replicative senescence after approximately 10 passages or 50 days in *in vitro* culture, so there is a time window when experiments should be performed.

It has been previously reported the spontaneous immortalization of two vertebral bones-derived fish cell lines (from the gilthead seabream *Sparus aurata*) able to differentiate either to osteoblasts or to chondrocytes in a mutually exclusive manner[240]. Under specific culture conditions, these cells were also able to differentiate into adipocytes (unpublished). This demonstrates both the conservation of the MSC differentiation system in teleosts and the

difference in behavior of MSC, not only when collected from different tissues, but also probably from different regions within the same tissue.

Side-by-side MSC cultures derived from rat bone morrow (BMSC) and from adipose tissue (ASC) were compared. Although similar in phenotype, ASC have a greater adipocytic differentiation potential but are difficult to differentiate into osteoblasts, whereas BMSC have a greater osteoblastic and lower adipocytic differentiation potential (Fig. 41).
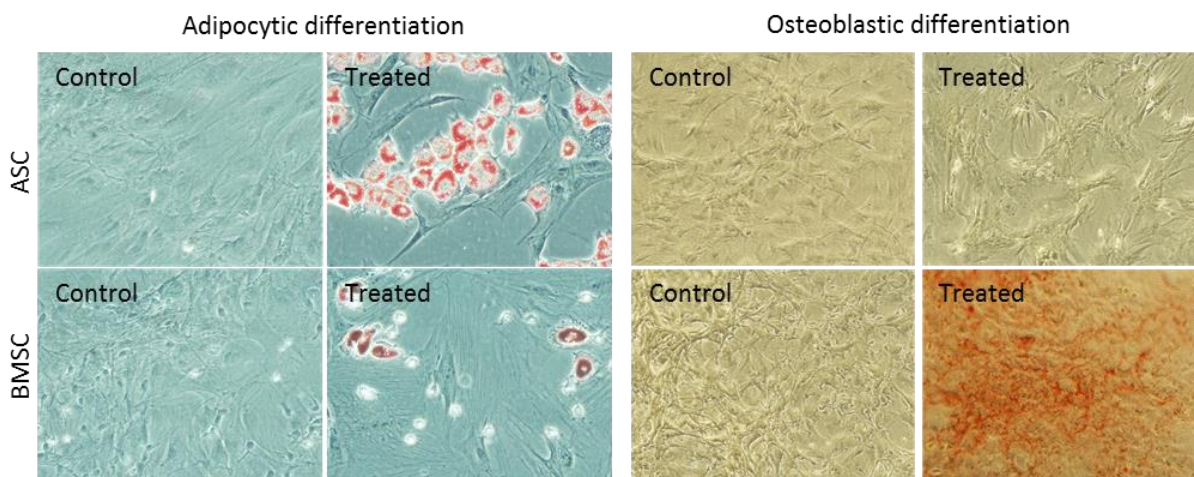
Figure 40: Rat MSC were derived from bone marrow aspirate (BMSC) and fat tissue (ASC). Differentiation was induced towards adipocytes and osteoblasts and cells were stained with Oil Red O and Alizarin Red respectively.

While colorimetric staining provides an easy visualization under a normal light microscope, it is not suitable for HCS. Oil Red O can be substituted by Nile Red and Alizarin Red can be replaced by calcein, which are fluorescent markers for lipid droplets in adipocytes and extracellular calcium matrix deposition by osteoblasts, respectively.

When planning for a phenotypic HCS screening, one should make some important decisions at early stages. One of them is the source of cells for screening. The use of established cell lines would hardly mimic the situation *in vivo* due to the accumulated mutations that results from immortalization and continuous passaging. Primary cells would then be a better choice. While the use of animal models may be useful in understanding the evolutionary aspects of the differentiation processes, it does not mean they represent with high fidelity what happens in humans. Accordingly, the best would probably be the use of human primary cells. Human ASC can be easily obtained from lipoaspirations and a perfect source to study adipocytic differentiation and for screening of compounds useful in the treatment of obesity, but, if they replicate the rat experiment, their osteoblastic differentiation would be more difficult to achieve. Osteotomies and bone marrow aspirations may provide

sources of MSC suitable for screening of compounds inducing osteoblastic differentiation and thus a source for transplantation. However, healthy people do not usually undergo osteotomies and cells from unhealthy patients may be biased towards some abnormal phenotype. At the end, a choice must be made and relevant secondary assays designed to validate the usefulness of hit compounds. The experiments with rat ASC resulted in a screening-unrelated publication concerning dermal scaffolds for hernia repair (Publication II).

4.2.1- Hematopoietic differentiation screen

Human umbilical cord blood was selected as starting point for the purification of hematopoietic stem cells (HSC), characterized by their expression of the membrane protein CD34. Using immunomagnetic cell sorting after Ficoll purification, a typical sample of human umbilical cord blood of 30 ml contained approximately half a million cells from which 1% were CD34 positive. This column-based cell sorting is very efficient in collecting the CD34$^+$ cells, which are rare in the flowthrough (Fig. 42). It is not as efficient in separating a pure population of CD34$^+$ cells. The approximate 20% of CD34$^-$ cells present in the collected fraction may be explained by the use of gravity as the force that is not strong enough to separate the cells magnetically bound to the column from the cells that should flowthrough.
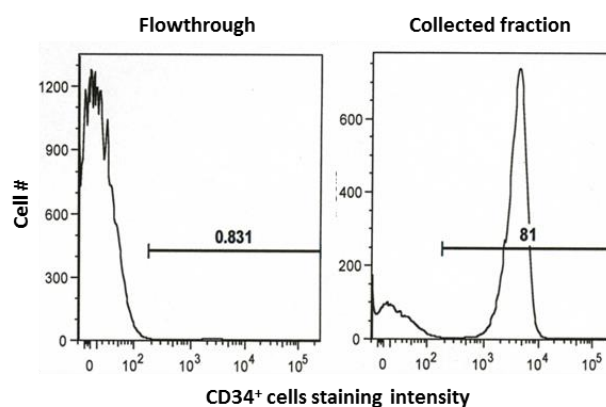
Figure 41: Flow cytometry analysis of the flowthrough and collected fractions from the magnetic assisted cell sorting of human umbilical cord blood using a labeled anti-CD34 antibody.

The library of bioactive compounds was chosen for the pilot screening of CD34$^+$ cells differentiation. After 5 days treatment with 1 µM compounds, cells were stained with a multiplex of seven directly conjugated antibodies directed at specific cell lineages, plus ethidium bromide for assessing cell viability, and analyzed by flow cytometry. The primary screen results indicated that from the 2448 compounds tested 2247 were inactive, 131 were toxic for the cells and 70 showed some activity. Analyzing cells treated with the primary hits

but without antibody staining revealed that 17 compounds are auto-fluorescent. The remaining compounds were then tested in duplicates, where 35 showed no activity and were consider as primary screen false positives. The activity of 18 compounds was confirmed (Fig. 43).
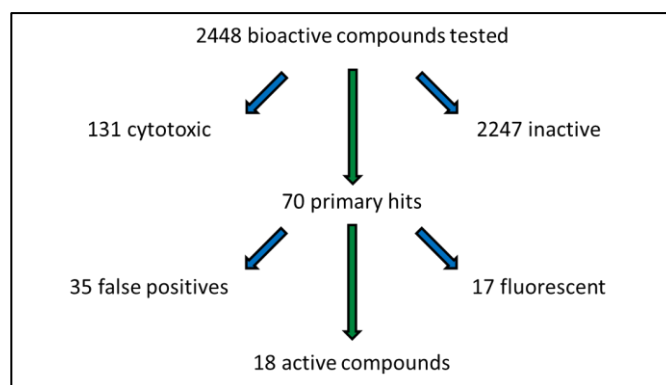
Figure 42: Flowchart representing the compounds flagging after primary screen and validation.

No active compound was found to direct differentiation of HSC specifically to the T cell lineage. To other specific lineages, 2 to 4 compounds were found to induce differentiation and 2 compounds promoted an increase in the number of progenitors. Compound CCG1811 induced an increase in the expression of markers for T and B cells, and it is probably inducing the differentiation of HSC to the lymphoid lineage. The same happens with compound CCG1357 towards the myeloid phenotype, because it elevates the number of all cells belonging to this lineage. The compounds activity classes were predominantly G-protein coupled receptors (GPCR) and ion channels modulators (Table 10).

A large variability was detected when working with human umbilical cord blood samples. The volume of the sample collected and the number of cells in the sample differ considerably, although the 1% of CD34$^+$ cells in the fraction collected after Ficoll gradient centrifugation remained almost constant. Also, the percentage of expression of the different lineage markers in control conditions varied substantially after 5 days in culture (not shown). Moreover, usually one cord blood sample is not enough to fill one 384-well plate which increases the complexity of the results.

Table 10: Small molecules active in the HSC differentiation screening

Compound ID	Progenitor	Lymphoid		Myeloid				Compound class
		T Cell	B Cell	Macrophages	Granulocytes	Platelets	Erythrocytes	
CCG2060	✓							GPCR
CCG1936	✓							GPCR
CCG286			✓					Nucleotide analog
CCG848			✓					GPCR
CCG2649			✓					Ion channel
CCG164				✓				GPCR
CCG983				✓				Antioxidant
CCG1741				✓				Ion channel
CCG1157					✓			Ion channel
CCG966					✓			Ion channel
CCG176						✓		Alkylating agent
CCG549						✓		GPCR
CCG1670						✓		GPCR
CCG1677						✓		GPCR
CCG1428							✓	Antiseptic
CCG2196							✓	Ion channel
CCG1811		✓	✓					GPCR
CCG1357				✓	✓	✓	✓	Ion channel

Another panel of directly conjugated antibodies for flow cytometry was built, with several markers for the same cell lineage, allowing the validation of the effect of the compounds with a single cell resolution, excluding artifacts of the unrelated single antibody staining. Activity of most of the compounds followed the pattern of variability in the assay. However, compound CCG1357 was repetitively able to induce the expression of the macrophage lineage CD41, CD42b and double-positive after 5 days treatment of CD34$^+$ cells (Fig. 44).
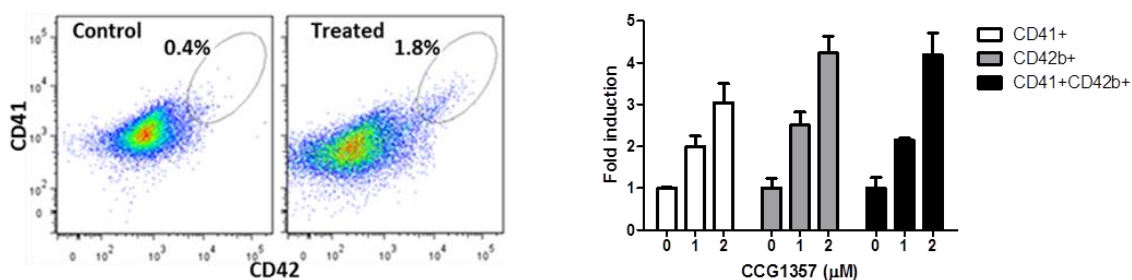

Figure 43: Flow cytometry analysis of CD34$^+$ cells incubated 5 days with compound CCG1357: Dot plot representation (left) and bar graph representation of fold induction (right).

In vitro and *in vivo* methods are being designed to validate the activity of the hit compounds, especially CCG1357. As for previous examples, the final goal would be to develop an automated assay suitable for HTS.

4.3- Pathways involved in cell death

The search for small molecules that selectively kill cancer cells or infectious unicellular organisms without harming the patient is an important area of research in drug discovery. A wide variety of assays for detecting and characterizing the type of death induced by a small molecule are available. These can range from low-throughput assays such as comet or DNA fragmentation assay, to HCS assays with fluorescent antibodies staining nuclear foci formation or changes in the cytoskeleton and to HTS using reporter or metabolic assays.

We have mainly used homogeneous assays for the discovery and characterization of small molecules inducing cell death: the fluorescent cell viability detection reagent CellTiter Blue (Promega) for HTS; the luminescent Caspase-Glo 3/7 Assay (Promega) and the fluorescent Cytotox-One (Promega) for subsequent determination of the cell death process. One example where this setup was applied concerned a new class of antibiotics: the lipophosphonoxins (Publication III and Publication V - Patent). These antibiotics displayed significant antibacterial properties against a panel of Gram-positive species, including multiresistant strains. There was then the need to determine the effect of these antibiotics on human cells. We used a human primary culture of erythroid progenitors and, although there was some toxicity detected, the concentration at which some of the antibiotics killed bacteria is considerable lower than the one killing the very sensitive progenitor cells (Fig. 45).
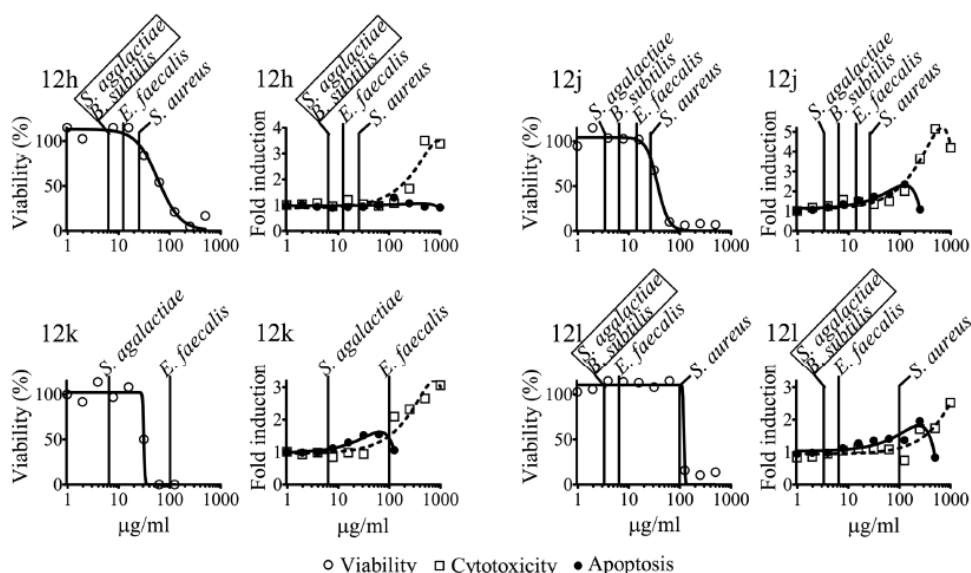

Figure 44: Cell viability, cytotoxicity, and apoptosis of erythroid progenitor cells after exposure to selected compounds. Vertical lines in the graphs represent the toxic concentration for the respective bacterial strains.

4.3.1- Small molecules sensitizers of cancer cells to TRAIL-induced apoptosis

TNF-related apoptosis-inducing ligand (TRAIL) is a protein ligand that induces apoptosis specifically in cancer cells. However, tumor cells rapidly acquire resistance and compounds that re-sensitize these cells to TRAIL could be useful for cancer therapy. The HTS procedure to discover such compounds was carried using the fluorescent CellTiter Blue assay for detection of cell viability followed by a counter-screen for detection of caspase activation using the luminescent Caspase-Glo 3/7 Assay. HT29, a colorectal cancer cell line and resistant to TRAIL-induced apoptosis was chosen for the assay. The screen was then performed in the presence and in the absence of TRAIL making it possible to distinguish between the killing effects of the compounds unrelated to TRAIL sensitization. Data analysis was performed by dividing the viability of cells in wells treated with compounds and TRAIL by the viability of cells in wells treated with compounds alone and the hit threshold was set at 0.5.

Among the positive hits (compounds able to sensitize cancer cells to TRAIL-induced apoptosis) were previously identified sensitizers such as camptothecin and thapsigargin (Fig. 46). Other validated hits were emetine and its analog cephaeline, the inhibitor of protein synthesis anisomycin, the alcohol dehydrogenase inhibitor disulfiram and homoharringtonine (HHT).
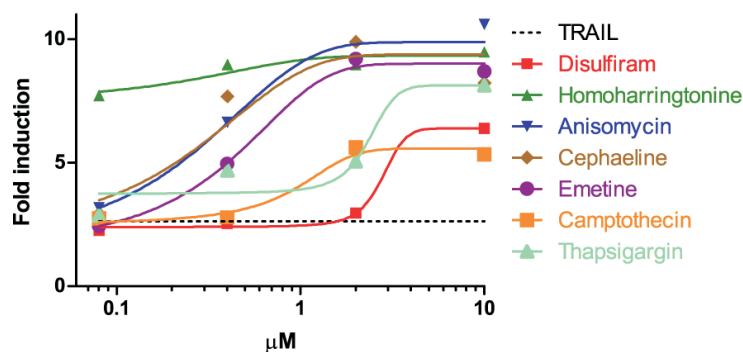

Figure 45: Caspase 3/7 activation of validated screening hits in combination with TRAIL (1 µg/ml) in HT29 cells.

From the validated hits, HHT was found to be the most potent TRAIL sensitizer with an IC$_{50}$ of 15 nM (Table 11), only followed by the 20 fold less potent anysomycin and cephaeline, which have similar maximum induction of 9 to 10 fold.

Table 11: Caspase 3/7 activation of validated screening hits in combination with TRAIL (1 μg/ml) in HT29 cells.

Compound	Max. fold induction	EC$_{50}$ (μM)
Disulfiram	6.387	3.0
Homoharringtonine	9.325	0.015
Anisomycin	9.875	0.3
Cephaeline	9.378	0.3
Emetine	9.003	0.5
Camptothecine	5.571	0.9
Thapsigargin	8.121	2.4

HHT is an alkaloid originally isolated from Cephalotaxus harringtonia (Fig. 47). Recently, its semisynthetic variant Omacetaxine mepesuccinate (marketed under the name Synribo) has been considered as an alternative therapeutic option in the treatment of imatinib-resistant chronic myeloid leukemias[241].
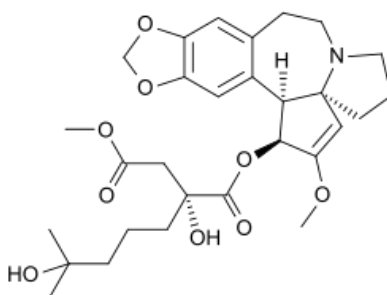

Figure 46: Chemical structure of homoharringtonine.

The combined effect of HHT and TRAIL was found not to be restricted to HT29 cells. Other colorectal carcinoma cell lines, ranging from completely resistant (COLO320) to partially sensitive (RKO, SW480 and LS147T) to TRAIL-induced apoptosis had much higher caspase activation when co-treated with HHT and TRAIL (Fig. 48). From the tested cell lines, HCT116 cells showed to be the most sensitive to TRAIL and this may be the reason why an increase in caspase activation was not seen in the combined treatment.
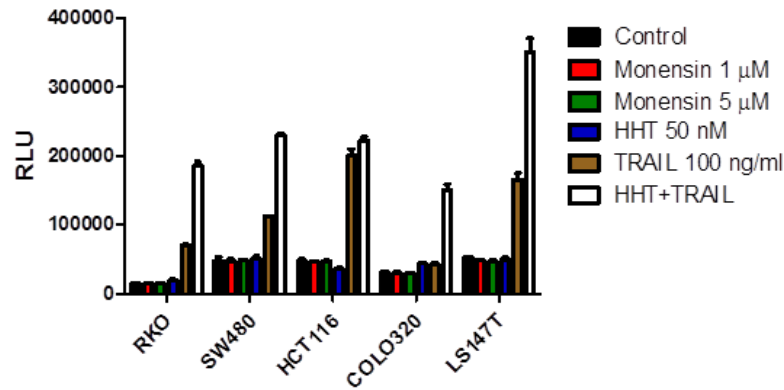
Figure 47: Effect of TRAIL, HHT and their combination in the caspase activation of different colorectal cancer cell lines.

It was also shown that HHT, in combination with TRAIL, effectively inhibits the growth of tumors implanted into immunodeficient mice (Fig. 49), without any apparent toxicity in mice.
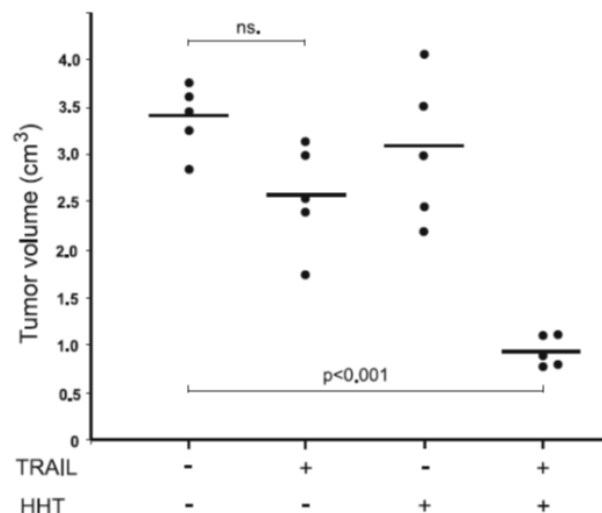

Figure 48: Effect of the combination of HHT and TRAIL on the growth of tumors implanted into immunodeficient mice.

At present, the molecular target of HHT responsible for the sensitization of colorectal cancer cells to TRAIL-induced apoptosis has not been identified. However, it was shown that HHT caused a drop in the cellular levels of the anti-apoptotic proteins Mcl-1 and cFLIP, two important regulators of TRAIL-induced apoptosis. A more detailed description of HHT and TRAIL combined actions can be found in Publication IV.

4.3.2- Small molecules with leishmanicidal properties

Leishmania major promastigotes are usually isolated from infected mice and stored frozen. By simply counting the number of parasites it was determined that *Leishmania* started losing their proliferation potential in the fourth week after thawing. Therefore, *Leishmania* were used for the screening in the second and third week after thawing. The first step of HTS assay development was to find the optimal parasite density for performing the CellTiter Blue viability assay in 384-well plates (Fig. 50).
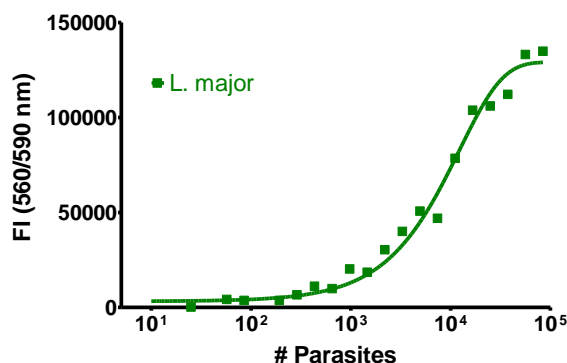

Figure 49: Determination of the optimal number of *Leishmania* per well of a 384-well plate for detection of parasite viability using the CellTiter Blue assay.

The HTS procedure was then performed with 15000 parasites per well, incubated with compounds for 48 hours and viability was measured using the CellTiter Blue assay. The library of bioactive compounds was screened and 20 compounds were identified as primary hits. From these, 12 were active when the assay was repeated in a dose-response experiment for their ability to kill *Leishmania* promastigotes (Fig. 51).
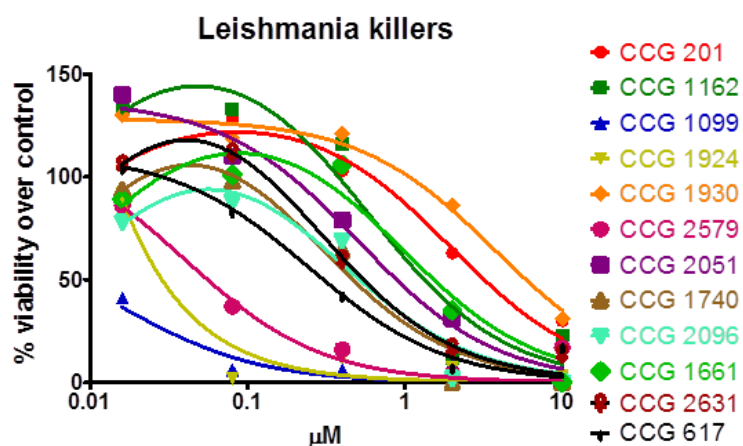
Figure 50: Validation of leishmanicidal screen primary hits in dose-response using the CellTiter Blue assay.

The next goal was to determine which of the 12 confirmed hits would be able to kill intracellular *Leishmania* (amastigotes). Mouse intraperitoneal macrophages were purified and co-cultured with *Leishmania* promastigotes stably expressing GFP in 96-well plates. The promastigotes infected the macrophages and metamorphosed to amastigotes. 24 hours later, the cells were washed, removing the free promastigotes. Then, compounds were added for 48 hours and the samples were visualized under a fluorescent microscope (Fig. 52) and analyzed by flow cytometry. The novel activity of two compounds was identified. From the images, it is visible that in control conditions approximately half of the macrophages are infected with *Leishmania* and that the treatment with the compounds did not apparently affect the phenotype of the macrophages. Although it would be difficult to assess the effect of calcimycin (compound CCG 2631) by visual inspection, the effect of diphenyleneiodonium chloride (DPI, compound CCG 2579) is clear as no fluorescent *Leishmania* can be seen in the image.
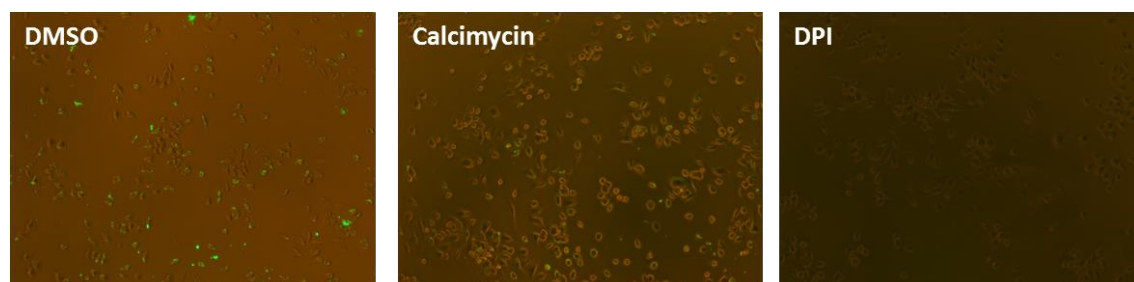

Figure 51: Merge of brightfield and fluorescent microscopy photos showing macrophages and GFP-*Leishmania* respectively, 48 hours after treatment with compounds (1 μM).

Flow cytometry analysis of macrophages infected with the GFP-*Leishmania*, after 48 hours incubation with DMSO, showed that 40.5% of the macrophages were infected (Fig. 53). Treatment with calcimycin or DPI drastically reduced the GFP-positive population without altering the number of macrophages. The flow cytometry dose-response analysis showed that both compounds are able to efficiently kill intracellular *Leishmania* (amastigotes) with DPI being effective at very low concentrations, in the range of nanomolar (IC$_{50} \approx 40$ nM), tenfold lower than calcimycin.

Efforts were therefore concentrated on these two compounds. The cytotoxicity of these compounds in normal cells was tested on primary human fibroblasts, the CCD 841 cells (Fig. 54). Calcimycin showed toxicity towards CCD 841 cells starting at 1 μM, concentration high enough to kill most of *Leishmania*. This indicates that there is probably some window of concentrations that can be used to kill the parasites but care must be taken due the possible

damage to normal cells. DPI, more potent at killing *Leishmania* is also less toxic to normal cells.
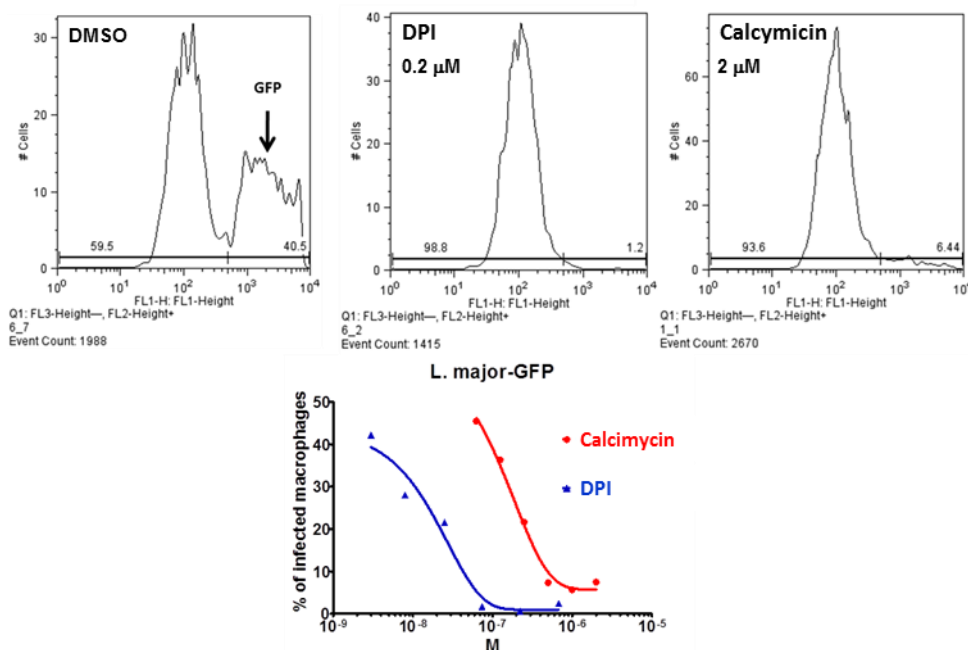
Figure 52: Flow cytometry graphs of macrophages infected with GFP-*Leishmania* 48 hours after compound treatment (top) and respective dose-response analysis (bottom).
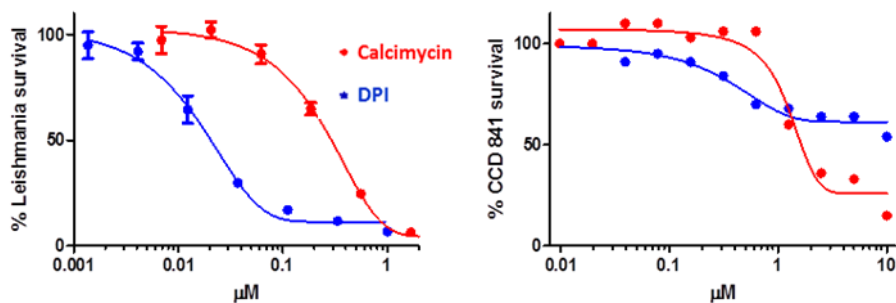

Figure 53: Dose-response analysis of the viability of *Leishmania* promastigotes and human primary fibroblasts CCD 841 after 48 hours incubation with compounds using the CellTiter Blue assay.

The next goal was to find the mechanism of action of DPI and calcimycin. Both of them were present in the library of bioactive compounds, therefore some information was available that helped in the design of the following experiments.

The toxicity of calcimycin was greatly reduced when *Leishmania* promastigotes were co-treated with ARL 17477, a selective nitric oxide synthase inhibitor, (Fig. 55). It remains to be tested if calcimycin induces the activity of nitric oxide synthase and if this is the cause of its toxicity in *Leishmania*.
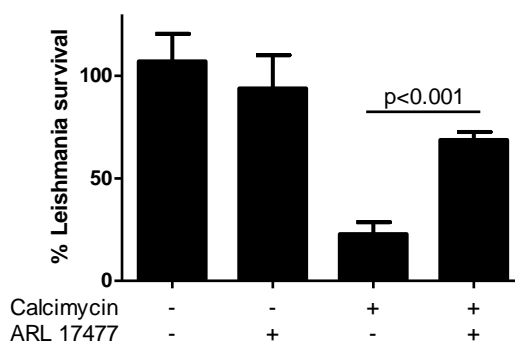
Figure 54: Effect of 48 hours ARL 17477 (50 μM) co-incubation with calcimycin (0.5 μM) on the *Leishmania* promastigotes viability using the CellTiter Blue assay.

For DPI, co-treatment of *Leishmania* promastigotes with bromosulfophthalein (BSP) practically abolishes its killing effect (Fig. 56). BSP is known to prevent glutathione efflux, so DPI may induce *Leishmania* glutathione depletion leading to cell cycle arrest, a hypothesis to be tested in the near future.
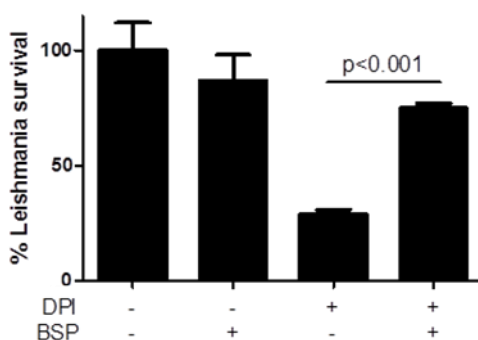
Figure 55: Effect of 48 hours BSP (0.6 M) co-incubation with DPI (50 nM) on the *Leishmania* promastigotes viability using the CellTiter Blue assay.

In order to prove the utility of these compounds for the treatment of leishmaniasis, testing in animal models is essential. *In vivo* experiments are underway. For that, *Leishmania* promastigotes were inoculated into mice rump. This caused the formation of a skin lesion representative of cutaneous leishmaniasis. In the same mice, *Leishmania* then migrate and infect internal organs as in human visceral leishmaniasis. We are trying to alleviate the infection by daily intraperitoneal injection of our selected compounds DPI and calcimycin, and hope that in the future they might be useful to ameliorate the life conditions of people living in risk areas.

5- Conclusions

Small chemical compounds that change the way cells behave are commonly used in academic laboratories as tools to help dissecting the molecular mechanisms and signaling pathways responsible for such phenotypic changes. Some of them were developed as drugs to treat a wide spectrum of diseases.

Several approaches can be used for the discovery of active small molecules. For this thesis, high-throughput screening (HTS) was applied to test libraries comprising of thousands of compounds, in the attempt to find some with novel and interesting activities. Assays were developed aiming at the discovery of compounds modulating the three stages of the cell life cycle: self-renewal, differentiation and cell death.

Maintenance of cell self-renewal is regulated by different signaling pathways, such as Wnt and Hypoxia. Homogeneous, luminescent-based HTS reporter assays led to the identification of monensin as an inhibitor of the Wnt pathway and of two compounds activators of the hypoxia pathway. Monensin inhibits the Wnt pathway both *in vitro* and *in vivo* and showed some promise that it might be used as an anticancer drug. While trying to find molecular target for monensin, a variety of secondary assays were developed and a pipeline suitable to the study of small molecules modulating the Wnt pathway has been established. Similarly, a pipeline is being developed for the Hypoxia pathway based on the two agonists found. So far, these agonists seem to stabilize HIF-1α through inhibition of prolyl-hydroxylase activity, preventing the access of the enzyme to iron. After full *in vitro* characterization of the compounds activity, in vivo assays could provide the necessary information about the specificity and toxicity of the compounds to organisms. A mouse model of diabetes is now being used to test the ability of the hypoxia pathway activators to accelerate wound healing, a process dependent on HIF-1α and its target VEGF that are inhibited in diabetes. In the near future, we would like to extend our screenings to other pathways involved in cell self-renewal, e.g. the Hedgehog pathway.

The study of small molecules influencing cellular differentiation is more complex than the reporter-based assays and the data acquisition requires special instruments such as an automated fluorescent microscope or flow cytometer. These instruments provide multiparametric readouts and screenings using them are termed high-content screenings. Primary ex vivo cells would be the most reliable source for differentiation studies. These cells are often difficult to obtain and the differentiation requires a multi-step procedure, cells pass through different maturation stages and terminally differentiate into the functional cell types.

Therefore, assay development for the neural and mesenchymal differentiation screens are still ongoing. The hematopoietic stem cell differentiation screen is more advanced and hit validation from a pilot screen is underway. To date, one compound was shown to be able to direct the differentiation towards the platelet phenotype, inducing the expression of both CD41 and CD42 and secondary assays are being designed to evaluate its mechanism of action.

Finally, for the discovery of compounds inducing death in a cell-type-specific manner, two viability homogeneous screens were performed and, for each of them, one compound was found with activities in the nanomolar range of concentrations. From the first screen, Homoharringtonine was found to efficiently sensitize resistant cancer cells to their TRAIL-mediated elimination both *in vitro* and in vivo while, within the therapeutic window, not being harmful to normal cells or the organism. From the second screen, DPI was identified as a potent killer of *Leishmania* both in their extracellular life stage (promastigotes) and in their intracellular stage (amastigotes) without harming the macrophage hosts. A mouse model of infection is now being tested for the ability of DPI to kill *Leishmania* in vivo. To extend our studies about compounds involved in pathways controlling cell death, assay development for both high-throughput and high-content screens of compounds influencing the DNA repair machinery are now underway.

6- References

1   Oron E & Ivanova N. Cell fate regulation in early mammalian development. *Phys Biol* **epub** (2012).

2   Takahashi K & Yamanaka S. Induction of pluripotent stem cells from mouse embryonic and adult fibroblast cultures by defined factors. *Cell* **126**, 663-676 (2006).

3   Suvà ML, Riggi N & Bernstein BE. Epigenetic reprogramming in cancer. *Science* **29**, 1567-1570 (2013).

4   Saunders JW Jr. Death in embryonic systems. *Science* **154**, 604-612 (1966).

5   Tau GZ1 & Peterson BS. Normal development of brain circuits. *Neuropsychopharmacology* **35**, 147-168 (2010).

6   Sokol SY. Maintaining embryonic stem cell pluripotency with Wnt signaling. *Development* **138**, 4341-4350 (2011).

7   Liu J, Sato C, Cerletti M & Wagers A. Notch signaling in the regulation of stem cell self-renewal and differentiation. *Curr Top Dev Biol* **92**, 367-409 (2010).

8   Stanton BZ & Peng LF. Small-molecule modulators of the Sonic Hedgehog signaling pathway. *Mol Biosyst* **6**, 44-54 (2010).

9   Sakaki-Yumoto M, Katsuno Y & Derynck R. TGF-β family signaling in stem cells. *Biochim Biophys Acta* **1830**, 2280-2296 (2013).

10   Gotoh N. Control of stemness by fibroblast growth factor signaling in stem cells and cancer stem cells. *Curr Stem Cell Res Ther* **4**, 9-15 (2009).

11   Mazumdar J, Dondeti V & Simon MC. Hypoxia-inducible factors in stem cells and cancer. *J Cell Mol Med* **13**, 4319-4328 (2009).

12   Gokhale PJ & Andrews PW. The development of pluripotent stem cells. *Curr Opin Genet Dev* **22**, 403-408 (2012).

13   Kusserow A, Pang K, Sturm C, Hrouda M, Lentfer J, Schmidt HA *et al.* Unexpected complexity of the Wnt gene family in a sea anemone. *Nature* **433**, 156-160 (2005).

14   Nüsslein-Volhard C & Wieschaus E. Mutations affecting segment number and polarity in Drosophila. *Nature* **287**, 795-801 (1980).

15   McMahon AP & Moon RT. Ectopic expression of the proto-oncogene int-1 in Xenopus embryos leads to duplication of the embryonic axis. *Cell* **58**, 1075-1084 (1989).

16   Janda CY, Waghray D, Levin AM, Thomas C & Garcia KC. Structural basis of Wnt recognition by Frizzled. *Science* **337**, 59-64 (2012).

17   Tamai K, Semenov M, Kato Y, Spokony R, Liu C, Katsuyama Y *et al.* LDL-receptor-related proteins in Wnt signal transduction. *Nature* **407**, 530-535 (2000).

18   Zeng X, Tamai K, Doble B, Li S, Huang H, Habas R *et al.* A dual-kinase mechanism for Wnt co-receptor phosphorylation and activation. *Nature* **438** (2005).

19   Červenka I, Wolf J, Mašek J, Krejci P, Wilcox WR, Kozubík A *et al.* Mitogen-activated protein kinases promote WNT/beta-catenin signaling via phosphorylation of LRP6. *Mol Cell Biol* **31**, 179-189 (2011).

20   Mao J, Wang J, Liu B, Pan W, Farr GH 3rd, Flynn C *et al.* Low-density lipoprotein receptor-related protein-5 binds to Axin and regulates the canonical Wnt signaling pathway. *Mol Cell* **7**, 801-809 (2001).

21   Chen W, ten Berge D, Brown J, Ahn S, Hu LA, Miller WE *et al.* Dishevelled 2 recruits beta-arrestin 2 to mediate Wnt5A-stimulated endocytosis of Frizzled 4. *Science* **301**, 1391-1394 (2003).

22   Rubinfeld B, Souza B, Albert I, Müller O, Chamberlain SH, Masiarz FR *et al.* Association of the APC gene product with beta-catenin. *Science* **262**, 1731-1734 (1993).

23   Liu C, Li Y, Semenov M, Han C, Baeg GH, Tan Y *et al.* Control of beta-catenin phosphorylation/degradation by a dual-kinase mechanism. *Cell* **108**, 837-847 (2002).

24   Aberle H, Bauer A, Stappert J, Kispert A & Kemler R. beta-catenin is a target for the ubiquitin-proteasome pathway. *EMBO J* **16**, 3797-3804 (1997).

25   MacDonald BT, Tamai K & He X. Wnt/beta-catenin signaling: components, mechanisms, and diseases. *Dev Cell* **17**, 9-26 (2009).

26   Li VS, Ng SS, Boersema PJ, Low TY, Karthaus WR, Gerlach JP *et al.* Wnt signaling through inhibition of β-catenin degradation in an intact Axin1 complex. *Cell* **149**, 1245-1256 (2012).

27   Clevers H & Nusse R. Wnt/β-catenin signaling and disease. *Cell* **149**, 1192-1205 (2012).

28   Sugioka K, Mizumoto K & Sawa H. Wnt regulates spindle asymmetry to generate asymmetric nuclear β-catenin in C. elegans. *Cell* **146**, 942-954 (2011).

29   Cavallo RA, Cox RT, Moline MM, Roose J, Polevoy GA, Clevers H *et al.* Drosophila Tcf and Groucho interact to repress Wingless signalling activity. *Nature* **395**, 604-608 (1998).

30   Roose J, Molenaar M, Peterson J, Hurenkamp J, Brantjes H, Moerer P *et al.* The Xenopus Wnt effector XTcf-3 interacts with Groucho-related transcriptional repressors. *Nature* **395**, 608-612 (1998).

31   Mosimann C, Hausmann G & Basler K. Beta-catenin hits chromatin: regulation of Wnt target gene activation. *Nat Rev Mol Cell Biol* **10**, 276-286 (2009).

32   *The Wnt Homepage*, http://www.stanford.edu/group/nusselab/cgi-bin/wnt/.

33   Huber AH, Nelson WJ & Weis WI. Three-dimensional structure of the armadillo repeat region of beta-catenin. *Cell* **90**, 871-882 (1997).

34   Xing Y, Takemaru K, Liu J, Berndt JD, Zheng JJ, Moon RT *et al.* Crystal structure of a full-length beta-catenin. *Structure* **16**, 478-487 (2008).

35   Orsulic S, P. M. An in vivo structure-function study of armadillo, the beta-catenin homologue, reveals both separate and overlapping regions of the protein required for cell adhesion and for wingless signaling. *J Cell Biol* **124**, 1283-1300 (1996).

36   Vleminckx K, Kemler R & Hecht A. The C-terminal transactivation domain of beta-catenin is necessary and sufficient for signaling by the LEF-1/beta-catenin complex in Xenopus laevis. *Mech Dev* **81**, 65-74 (1999).

37   Korinek V, Barker N, Moerer P, van Donselaar E, Huls G, Peters PJ *et al.* Depletion of epithelial stem-cell compartments in the small intestine of mice lacking Tcf-4. *Nat Genet* **19**, 379-383 (1998).

38   Zeng YA & Nusse R. Wnt proteins are self-renewal factors for mammary stem cells and promote their long-term expansion in culture. *Cell Stem Cell* **6**, 568-577 (2010).

39   Miyoshi Y, Nagase H, Ando H, Horii A, Ichii S, Nakatsuru S *et al.* Somatic mutations of the APC gene in colorectal tumors: mutation cluster region in the APC gene. *Hum Mol Genet* **1**, 229-233 (1992).

40   Malanchi I, Peinado H, Kassen D, Hussenet T, Metzger D, Chambon P *et al.* Cutaneous cancer stem cell maintenance is dependent on beta-catenin signalling. *Nature* **452**, 650-653 (2008).

41   Jamieson CH, Ailles LE, Dylla SJ, Muijtjens M, Jones C, Zehnder JL *et al.* Granulocyte-macrophage progenitors as candidate leukemic stem cells in blast-crisis CML. *N Engl J Med* **351**, 657-667 (2004).

42   Huelsken J & Birchmeier W. New aspects of Wnt signaling pathways in higher vertebrates. *Curr Opin Genet Dev* **11**, 547-553 (2001).

43   Strutt DI, Weber U & Mlodzik M. The role of RhoA in tissue polarity and Frizzled signalling. *Nature* **387**, 292-295 (1997).

44   Heisenberg CP, Tada M, Rauch GJ, Saúde L, Concha ML, Geisler R *et al.* Silberblick/Wnt11 mediates convergent extension movements during zebrafish gastrulation. *Nature* **405**, 76-81 (2000).

45   Dabdoub A, Donohue MJ, Brennan A, Wolf V, Montcouquiol M, Sassoon DA *et al.* Wnt signaling mediates reorientation of outer hair cell stereociliary bundles in the mammalian cochlea. *Development* **130**, 2375-2384 (2003).

46   Ciani L & Salinas PC. WNTs in the vertebrate nervous system: from patterning to neuronal connectivity. *Nat Rev Neurosci* **6**, 351-362 (2005).

47   Saneyoshi T, Kume S, Amasaki Y & Mikoshiba K. The Wnt/calcium pathway activates NF-AT and promotes ventral cell fate in Xenopus embryos. *Nature* **417**, 295-299 (2002).

48   Veeman MT, Slusarski DC, Kaykas A, Louie SH & Moon RT. Zebrafish prickle, a modulator of noncanonical Wnt/Fz signaling, regulates gastrulation movements. *Curr Biol* **13**, 680-685 (2003).

49   Sheldahl LC, Slusarski DC, Pandur P, Miller JR, Kühl M & Moon RT. Dishevelled activates Ca2+ flux, PKC, and CamKII in vertebrate embryos. *J Cell Biol* **161**, 769-777 (2003).

50   Kühl M, Sheldahl LC, Park M, Miller JR & Moon RT. The Wnt/Ca2+ pathway: a new vertebrate Wnt signaling pathway takes shape. *Trends Genet* **16**, 279-283 (2000).

51   Avila ME, Sepúlveda FJ, Burgos CF, Moraga-Cid G, Parodi J, Moon RT *et al.* Canonical Wnt3a modulates intracellular calcium and enhances excitatory neurotransmission in hippocampal neurons. *J Biol Chem* **285**, 18939-18947 (2010).

52   Huang T, Xie Z, Wang J, Li M, Jing N & Li L. Nuclear factor of activated T cells (NFAT) proteins repress canonical Wnt signaling via its interaction with Dishevelled (Dvl) protein and participate in regulating neural progenitor cell proliferation and differentiation. *J Biol Chem* **286**, 37399-37405 (2011).

53   Lu D & Carson DA. Spiperone enhances intracellular calcium level and inhibits the Wnt signaling pathway. *BMC Pharmacol* **9** (2009).

54   Chen B, Dodge ME, Tang W, Lu J, Ma Z, Fan CW *et al.* Small molecule-mediated disruption of Wnt-dependent signaling in tissue regeneration and cancer. *Nat Chem Biol* **5**, 100-107 (2009).

55   Chen M, Wang J, Lu J, Bond MC, Ren XR, Lyerly HK *et al.* The anti-helminthic niclosamide inhibits Wnt/Frizzled1 signaling. *Biochemistry* **48**, 10267-10274 (2009).

56   Shan J, Shi DL, Wang J & Zheng J. Identification of a specific inhibitor of the dishevelled PDZ domain. *Biochemistry* **44**, 15495-15503 (2005).

57   Thorne CA, Hanson AJ, Schneider J, Tahinci E, Orton D, Cselenyi CS *et al.* Small-molecule inhibition of Wnt signaling through activation of casein kinase 1α. *Nat Chem Biol* **6**, 829-836 (2010).

58   Huang SM, Mishina YM, Liu S, Cheung A, Stegmeier F, Michaud GA *et al.* Tankyrase inhibition stabilizes axin and antagonizes Wnt signalling. *Nature* **461**, 614-620 (2009).

59   Waaler J, Machon O, Tumova L, Dinh H, Korinek V, Wilson SR *et al.* A novel tankyrase inhibitor decreases canonical Wnt signaling in colon carcinoma cells and reduces tumor growth in conditional APC mutant mice. *Cancer Res.* **72**, 2822-2832 (2012).

60   James RG, Davidson KC, Bosch KA, Biechele TL, Robin NC, Taylor RJ *et al.* WIKI4, a Novel Inhibitor of Tankyrase and Wnt/ß-Catenin Signaling. *PLoS One* **7**, epub (2012).

61   Chen Z, Venkatesan AM, Dehnhardt CM, Dos Santos O, Delos Santos E, Ayral-Kaloustian S *et al.* 2,4-Diamino-quinazolines as inhibitors of beta-catenin/Tcf-4 pathway: Potential treatment for colorectal cancer. *Bioorg Med Chem Lett* **19**, 4980-4983 (2009).

62   Lepourcelet M, Chen YN, France DS, Wang H, Crews P, Petersen F *et al.* Small-molecule antagonists of the oncogenic Tcf/beta-catenin protein complex. *Cancer Cell* **5**, 91-102 (2004).

63   Park CH, Chang JY, Hahm ER, Park S, Kim HK & Yang CH. Quercetin, a potent inhibitor against beta-catenin/Tcf signaling in SW480 colon cancer cells. *Biochem Biophys Res Commun* **328**, 227-234 (2005).

64   Yao H, Ashihara E, Strovel JW, Nakagawa Y, Kuroda J, Nagao R *et al.* AV-65, a novel Wnt/β-catenin signal inhibitor, successfully suppresses progression of multiple myeloma in a mouse model. *Blood Cancer J* **1**, epub (2011).

65   Dihlmann S, Siermann A & von Knebel Doeberitz M. The nonsteroidal anti-inflammatory drugs aspirin and indomethacin attenuate beta-catenin/TCF-4 signaling. *Oncogene* **20**, 645-653 (2001).

66   Handeli S & Simon JA. A small-molecule inhibitor of Tcf/beta-catenin signaling down-regulates PPARgamma and PPARdelta activities. *Mol Cancer Ther* **7**, 521-529 (2008).

67   Emami KH, Nguyen C, Ma H, Kim DH, Jeong KW, Eguchi M *et al.* A small molecule inhibitor of beta-catenin/CREB-binding protein transcription [corrected]. *Proc Natl Acad Sci U S A* **101**, 12682-12687 (2004).

68   Lu D, Choi MY, Yu J, Castro JE, Kipps TJ & Carson DA. Salinomycin inhibits Wnt signaling and selectively induces apoptosis in chronic lymphocytic leukemia cells. *Proc Natl Acad Sci U S A* **108**, 13253-13257 (2011).

69   Lu W, Lin C, King TD, Chen H, Reynolds RC & Li Y. Silibinin inhibits Wnt/β-catenin signaling by suppressing Wnt co-receptor LRP6 expression in human prostate and breast cancer cells. *Cell Signal.* **24**, 2291-2296 (2012).

70   Waki H, Park KW, Mitro N, Pei L, Damoiseaux R, Wilpitz DC *et al.* The small molecule harmine is an antidiabetic cell-type-specific regulator of PPARgamma expression. *Cell Metab* **5**, 357-370 (2007).

71   Rey JP & Ellies DL. Wnt modulators in the biotech pipeline. *Dev Dyn* **239**, 102-114 (2010).

72   Wenger RH, Stiehl DP & Camenisch G. Integration of oxygen signaling at the consensus HRE. *Sci STKE* **306** (2005).

73   Greer SN, Metcalf JL, Wang Y & Ohh M. The updated biology of hypoxia-inducible factor. *EMBO J* **31**, 2448-2460 (2012).

74   Goda N & Kanai M. Hypoxia-inducible factors and their roles in energy metabolism. *Int J Hematol.* **95**, 457-463 (2012).

75   Krock BL, Skuli N & Simon MC. Hypoxia-induced angiogenesis: good and evil. *Genes Cancer* **2**, 1117-1133 (2011).

76   Epstein AC, Gleadle JM, McNeill LA, Hewitson KS, O'Rourke J, Mole DR *et al.* C. elegans EGL-9 and mammalian homologs define a family of dioxygenases that regulate HIF by prolyl hydroxylation. *Cell* **107**, 43-54 (2001).

77   Schofield CJ & Ratcliffe PJ. Oxygen sensing by HIF hydroxylases. *Nat Rev Mol Cell Biol* **5**, 343-354 (2004).

78   Kaelin WG Jr & Ratcliffe PJ. Oxygen sensing by metazoans: the central role of the HIF hydroxylase pathway. *Mol Cell* **30**, 393-402 (2008).

79   Finley LW, Carracedo A, Lee J, Souza A, Egia A, Zhang J *et al.* SIRT3 opposes reprogramming of cancer cell metabolism through HIF1α destabilization. *Cancer Cell* **19**, 416-428 (2011).

80   Maxwell PH, Wiesener MS, Chang GW, Clifford SC, Vaux EC, Cockman ME *et al.* The tumour suppressor protein VHL targets hypoxia-inducible factors for oxygen-dependent proteolysis. *Nature* **399**, 271-275 (1999).

81   Lando D, Peet DJ, Whelan DA, Gorman JJ & Whitelaw ML. Asparagine hydroxylation of the HIF transactivation domain a hypoxic switch. *Science* **295**, 858-861 (2002).

82   Hudson CC, Liu M, Chiang GG, Otterness DM, Loomis DC, Kaper F *et al.* Regulation of hypoxia-inducible factor 1alpha expression and function by the mammalian target of rapamycin. *Mol Cell Biol* **22**, 7004-7014 (2002).

83   Dang EV, Barbi J, Yang HY, Jinasena D, Yu H, Zheng Y *et al.* Control of T(H)17/T(reg) balance by hypoxia-inducible factor 1. *Cell* **146**, 772-784 (2011).

84   Zhong L, D'Urso A, Toiber D, Sebastian C, Henry RE, Vadysirisack DD *et al.* The histone deacetylase Sirt6 regulates glucose homeostasis via Hif1alpha. *Cell* **140**, 280-293 (2010).

85   Wang GL, Jiang BH, Rue EA & Semenza GL. Hypoxia-inducible factor 1 is a basic-helix-loop-helix-PAS heterodimer regulated by cellular O2 tension. *Proc Natl Acad Sci U S A* **92**, 5510-5514 (1995).

86   Ebert BL & Bunn HF. Regulation of transcription by hypoxia requires a multiprotein complex that includes hypoxia-inducible factor 1, an adjacent transcription factor, and p300/CREB binding protein. *Mol Cell Biol* **18**, 4089-4096 (1998).

87   Luo W, Hu H, Chang R, Zhong J, Knabel M, O'Meally R *et al.* Pyruvate kinase M2 is a PHD3-stimulated coactivator for hypoxia-inducible factor 1. *Cell* **145**, 732-744 (2011).

88   Liu Y, Cox SR, Morita T & Kourembanas S. Hypoxia regulates vascular endothelial growth factor gene expression in endothelial cells. Identification of a 5' enhancer. *Circ Res* **77**, 638-643 (1995).

89   Compernolle V, Brusselmans K, Acker T, Hoet P, Tjwa M, Beck H *et al.* Loss of HIF-2alpha and inhibition of VEGF impair fetal lung maturation, whereas treatment with VEGF prevents fatal respiratory distress in premature mice. *Nat Med* **8**, 702-710 (2002).

90   Jiang BH, Jiang G, Zheng JZ, Lu Z, Hunter T & Vogt PK. Phosphatidylinositol 3-kinase signaling controls levels of hypoxia-inducible factor 1. *Cell Growth Differ* **12**, 363-369 (2001).

91   Del Bufalo D, Ciuffreda L, Trisciuoglio D, Desideri M, Cognetti F, Zupi G *et al.* Antiangiogenic potential of the Mammalian target of rapamycin inhibitor temsirolimus. *Cancer Res.* **66**, 5549-5554 (2006).

92   Rapisarda A, Uranchimeg B, Sordet O, Pommier Y, Shoemaker RH & Melillo G. Topoisomerase I-mediated inhibition of hypoxia-inducible factor 1: mechanism and therapeutic implications. *Cancer Res.* **64**, 1475-1482 (2004).

93   Mabjeesh NJ, Escuin D, LaVallee TM, Pribluda VS, Swartz GM, Johnson MS *et al.* 2ME2 inhibits tumor growth and angiogenesis by disrupting microtubules and dysregulating HIF. *Cancer Cell* **3**, 363-375 (2003).

94   Mabjeesh NJ, Post DE, Willard MT, Kaur B, Van Meir EG, Simons JW *et al.* Geldanamycin induces degradation of hypoxia-inducible factor 1alpha protein via the proteosome pathway in prostate cancer cells. *Cancer Res.* **62**, 2478-2482 (2002).

95   Hur E, Kim HH, Choi SM, Kim JH, Yim S, Kwon HJ *et al.* Reduction of hypoxia-induced transcription through the repression of hypoxia-inducible factor-1alpha/aryl hydrocarbon receptor nuclear translocator DNA binding by the 90-kDa heat-shock protein inhibitor radicicol. *Mol Pharmacol* **62**, 975-982 (2002).

96   Han JY, Oh SH, Morgillo F, Myers JN, Kim E, Hong WK *et al.* Hypoxia-inducible factor 1alpha and antiangiogenic activity of farnesyltransferase inhibitor SCH66336 in human aerodigestive tract cancer. *J Natl Cancer Inst* **97**, 1272-1286 (2005).

97   Osada M, Imaoka S & Funae Y. Apigenin suppresses the expression of VEGF, an important factor for angiogenesis, in endothelial cells via degradation of HIF-1alpha protein. *FEBS Lett* **575**, 59-63 (2004).

98   Qian DZ, Kachhap SK, Collis SJ, Verheul HM, Carducci MA, Atadja P *et al.* Class II histone deacetylases are associated with VHL-independent regulation of hypoxia-inducible factor 1 alpha. *Cancer Res.* **66**, 8814-8821 (2006).

99   Mie Lee Y, Kim SH, Kim HS, Jin Son M, Nakajima H, Jeong Kwon H *et al.* Inhibition of hypoxia-induced angiogenesis by FK228, a specific histone deacetylase inhibitor, via suppression of HIF-1alpha activity. *Biochem Biophys Res Commun* **300**, 241-246 (2003).

100   Kong X, Lin Z, Liang D, Fath D, Sang N & Caro J. Histone deacetylase inhibitors induce VHL and ubiquitin-independent proteasomal degradation of hypoxia-inducible factor 1alpha. *Mol Cell Biol* **26**, 2019-2028 (2006).

101   Chun YS, Yeo EJ, Choi E, Teng CM, Bae JM, Kim MS *et al.* Inhibitory effect of YC-1 on the hypoxic induction of erythropoietin and vascular endothelial growth factor in Hep3B cells. *Biochem Pharmacol* **61**, 947-954 (2001).

102   Welsh S, Williams R, Kirkpatrick L, Paine-Murrieta G & Powis G. Antitumor activity and pharmacodynamic properties of PX-478, an inhibitor of hypoxia-inducible factor-1alpha. *Mol Cancer Ther* **3**, 233-244 (2004).

103   Welsh SJ, Williams RR, Birmingham A, Newman DJ, Kirkpatrick DL & Powis G. The thioredoxin redox inhibitors 1-methylpropyl 2-imidazolyl disulfide and pleurotin inhibit hypoxia-induced factor 1alpha and vascular endothelial growth factor formation. *Mol Cancer Ther* **2**, 235-243 (2003).

104   Jones DT, Pugh CW, Wigfield S, Stevens MF & Harris AL. Novel thioredoxin inhibitors paradoxically increase hypoxia-inducible factor-alpha expression but decrease functional transcriptional activity, DNA binding, and degradation. *Clin Cancer Res* **12**, 5384-5394 (2006).

105   Kong D, Park EJ, Stephen AG, Calvani M, Cardellina JH, Monks A *et al.* Echinomycin, a small-molecule inhibitor of hypoxia-inducible factor-1 DNA-binding activity. *Cancer Res* **65**, 9047-9055 (2005).

106   Kung AL, Zabludoff SD, France DS, Freedman SJ, Tanner EA, Vieira A *et al.* Small molecule blockade of transcriptional coactivation of the hypoxia-inducible factor pathway. *Cancer Cell* **6**, 33-43 (2004).

107   Kaluz S, Kaluzová M & Stanbridge EJ. Proteasomal inhibition attenuates transcriptional activity of hypoxia-inducible factor 1 (HIF-1) via specific effect on the HIF-1alpha C-terminal activation domain. *Mol Cell Biol* **26**, 5895-5907 (2006).

108   Yeo EJ, Ryu JH, Cho YS, Chun YS, Huang LE, Kim MS *et al.* Amphotericin B blunts erythropoietin response to hypoxia by reinforcing FIH-mediated repression of HIF-1. *Blood* **107**, 916-923 (2006).

109   Jaakkola P, Mole DR, Tian YM, Wilson MI, Gielbert J, Gaskell SJ *et al.* Targeting of HIF-alpha to the von Hippel-Lindau ubiquitylation complex by O2-regulated prolyl hydroxylation. *Science* **292**, 468-472 (2001).

110   McDonough MA, McNeill LA, Tilliet M, Papamicaël CA, Chen QY, Banerji B *et al.* Selective inhibition of factor inhibiting hypoxia-inducible factor. *J Am Chem Soc* **127**, 7680-7681 (2005).

111   Wang GL1 & Semenza GL. Desferrioxamine induces erythropoietin gene expression and hypoxia-inducible factor 1 DNA-binding activity: implications for models of hypoxia signal transduction. *Blood* **82**, 3610-3615 (1993).

112   Knowles HJ, Tian YM, Mole DR & Harris AL. Novel mechanism of action for hydralazine: induction of hypoxia-inducible factor-1alpha, vascular endothelial growth factor, and angiogenesis by inhibition of prolyl hydroxylases. *Circ Res* **95**, 162-169 (2004).

113   Majamaa K, Günzler V, Hanauske-Abel HM, Myllylä R & Kivirikko KI. Partial identity of the 2-oxoglutarate and ascorbate binding sites of prolyl 4-hydroxylase. *J Biol Chem.* **261**, 7819-7823 (1986).

114   Ivan M, Haberberger T, Gervasi DC, Michelson KS, Günzler V, Kondo K *et al.* Biochemical purification and pharmacological inhibition of a mammalian prolyl hydroxylase acting on hypoxia-inducible factor. *Proc Natl Acad Sci USA* **99**, 13459-13464 (2002).

115   Wanner RM, Spielmann P, Stroka DM, Camenisch G, Camenisch I, Scheid A *et al.* Epolones induce erythropoietin expression via hypoxia-inducible factor-1 alpha activation. *Blood* **96**, 1558-1565 (2000).

116   Robinson A, Keely S, Karhausen J, Gerich ME, Furuta GT & Colgan SP. Mucosal protection by hypoxia-inducible factor prolyl hydroxylase inhibition. *Gastroenterology* **134**, 145-155 (2008).

117   Nangaku M, Izuhara Y, Takizawa S, Yamashita T, Fujii-Kuriyama Y, Ohneda O *et al.* A novel class of prolyl hydroxylase inhibitors induces angiogenesis and exerts organ protection against ischemia. *Arterioscler Thromb Vasc Biol* **27**, 2548-2554 (2007).

118   McCaffrey TA, Pomerantz KB, Sanborn TA, Spokojny AM, Du B, Park MH *et al.* Specific inhibition of eIF-5A and collagen hydroxylation by a single agent. Antiproliferative and fibrosuppressive effects on smooth muscle cells from human coronary arteries. *J Clin Invest* **95**, 446-455 (1995).

119   Schlemminger I, Mole DR, McNeill LA, Dhanda A, Hewitson KS, Tian YM *et al.* Analogues of dealanylalahopcin are inhibitors of human HIF prolyl hydroxylases. *Bioorg Med Chem Lett* **13**, 1451-1454 (2003).

120   Warshakoon NC, Wu S, Boyer A, Kawamoto R, Sheville J, Renock S *et al.* Structure-based design, synthesis, and SAR evaluation of a new series of 8-hydroxyquinolines as HIF-1alpha prolyl hydroxylase inhibitors. *Bioorg Med Chem Lett* **16**, 5517-5522 (2006).

121   Warshakoon NC, Wu S, Boyer A, Kawamoto R, Renock S, Xu K *et al.* Design and synthesis of a series of novel pyrazolopyridines as HIF-1alpha prolyl hydroxylase inhibitors. *Bioorg Med Chem Lett* **16**, 5687-5690 (2006).

122   Pera MF. Stem cells: The dark side of induced pluripotency. *Nature* **471**, 46-47 (2011).

123   Xu T1, Zhang M, Laurent T, Xie M & Ding S. Concise review: chemical approaches for modulating lineage-specific stem cells and progenitors. *Stem Cells Transl Med* **2**, 355-361 (2013).

124   Gage FH. Mammalian neural stem cells. *Science* **287**, 1433-1438 (2000).

125   Basak O & Taylor V. Stem cells of the adult mammalian brain and their niche. *Cell Mol Life Sci* **66**, 1057-1072 (2009).

126   Gage FH, Kempermann G, Palmer TD, Peterson DA & Ray J. Multipotent progenitor cells in the adult dentate gyrus. *J Neurobiol* **36**, 249-266 (1998).

127 Pollard SM, Conti L, Sun Y, Goffredo D & Smith A. Adherent neural stem (NS) cells from fetal and adult forebrain. *Cereb Cortex* **16**, 112-120 (2006).

128 Conti L, Pollard SM, Gorba T, Reitano E, Toselli M, Biella G *et al.* Niche-independent symmetrical self-renewal of a mammalian tissue stem cell. *PLoS Biol* **3**, epub (2005).

129 Brüstle O, Spiro AC, Karram K, Choudhary K, Okabe S & McKay RD. In vitro-generated neural precursors participate in mammalian brain development. *Proc Natl Acad Sci U S A* **94**, 14809-14814 (1997).

130 Rich JN. The Implications of the Cancer Stem Cell Hypothesis for Neuro-Oncology and Neurology. *Future Neurol.* **3**, 265-273 (2008).

131 Yoo J, Kim HS & Hwang DY. Stem cells as promising therapeutic options for neurological disorders. *J Cell Biochem* **114**, 743-753 (2013).

132 Kopen GC, Prockop DJ & Phinney DG. Marrow stromal cells migrate throughout forebrain and cerebellum, and they differentiate into astrocytes after injection into neonatal mouse brains. *Proc Natl Acad Sci U S A* **96**, 10711-10716 (1999).

133 Petersen BE, Bowen WC, Patrene KD, Mars WM, Sullivan AK, Murase N *et al.* Bone marrow as a potential source of hepatic oval cells. *Science* **284**, 1168-1170 (1999).

134 Uccelli A, Moretta L & Pistoia V. Mesenchymal stem cells in health and disease. *Nat Rev Immunol* **8**, 726-736 (2008).

135 da Silva Meirelles L, Chagastelles PC & Nardi NB. Mesenchymal stem cells reside in virtually all post-natal organs and tissues. *J Cell Sci* **119**, 2204-2213 (2006).

136 Horwitz EM, Le Blanc K, Dominici M, Mueller I, Slaper-Cortenbach I, Marini FC *et al.* Clarification of the nomenclature for MSC: The International Society for Cellular Therapy position statement. *Cytotherapy* **7**, 393-395 (2005).

137 Horwitz EM, Prockop DJ, Fitzpatrick LA, Koo WW, Gordon PL, Neel M *et al.* Transplantability and therapeutic effects of bone marrow-derived mesenchymal cells in children with osteogenesis imperfecta. *Nat Med* **5**, 309-313 (1999).

138 Maximow, A. Der Lymphozyt als gemeinsame Stammzelle der verschiedenen Blutelemente in der embryonalen Entwicklung und im postfetalen Leben der Saugetiere. *Folia Haematol. (Frankf.)* **8**, 125-134 (1909).

139 Wang JC, Doedens M & Dick JE. Primitive human hematopoietic cells are enriched in cord blood compared with adult bone marrow or mobilized peripheral blood as measured by the quantitative in vivo SCID-repopulating cell assay. *Blood* **89**, 3919-3924 (1997).

140 Doulatov S, Notta F, Laurenti E & Dick JE. Hematopoiesis: a human perspective. *Cell Stem Cell* **10**, 120-136 (2012).

141 Kobayashi Y. Molecular target therapy in hematological malignancy: front-runners and prototypes of small molecule and antibody therapy. *Jpn J Clin Oncol* **41**, 157-164 (2011).

142 Goldman JM. Initial treatment for patients with CML. *Hematology Am Soc Hematol Educ Program*, 453-460 (2009).

143 de Lichtervelde L, Antal CE, Boitano AE, Wang Y, Krastel P, Petersen F *et al.* Euphohelioscopin A is a PKC activator capable of inducing macrophage differentiation. *Chem Biol* **19**, 994-1000 (2012).

144 Boitano AE, Wang J, Romeo R, Bouchez LC, Parker AE, Sutton SE *et al.* Aryl hydrocarbon receptor antagonists promote the expansion of human hematopoietic stem cells. *Science* **329**, 1345-1348 (2010).

145 North TE1, Goessling W, Walkley CR, Lengerke C, Kopani KR, Lord AM *et al.* Prostaglandin E2 regulates vertebrate haematopoietic stem cell homeostasis. *Nature* **447**, 1007-1011 (2007).

146 Galluzzi L, Vitale I, Abrams JM, Alnemri ES, Baehrecke EH, Blagosklonny MV *et al.* Molecular definitions of cell death subroutines: recommendations of the Nomenclature Committee on Cell Death 2012. *Cell Death Differ* **19**, 107-120 (2012).

147 Wei MC, Zong WX, Cheng EH, Lindsten T, Panoutsakopoulou V, Ross AJ *et al.* Proapoptotic BAX and BAK: a requisite gateway to mitochondrial dysfunction and death. *Science* **292**, 727-730 (2001).

148 Smith CA, Farrah T & Goodwin RG. The TNF receptor superfamily of cellular and viral proteins: activation, costimulation, and death. *Cell* **76**, 959-962 (1994).

149 Wiley SR, Schooley K, Smolak PJ, Din WS, Huang CP, Nicholl JK *et al.* Identification and characterization of a new member of the TNF family that induces apoptosis. *Immunity* **3**, 673-682 (1995).

150 Walczak H, Miller RE, Ariail K, Gliniak B, Griffith TS, Kubin M *et al.* Tumoricidal activity of tumor necrosis factor-related apoptosis-inducing ligand in vivo. *Nat Med* **5**, 157-163 (1999).

151 Pan G, O'Rourke K, Chinnaiyan AM, Gentz R, Ebner R, Ni J *et al.* The receptor for the cytotoxic ligand TRAIL. *Science* **276**, 111-113 (1997).

152 Pan G, Ni J, Wei YF, Yu G, Gentz R & Dixit VM. An antagonist decoy receptor and a death domain-containing receptor for TRAIL. *Science* **277** (1997).

153 Marsters SA, Sheridan JP, Pitti RM, Huang A, Skubatch M, Baldwin D *et al.* A novel receptor for Apo2L/TRAIL contains a truncated death domain. *Curr Biol* **7**, 1003-1006 (1997).

154 Emery JG, McDonnell P, Burke MB, Deen KC, Lyn S, Silverman C *et al.* Osteoprotegerin is a receptor for the cytotoxic ligand TRAIL. *J Biol Chem* **273**, 14363-14367 (1998).

155 Sedger LM, Glaccum MB, Schuh JC, Kanaly ST, Williamson E, Kayagaki N *et al.* Characterization of the in vivo function of TNF-alpha-related apoptosis-inducing ligand, TRAIL/Apo2L, using TRAIL/Apo2L gene-deficient mice. *Eur J Immunol* **32**, 2246-2254 (2002).

156 Sheridan JP, Marsters SA, Pitti RM, Gurney A, Skubatch M, Baldwin D *et al.* Control of TRAIL-induced apoptosis by a family of signaling and decoy receptors. *Science* **277**, 818-821 (1997).

157 Mongkolsapaya J, Grimes JM, Chen N, Xu XN, Stuart DI, Jones EY *et al.* Structure of the TRAIL-DR5 complex reveals mechanisms conferring specificity in apoptotic initiation. *Nat Struct Biol* **6**, 1048-1053 (1999).

158 Pennarun B, Meijer A, de Vries EG, Kleibeuker JH, Kruyt F & de Jong S. Playing the DISC: turning on TRAIL death receptor-mediated apoptosis in cancer. *Biochim Biophys Acta* **1805**, 123-140 (2010).

159 Kischkel FC, Lawrence DA, Chuntharapai A, Schow P, Kim KJ & Ashkenazi A. Apo2L/TRAIL-dependent recruitment of endogenous FADD and caspase-8 to death receptors 4 and 5. *Immunity* **12**, 611-620 (2000).

160 Li H, Zhu H, Xu CJ & Yuan J. Cleavage of BID by caspase 8 mediates the mitochondrial damage in the Fas pathway of apoptosis. *Cell* **94**, 491-501 (1998).

161 Barnhart BC, Alappat EC & Peter ME. The CD95 type I/type II model. *Semin Immunol* **15**, 185-193 (2003).

162 Odoux C & Albers A. Additive effects of TRAIL and paclitaxel on cancer cells: implications for advances in cancer therapy. *Vitam Horm* **67**, 385-407 (2004).

163 Holoch PA & Griffith TS. TNF-related apoptosis-inducing ligand (TRAIL): a new path to anti-cancer therapies. *Eur J Pharmacol* **625**, 63-72 (2009).

164   Du C, Fang M, Li Y, Li L & Wang X. Smac, a mitochondrial protein that promotes cytochrome c-dependent caspase activation by eliminating IAP inhibition. *Cell* **102**, 33-42 (2000).

165   Verhagen AM, Ekert PG, Pakusch M, Silke J, Connolly LM, Reid GE *et al.* Identification of DIABLO, a mammalian protein that promotes apoptosis by binding to and antagonizing IAP proteins. *Cell* **102**, 43-53 (2000).

166   Holcik M, Gibson H & Korneluk RG. XIAP: apoptotic brake and promising therapeutic target. *Apoptosis* **6**, 253-261 (2001).

167   Li P, Nijhawan D, Budihardjo I, Srinivasula SM, Ahmad M, Alnemri ES *et al.* Cytochrome c and dATP-dependent formation of Apaf-1/caspase-9 complex initiates an apoptotic protease cascade. *Cell* **91**, 479-489 (1997).

168   Greco FA, Bonomi P, Crawford J, Kelly K, Oh Y, Halpern W *et al.* Phase 2 study of mapatumumab, a fully human agonistic monoclonal antibody which targets and activates the TRAIL receptor-1, in patients with advanced non-small cell lung cancer. *Lung Cancer* **61**, 82-90 (2008).

169   Plummer R, Attard G, Pacey S, Li L, Razak A, Perrett R *et al.* Phase 1 and pharmacokinetic study of lexatumumab in patients with advanced cancers. *Clin Cancer Res* **13**, 6187-6194 (2007).

170   Forero-Torres A, Shah J, Wood T, Posey J, Carlisle R, Copigneaux C *et al.* Phase I trial of weekly tigatuzumab, an agonistic humanized monoclonal antibody targeting death receptor 5 (DR5). *Cancer Biother Radiopharm* **25**, 13-19 (2010).

171   Kaplan-Lefko PJ, Graves JD, Zoog SJ, Pan Y, Wall J, Branstetter DG *et al.* Conatumumab, a fully human agonist antibody to death receptor 5, induces apoptosis via caspase activation in multiple tumor types. *Cancer Biol Ther* **9**, 618-631 (2010).

172   Sheikh MS, Huang Y, Fernandez-Salas EA, El-Deiry WS, Friess H, Amundson S *et al.* The antiapoptotic decoy receptor TRID/TRAIL-R3 is a p53-regulated DNA damage-inducible gene that is overexpressed in primary tumors of the gastrointestinal tract. *Oncogene* **19**, 4153-4159 (1999).

173   Sanlioglu AD, Dirice E, Aydin C, Erin N, Koksoy S & Sanlioglu S. Surface TRAIL decoy receptor-4 expression is correlated with TRAIL resistance in MCF7 breast cancer cells. *BMC Cancer* **5**, 54 (2005).

174   Zhang XD, Franco A, Myers K, Gray C, Nguyen T & Hersey P. Relation of TNF-related apoptosis-inducing ligand (TRAIL) receptor and FLICE-inhibitory protein expression to TRAIL-induced apoptosis of melanoma. *Cancer Res.* **59**, 2747-2753 (1999).

175   Lee SH, Shin MS, Kim HS, Lee HK, Park WS, Kim SY *et al.* Somatic mutations of TRAIL-receptor 1 and TRAIL-receptor 2 genes in non-Hodgkin's lymphoma. *Oncogene* **20**, 399-403 (2001).

176   Jin Z, Dicker DT & El-Deiry WS. Enhanced sensitivity of G1 arrested human cancer cells suggests a novel therapeutic strategy using a combination of simvastatin and TRAIL. *Cell Cycle* **1**, 82-89 (2002).

177   Mazurek N, Byrd JC, Sun Y, Hafley M, Ramirez K, Burks J *et al.* Cell-surface galectin-3 confers resistance to TRAIL by impeding trafficking of death receptors in metastatic colon adenocarcinoma cells. *Cell Death Differ* **19**, 523-533 (2012).

178   Wagner KW, Punnoose EA, Januario T, Lawrence DA, Pitti RM, Lancaster K *et al.* Death-receptor O-glycosylation controls tumor-cell sensitivity to the proapoptotic ligand Apo2L/TRAIL. *Nat Med* **13**, 1070-1077 (2007).

179   Irmler M, Thome M, Hahne M, Schneider P, Hofmann K, Steiner V *et al.* Inhibition of death receptor signals by cellular FLIP. *Nature* **388**, 190-195 (1997).

180   Deveraux QL, Takahashi R, Salvesen GS & Reed JC. X-linked IAP is a direct inhibitor of cell-death proteases. *Nature* **388**, 300-304 (1997).

181   Sinicrope FA, Penington RC & Tang XM. Tumor necrosis factor-related apoptosis-inducing ligand-induced apoptosis is inhibited by Bcl-2 but restored by the small molecule Bcl-2 inhibitor, HA 14-1, in human colon cancer cells. *Clin Cancer Res* **10**, 8284-8292 (2004).

182   Clohessy JG, Zhuang J, de Boer J, Gil-Gómez G & Brady HJ. Mcl-1 interacts with truncated Bid and inhibits its induction of cytochrome c release and its role in receptor-mediated apoptosis. *J Biol Chem* **284**, 5750-5759 (2006).

183   Ehrhardt H, Fulda S, Schmid I, Hiscott J, Debatin KM & Jeremias I. TRAIL induced survival and proliferation in cancer cells resistant towards TRAIL-induced apoptosis mediated by NF-kappaB. *Oncogene* **22**, 3842-3852 (2003).

184   Gupta SC, Reuter S, Phromnoi K, Park B, Hema PS, Nair M *et al.* Nimbolide sensitizes human colon cancer cells to TRAIL through reactive oxygen species- and ERK-dependent up-regulation of death receptors, p53, and Bax. *J Biol Chem* **286**, 1134-1146 (2011).

185   Ding J, Polier G, Köhler R, Giaisi M, Krammer PH & Li-Weber M. Wogonin and related natural flavones overcome tumor necrosis factor-related apoptosis-inducing ligand (TRAIL) protein resistance of tumors by down-regulation of c-FLIP protein and up-regulation of TRAIL receptor 2 expression. *J Biol Chem* **287**, 641-649 (2012).

186   Mitsiades CS, Treon SP, Mitsiades N, Shima Y, Richardson P, Schlossman R *et al.* TRAIL/Apo2L ligand selectively induces apoptosis and overcomes drug resistance in multiple myeloma: therapeutic applications. *Blood* **98**, 795-804 (2001).

187   Tang SY, Zhong MZ, Yuan GJ, Hou SP, Yin LL, Jiang H *et al.* Casticin, a flavonoid, potentiates TRAIL-induced apoptosis through modulation of anti-apoptotic proteins and death receptor 5 in colon cancer cells. *Oncol Rep* **epub** (2012).

188   Oh B, Park S, Pak JH & Kim I. Downregulation of Mcl-1 by daunorubicin pretreatment reverses resistance of breast cancer cells to TNF-related apoptosis-inducing ligand. *Biochem Biophys Res Commun* **422**, 42-47 (2012).

189   Kim HB, Kim MJ, Lee SH, Lee JW, Bae JH, Kim DW *et al.* Amurensin G, a novel SIRT1 inhibitor, sensitizes TRAIL-resistant human leukemic K562 cells to TRAIL-induced apoptosis. *Biochem Pharmacol* **84**, 402-410 (2012).

190   Sidler D, Brockmann A, Mueller J, Nachbur U, Corazza N, Renzulli P *et al.* Thiazolide-induced apoptosis in colorectal cancer cells is mediated via the Jun kinase-Bim axis and reveals glutathione-S-transferase P1 as Achilles' heel. *Oncogene* **31**, 4095-4106 (2012).

191   Liu F, Liu Q, Yang D, Bollag WB, Robertson K, Wu P *et al.* Verticillin A overcomes apoptosis resistance in human colon carcinoma through DNA methylation-dependent upregulation of BNIP3. *Cancer Res.* **71**, 6807-6816 (2011).

192   Waiwut P, Inujima A, Inoue H, Saiki I & Sakurai H. Bufotalin sensitizes death receptor-induced apoptosis via Bid- and STAT1-dependent pathways. *Int J Oncol* **40**, 203-208 (2012).

193   Badr CE, Wurdinger T, Nilsson J, Niers JM, Whalen M, Degterev A *et al.* Lanatoside C sensitizes glioblastoma cells to tumor necrosis factor-related apoptosis-inducing ligand and induces an alternative cell death pathway. *Neuro Oncol* **13**, 1213-1224 (2011).

194   Kim HB, Kim MJ, Kim DY, Lee JW, Bae JH, Kim DW *et al.* High susceptibility of metastatic cells derived from human prostate and colon cancer cells to TRAIL and sensitization of TRAIL-insensitive primary cells to TRAIL by 4,5-dimethoxy-2-nitrobenzaldehyde. *Mol Cancer Ther* **10**, 1969-1981 (2011).

195   Kong CK, Lam WS, Chiu LC, Ooi VE, Sun SS & Wong YS. A rice bran polyphenol, cycloartenyl ferulate, elicits apoptosis in human colorectal adenocarcinoma SW480 and sensitizes metastatic SW620 cells to TRAIL-induced apoptosis. *Biochem Pharmacol* **77**, 1487-1496 (2009).

196   Raja SM, Chen S, Yue P, Acker TM, Lefkove B, Arbiser JL *et al.* The natural product honokiol preferentially inhibits cellular FLICE-inhibitory protein and augments death receptor-induced apoptosis. *Mol Cancer Ther* **7**, 2212-2223 (2008).

197   Carter BZ, Mak DH, Schober WD, Dietrich MF, Pinilla C, Vassilev LT *et al.* Triptolide sensitizes AML cells to TRAIL-induced apoptosis via decrease of XIAP and p53-mediated increase of DR5. *Blood* **11**, 3742-3750 (2008).

198   Retzer-Lidl M, Schmid RM & Schneider G. Inhibition of CDK4 impairs proliferation of pancreatic cancer cells and sensitizes towards TRAIL-induced apoptosis via downregulation of survivin. *Int J Cancer* **121**, 66-75 (2007).

199   Nakata S, Yoshida T, Shiraishi T, Horinaka M, Kouhara J, Wakada M *et al.* 15-Deoxy-Delta12,14-prostaglandin J(2) induces death receptor 5 expression through mRNA stabilization independently of PPARgamma and potentiates TRAIL-induced apoptosis. *Mol Cancer Ther* **5**, 1827-1835 (2006).

200   Kim YH, Park JW, Lee JY & Kwon TK. Sodium butyrate sensitizes TRAIL-mediated apoptosis by induction of transcription from the DR5 gene promoter through Sp1 sites in colon cancer cells. *Carcinogenesis* **25**, 1813-1820 (2004).

201   Fulda S & Debatin KM. Sensitization for tumor necrosis factor-related apoptosis-inducing ligand-induced apoptosis by the chemopreventive agent resveratrol. *Cancer Res.* **64**, 337-346 (2004).

202   Rosato RR, Almenara JA, Coe S & Grant S. The multikinase inhibitor sorafenib potentiates TRAIL lethality in human leukemia cells in association with Mcl-1 and cFLIPL down-regulation. *Cancer Res.* **67**, 9490-9500 (2007).

203   Zhang XD, Gillespie SK, Borrow JM & Hersey P. The histone deacetylase inhibitor suberic bishydroxamate: a potential sensitizer of melanoma to TNF-related apoptosis-inducing ligand (TRAIL) induced apoptosis. *Biochem Pharmacol* **66**, 1537-1545 (2003).

204   Jeon KI, Rih JK, Kim HJ, Lee YJ, Cho CH, Goldberg ID *et al.* Pretreatment of indole-3-carbinol augments TRAIL-induced apoptosis in a prostate cancer cell line, LNCaP. *FEBS Lett* **544**, 246-251 (2003).

205   Chanvorachote P & Pongrakhananon V. Ouabain down-regulates Mcl-1 and sensitizes lung cancer cells to TRAIL-induced apoptosis. *Am J Physiol Cell Physiol*, epub (2012).

206   Frese S, Schüller A, Frese-Schaper M, Gugger M & Schmid RA. Cytotoxic effects of camptothecin and cisplatin combined with tumor necrosis factor-related apoptosis-inducing ligand (Apo2L/TRAIL) in a model of primary culture of non-small cell lung cancer. *Anticancer Res* **29**, 2905-2911 (2009).

207   Chen LH, Jiang CC, Kiejda KA, Wang YF, Thorne RF, Zhang XD *et al.* Thapsigargin sensitizes human melanoma cells to TRAIL-induced apoptosis by up-regulation of TRAIL-R2 through the unfolded protein response. *Carcinogenesis* **28**, 2328-2336 (2007).

208   Herwaldt BL. Leishmaniasis. *Lancet* **354**, 1191-1199 (1999).

209   Bates PA. Transmission of Leishmania metacyclic promastigotes by phlebotomine sand flies. *Int J Parasitol* **37**, 1097-1106 (2007).

210   Lipoldová M & Demant P. Genetic susceptibility to infectious disease: lessons from mouse models of leishmaniasis. *Nat Rev Genet* **7**, 294-305 (2006).

211   Machado CM, Martins TC, Colturato I, Leite MS, Simione AJ, Souza MP *et al.* Epidemiology of neglected tropical diseases in transplant recipients. Review of the literature and experience of a Brazilian HSCT center. *Rev Inst Med Trop Sao Paulo* **51**, 309-324 (2009).

212   Desjeux P. Leishmaniasis. Public health aspects and control. *Clin Dermatol* **14**, 417-423 (1996).

213   Dujardin JC, Campino L, Cañavate C, Dedet JP, Gradoni L, Soteriadou K *et al.* Spread of vector-borne diseases and neglect of Leishmaniasis, Europe. *Emerg Infect Dis* **14**, 1013-1018 (2008).

214   Kobets T, Grekov I & Lipoldova M. Leishmaniasis: prevention, parasite detection and treatment. *Curr Med Chem* **19**, 1443-1474 (2012).

215   Denton H, McGregor JC & Coombs GH. Reduction of anti-leishmanial pentavalent antimonial drugs by a parasite-specific thiol-dependent reductase, TDR1. *Biochem J* **381**, 405-412 (2004).

216   Berman JD, Gallalee JV & Best JM. Sodium stibogluconate (Pentostam) inhibition of glucose catabolism via the glycolytic pathway, and fatty acid beta-oxidation in Leishmania mexicana amastigotes. *Biochem Pharmacol* **36**, 197-201 (1987).

217   Chakraborty AK & Majumder HK. Mode of action of pentavalent antimonials: specific inhibition of type I DNA topoisomerase of Leishmania donovani. *Biochem Biophys Res Commun* **152**, 605-611 (1988).

218   Wyllie S, Cunningham ML & Fairlamb AH. Dual action of antimonial drugs on thiol redox metabolism in the human pathogen Leishmania donovani. *J Biol Chem* **279**, 39952-39932 (2004).

219   Vanaerschot M, De Doncker S, Rijal S, Maes L, Dujardin JC & Decuypere S. Antimonial resistance in Leishmania donovani is associated with increased in vivo parasite burden. *PLoS One* **epub** (2011).

220   Carter KC, Hutchison S, Henriquez FL, Légaré D, Ouellette M, Roberts CW *et al.* Resistance of Leishmania donovani to sodium stibogluconate is related to the expression of host and parasite gamma-glutamylcysteine synthetase. *Antimicrob Agents Chemother* **50**, 88-95 (2006).

221   Herwaldt BL & Berman JD. Recommendations for treating leishmaniasis with sodium stibogluconate (Pentostam) and review of pertinent clinical studies. *Am J Trop Med Hyg* **46**, 296-306 (1992).

222   Goto H & Lindoso JA. Current diagnosis and treatment of cutaneous and mucocutaneous leishmaniasis. *Expert Rev Anti Infect Ther* **8**, 419-433 (2010).

223   Croft SL, Seifert K & Yardley V. Current scenario of drug development for leishmaniasis. *Indian J Med Res* **123**, 399-410 (2006).

224   Sundar S & Chatterjee M. Visceral leishmaniasis - current therapeutic modalities. *Indian J Med Res* **123**, 345 (2006).

225   Ramos H, Valdivieso E, Gamargo M, Dagger F & Cohen BE. Amphotericin B kills unicellular leishmanias by forming aqueous pores permeable to small cations and anions. *J Membr Biol* **152**, 65-75 (1996).

226   Bray PG, Barrett MP, Ward SA & de Koning HP. Pentamidine uptake and resistance in pathogenic protozoa: past, present and future. *Trends Parasitol* **19**, 232-239 (2003).

227   Cruz AK, de Toledo JS, Falade M, Terrão MC, Kamchonwongpaisan S, Kyle DE *et al.* Current treatment and drug discovery against Leishmania spp. and Plasmodium spp.: a review. *Curr Drug Targets* **10**, 178-192 (2009).

228   Report of the Fifth Consultative Meeting on Leishmania/HIV Coinfection. *WHO Document Production Services: Geneva, Switzerland.*, 24 (2007).

229 Maarouf M, Lawrence F, Brown S & Robert-Gero M. Biochemical alterations in paromomycin-treated Leishmania donovani promastigotes. *Parasitol Res* **83**, 198-202 (1997).

230 Luque-Ortega JR & Rivas L. Miltefosine (hexadecylphosphocholine) inhibits cytochrome c oxidase in Leishmania donovani promastigotes. *Antimicrob Agents Chemother* **51**, 1327-1332 (2007).

231 Lux H, Heise N, Klenner T, Hart D & Opperdoes FR. Ether--lipid (alkyl-phospholipid) metabolism and the mechanism of action of ether--lipid analogues in Leishmania. *Mol Biochem Parasitol* **111**, 1-14 (2000).

232 Carvalho L, Luque-Ortega JR, López-Martín C, Castanys S, Rivas L & Gamarro F. The 8-aminoquinoline analogue sitamaquine causes oxidative stress in Leishmania donovani promastigotes by targeting succinate dehydrogenase. *Antimicrob Agents Chemother* **55**, 4204-4210 (2011).

233 Grekov I, Svobodová M, Nohýnková E & Lipoldová M. Preparation of highly infective Leishmania promastigotes by cultivation on SNB-9 biphasic medium. *J Microbiol Methods* **87**, 273-277 (2011).

234 Xu Q, Wang Y, Dabdoub A, Smallwood PM, Williams J, Woods C *et al.* Vascular development in the retina and inner ear: control by Norrin and Frizzled-4, a high-affinity ligand-receptor pair. *Cell* **116**, 883-895 (2004).

235 Hughes K, Nikolakaki E, Plyte SE, Totty NF & Woodgett JR. Modulation of the glycogen synthase kinase-3 family by tyrosine phosphorylation. *EMBO J* **12**, 803-808 (1993).

236 Rayasam GV, Tulasi VK, Sodhi R, Davis JA & Ray A. Glycogen synthase kinase 3: more than a namesake. *Br J Pharmacol* **156**, 885-898 (2009).

237 Thangarajah H, Yao D, Chang EI, Shi Y, Jazayeri L, Vial IN *et al.* The molecular basis for impaired hypoxia-induced VEGF expression in diabetic tissues. *Proc Natl Acad Sci U S A* **106**, 13505-13510 (2009).

238 Bao P1, Kodra A, Tomic-Canic M, Golinko MS, Ehrlich HP & Brem H. The role of vascular endothelial growth factor in wound healing. *J Surg Res* **153**, 347-358 (2009).

239 Chou E, Suzuma I, Way KJ, Opland D, Clermont AC, Naruse K *et al.* Decreased cardiac expression of vascular endothelial growth factor and its receptors in insulin-resistant and diabetic States: a possible explanation for impaired collateral formation in cardiac tissue. *Circulation* **105**, 373-379 (2002).

240 Pombinho AR, Laizé V, Molha DM, Marques SM & Cancela ML. Development of two bone-derived cell lines from the marine teleost Sparus aurata; evidence for extracellular matrix mineralization and cell-type-specific expression of matrix Gla protein and osteocalcin. *Cell Tissue Res* **315**, 393-406 (2004).

241 Klag T, Härtel N, Erben P, Schwaab J, Schnetzke U, Schenk T *et al.* Omacetaxine mepesuccinate prevents cytokine-dependent resistance to nilotinib in vitro: potential role of the common β-subunit c of cytokine receptors. *Leukemia* **26**, 1321-1328 (2012).

7- Abbreviations

APC   adenomatous polyposis coli

Arnt   Aryl hydrocarbon nuclear translocator

ASC   adipose stem cells

Bcl   B-cell leukemia/lymphoma

BM   bone marrow

BMSC   bone marrow mesenchymal stem cells

BSP   bromosulfophthalein

CaMKII   calcium/calmodulin dependent protein kinase II

CBP   cyclic adenosine monophosphate response element-binding protein

CD   complex of differentiation

cDNA   complementary deoxyribonucleic acid

cFLIP   FADD-like IL-1β-converting enzyme inhibitory protein

CK   casein kinase

CML   chronic myeloid leukemia

CL   cutaneous leishmaniasis

DcR   decoy receptor

DISC   death-inducing signaling complex

DNA   deoxyribonucleic acid

DPI   diphenyleneiodonium chloride

DR   death receptor

DVL   disheveled

EGF   epidermal growth factor

ESC   embryonic stem cells

FADD   Fas-associated death domain

FBS   fetal bovine serum

FGF   fibroblast growth factor

FIH   factor inhibiting HIF

Fz   frizzled

GFP   green fluorescent protein

GSK   glycogen synthase kinase

HCS   high-content screening

HIF	hypoxia-inducible factor
HRE	hypoxia responsive element
HSC	hematopoietic stem cell
HTS	high-throughput screening
LEF	lymphoid enhancer-binding factor
LRP	low-density lipoprotein receptor-related proteins
ML	mucocutaneous leishmaniasis
mRNA	messenger ribonucleic acid
MSC	mesenchymal stem cells
mTOR	mammalian target of rapamycin
NF-AT	nuclear factor of activated T cells
NSC	neural stem cells
PCP	planar cell polarity
PCR	polymerase chain reaction
PHDs	prolyl-hydroxylases
PKC	protein kinase C
pVHL	von Hippel-Lindau tumor suppressor protein
RLU	relative luminescence units
RNA	ribonucleic acid
RT-PCR	reverse transcription polymerase chain reaction
STF	SuperTOPFLASH HEK293
TCF	T cell factor
TRAIL	tumor necrosis factor-related apoptosis-inducing ligand
VL	visceral leishmaniasis

8- Publications

Publication I

Tumova L*, <u>Pombinho AR</u>*, Vojtechova M, Stancikova J, Gradl D, Krausova M, Sloncova E, Horazna M, Kriz V, Machonova O, Jindrich J, Zdrahal Z, Bartunek P, Korinek V. Monensin inhibits canonical Wnt signaling in human colorectal cancer cells and suppresses tumor growth in multiple intestinal neoplasia mice. Mol Cancer Ther. 2014 Apr;13(4):812-22.

Publication II

Mestak O, Matouskova E, Spurkova Z, Benkova K, Vesely P, Mestak J, Molitor M, <u>Pombinho A</u>, Sukop A. Mesenchymal stem cells seeded on cross-linked and noncross-linked acellular porcine dermal scaffolds for long-term full-thickness hernia repair in a small animal model. Artif Organs. 2014 Jul;38(7):572-9.

Publication III

Rejman D, Rabatinová A, <u>Pombinho AR</u>, Kovačková S, Pohl R, Zborníková E, Kolář M, Bogdanová K, Nyč O, Sanderová H, Látal T, Bartůněk P, Krásný L. Lipophosphonoxins: new modular molecular structures with significant antibacterial properties. J Med Chem. 2011 Nov 24;54(22):7884-98.

Publication IV

Beranova L*, <u>Pombinho AR</u>*, Spegarova J, Koc M, Klanova M, Molinsky J, Klener P, Bartunek P, Andera L. The plant alkaloid and anti-leukemia drug homoharringtonine sensitizes resistant human colorectal carcinoma cells to TRAIL-induced apoptosis via multiple mechanisms. Apoptosis. 2013 Jun;18(6):739-50.

*These authors contributed equally to this work

Publication V - Patent

Rejman D, Pohl R, Bartůněk P, <u>Pombinho AR</u>, Krásný L, Látal T. Lipophosphonoxins, method of their preparation and use. EP2527351B1, 2012.

Small Molecule Therapeutics

Monensin Inhibits Canonical Wnt Signaling in Human Colorectal Cancer Cells and Suppresses Tumor Growth in Multiple Intestinal Neoplasia Mice

Lucie Tumova[1], Antonio R. Pombinho[2], Martina Vojtechova[1], Jitka Stancikova[1], Dietmar Gradl[5], Michaela Krausova[1], Eva Sloncova[1], Monika Horazna[1], Vitezslav Kriz[1], Olga Machonova[2], Jindrich Jindrich[2,3], Zbynek Zdrahal[4], Petr Bartunek[2], and Vladimir Korinek[1]

Abstract

The Wnt signaling pathway is required during embryonic development and for the maintenance of homeostasis in adult tissues. However, aberrant activation of the pathway is implicated in a number of human disorders, including cancer of the gastrointestinal tract, breast, liver, melanoma, and hematologic malignancies. In this study, we identified monensin, a polyether ionophore antibiotic, as a potent inhibitor of Wnt signaling. The inhibitory effect of monensin on the Wnt/β-catenin signaling cascade was observed in mammalian cells stimulated with Wnt ligands, glycogen synthase kinase-3 inhibitors, and in cells transfected with β-catenin expression constructs. Furthermore, monensin suppressed the Wnt-dependent tail fin regeneration in zebrafish and Wnt- or β-catenin–induced formation of secondary body axis in Xenopus embryos. In Wnt3a-activated HEK293 cells, monensin blocked the phoshorylation of Wnt coreceptor low-density lipoprotein receptor related protein 6 and promoted its degradation. In human colorectal carcinoma cells displaying deregulated Wnt signaling, monensin reduced the intracellular levels of β-catenin. The reduction attenuated the expression of Wnt signaling target genes such as *cyclin D1* and *SP5* and decreased the cell proliferation rate. In multiple intestinal neoplasia (Min) mice, daily administration of monensin suppressed progression of the intestinal tumors without any sign of toxicity on normal mucosa. Our data suggest monensin as a prospective anticancer drug for therapy of neoplasia with deregulated Wnt signaling. *Mol Cancer Ther; 13(4); 1–11. ©2014 AACR.*

Introduction

The Wnt pathway is an evolutionarily conserved signaling mechanism that evolved in metazoans. During embryonic development, the pathway is essential for cell proliferation, differentiation, and migration. In adult organisms, Wnt signaling is involved in somatic tissue homeostasis and tissue regeneration upon injury (reviewed in ref. 1); moreover, deregulation of Wnt signaling is a hallmark of various types of cancer (reviewed in ref. 2). The key component of the canonical the Wnt signaling pathway is β-catenin (reviewed in ref. 3). In unstimulated cells, β-catenin is phosphorylated at the N-terminus by the cytoplasmic "destruction complex" that includes axis inhibition protein (Axin), adenomatous polyposis coli (APC) and serine/threonine kinases casein kinase-1α (CK1α), and glycogen synthase kinase-3 (GSK-3). The phosphorylation promotes ubiquitination and subsequent degradation of the protein keeping the cellular level of the free pool of β-catenin low. Binding of the secreted Wnt ligands to the Frizzled (Fz) receptor and Wnt coreceptor lipoprotein receptor related protein (LRP)-5/6 initiates the CK1ε-dependent phoshorylation of multidomain cytoplasmic transducer Dishevelled (Dvl). In addition, LRP is phosphorylated at its intracellular part by CK1γ and GSK3. The latter event leads to the formation of the LRP–Axin complex and dephosphorylation of Axin. Dephosphorylated Axin constitutes inactive conformation that is unable to interact with LRP and β-catenin. Without the Axin scaffold β-catenin phosphorylation is inhibited and, consequently, the protein accumulates in the cell cytoplasm and nucleus. In the nucleus, β-catenin forms complexes with DNA-binding factors of the lymphoid enhancer factor/T-cell factor (LEF/TCF) family (further referred to as TCFs). The complexes act as

Authors' Affiliations: [1]Department of Cell and Developmental Biology, [2]CZ-OPENSCREEN, Institute of Molecular Genetics AS CR; [3]Department of Organic Chemistry, Faculty of Science, Charles University in Prague, Prague; and [4]Central European Institute of Technology, Masaryk University, Brno, Czech Republic; and [5]Zoologisches Institut II, Universität Karlsruhe, Karlsruhe, Germany

Note: Supplementary data for this article are available at Molecular Cancer Therapeutics Online (http://mct.aacrjournals.org/).

L. Tumova and A.R. Pombinho contributed equally to this work.

Corresponding Authors: Vladimir Korinek, Institute of Molecular Genetics, Videnska 1083, 14220 Prague 4, Czech Republic. Phone: 420-241-063-146; Fax: 420-244-472-282; E-mail: korinek@img.cas.cz; and Petr Bartunek, E-mail: bartunek@img.cas.cz

bipartite transcriptional activators of specific Wnt signaling target genes.

Cancer affecting colon and rectum constitutes one of the most commonly diagnosed neoplasia in developed countries (4). Intriguingly, pathogenesis of the colorectal carcinoma is connected with the aberrant activity of the Wnt/β-catenin signaling cascade. Germinal mutations of the *APC* gene underlie the hereditary familial adenomatous polyposis (FAP) syndrome (5). Similarly, about 50% of sporadic colorectal tumors arise upon biallelic loss of *APC* (6). Hyperactive Wnt signaling might also result upon activation mutations in the β-catenin (also designated as *CTNNB1*) gene (7). In either case, stabilized β-catenin mediates inappropriate transcriptional activation of TCF/β-catenin target genes, thus driving pathologic transformation of the gut epithelium (8).

In the present study, we performed a reporter gene-based high-throughput screen (HTS) to identify inhibitors of the Wnt signaling pathway. We identified monensin, an antibiotic isolated from *Streptomyces cinnamonensis* bacteria (9), as a potent blocker of the Wnt-induced transcription in cells stimulated with Wnt ligands or GSK3 inhibitors. The suppressive effect of monensin on Wnt signaling was also observed in the tail fin regeneration assay in zebrafish and Xenopus body axis duplication experiment. In human colorectal carcinoma cells harboring mutations in *APC* or β-*catenin*, the monensin-mediated block of the TCF/β-catenin transcription activity led to slowdown in cell-cycle progression. Finally, monensin treatment reduced the size of the *Apc*-deficient tumors in the mouse model of intestinal cancer.

Materials and Methods

Cell lines and generation of Wnt1-producing cells

SuperTOPFLASH HEK293 (STF) cells (10) harboring the genome-integrated Wnt-responsive luciferase reporter SuperTOPFLASH were a gift of Q. Xu and J. Nathans (Johns Hopkins University, Baltimore, MD). COLO320, HCT116, HEK293, L, LS174T, RKO, and SW480 cell lines were purchased from the American Type Culture Collection. All cell lines were obtained in 2006 and maintained in Dulbecco's modified Eagle medium (Sigma) supplemented with 10% FBS (Gibco), penicillin, streptomycin, and gentamicin (Invitrogen). Upon receipt, cells were expanded and aliquots of cells at passage number <10 were stored frozen in liquid nitrogen. Cells from one aliquot were kept in culture for less than 2 months after resuscitation. The cell identity was not authenticated by the authors. Mouse Wnt1 cDNA (11) was cloned into the lentiviral vector pCDH1 (System Biosciences). Lentiviruses were prepared using the Trans-Lentiviral Packaging System (Open Biosystems). Transduced STF cells were selected without subcloning using puromycin (Alexis; 5 μg/mL).

Compounds, luciferase reporters and assays, transfections, and biochemistry

The small compound collections included the Library of Pharmacologically Active Compounds (LOPAC1280; Sigma-Aldrich), Prestwick Chemical Library (Illkirch, France), and NIH Clinical Trial Collection. Monensin sodium salt, (2′Z,3′E)-6-Bromoindirubin-3′-oxime (BIO) and bafilomycin A1 were purchased from Sigma, and CHIR99021 from Selleckchem. Luciferase reporter constructs, NF-κB-Luc and pRL-TK, were purchased from Promega. The TCF/β-catenin–dependent reporter TOPFLASH and negative control reporter FOPFLASH were described previously (8). The luciferase assays were performed as described previously (11) using the ONE-Glo Luciferase Assay System (Promega) for HTS and Dual-Glo Luciferase Assay System (Promega) for subsequent analysis. Mouse Wnt3a ligand was isolated from the culture medium of Wnt3a-producing L cells as described previously (12). Human recombinant lymphotoxin-α (LTα) was purchased from R&D Systems. Transfections were performed using Lipofectamine 2000 reagent (Invitrogen). RNA purification, quantitative reverse transcription PCR (qRT-PCR), coimmunoprecipitations, and immunoblotting were performed as described previously (11). The primers for qRT-PCR are listed in Supplementary Table S1.

Cell viability, apoptosis, and cell proliferation assays

Cell viability and apoptosis were determined after overnight incubation with respective compounds using the Cell Titer-Blue Cell Viability Assay Kit and Caspase-Glo 3/7 Assay Kit, respectively (Promega). In control experiments, cells were incubated with recombinant TRAIL (kindly provided by L. Andera, Institute of Molecular Genetics, Prague, Czech Republic). Apoptotic cells in the mouse intestine were detected using TumorTACS Detection Kit (RD Systems). Metabolic incorporation of [^{3}H]-thymidine (MP Radiochemicals; final concentration 0.1 mCi/μL) was measured using MicroBeta2 Microplate Counter (PerkinElmer) after overnight incubation at 37°C.

Monitoring cell proliferation and attachment in "real time"

xCELLigence Real-Time Cell Analysis System (Roche Applied Science) was used according to the instructions of the manufacturer. Cells were seeded at the density of 1,500 cells per well. The electronic impedance of sensor electrodes was monitored every 15 minutes. Eighteen hours after seeding, monensin or dimethyl sulfoxide (DMSO) was added to the wells and the measurement continued for additional 24 hours. Cell index was quantified as described previously (13).

Immunocytochemistry and immunohistochemistry

The techniques were performed as described previously (14, 15).

Zebrafish tailfin regeneration assay

Zebrafish (less than 6 months of age) were kept in E3 medium (5 mmol/L NaCl, 0.17 mmol/L KCl, 0.33 mmol/L CaCl$_2$, and 0.33 mmol/L MgSO$_4$ in distilled H$_2$O) at 28°C. Fishes that were approximately 2.5 cm long were anesthetized with tricaine (Sigma) and tips of their tail fin were

carefully amputated using scissors. The animals were randomly distributed into aquaria (4–5 fish per tank) containing E3 medium with 2 µmol/L (prepared from stock solution of 20 mmol/L monensin in ethanol) or equivalent volume of ethanol alone. One week later, fishes were anesthetized and photographed. The regenerated area (recognizable by lack of pigmentation) was scored in three independent experiments using ImageJ software.

Xenopus double axis formation assay

The assay was performed as described previously (16). A marginal zone of the ventral blastomeres of 4-cell stage *Xenopus laevis* embryos was injected (4 nL) using 20 or 800 pg of *XWnt8* or β-CATENIN mRNA, respectively. Messenger RNA was injected together with monensin (0.04 pmol) or vehicle (DMSO). The developing embryos were kept at 20°C; the duplication of the body axis was scored 36 hours after injection.

Tumor treatment in mice

Multiple intestinal neoplasia (Min) mice (further referred to as the Apc$^{+/Min}$ strain) were purchased from the Jackson Laboratory. Animals were housed and handled in accordance with the approved guidelines. Four-week-old pups were weaned, genotyped, and randomized. The animals were divided into two groups and treated with monensin (10 mg/kg) or vehicle (DMSO). Daily oral applications continued for 6 weeks. In addition, six pairs of Apc$^{+/Min}$ mice ages 7, 10, 13, 16, 19, and 22 weeks were treated with monensin or vehicle for 5 weeks. The mice were sacrificed and the intestines were dissected, washed in PBS, and fixed in 4% formaldehyde (v/v) in PBS for 3 days. Fixed intestines were embedded in paraffin, sectioned and stained. The number and size of the neoplastic lesions were quantified using Ellipse software (ViDiTo).

Statistical analysis

Fisher exact test was used to analyze the statistical significance of the results of the double axis formation assay. Data obtained in the gene reporter and qRT-PCR analyses were evaluated by Student t test.

Additional materials and methods, including details of HTS, plasmid constructs, and antibodies, are given in Supplementary Materials and Methods.

Results

HTS for inhibitors of the Wnt signaling pathway

Luciferase reporter gene assay in STF cells was used to search for novel inhibitors of Wnt/β-catenin signaling. The screen included 2,448 compounds from three commercially available collections. STF cells were stimulated with recombinant Wnt3a ligand and, simultaneously, the tested compounds were added to culture medium to 1 µmol/L concentration. The luciferase activity was quantified 18 hours later using bioluminescent signal detection. The primary screen identified seven "small molecules" displaying a profound inhibitory effect on the SuperTOP-

FLASH activity. These molecules included the previously identified Wnt pathway inhibitors indometacin (17), thapsigargin (18), and harmine (19). In addition, four compounds without any (published) relation to Wnt signaling were discovered. The putative novel Wnt pathway modulators were examined for their effective concentration range, cell toxicity, and direct repressive effect on the luciferase reaction. Moreover, because the zebrafish has the ability to regrow damaged tissues in the process that depends on active Wnt/β-catenin signaling (20), we used the tail fish regeneration assay to validate the action of the identified Wnt pathway inhibitors *in vivo*. Polyether antibiotic monensin, which suppressed the activity of the TCF/β-catenin reporter SuperTOPFLASH at concentrations 0.2 to 5 µmol/L and decreased the tail fish regeneration to 50% (compared with control vehicle-treated animals), was selected for subsequent studies (Fig. 1).

Monensin inhibits the Wnt signaling cascade at multiple levels

To confirm the specificity of the monensin action, reporter gene assays in HEK293 cells were performed using the Wnt-responsive reporter TOPFLASH (8), negative-control reporter FOPFLASH, and the NF-κB pathway luciferase reporter plasmid NF-κB-Luc. Cells transiently transfected with the reporters were stimulated with recombinant Wnt3a or LTα to activate Wnt or NK-κB signaling, respectively. In agreement with the results obtained in STF cells, 1 and 5 µmol/L monensin reduced the TOPFLASH activity to 34% and 32%, respectively (Fig. 2A). Conversely, monensin had no effect on the transcription from the NF-κB-Luc and FOPFLASH reporters (Fig. 2A; data not shown). In addition, we performed qRT-PCR analysis of HEK293 cells. Monensin treatment resulted in downregulation of the previously described Wnt target genes *AXIN2*, *CYCLIN D1*, *LGR5*, *NKD1*, and *SP5* (Fig. 2B). To verify these results in a different cell type, the β-catenin stabilization was visualized in L cells (15). In these mouse fibroblasts, monensin reduced Wnt3a-mediated accumulation of β-catenin in the cytoplasm and nucleus (Fig. 2C). Recently, Morrell and colleagues have reported that some inhibitors of the Wnt pathway antagonize recombinant Wnt3a protein but are ineffective against ectopically expressed Wnt ligands (21). To exclude this possibility, the results of luciferase and qRT-PCR assays were confirmed using Wnt1-transduced STF cells (not shown). In addition, Western blot analysis of Wnt1-producing STF cells showed that monensin treatment decreased the cellular levels of β-catenin, including the presumably transcriptionally active forms of the protein either nonphoshorylated at the N-terminus (non-P-β-CATENIN) or containing the phosphorylated serine residue at position 675 (P-S675-β-CATENIN; ref. 22). Reduction in the production of the AXIN2 protein was also observed, indicating that monensin did not inhibit tankyrase (14). In contrast, monensin had no effect on the cellular levels of nuclear Wnt signaling effector TCF4 (Fig. 2D).
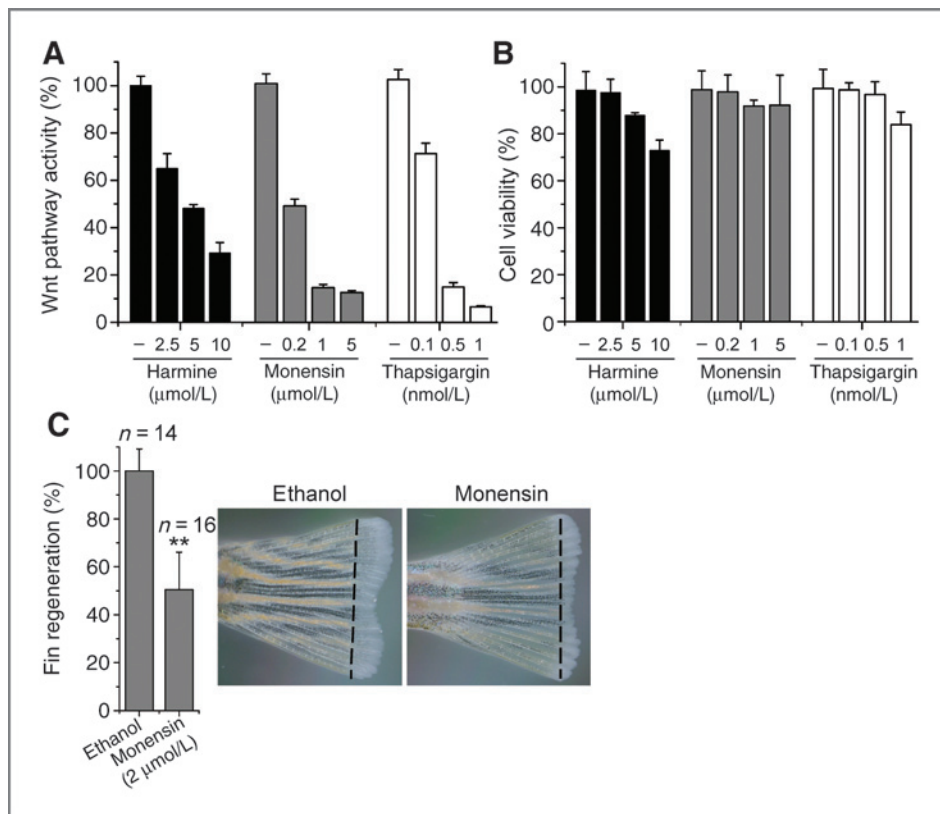
Figure 1. Monensin inhibits the SuperTOPFLASH reporter and suppresses tail fin regeneration. A, luciferase reporter assay in Wnt3a-stimulated STF cells. The reporter activity in cells treated with Wnt3a and vehicle (DMSO) was arbitrarily set to 100%. B, results of the cell viability test. The histograms represent mean values of triplicate experiments; SDs are shown by error bars. C, monensin blocks the zebrafish tail fin regeneration. The amputation plane is indicated by a dashed line. The average area of regrown fins obtained in control experiment was arbitrarily set to 100%; error bars, SD. **, $P < 0.01$ (Student t test); n, number of examined animals.

To identify the molecular mechanism of the monensin action in more detail, we used GSK3 inhibitors BIO (23) and CHIR99021 (24) to trigger Wnt signaling. Monensin suppressed the activity of both compounds in STF and L cells (Fig. 3A and B; data not shown). In HEK293 cells, BIO increased the cellular levels of total and "active" non-P-β-CATENIN. Combined cell treatment with BIO and monensin caused a moderate decrease in all tested β-catenin forms (Fig. 3C and Supplementary Fig. S1). We noted that monensin antagonized GSK3 inhibitors less efficiently than the signaling initiated by Wnt ligands, indicating that monensin "hits" the Wnt pathway upstream and at the level (or downstream) of the β-catenin destruction complex. This conclusion was confirmed in STF cells displaying aberrant Wnt signaling after disruption of the *APC* gene induced by transcription activator-like effector nucleases (Supplementary Fig. S2). One of the proximal events of Wnt signaling is phosphorylation of cytoplasmic protein Dvl followed by phosphorylation of Wnt coreceptor LRP (25). Immunoblotting of HEK293 cells revealed that the phoshorylation of Dvl was not influenced by monensin (Supplementary Fig. S3); however, the compound blocked the phoshorylation of LRP6 and induced its degradation (Fig. 3D). To determine which protein kinase is inhibited by monensin, selectivity profiling was performed. Nevertheless, none of the 50 enzymes representing the main protein kinase families was affected by monensin (Supplementary Table S2).

We next tested whether monensin inhibits Wnt-induced dorsalization of Xenopus embryos. Injection of *XWnt8* with vehicle alone resulted in 65.9% embryos with a duplicated body axis. In contrast, coinjection of *XWnt8* with monensin caused a significant ($P = 0.002$) decrease in the proportion of dorsalized animals to 30.7%. Interestingly, monensin also reduced the secondary body axis formation initiated by β-*catenin* mRNA (Fig. 3E). In agreement with the results obtained in Xenopus embryos, in STF cells monensin suppressed the transcription activity of wild-type (wt) β-catenin. Strikingly, monensin also inhibited stable forms of β-catenin mutated at the N-terminal regulatory residues but had no effect on transcription induced by the Lef1-VP16 fusion protein (Fig. 3F).

Disruption of intracellular pH homeostasis suppresses paracrine Wnt signaling; moreover, inhibition of vacuolar acidification interferes with Wnt secretion (26). Because monensin acts as a ionophore blocking cellular acidification, we compared its effect on Wnt signaling with bafilomycin A, a compound disrupting vacuolar acidification through pharmacologic inhibition of V-ATPase (27). In contrast with monensin, bafilomycin inhibited the signaling activity of the recombinant and ectopically expressed Wnt ligand, but the inhibitor was not effective against signaling stimulated by β-catenin or constitutively active LRP6 (ΔN-LRP6; Supplementary Fig. S4). Taken together, these results provided evidence that monensin
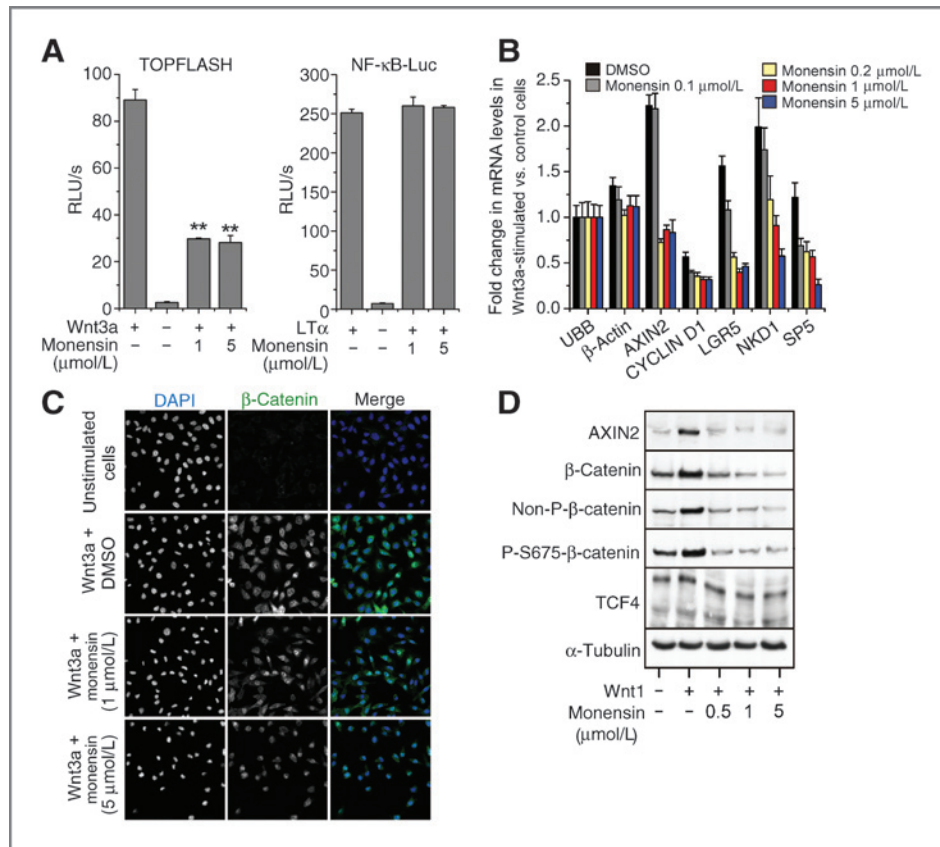
Figure 2. The inhibitory effect of monensin is specific for Wnt signaling. A, luciferase reporter assays in HEK293. Cells transfected with the indicated reporters were stimulated with recombinant Wnt3a or LTα (10 ng/mL), respectively, and grown with vehicle or monensin. The histograms represent average luciferase light units per second (RLU/second) of a triplicate corrected for the efficiency of transfection using *Renilla* luciferase as the internal control; **, $P < 0.01$. B, qRT-PCR analysis. HEK293 cells treated with vehicle or monensin were stimulated with Wnt3a and analyzed 20 hours later. The levels of input cDNAs were normalized to the *UBIQUITIN B* (*UBB*) housekeeping gene. The expression level of the respective gene in unstimulated cells was arbitrarily set to 1. C, monensin suppresses accumulation of β-catenin in mouse L cells. Microscopy images of cells stained with an anti-β-catenin monoclonal antibody (green) or 4′,6-diamidino-2-phenylindole dihydrochloride (DAPI) nuclear stain (blue). Original magnification, ×630. D, immunoblotting analysis of STF cells transduced with Wnt1-expressing lentivirus; cells were grown with vehicle or monensin for 20 hours; non-P-β-CATENIN, β-catenin unphosphorylated at S33, S37, and T41; P-S675-β-CATENIN, β-catenin phosphorylated at S675; α-TUBULIN, loading control. Densitometric analysis of the Western blot analyses is given in Supplementary Fig. S1A.

specifically antagonized the Wnt signaling pathway at the LRP and β-catenin levels.

Monensin attenuates aberrant Wnt signaling in human colorectal carcinoma cells

The effect of monensin was investigated in four colorectal carcinoma-derived cell lines. SW480 and COLO320 cells are *APC* deficient, whereas LS174T and HCT116 cells contain intact APC but produce stabilized S45A and ΔS45 β-catenin proteins, respectively (28). Interestingly, monensin decreased the activity of the TOPFLASH reporter and the expression of Wnt signaling target genes in SW480, COLO320, and LS174T cells but not in HCT116 cells (Fig. 4A and B; Supplementary Table S3; Supplementary Fig. S5A). Microscopy supported this finding, showing reduced anti-β-catenin staining in monensin-treated SW480, COLO320, and LS174T cells. No reduction in the anti-β-catenin signal was observed in HCT116 cells, although the treated cells

gained a spindle-like shape (Fig. 4C and Supplementary Fig. S5B). Using immunoblotting, we detected a decrease in all forms of β-catenin in SW480 cells. In the other colorectal carcinoma-derived cells, the decrease in the stability of different β-catenin forms was moderate (COLO320 and HCT116 cells) or negligible (LS174T cells; Fig. 4D and Supplementary Fig. S5C). We noted a discrepancy between clear reduction of the β-catenin signal as documented by microscopy and rather moderate changes in the β-catenin levels obtained by immunoblotting. The phenomenon was not associated with the specificity of the monoclonal antibody because another two anti-β-catenin monoclonal antibodies displayed a similar variation in the β-catenin detection (data not shown). The observed discrepancy possibly reflects differences in the robustness of these two readouts, and monensin to some extent promoted β-catenin degradation in three (SW480, COLO320, and LS174T) out of four colorectal carcinoma cells tested.
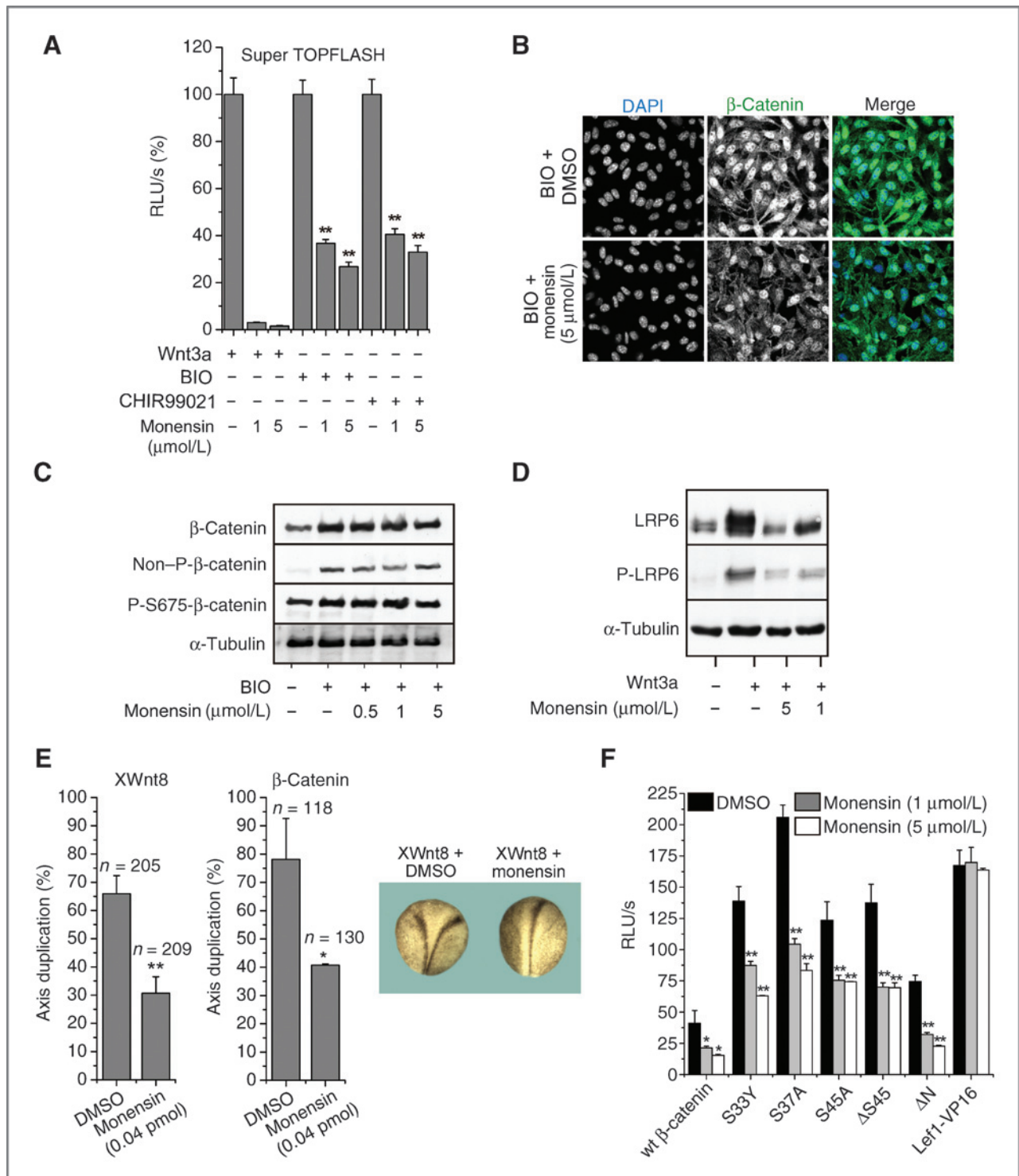
Figure 3. Monensin suppresses Wnt signaling initiated by GSK3 inhibitors and ectopic β-catenin. A, luciferase reporter assays in STF cells stimulated with recombinant Wnt3a or GSK3 inhibitors BIO (1 μmol/L) and CHIR99021 (3 μmol/L); error bars, SDs. B, fluorescent microscopy images of L cells treated overnight with BIO in combination with vehicle or monensin. C, immunoblotting of lysates obtained from STF cells stimulated overnight with BIO in combination with vehicle or monensin. Densitometric analysis of the Western blot analyses is given in Supplementary Fig. S1B. D, monensin reduces the protein level and phosphorylation of the Wnt coreceptor LRP6 in HEK293 cells; P-LRP6, LRP6 phosphorylated at S1490. E, monensin reduces double axis formation in Xenopus embryos; representative images of embryos are shown at the right. *n*, total number of injected embryos; error bars, SEM. F, results of the luciferase reporter assays performed in STF cells transfected with the indicated β-catenin–expressing constructs. S33Y, S37A, S45A, stable β-catenin with the amino acid changes at the serine residue in positions 33, 37, and 45; ΔS45, S45 deleted; ΔN, the N-terminally truncated variant of β-catenin; Lef1-VP16, Lef1 lacking the N-terminal β-catenin–interaction domain fused to the transcription transactivation domain of herpes simplex virus protein VP16; *, $P < 0.05$; **, $P < 0.01$.

Figure 4. Differential sensitivity of SW480 and HCT116 colorectal carcinoma cells to monensin. A, monensin inhibits the activity of the TOPFLASH reporter in SW480 but not in HCT116 cells. *, $P < 0.05$; error bars, SD. B, qRT-PCR analysis of cells treated with vehicle or monensin for 36 hours before harvesting. The expression level of the respective gene in unstimulated cells was arbitrarily set to 1. C, fluorescent microscopy images of SW480 and HCT116 cells treated with vehicle or monensin for 36 hours; original magnification, ×400. D, immunoblot analyses of SW480 and HCT116 cells incubated for 36 hours with DMSO or monensin. Densitometric analysis of the Western blot analyses is given in Supplementary Fig. S1C. E, cell proliferation assay. The ^{3}H-thymidine counts in cells cultured with vehicle (DMSO) was arbitrarily set to 100%. F, impedance-based measurement of growth and dimensional changes of SW480 and HCT116 cells treated with monensin or vehicle. G, monensin does not induce apoptosis of colorectal carcinoma cells. TRAIL-sensitive RKO colorectal carcinoma cells were also included in the test. The assay was performed in triplicate; the average luminescence units (LU)/second are shown; error bars, SD.
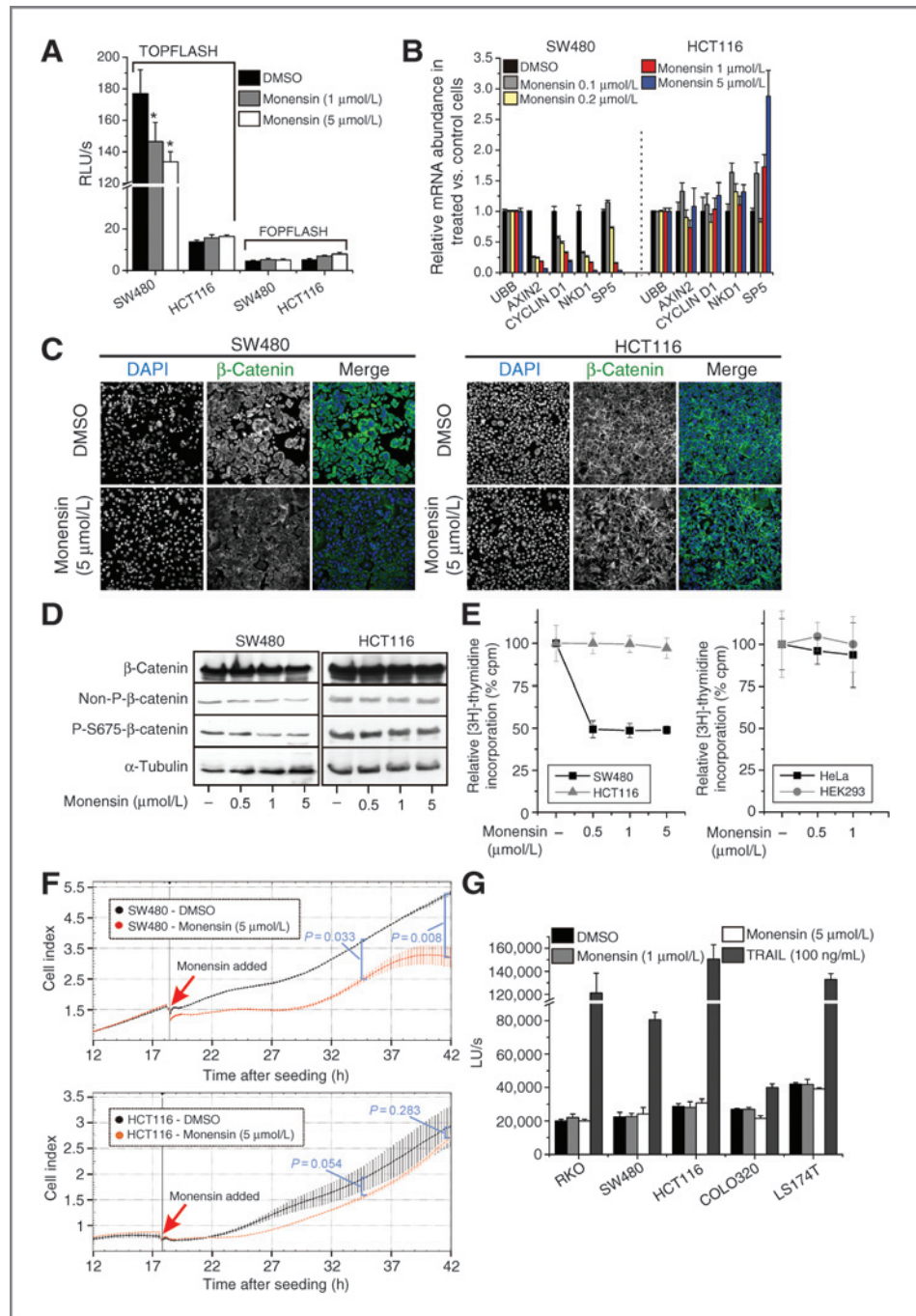
Cell proliferation assays in SW480 and COLO320 cells revealed more than 50% decrease in [^{3}H]-thymidine incorporation in cultures with monensin when compared with controls treated with DMSO alone. The proliferation rate of LS174T cells was affected by monensin to a lesser extent; nevertheless, the antibiotic caused 25% decline in [^{3}H]-thymidine counts. No substantial changes in proliferation of HCT116 and Wnt "signaling inactive" HEK293 and HeLa cells were recorded (Fig. 4E and Supplementary Fig. S5D). Subsequently, cell-cycle analysis showed that

monensin reduced the fraction of SW480 cells in S and G$_2$–M phases. Conversely, the cell fraction in G$_1$ phase was increased (Supplementary Table S4). In addition, we used the xCELLigence system to gain continuous information about the cell growth, death, and morphological changes of SW480 and HCT116 cells. As shown in Fig. 4F, monensin significantly influenced the cell index (this parameter depends on the number and dimensional changes of attached cells) of SW480 cells. In HCT116, the cell index fluctuations were possibly attributed to the

changes in cellular shape because monensin did not induce apoptosis in any of the colorectal carcinoma cells tested (Fig. 4G). In prostate cancer cells, monensin treatment reduced the amount of androgen receptor mRNA and elevated oxidative stress (29). However, monensin did not increase the levels of reactive oxygen species (ROS) in HEK293 and SW480 cells (Supplementary Fig. S6); thus, we could exclude that its effect on Wnt signaling was indirectly mediated by changes in the intracellular ROS concentration.

The insensitivity of HCT116 cells to monensin was peculiar as LS174T cells, which also express mutant β-catenin, were sensitive to the antibiotic. Interestingly, HCT116 cells show considerably less TOPFLASH activity than other colorectal carcinoma cells carrying APC truncations or β-catenin mutations (Fig. 4A; ref. 28). Moreover, in HCT116 cells, β-catenin is mainly associated with the cellular membrane (Supplementary Fig. S7). Recently, several studies documented that β-catenin localization or intracellular concentration can be regulated by several kinases, including RAF1, c-*Jun* NH$_2$-terminal kinase 2, AKT, protein kinase A (PKA), and P21-activated kinase 1 (22, 30–33). We therefore evaluated the effect of monensin on the phosphorylation of β-catenin. The endogenous protein was precipitated from control and monensin-treated SW480 and HCT116 cells, and phosphorylated peptides were determined using liquid chromatography/tandem mass spectrometry (LC/MS–MS). The analysis revealed that β-catenin is indeed phosphorylated at S191 (HCT116 cells only), S552, and S675; however, the observed modifications did not change in monensin-sensitive SW480 cells upon the treatment (Supplementary Table S5). Because acetylation influences β-catenin stability and transcriptional activity (34), the impact of monensin on β-catenin acetylation was also determined. Nevertheless, the extent of β-catenin acetylation did not change in the cells cultured with monensin (Supplementary Fig. S8).

Monensin reduces tumor size in the APC$^{+/Min}$ mouse model of intestinal cancer

The possible antitumor activity of monensin was analyzed in Apc$^{+/Min}$ mice. The mice harbor a truncation mutation in one allele of the *Apc* gene, and all adult animals eventually develop large amounts of intestinal polyps and die of cancer (35). The initial daily oral applications of monensin (dose 10 mg/kg) started at the weaning age. Animals in the control group received vehicle (DMSO) only. No effect on body weight was noticed throughout the experiment and individuals in both groups were steadily gaining weight as they were reaching sexual maturity (not shown). After six weeks, the mice were sacrificed and the dissected intestines were embedded in paraffin and sectioned. Immunohistochemical staining showed elevated production of β-catenin in neoplastic lesions found mainly in the small intestine (Fig. 5A). Stained tumors contrasted with the healthy mucosa enabled quantitative analysis of the tumor size and num-

bers using the image analysis software Ellipse (14). Although the numbers of tumors did not change substantially, a significant ($P = 0.0144$) reduction in the average size of lesions was observed in monensin-treated Apc$^{+/Min}$ mice when compared with control animals (mean 0.199 mm^2 vs. 0.299 mm^2). Consequently, the total tumor area estimated in one animal was decreased in individuals receiving monensin (mean 10.16 mm^2 vs. 16.46 mm^2; $P = 0.0125$; Fig. 5B). The inhibitory effect of monensin on the tumor growth was also observed in the second experiment, in which the compound (or vehicle) was administered to paired adult animals at various ages (Fig. 5C). Interestingly, the proportion of proliferating cells positive for the Ki-67 or proliferating cell nuclear antigen marker did not change in adenomas exposed to monensin (Fig. 5D, c and d' and Supplementary Fig. S9). However, monensin treatment increased the numbers of apoptotic cells and cells expressing the p21 cell-cycle inhibitor at the surface area of the neoplastic outgrowths (Fig. 5D, e–h'). This indicated that the smaller size of lesions in monensin-treated APC$^{+/Min}$ mice was related to the cell-cycle arrest and/or cell death at the tumor periphery. Importantly, no changes in the cell proliferation, differentiation, and tissue architecture in the healthy parts of mucosa were noted after exposure to monensin (Fig. 5E, i–l).

Discussion

Monensin belongs to the group of natural carboxylic polyether ionophores (36). The ionophoric antibiotics, the group currently includes more than 100 compounds, are studied mainly for their antibacterial, antifungal, and antiparasitic biologic activity (9). Monensin was approved by the U.S. Food and Drug Administration for use in veterinary practice as a coccidiostat in poultry and growth-promoting agent in cattle (New Animal Drug Application No. 95-735). The antibiotic increased dairy cattle milk production with no negative side effects on the animal health or reproduction (37, 38). Stimulation of growth in ruminants is associated with changes in intestinal microflora that lead to increased amounts of digestible proteins (39). Monensin antibacterial and antiparasitic activity is related to the intracellular changes in pH and sodium–potassium balance that can result in cell death (40). Several recent studies have demonstrated that monensin inhibits growth and induces apoptosis of cells derived from renal, prostate, and colon carcinoma (29, 41, 42). In addition, monensin induced cell-cycle arrest of acute myelogenous leukemia and lymphoma cells (43, 44). In glioma cells, monensin provoked endoplasmic reticulum stress and sensitized these cells to TRAIL-induced apoptosis (45). According to our results, monensin antagonized the Wnt signaling cascade at multiple levels involving LRP6 and β-catenin. Interestingly, a similar "mode of action" was described for other potassium ionophores salinomycin and nigericin in chronic lymphocytic leukemia

Figure 5. Monensin treatment decreases the size of adenomas in APC$^{+/Min}$ mice. A, hematoxylin and anti-β-catenin–stained sections of the jejunum of APC$^{+/Min}$ mice. Tumors are indicated by black arrowheads. B and C, quantification of the tumor size and count in the ileum of vehicle- and monensin-treated APC$^{+/Min}$ mice; the treatment started either in 4-week-old animals just after weaning (B) or in adult animals 7 to 22 weeks of age (C). The total tumor area determined in each individual is indicated in the boxplots. The boxed areas correspond to the second and third quartiles; the spread of the values is given by "whiskers" above and below each box. Median (transverse line) and mean (cross) is marked inside each box; statistical significance was determined using Student (B) or paired (C) t test; *, $P < 0.05$; error bars, SD. D, detection of proliferation marker Ki-67 (c and d), cell-cycle inhibitor p21 (e and f), and apoptotic cells (TACS; g and h) in the small intestinal tumors. Detailed images are shown in panels c′, d′, e′, f′, g′, and h′. E, phenotype of healthy parts of the small intestine is not affected by monensin. The specimens were stained with Ki-67 (i and k) and cytokeratin 20 (Krt20; j and l) to label proliferating cells in the crypts and terminally differentiated epithelial cells on the villi, respectively. Bar, 0.5 mm (a and b), 0.15 mm (a′, b′, c, d, e, f, g, and h), 0.08 mm (i, j, k, and l), 0.05 mm (c′, d′, e′, f′, g′, and h′).
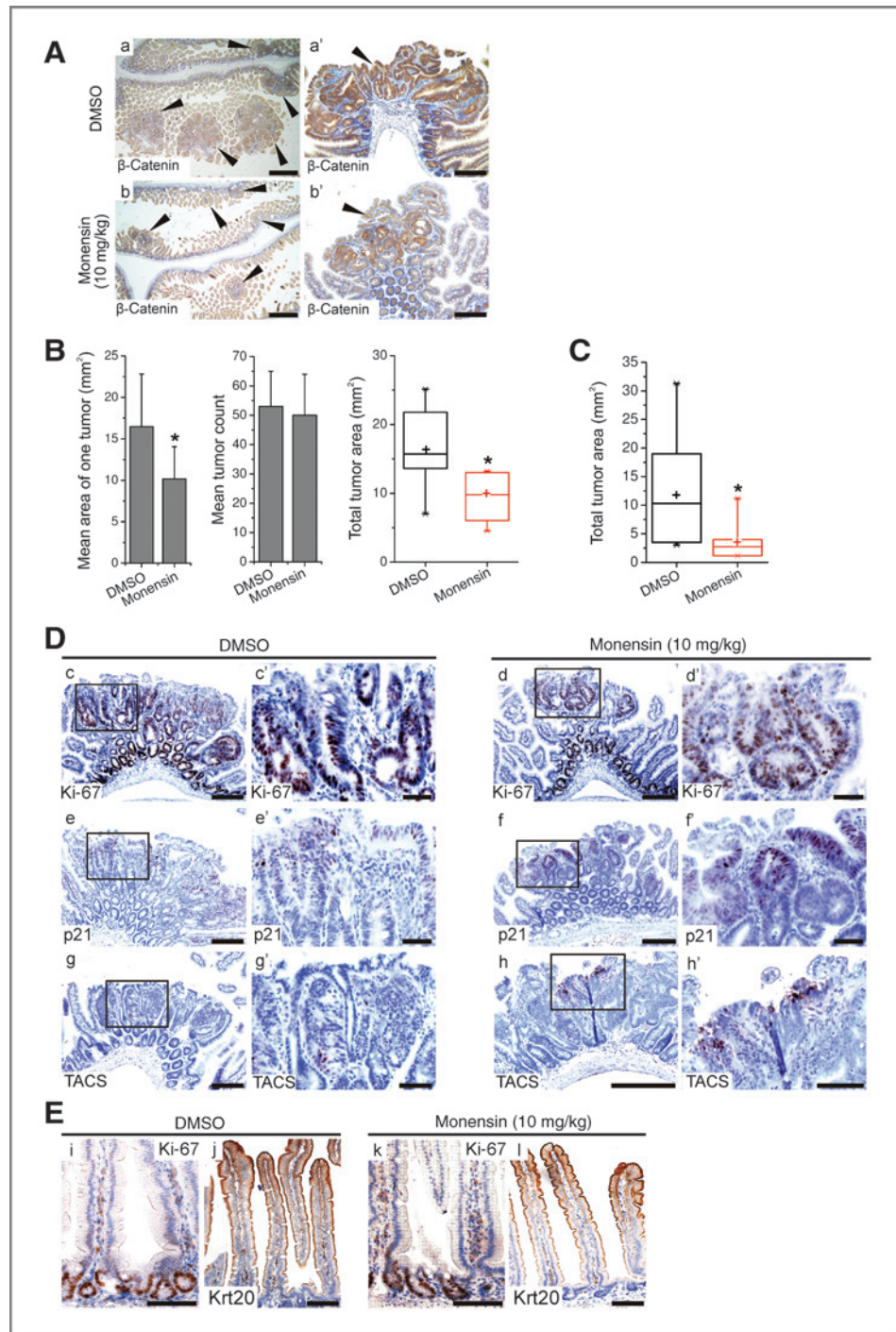
cells (46). However, the detailed inhibitory mechanism of these antibiotics on the Wnt signaling pathway has not been identified.

Protein phosphorylation is the key modification in virtually all signaling cascades. Therefore, we performed kinase selectivity profiling, but no conclusive result was obtained. This would imply that (i) the monensin action is highly specific and monensin-sensitive kinase was not included in the test, (ii) the selected concentrations of the antibiotic were too low to elicit any effect in this particular type of experiment, and (iii) the monensin action is not related to the inhibition of any protein kinase. The last possibility seems to be most likely, at least in relation to β-catenin, because LC/MS-MS analysis did not identify any phosphorylation sites that changed in monensin-sensitive SW480 cells.

In APC$^{+/Min}$ mice, monensin suppressed tumor growth without any noticeable negative impact on healthy mucosa. In the treated animals, the size of neoplastic lesions was decreased, but the average number of tumors remained unchanged. This result indicated that monensin inhibited tumor progression rather than the tumor initiation process. The conclusion was confirmed by immunohistochemical staining that showed markers of cell-cycle arrest and apoptosis at the surface of neoplastic outgrowths. In colorectal carcinoma cells, this proapoptotic activity of monensin was not observed, presumably due to the genetic alterations impairing cell death-inducing mechanisms (47).

In HCT116 cells, β-catenin displayed clear membrane localization; however, in LS174T cells, the protein was detected not only at the cellular membrane, but also in the cytoplasm and nucleus. As reported previously, the level of aberrant TCF/β-catenin–driven transcription depends on mutations in the genome of colorectal carcinoma cells. Cells expressing "short" APC mutants lacking the nuclear export signals exhibit high activity of the TOPFLASH reporter when compared with cells with wt *APC* but mutant β-*catenin* (28). HCT116 cells harbor one wt and one mutant (ΔS45) allele of β-catenin, whereas LS174T are homozygous for *missense* mutations (S45A) in the same triplet of the gene. This implies that subcellular distribution of β-catenin is related to the partially retained ability of HCT116 cells to regulate Wnt/β-catenin signaling. Nevertheless, because both mutant alleles (i.e., ΔS45 and S45A) are inhibited by monensin in reporter gene assays, the reason why HCT116 and LS174T cells display differential sensitivity to monensin is unclear. We suggest that particular cellular "wiring" of various signaling pathways or networks can contribute to the response of the respective cell to monensin.

Despite some prevailing uncertainties about the detailed inhibitory mechanism of monensin, our data imply that the antibiotic might be used as an anticancer drug, especially in neoplasia displaying aberrant Wnt signaling.

Disclosure of Potential Conflicts of Interest

No potential conflicts of interest were disclosed.

Authors' Contributions

Conception and design: P. Bartunek, V. Korinek
Development of methodology: A.R. Pombinho, P. Bartunek, V. Korinek
Acquisition of data (provided animals, acquired and managed patients, provided facilities, etc.): L. Tumova, A.R. Pombinho, M. Vojtechova, J. Stancikova, D. Gradl, M. Krausova, E. Sloncova, M. Horazna, V. Kriz, O. Machonova, Z. Zdrahal, V. Korinek
Analysis and interpretation of data (e.g., statistical analysis, biostatistics, computational analysis): L. Tumova, A.R. Pombinho, D. Gradl, Z. Zdrahal, V. Korinek
Writing, review, and/or revision of the manuscript: L. Tumova, V. Korinek
Administrative, technical, or material support (i.e., reporting or organizing data, constructing databases): J. Jindrich, P. Bartunek
Study supervision: P. Bartunek, V. Korinek

References

1. Clevers H, Nusse R. Wnt/beta-catenin signaling and disease. Cell 2012;149:1192–205.
2. Polakis P. Wnt signaling in cancer. Cold Spring Harb Perspect Biol 2012;4.
3. Valenta T, Hausmann G, Basler K. The many faces and functions of beta-catenin. Embo J 2012;31:2714–36.
4. Siegel R, Naishadham D, Jemal A. Cancer statistics, 2012. CA Cancer J Clin 2012;62:10–29.
5. Kinzler KW, Nilbert MC, Su LK, Vogelstein B, Bryan TM, Levy DB, et al. Identification of FAP locus genes from chromosome 5q21. Science 1991;253:661–5.
6. Kinzler KW, Vogelstein B. Lessons from hereditary colorectal cancer. Cell 1996;87:159–70.
7. Morin PJ, Sparks AB, Korinek V, Barker N, Clevers H, Vogelstein B, et al. Activation of beta-catenin-Tcf signaling in colon cancer by mutations in beta-catenin or APC. Science 1997;275:1787–90.
8. Korinek V, Barker N, Morin PJ, van Wichen D, de Weger R, Kinzler KW, et al. Constitutive transcriptional activation by a beta-catenin-Tcf complex in APC−/− colon carcinoma. Science 1997;275:1784–7.
9. Huczynski A, Janczak J, Lowicki D, Brzezinski B. Monensin A acid complexes as a model of electrogenic transport of sodium cation. Biochim Et Biophys Acta 2012;1818:2108–19.
10. Xu Q, Wang Y, Dabdoub A, Smallwood PM, Williams J, Woods C, et al. Vascular development in the retina and inner ear: control by Norrin and Frizzled-4, a high-affinity ligand-receptor pair. Cell 2004; 116:883–95.
11. Lukas J, Mazna P, Valenta T, Doubravska L, Pospichalova V, Vojtechova M, et al. Dazap2 modulates transcription driven by the Wnt effector TCF-4. Nucleic Acids Res 2009;37:3007–20.
12. Willert K, Brown JD, Danenberg E, Duncan AW, Weissman IL, Reya T, et al. Wnt proteins are lipid-modified and can act as stem cell growth factors. Nature 2003;423:448–52.
13. Urcan E, Haertel U, Styllou M, Hickel R, Scherthan H, Reichl FX. Real-time xCELLigence impedance analysis of the cytotoxicity of dental composite components on human gingival fibroblasts. Dent Mater 2010;26:51–8.
14. Waaler J, Machon O, Tumova L, Dinh H, Korinek V, Wilson SR, et al. A novel tankyrase inhibitor decreases canonical Wnt signaling in colon carcinoma cells and reduces tumor growth in conditional APC mutant mice. Cancer Res 2012;72:2822–32.
15. Doubravska L, Krausova M, Gradl D, Vojtechova M, Tumova L, Lukas J, et al. Fatty acid modification of Wnt1 and Wnt3a at serine is prerequisite for lipidation at cysteine and is essential for Wnt signalling. Cell Signal 2011;23:837–48.

16. Gradl D, Kuhl M, Wedlich D. Keeping a close eye on Wnt-1/wg signaling in Xenopus. Mech Dev 1999;86:3–15.
17. Hawcroft G, D'Amico M, Albanese C, Markham AF, Pestell RG, Hull MA. Indomethacin induces differential expression of beta-catenin, gamma-catenin and T-cell factor target genes in human colorectal cancer cells. Carcinogenesis 2002;23:107–14.
18. Lu D, Carson DA. Spiperone enhances intracellular calcium level and inhibits the Wnt signaling pathway. BMC Pharmacol 2009;9:13.
19. Waki H, Park KW, Mitro N, Pei L, Damoiseaux R, Wilpitz DC, et al. The small molecule harmine is an antidiabetic cell-type-specific regulator of PPARgamma expression. Cell Metab 2007;5:357–70.
20. Stoick-Cooper CL, Weidinger G, Riehle KJ, Hubbert C, Major MB, Fausto N, et al. Distinct Wnt signaling pathways have opposing roles in appendage regeneration. Development 2007;134:479–89.
21. Morrell NT, Leucht P, Zhao L, Kim JB, ten Berge D, Ponnusamy K, et al. Liposomal packaging generates Wnt protein with in vivo biological activity. PLoS ONE 2008;3:e2930.
22. Zhu G, Wang Y, Huang B, Liang J, Ding Y, Xu A, et al. A Rac1/PAK1 cascade controls beta-catenin activation in colon cancer cells. Oncogene 2012;31:1001–12.
23. Meijer L, Skaltsounis AL, Magiatis P, Polychronopoulos P, Knockaert M, Leost M, et al. GSK-3-selective inhibitors derived from Tyrian purple indirubins. Chem Biol 2003;10:1255–66.
24. Ring DB, Johnson KW, Henriksen EJ, Nuss JM, Goff D, Kinnick TR, et al. Selective glycogen synthase kinase 3 inhibitors potentiate insulin activation of glucose transport and utilization in vitro and in vivo. Diabetes 2003;52:588–95.
25. Bernatik O, Ganji RS, Dijksterhuis JP, Konik P, Cervenka I, Polonio T, et al. Sequential activation and inactivation of Dishevelled in the Wnt/beta-catenin pathway by casein kinases. J Biol Chem 2011;286:10396–410.
26. Coombs GS, Yu J, Canning CA, Veltri CA, Covey TM, Cheong JK, et al. WLS-dependent secretion of WNT3A requires Ser209 acylation and vacuolar acidification. J Cell Sci 2010;123:3357–67.
27. Cruciat CM, Ohkawara B, Acebron SP, Karaulanov E, Reinhard C, Ingelfinger D, et al. Requirement of prorenin receptor and vacuolar H+-ATPase-mediated acidification for Wnt signaling. Science 2010;327:459–63.
28. Rosin-Arbesfeld R, Cliffe A, Brabletz T, Bienz M. Nuclear export of the APC tumour suppressor controls beta-catenin function in transcription. Embo J 2003;22:1101–13.
29. Ketola K, Vainio P, Fey V, Kallioniemi O, Iljin K. Monensin is a potent inducer of oxidative stress and inhibitor of androgen signaling leading to apoptosis in prostate cancer cells. Mol Cancer Ther 2010;9:3175–85.
30. Phelps RA, Chidester S, Dehghanizadeh S, Phelps J, Sandoval IT, Rai K, et al. A two-step model for colon adenoma initiation and progression caused by APC loss. Cell 2009;137:623–34.
31. Wu X, Tu X, Joeng KS, Hilton MJ, Williams DA, Long F. Rac1 activation controls nuclear localization of beta-catenin during canonical Wnt signaling. Cell 2008;133:340–53.
32. Hino S, Tanji C, Nakayama KI, Kikuchi A. Phosphorylation of beta-catenin by cyclic AMP-dependent protein kinase stabilizes beta-catenin through inhibition of its ubiquitination. Mol Cell Biol 2005;25:9063–72.
33. Fang D, Hawke D, Zheng Y, Xia Y, Meisenhelder J, Nika H, et al. Phosphorylation of beta-catenin by AKT promotes beta-catenin transcriptional activity. J Biol Chem 2007;282:11221–9.
34. Levy L, Wei Y, Labalette C, Wu Y, Renard CA, Buendia MA, et al. Acetylation of beta-catenin by p300 regulates beta-catenin-Tcf4 interaction. Mol Cell Biol 2004;24:3404–14.
35. Su LK, Kinzler KW, Vogelstein B, Preisinger AC, Moser AR, Luongo C, et al. Multiple intestinal neoplasia caused by a mutation in the murine homolog of the APC gene. Science 1992;256:668–70.
36. Kevin Ii DA, Meujo DA, Hamann MT. Polyether ionophores: broad-spectrum and promising biologically active molecules for the control of drug-resistant bacteria and parasites. Expert Opin Drug Discov 2009;4:109–46.
37. Beckett S, Lean I, Dyson R, Tranter W, Wade L. Effects of monensin on the reproduction, health, and milk production of dairy cows. J Dairy Sci 1998;81:1563–73.
38. Duffield T, Bagg R, Kelton D, Dick P, Wilson J. A field study of dietary interactions with monensin on milk fat percentage in lactating dairy cattle. J Dairy Sci 2003;86:4161–6.
39. Goren E, de Jong WA, Doornenbal P, Koopman JP, Kennis HM. Protection of chicks against Salmonella infantis infection induced by strict anaerobically cultured intestinal microflora. Vet Q 1984;6:22–6.
40. Mollenhauer HH, Morre DJ, Rowe LD. Alteration of intracellular traffic by monensin; mechanism, specificity and relationship to toxicity. Biochim Biophys Acta 1990;1031:225–46.
41. Park WH, Kim ES, Jung CW, Kim BK, Lee YY. Monensin-mediated growth inhibition of SNU-C1 colon cancer cells via cell cycle arrest and apoptosis. Int J Oncol 2003;22:377–82.
42. Park WH, Jung CW, Park JO, Kim K, Kim WS, Im YH, et al. Monensin inhibits the growth of renal cell carcinoma cells via cell cycle arrest or apoptosis. Int J Oncol 2003;22:855–60.
43. Park WH, Lee MS, Park K, Kim ES, Kim BK, Lee YY. Monensin-mediated growth inhibition in acute myelogenous leukemia cells via cell cycle arrest and apoptosis. Int J Cancer 2002;101:235–42.
44. Park WH, Seol JG, Kim ES, Kang WK, Im YH, Jung CW, et al. Monensin-mediated growth inhibition in human lymphoma cells through cell cycle arrest and apoptosis. Br J Haematol 2002;119:400–7.
45. Yoon MJ, Kang YJ, Kim IY, Kim EH, Lee JA, Lim JH, et al. Monensin, a polyether ionophore antibiotic, overcomes TRAIL resistance in glioma cells via endoplasmic reticulum stress, DR5 upregulation and c-FLIP downregulation. Carcinogenesis 2013;34:1918–28.
46. Lu D, Choi MY, Yu J, Castro JE, Kipps TJ, Carson DA. Salinomycin inhibits Wnt signaling and selectively induces apoptosis in chronic lymphocytic leukemia cells. Proc Natl Acad Sci U S A 2011;108:13253–7.
47. Vogelstein B, Kinzler KW. Cancer genes and the pathways they control. Nat Med 2004;10:789–99.

Mesenchymal Stem Cells Seeded on Cross-Linked and Noncross-Linked Acellular Porcine Dermal Scaffolds for Long-Term Full-Thickness Hernia Repair in a Small Animal Model

*Ondrej Mestak, †Eva Matouskova, ‡Zuzana Spurkova, ‡Kamila Benkova, *Pavel Vesely, *Jan Mestak, *Martin Molitor, §Antonio Pombinho, and **Andrej Sukop

*Department of Plastic Surgery, 1st Faculty of Medicine, Charles University in Prague, Bulovka Hospital; †Laboratory of Cell Biology, Prague Burn Centre, 3rd Faculty of Medicine, Charles University in Prague; ‡Department of Pathology, Bulovka Hospital; §Laboratory of Cell Differentiation, Institute of Molecular Genetics, Czech Academy of Sciences; and **Department of Plastic Surgery, 3rd Faculty of Medicine, Charles University in Prague, University Hospital Kralovske Vinohrady, Prague, Czech Republic

Abstract: Biological meshes are biomaterials consisting of extracellular matrix that are used in surgery particularly for hernia treatment, thoracic wall reconstruction, or silicone implant-based breast reconstruction. We hypothesized that combination of extracellular matrices with autologous mesenchymal stem cells used for hernia repair would result in increased vascularization and increased strength of incorporation. We cultured autologous adipose-derived stem cells harvested from the inguinal region of Wistar rats on cross-linked and noncross-linked porcine extracellular matrices. In 24 Wistar rats, a standardized 2×4 cm fascial defect was created and repaired with either cross-linked or noncross-linked grafts enriched with stem cells. Non-MSC-enriched grafts were used as controls. The rats were sacrificed at 3 months of age. The specimens were examined for the strength of incorporation, vascularization, cell invasion, foreign body reaction, and capsule formation. Both materials showed cellular ingrowth and neovascularization. Comparison of both tested groups with the controls showed no significant differences in the capsule thickness, foreign body reaction, cellularization, or vascularization. The strength of incorporation of the stem cell-enriched cross-linked extracellular matrix specimens was higher than in acellular specimens, but this result was statistically nonsignificant. In the noncross-linked extracellular matrix, the strength of incorporation was significantly higher in the stem cell group than in the acellular group. Seeding of biological meshes with stem cells does not significantly contribute to their increased vascularization. In cross-linked materials, it does not ensure increased strength of incorporation, in contrast to noncross-linked materials. Owing to the fact that isolation and seeding of stem cells is a very complex procedure, we do not see sufficient benefits for its use in the clinical setting. **Key Words:** Extracellular matrix—Scaffold—Acellular matrix—Biocompatibility—Animal model—Cross-linking—Hernia—Mesenchymal stem cells—Adipose-derived stem cells.

There are many materials used for tissue replacement in modern surgery including those derived from extracellular matrix (ECM). These biological meshes are derived from different human and animal tissues such as human dermis, porcine dermis, porcine small intestine submucosa, or bovine pericardium. The largest benefit of these materials is their ability of better vascularization and integration into the host tissue in comparison to synthetic materials (1–3). This increases the safety of mesh use in contaminated areas with large risk of synthetic mesh infection (4,5). ECMs are used particularly for hernia treatment (6–9), thoracic wall reconstruction, or silicone implant-based breast reconstruction (10). These biological meshes can be used without further processing (noncross-linked [non-CL] materials) or can be

cross-linked (CL) to make them more stable. However, cross-linking decreases the biocompatibility of the material and the strength of incorporation into host tissues (9).

Cross-linking can also deteriorate potential penetration of cells, including stem cells, into the biomaterial. Stem cells are cells that have potential of differentiating into different cell lines. There are two basic types of stem cells—embryonic and adult stem cells. Adult stem cells play a crucial role in evolution and progress of regenerative medicine (11). They can be found in almost any tissue including skin, brain, or fat. By far, the most accessible and abundant tissue for stem cell harvesting is fat (12). In humans, it can be harvested by liposuction, or in small animals by excision, both with very low donor site morbidity. Autologous cells are the body's own and, therefore, they do not evoke any reaction. Sufficient numbers of cells can be easily cultivated from a relatively small amount of fat.

Stem cells have angiogenic properties, probably caused by secretion of cytokines (13). We therefore hypothesized that combining ECM with autologous mesenchymal stem cells (MSCs) from fat (adipose-derived stem cells [ADSCs]) used for hernia repair would result in increased vascularization and increased strength of incorporation compared with repairing hernias with acellular ECM. This would result in improved outcomes of clinical ventral hernia repairs in terms of infection and hernia recurrence.

So far, no study has evaluated the histological and mechanical properties of CL and non-CL ECM combined with ADSCs used for hernia repair. Both CL ECM and non-CL ECM are frequently used in surgery. As these materials differ in their ability for tissue ingrowth, we considered it beneficial to use both of them in our study and compare the influence of MSCs on their properties.

The standard test to confirm multipotency is the ability of the cells to differentiate into osteoblasts and adipocytes (and chondrocytes as well as myocytes, and possibly neuron-like cells) (14).

MATERIALS AND METHODS

This study was carried out in strict accordance with the recommendations of the Guide for the Care and Use of Laboratory Animals of the Ministry of Agriculture of the Czech Republic. The protocol was approved by the Committee on the Ethics of Animal Experiments of the 1st Faculty of Medicine, Charles University in Prague. All surgery was performed under anesthesia, and all efforts were made to minimize suffering.

ECMs used

We used non-CL ECM (Medicem Technology, Kamenne Zehrovice, Czech Republic) produced by harvesting split-thickness porcine skin grafts with a thickness of about 0.8 mm. Then, the material underwent trypsinization (0.3%) for cell removal, was dehydrated by desiccation attached to a glass substrate, and sterilized by gamma irradiation. We compared this non-CL ECM to commercially available CL ECM Permacol (Covidien, Dublin, Ireland). Permacol is one of the most widely used and well-studied surgical dermal scaffold materials (8,15,16). It is a porcine-derived acellular dermal scaffold manufactured by trypsinization (to remove all living cells), solvent extraction (to remove all lipid and fat deposits), gamma irradiation, and cross-linking using hexamethylene diisocyanate.

Isolation and cultivation of MSCs

Female Wistar rats ($n = 12$) weighing 340–400 g were anesthetized with an intramuscular injection of 50 mg/kg body weight Zoletil (Virbac Laboratories, Carros, France) 30 min before surgery. After shaving the inguinal area, incision was made, and a sample of fat around 1 cc was harvested. This sample was then transferred to our tissue engineering laboratory. The wound was sutured by interrupted sutures using Vicryl 3/0 (Ethicon, Inc., Somerville, NJ, USA). Adipose tissue was cut into small pieces and incubated for 1–2 h in 0.1% collagenase A (Roche, Basel, Switzerland) at 37°C. The digested tissue was disrupted by shaking and repeated pipetting. An excess (10-fold) of minimum essential medium Eagle with Hanks' salts (H-MEM; Sigma Aldrich, St. Louis, MO, USA) with 10% bovine serum was added, and the suspension was centrifuged at $500 \times g$ for 8 min. The resultant cell pellet was seeded into 25 cm^2 tissue culture flasks and cultured in the H-MEM medium enriched with nonessential amino acids, 0.12 g/L sodium pyruvate, 1 g/L NaHCO$_3$, 10% bovine serum, and 2% fetal bovine serum (MSC growth medium) at 37°C in an incubator with 3.5% CO$_2$. The medium was changed every 2–4 days, and passages were carried out at 70–90% confluence. Cells from the second passage were used for seeding on ECM. MSCs (passage 2) were seeded in the amount of 3×10^5 cells/dish with ECM or without ECM control. The cell layer on the dish was confluent in 4 days. There was no difference between growth in the medium containing ECM and control (no cytotoxicity was observed). A small thin piece of each ECM group was stained by May-Grünwald and Giemsa-Romanovski solutions to visualize the cells.

Identity control of MSCs

MSCs were cultured in the MSC growth medium enriched with growth factors for adipocyte and osteoblast differentiation (17). For adipocyte differentiation, dexamethasone (1 µM), IBMX (0.5 µM), insulin (10 µg/mL), and indomethacin (60 µM) were added into the medium. The cells were cultured for 5 days. MSCs in the third passage were cultured to subconfluence. The MSC medium was then replaced by adipocyte medium (changed every 2–3 days). After 5 days, the culture was stained by Oil Red O for histological assay. For osteoblast differentiation, dexamethasone (1 µM), ascorbic acid (50 µg/mL), and β-glycerophosphate (10 mM) were added. Cells were cultured for 2 weeks. MSCs in the third passage were cultured to confluence. The MSC medium was then replaced by osteoblast medium (changed every 3–4 days). After 16 days, the culture was stained by Alizarin Red S for calcium visualization.

Seeding of cultured MSCs onto ECM

Six pieces of non-CL-ECM and six pieces of CL-ECM measuring approx. 2×3 cm were placed individually in 60-mm culture dishes and bathed overnight in the MSC growth medium. MSCs (ADSC) were seeded next day in fresh medium in the amount of 3×10^5 cells/dish. The cells on ECM were cultured for 4 days. ECM with cells was used for the surgical procedure of hernia repair.

Surgical procedure

For hernia repair, the group of female Wistar rats used for fat harvesting (A; $n = 12$) and a control group of female Wistar rats (B; $n = 12$) were anesthetized with an intramuscular injection of 50 mg/kg body weight Zoletil (Virbac Laboratories) 30 min
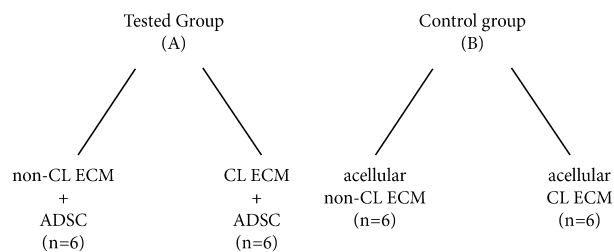
FIG. 1. Rats from the tested group (A) were randomly divided into two subgroups. The first subgroup ($n = 6$) received non-CL ECM seeded with MSCs for abdominal wall repair. The second subgroup ($n = 6$) received CL ECM seeded with MSCs for abdominal wall repair. Rats from the control group (B) were randomly divided into two subgroups as well. The first subgroup received non-MSC-enriched CL ECM for abdominal wall repair ($n = 6$). The second subgroup received non-MSC-enriched non-CL ECM for abdominal wall repair ($n = 6$).
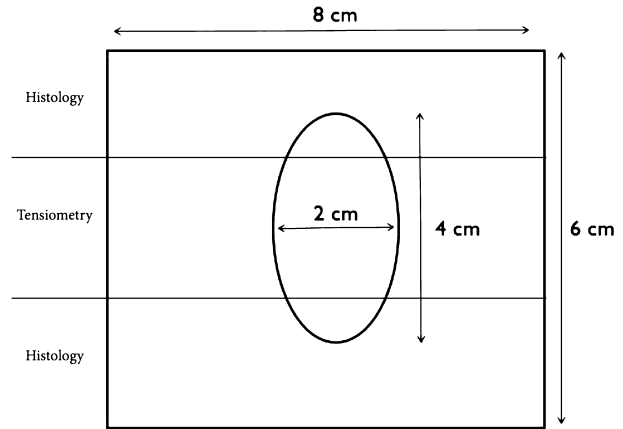
FIG. 2. A square block of abdominal wall measuring 8×6 cm was excised en bloc and divided into three parts. The ventral and dorsal parts were processed for histological evaluation. The middle part of the excision (15-mm wide strip) was transported for tensile testing.

before surgery. After shaving the abdominal area and treating with antibiotic solution, an abdominal midline incision (5 cm) through the skin and subcutaneous tissue was made. Carinal shape full-thickness excision (4×2 cm) of the abdominal wall was made. Materials were sutured to the edges of the abdominal wall defects as a patch using Prolene 4/0 (Ethicon, Inc.) continuous suture. Rats from the tested group were randomly divided into two subgroups. The first subgroup ($n = 6$) received non-CL-ECM seeded with MSCs for abdominal wall repair. The second subgroup ($n = 6$) received CL ECM seeded with MSCs for abdominal wall repair. Rats from the control group were randomly divided into two subgroups as well. The first subgroup received acellular CL ECM for abdominal wall repair ($n = 6$). The second subgroup received acelullar non-CL ECM for abdominal wall repair ($n = 6$) (Fig. 1). The wound was sutured by interrupted sutures using Vicryl 3/0 (Ethicon, Inc.). Postoperative analgesic treatment was provided by intramuscular application of Butomidor (Richter Pharma, Wels, Austria) 0.01 mg per rat. The postoperative course and observation period were without undesirable events.

All animals were sacrificed after 3 months by injection of ketamine 0.1 mL/100 g + medetomidine 0.01 mL/100 g intramuscularly and T61 3 mL/100 g intracardially. The incidence of herniation was evaluated. A square block of abdominal wall measuring 8×6 cm was excised en bloc and divided into three parts (Fig. 2). The ventral and dorsal parts were processed for histological evaluation. The middle part of the excision (15-mm wide strip) was transported in saline solution for tensile testing.

Cell/ reaction	Scoring				
	0	1	2	3	4
Implant cellularization	0	Rare, 1-5/phf	5-10/ phf	Heavy infiltrate	Packed
Leukocytes	0	Rare, 1-5/phf	5-10/ phf	Heavy infiltrate	Packed
Giant cells	0	Rare, 1-2/phf	3-5/ phf	Heavy infiltrate	Sheets
phf, per high powered field (400x)					

Histopathological scoring system: cell type/response

FIG. 3. Semiquantitative histopatholo-gical evaluation of each explant, as described in ISO 10993-6.

Reaction	Scoring				
	0	1	2	3	4
Neovascularization	0	Minimal capillary proliferation, focal 1-3 buds	Group of 4-7 capillaries with supporting fibroblastic structures	Broad band of capillaries with supporting structures	Extensive band of capillaries with supporting fibroblastic structures
Capsule thickness	0	Narrow band	Moderately thick band	Thick band	Extensive band

Histopathological scoring system: response

Histological examination

After explantation, tissue samples were fixed in formaldehyde and subjected to histological examination with hemotoxylin and eosin staining using an Olympus BX50 microscope (Olympus, Tokyo, Japan) with 40, 100, and $200 \times$ magnification. Semiquantitative histopathological evaluation of each explant was performed by the scoring system described in ISO 10993-6 (Fig. 3). The scores for microscopic evaluation of each parameter of each animal were added to obtain the sum for a group and divided by the number of animals in the group to obtain a test or reference group average. Samples were scored independently by two pathologists (KM and ZS).

Mechanical properties

The strength of incorporation was evaluated by Inspekt table 10 kN with 100 N load cell and Labmaster software (Hegewald & Peschke, Nossen, Germany). Preload 0.05 N and speed of crosshead travel 200 mm/min was set at the machine. The thickness of materials was evaluated by Mitutoyo ABSO-LUTE calipers (Mitutoyo, Inc., Kawasaki, Japan). Each specimen was oriented horizontally, with each end secured inside the grips. We evaluated the pull firmness and maximal breaking strength normalized for thickness, width, and cross-section of the strip and place of specimen rupture (implant, implant-tissue conjunction, and tissue). The degree of strength of incorporation (SOI) was expressed by several values. Maximum load was recorded in newtons (N). Tensile stress per unit width was determined by dividing the maximum load sustained by the material by the width of the specimen (N/mm). Tensile strength needed for specimen rupture was recorded in megapascals (MPa). The breaking strength was recorded as the maximum tension developed across the fascia-patch interface before rupture.

Statistical analysis

The data were analyzed statistically: quantitative data using the Wilcoxon test, and categorical data using the nonparametric Pearson's chi-square test, Mann–Whitney test, and Fisher's test.

RESULTS

Cell cultivation, differentiation, and identity control

The surface coverage by cells was about 50% in both materials examined after staining by May-Grünwald and Giemsa-Romanovski to visualize the cells.

Adipocyte differentiation: an accumulation of lipid-rich vacuoles was observed within the cells (Fig. 4). Eventually, the lipid vacuoles combined and filled the cells.

Osteoblast differentiation: the MSCs formed aggregates or nodules, which were stained positively by Alizarin Red S (Fig. 5).

Local findings after explantation

No seroma was found surrounding the materials. There were no hernias observed at the time of explantation in any group. There were no bowel adhesions in any group. We noticed only omentum adhesions to the peritoneal side of the material. The
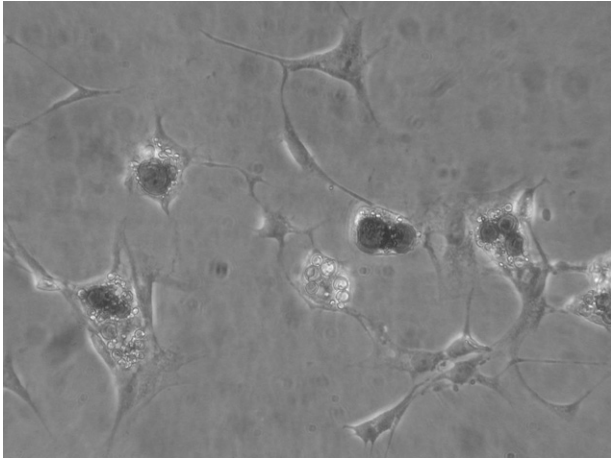
FIG. 4. MSCs were cultured in the adipocyte medium (MSC medium with addition of dexamethasone, insulin, isobutyl methylxanthine, and indomethacin) for 10 days. The cells were stained by Oil Red O. Accumulation of lipid (red) in vacuoles filling the cells is visible.

incidence of these adhesions was evenly distributed between both materials. All materials showed macroscopic evidence of early vascularization with blood vessels on both sides of the material. There were no signs of inflammation, fibrosis, calcification, or granulomatous reaction. Materials were stably ingrown in the subcutaneous tissues and abdominal wall. Non-CL ECM showed macroscopically significant degrading, looking like a thin, almost transparent membrane. CL ECM samples did not exhibit any macroscopic degradation throughout the entire study. Their appearance during the explantation was the same as at the time of implantation.

Histology

Both materials showed cellular ingrowth and neovascularization. Comparison of both tested groups with control groups did not show any significant differences in the capsule thickness, foreign body reaction, cellularization, or vascularization. Notably, the mean cellularization of 1.25 in the CL ECM non-MSC-enriched subgroup was higher than 1.167 in the MSC-enriched subgroup ($P = 0.375$). Vascularization in the CL ECM group was 1.75 in the non-MSC-enriched subgroup and only 1.167 in the MSC-enriched subgroup ($P = 0.375$). The mean capsule thickness in the CL ECM group was 0.33 in the non-MSC-enriched subgroup and 1 in the MSC-enriched subgroup ($P = 0.830$). Similarly as in the CL ECM group, the mean cellularization in non-CL ECM was higher in the non-MSC-enriched subgroup (2) than in the MSC-enriched subgroup (1.2, $P = 0.445$). Mean vascularization in the non-CL ECM group was 2 in

the non-MSC-enriched subgroup and 1.4 in the MSC-enriched subgroup ($P = 0.542$). The mean capsule thickness in the non-CL ECM group was 0.8 in the non-MSC-enriched subgroup and 1 in the MSC-enriched subgroup ($P = 0.638$) (Fig. 6).

Tensiometry

The place of rupture was evenly distributed between the implant, implant-tissue conjunction, and tissue.

SOI of the MSC-enriched CL ECM specimens was higher than that of the non-MSC-enriched CL ECM, but this result was statistically nonsignificant (0.59 MPa vs. 0.7 MPa, $P = 0.66$) (Fig. 7A). In the non-CL ECM group, there was a statistically significant difference between non-MSC-enriched ECM (0.75 MPa) and MSC-enriched ECM (3.37 MPa; $P = 0.018$) (Fig. 7A). This result might indicate better ingrowth of cells into the less compact material.

DISCUSSION

Biological meshes are materials that possess excellent biocompatibility and an ability to incorporate into host tissues. They undergo vascularization, which increases their resistance to infection. Their biostability can be increased by cross-linking. However, attempts of biological mesh producers to improve firmness by cross-linking deteriorate the biocompatibility and strength of attachment of the mesh to the host tissues. The materials are too compact for vessels and other host tissues to grow inside them, resulting in a weaker connection between the material and host tissues, for example, abdominal wall, and lesser resistance to infection.
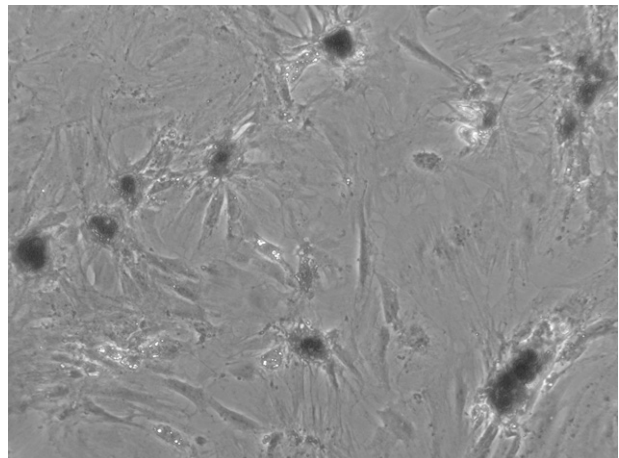
FIG. 5. MSCs were cultured in the osteoblast medium (MSC medium with addition of dexamethasone, ascorbic acid, and β-glycerophosphate) for 16 days. The cell clusters were positive for calcium, as visible by staining with Alizarin Red S.
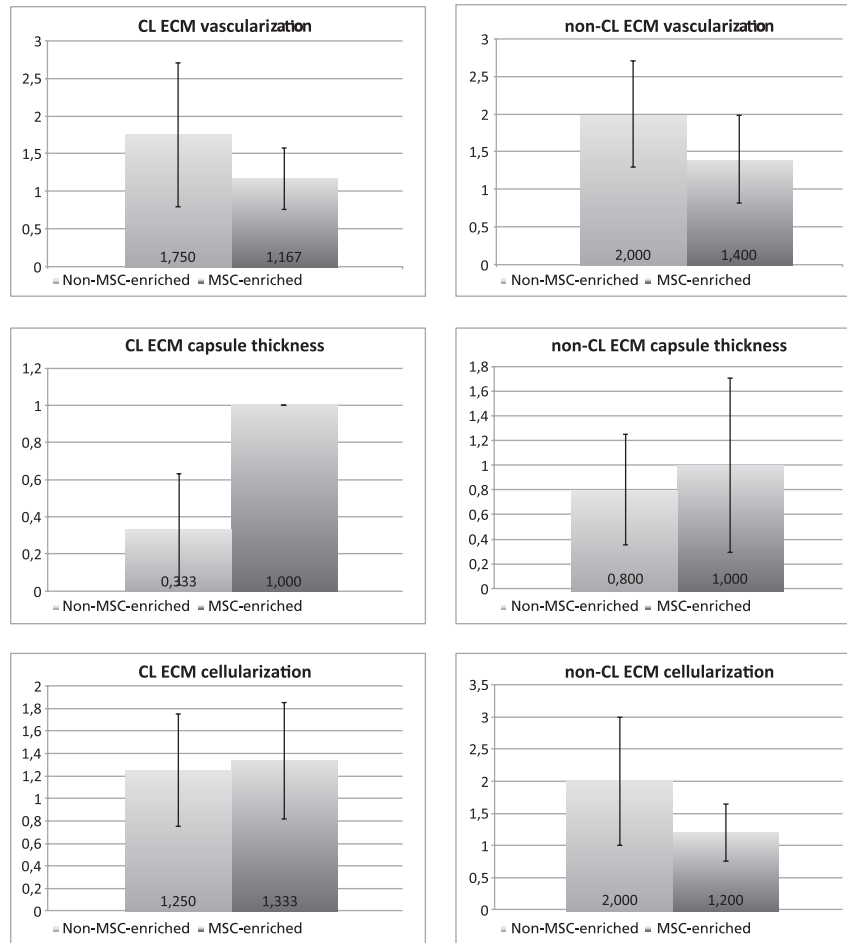
FIG. 6. Results of histological examination. Notably, mean cellulization of 1.25 in the cross-linked extracellular matrix (CL ECM) non-MSC-enriched subgroup was higher than 1.167 in the MSC-enriched subgroup ($P = 0.375$). Vascularization in the CL ECM group was 1.75 in the non-MSC-enriched subgroup and only 1.167 in the MSC-enriched subgroup ($P = 0.375$). The mean capsule thickness in the CL ECM group was 0.33 in the non-MSC-enriched subgroup and 1 in the MSC-enriched subgroup ($P = 0.830$). Similarly as in the CL ECM group, mean cellulization in noncross-linked extracellular matrix (non-CL ECM) was higher in the non-MSC-enriched subgroup (2) than in the MSC-enriched subgroup (1.2, $P = 0.445$). Mean vascularization in the non-CL ECM group was 2 in the non-MSC-enriched subgroup and 1.4 in the MSC-enriched subgroup ($P = 0.542$). The mean capsule thickness in the non-CL ECM group was 0.8 in the non-MSC-enriched subgroup and 1 in the MSC-enriched subgroup ($P = 0.638$).
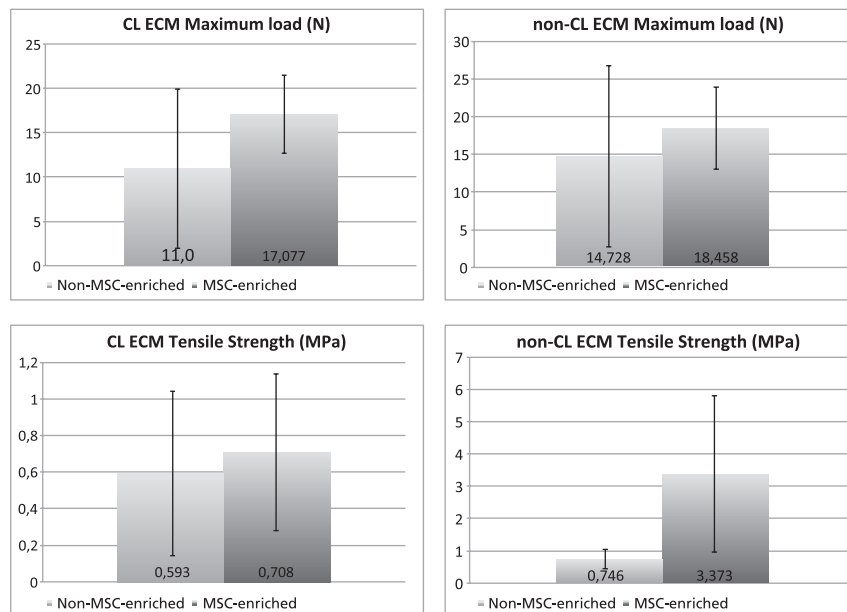
FIG. 7. Results of tensiometry. The strength of incorporation of the MSC-enriched cross-linked extracellular matrix (CL ECM) specimens was higher than that of the non-MSC-enriched CL ECM, but this result was statistically nonsignificant (0.59 MPa vs. 0.7 MPa, $P = 0.66$). In the noncross-linked extracellular matrix (non-CL ECM) group, there was a statistically significant difference between non-MSC-enriched ECM (0.75 MPa) and MSC-enriched ECM (3.37 MPa; $P = 0.018$).

Many experimental studies have been devoted to evaluation of the performance of ECMs for hernia repair. Primates (18), minipigs (19), or guinea pigs (9) have been used as animal models. However, by far, the most common animal for these tests is the rat, which has been used in most of the studies (16,20–24). The reason is that explants from this small animal model are sufficient for histological evaluation and tensiometry testing.

Our study was aimed to evaluate the outcomes of experimental hernia repair by CL ECM and non-CL ECM seeded with MSCs compared to acellular ECM either enriched or nonenriched with MSCs.

Similar studies have been presented in the literature. One study of acellular dermal matrix seeded with autologous bone marrow-derived MSCs described its use for experimental hernia repair in the rabbit (25). Another study by Japanese authors evaluated resorption of acellular dermal matrix seeded with ADSCs implanted as subcutaneous implant (26).

Zhao et al. (25) and Orbay et al. (26) reported that simple ECM undergoes degradation after implantation, and seeding it with stem cells significantly increases vascularization and SOI. We did not find slower degradation or increased vascularization after seeding ECM with cells. In our opinion, cross-linking is the only approach available at present to decrease degradation of biologic meshes (20,27–29). The use of bone marrow-derived MSCs for seeding ECM is questionable in clinical practice. However, adipose-derived MSCs are very easily harvestable, with minimum donor site morbidity. In addition, currently we have available instruments that are capable of isolating substantial numbers of ADSCs during an operation (30).

The results of our study were different than anticipated in many aspects. Vascularization and cellularization in both CL ECM and non-CL ECM groups were lower in the acellular subgroup, but these results were not significant. This outcome can be explained by the minimal impact of MSCs on ECM properties and also by the limited number of studied subjects. The only significant difference was the tensile strength in the non-CL ECM group. The SOI of the acellular subgroup was significantly lower than in the MSCs subgroup.

Contrary to the opinion of other authors (25,26), a tremendous number of studies have demonstrated an exceptional performance of ECM without seeded MSCs for hernia repair, especially in difficult cases (3,7,31).

Zhao et al. (25) described increased peritoneum regeneration in a group of MSC-enriched ECMs. This benefit might be helpful for decreasing bowel adhesions to the abdominal wall. In our opinion, isolation and seeding of cells on the mesh for hernia repair is a very complex procedure that cannot outweigh the possible clinical benefit.

CONCLUSION

Seeding of extracellular scaffolds with mesenchymal stem cells does not contribute significantly to increased vascularization in either cross-linked or noncross-linked extracellular matrix. In addition, in CL ECM, it does not ensure increased strength of incorporation. However, our findings showed significantly increased strength of incorporation in non-CL ECM. Owing to the fact that isolation and seeding of MSCs on ECM represents a very complex procedure, we do not see sufficient benefits for its use in the clinical setting.

Author contributions: Ondrej Mestak: concept/design, data analysis/interpretation, drafting the article, critical revision of article, and data collection. Eva Matouskova: data collection and drafting the article. Zuzana Spurkova: data collection. Kamila Benkova: data collection. Pavel Vesely: concept/design. Jan Mestak: funding secured by and approval of article. Martin Molitor: approval of article. Andrej Sukop: approval of article and concept/design.

REFERENCES

1. Catena F, Ansaloni L, Gazzotti F, et al. Use of porcine dermal collagen graft (Permacol) for hernia repair in contaminated fields. *Hernia* 2007;11:57–60.
2. Mahmoud Uslu HY, Erkek AB, Cakmak A, et al. Incisional hernia treatment with polypropylene graft: results of 10 years. *Hernia* 2006;10:380–4.
3. Iannitti DA, Hope WW, Norton HJ, et al. Technique and outcomes of abdominal incisional hernia repair using a synthetic composite mesh: a report of 455 cases. *J Am Coll Surg* 2008; 206:83–8.
4. Voyles CR, Richardson JD, Bland KI, Tobin GR, Flint LM, Polk HCJ. Emergency abdominal wall reconstruction with polypropylene mesh: short-term benefits versus long-term complications. *Ann Surg* 1981;194:219–23.
5. Szczerba SR, Dumanian GA. Definitive surgical treatment of infected or exposed ventral hernia mesh. *Ann Surg* 2003;237: 437–41.
6. Parker DM, Armstrong PJ, Frizzi JD, North JHJ. Porcine dermal collagen (Permacol) for abdominal wall reconstruction. *Curr Surg* 2006;63:255–8.

7. Hiles M, Record Ritchie RD, Altizer AM. Are biologic grafts effective for hernia repair?: a systematic review of the literature. *Surg Innov* 2009;16:26–37.

8. Hsu PW, Salgado CJ, Kent K, et al. Evaluation of porcine dermal collagen (Permacol) used in abdominal wall reconstruction. *J Plast Reconstr Aesthet Surg* 2009;62:1484–9.

9. Butler CE, Burns NK, Campbell KT, Mathur AB, Jaffari MV, Rios CN. Comparison of cross-linked and non-cross-linked porcine acellular dermal matrices for ventral hernia repair. *J Am Coll Surg* 2010;211:368–76.

10. Nahabedian MY. AlloDerm performance in the setting of prosthetic breast surgery, infection, and irradiation. *Plast Reconstr Surg* 2009;124:1743–53.

11. Behr B, Ko SH, Wong VW, Gurtner GC, Longaker MT. Stem cells. *Plast Reconstr Surg* 2010;126:1163–71.

12. Strem BM, Hedrick MH. The growing importance of fat in regenerative medicine. *Trends Biotechnol* 2005;23:64–6.

13. Utsunomiya T, Shimada M, Imura S, et al. Human adipose-derived stem cells: potential clinical applications in surgery. *Surg Today* 2011;41:18–23.

14. Dominici M, Le Blanc K, Mueller I, et al. Minimal criteria for defining multipotent mesenchymal stromal cells. The International Society for Cellular Therapy position statement. *Cytotherapy* 2006;8:315–7.

15. Macleod TM, Williams G, Sanders R, Green CJ. Histological evaluation of Permacol as a subcutaneous implant over a 20-week period in the rat model. *Br J Plast Surg* 2005;58:518–32.

16. Ayubi FS, Armstrong PJ, Mattia MS, Parker DM. Abdominal wall hernia repair: a comparison of Permacol and Surgisis grafts in a rat hernia model. *Hernia* 2008;12:373–8.

17. Zuk PA, Zhu M, Ashjian P, et al. Human adipose tissue is a source of multipotent stem cells. *Mol Biol Cell* 2002;13:4279–95.

18. Sandor M, Xu H, Connor J, et al. Host response to implanted porcine-derived biologic materials in a primate model of abdominal wall repair. *Tissue Eng Part A* 2008;14:2021–31.

19. Melman L, Jenkins ED, Hamilton NA, et al. Early biocompatibility of crosslinked and non-crosslinked biologic meshes in a porcine model of ventral hernia repair. *Hernia* 2011;15:157–64.

20. de Castro Bras LE, Shurey S, Sibbons PD. Evaluation of cross-linked and non-crosslinked biologic prostheses for abdominal hernia repair. *Hernia* 2012;16:77–89.

21. Rice RD, Ayubi FS, Shaub ZJ, Parker DM, Armstrong PJ, Tsai JW. Comparison of Surgisis, AlloDerm, and Vicryl Woven Mesh grafts for abdominal wall defect repair in an animal model. *Aesthetic Plast Surg* [Internet] 2009;34:290–6. Available at: http://link.springer.com/10.1007/s00266-009-9449-2. Accessed April 27, 2013.

22. Keller JE, Dolce CJ, Walters KC, et al. Effect of bacterial exposure on acellular human dermis in a rat ventral hernia model. *J Surg Res* 2010;162:148–52.

23. Mulier KE, Nguyen AH, Delaney JP, Marquez S. Comparison of Permacol and Strattice for the repair of abdominal wall defects. *Hernia* 2011;15:315–9.

24. Petter-Puchner AH, Fortelny RH, Walder N, et al. Adverse effects associated with the use of porcine cross-linked collagen implants in an experimental model of incisional hernia repair. *J Surg Res* 2008;145:105–10.

25. Zhao Y, Zhang Z, Wang J, et al. Abdominal hernia repair with a decellularized dermal scaffold seeded with autologous bone marrow-derived mesenchymal stem cells. *Artif Organs* 2011; 36:247–55.

26. Orbay H, Takami Y, Hyakusoku H, Mizuno H. Acellular dermal matrix seeded with adipose-derived stem cells as a subcutaneous implant. *Aesthetic Plast Surg* 2011;35:756–63.

27. de Castro Bras LE, Proffitt JL, Bloor S, Sibbons PD. Effect of crosslinking on the performance of a collagen-derived biomaterial as an implant for soft tissue repair: a rodent model. *J Biomed Mater Res B Appl Biomater* 2010;95:239–49.

28. Oliver RF, Grant RA, Cox RW, Cooke A. Effect of aldehyde cross-linking on human dermal collagen implants in the rat. *Br J Exp Pathol* 1980;61:544–9.

29. Oliver RF, Barker H, Cooke A, Stephen L. 3H-collagen turnover in non-cross-linked and aldehyde-cross-linked dermal collagen grafts. *Br J Exp Pathol* 1982;63:13–7.

30. Lin K, Matsubara Y, Masuda Y, et al. Characterization of adipose tissue-derived cells isolated with the celution system. *Cytotherapy* 2008;10:417–26.

31. Butler CE. The role of bioprosthetics in abdominal wall reconstruction. *Clin Plast Surg* 2006;33:199–211, v–vi.

Lipophosphonoxins: New Modular Molecular Structures with Significant Antibacterial Properties

Dominik Rejman,*,[†] Alžbeta Rabatinová,[‡] António R. Pombinho,[§] Soňa Kovačková,[†] Radek Pohl,[†] Eva Zborníková,[†] Milan Kolář,[∥,⊥] Kateřina Bogdanová,[⊥] Otakar Nyč,[#] Hana Šanderová,[‡] Tomáš Látal,[∥] Petr Bartůněk,[§] and Libor Krásný*,[‡]

[†]Institute of Organic Chemistry and Biochemistry, Academy of Sciences of the Czech Republic v.v.i., Flemingovo nám. 2, 166 10 Prague 6, Czech Republic

[‡]Institute of Microbiology, Academy of Sciences of the Czech Republic v.v.i., Vídeňská 1083, 142 20 Prague 4, Czech Republic

[§]Center for Chemical Genetics and CZ-OPENSCREEN, Institute of Molecular Genetics, Academy of Sciences of the Czech Republic v.v.i., Vídeňská 1083, 142 20 Prague 4, Czech Republic

[∥]TRIOS, Ltd., Zakouřilova 142, Prague 4, 149 00, Prague, Czech Republic

[⊥]Department of Microbiology, Faculty of Medicine and Dentistry, Palacký University Olomouc, 779 00 Olomouc, Czech Republic

[#]Department of Medical Microbiology, Teaching Hospital Motol and Charles University in Prague, Second Faculty of Medicine, V Úvalu 84, 150 06, Prague 5, Czech Republic

Ⓢ *Supporting Information*
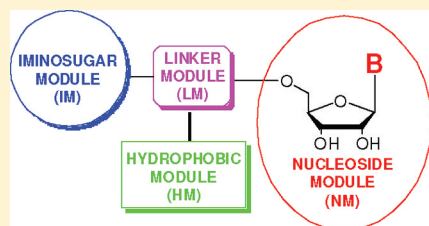
	MIC μg/ml			
	E. faecalis CCM 4224	*S. aureus* CCM 4223	*B. subtilis*	*S. agalactiae*
12a	12.50	-	6.25	3.13
12b	6.25	25.00	3.13	3.13
12h	12.50	25.00-12.50	6.25	6.25
12i	6.25	12.50- 6.25	3.13	1.56

ABSTRACT: Novel compounds termed lipophosphonoxins were prepared using a simple and efficient synthetic approach. The general structure of lipophosphonoxins consists of four modules: (i) a nucleoside module, (ii) an iminosugar module, (iii) a hydrophobic module (lipophilic alkyl chain), and (iv) a phosphonate linker module that holds together modules i–iii. Lipophosphonoxins displayed significant antibacterial properties against a panel of Gram-positive species, including multiresistant strains. The minimum inhibitory concentration (MIC) values of the best inhibitors were in the 1–12 μg/mL range, while their cytotoxic concentrations against human cell lines were significantly above this range. The modular nature of this artificial scaffold offers a large number of possibilities for further modifications/exploitation of these compounds.

■ INTRODUCTION

The use of antibiotics has been generally beneficial for public health. However, very few new antibiotics have been marketed in the last 40 years.[1] Moreover, the advantages offered by antibiotics in the treatment of infectious diseases are endangered due to the increase in the number of antibiotic-resistant bacterial strains. This reduces the efficiency of antibiotic treatments and poses a serious health and economic problem. Currently, the need for novel antibiotics is becoming increasingly apparent.[2,3]

We previously synthesized an effective inhibitor of *Giardia* trophozoite growth termed phosphonoxin (1) (Figure 1) with an activity that rivaled existing therapeutics. Phosphonoxin was designed as a transition-state inhibitor of a glycosyl transferase, cyst wall synthase (CWS). CWS catalyzes synthesis of the chitin-like poly β-1–3-linked *N*-acetylgalactosamine [poly-(GalNAc)] that comprises about 63% of the giardia cyst wall utilizing UDP-GalNAc (2) as a substrate. Although phospho-

noxin did not specifically inhibit cyst formation, it potently inhibited vegetative growth.[4]

Phosphonoxin bears structural similarities with several types of nucleoside antimicrobials: (i) polyoxins (3), (ii) muraymycins (4), and (iii) caprazamycins (5) (Figure 1).

The polyoxins of general formula 3 are a new group of antifungal antibiotics isolated from *Streptomyces cacaoi* that inhibit the growth of a number of mycelial fungi[5,6] by interfering with chitin synthesis.[7,8] Polyoxin D is a strong competitive inhibitor of chitin synthase in *Neurospora crassa*. Polyoxin D shares a gross structural similarity with uridine diphospho-*N*-acetyl-D-glucosamine (UDP-GlcNAc 2), in agreement with its role as a competitive inhibitor.

The caprazamycins (CPZs) (4) were isolated from a culture broth of the actinomycete strain *Streptomyces* spp. MK730–
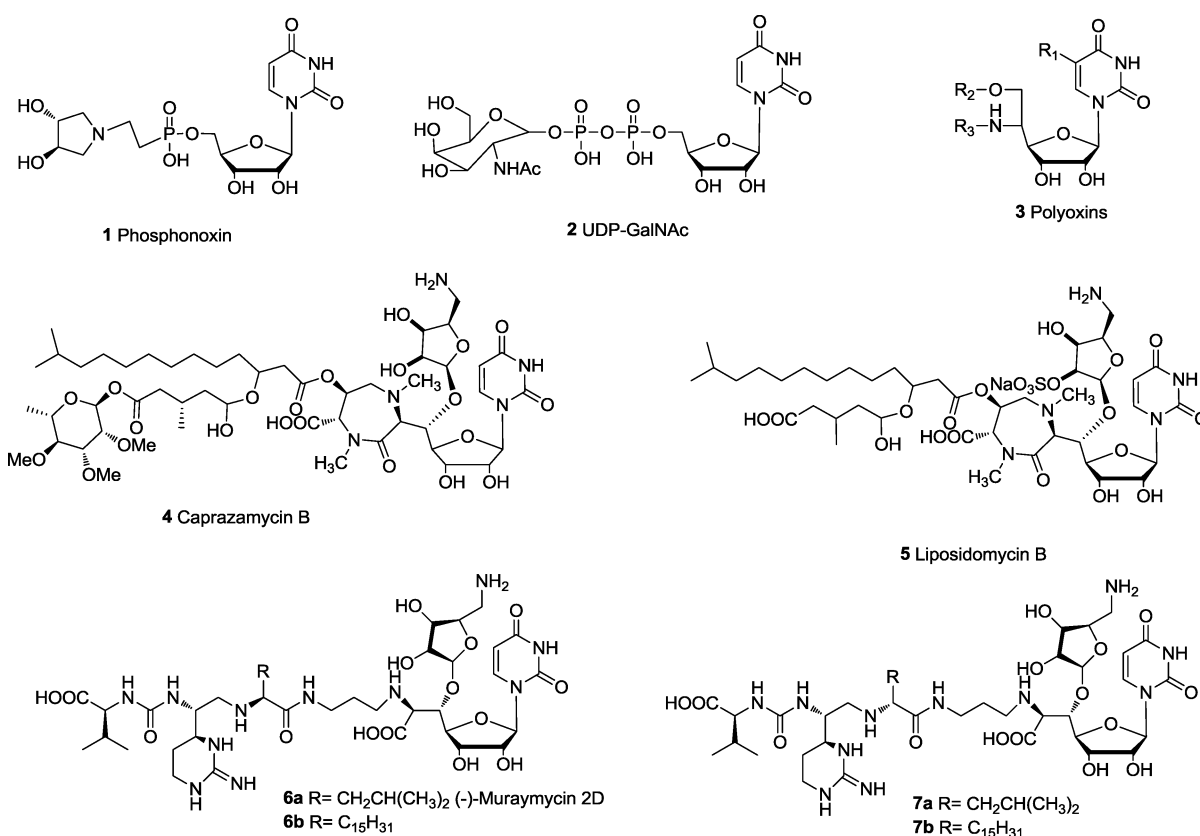
Figure 1. Structures of phosphonoxin, UDP-GlcNAc, and structurally related natural antimicrobials and their derivatives.

Table 1. Antibacterial Activity of Muraymycin Analogues

compd	MIC (μg/mL)					
	S. aureus ATCC 29213 (MSSA)	S. aureus SR3637 (MRSA)	E. feacalis ATCC 29212	E. feacalis SR7914 (VRE)	E. faecium ATCC 19434	E. faecium SR7917 (VRE)
6a	>64	>64	>64	>64	>64	>64
7a	>64	>64	>64	>64	>64	>64
6b	2	4	4	4	4	2
7b	2	4	2	4	0.5	0.25
vancomycin	1	1	1	>64	0.5	>64

62F2 in 2003[9,10] and represent the most recent members of the class of naturally occurring 6′-N-alkyl-5′-β-O-aminoribosyl-C-glycyluridine antibiotics that include the liposidomycins (**5**) (LPMs). The CPZs have shown excellent antimycobacterial activity *in vitro* not only against drug-susceptible (MIC = 3.13 μg/mL) but also multidrug-resistant *Mycobacterium tuberculosis* strains (MIC = 3.13 μg/mL) and exhibit no significant toxicity in mice. The biological target of the 6′-N-alkyl-5′-β-O-aminoribosyl-C-glycyluridine class of antibiotics is believed to be MraY translocase (IC$_{50}$ = 0.05 μg/mL for LPMs).[11]

The muraymycins (**6a**), isolated from a culture broth of *Streptomyces* species,[12] are members of a class of naturally occurring 6′-N-alkyl-5′-β-O-aminorybosyl-C-glycyluridine antibiotics. Members of this family showed antibacterial activity against *Staphylococcus aureus* and *Enterococci* and were able to protect mice against *S. aureus* infection (ED$_{50}$ = 1.1 mg/kg). The muraymycins inhibit the formation of lipid II and peptidoglycan and are believed to be inhibitors of phospho-MurNAc-pentapeptide translocase (MraY), which is responsible for the formation of lipid I in the peptidoglycan biosynthesis pathway.[13−17] Tanino recently described the

synthesis of lipophilic muraymycin analogues **6b** and **7b** that differ in the stereochemistry at the carbon atom, where the lipophilic moiety is attached. These compounds exhibited significant activity against methicillin-resistant *Staphylococcus aureus* (MRSA) and vancomycin-resistant *Enterococci* (VRE) (Table 1).[18]

At the beginning of this study, we tested phosphonoxin for potential antibacterial properties. However, no significant activity was observed. We reasoned that the negative charge on the phosphonate moiety may hamper cellular uptake. Thus, to facilitate the cell entry, we introduced the lipophilic hexadecyloxypropyl ester group[19] to the structure and synthesized several variants based on this structure. The obtained structures were collectively termed lipophosphonoxins (LPPOs), and they showed promising activities against several Gram-positive bacterial species and low to moderate cytotoxicities. LPPOs represent an artificial modular structure that could be easily synthesized in few simple reaction steps.

Here we present synthesis, antibacterial activity, and cytotoxicity of several members of the lipophosphonoxin family.

■ RESULTS AND DISCUSSION

General Structure of Lipophosphonoxins. LPPOs are modular molecules consisting of these parts: a nucleoside module (NM), a linker module (LM), an iminosugar module (IM), and a hydrophobic module (HM) (Figure 2).
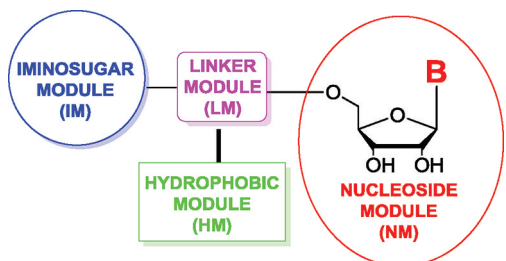
Figure 2. General structure of lipophosphonoxins.

The parent phosphonoxin (**1**) contained uridine as the NM. Cytidine was subsequently evaluated as an NM alternative. LPPOs containing hexadecyloxypropyl, ethyl, pivaloylthioethyl (SATE),[20] tetradecyl, hexadecyl, octadecyl, or eicosanyl ester groups as the HM were synthesized. Several hydroxylated pyrrolidines and piperidines were used as the IM. The LM was in all cases ethylphosphonic acid.

Chemistry. Vinylphosphonate synthons **9a−b** were prepared from nucleobase protected 2′,3′-isopropylidene nucleosides **8a−b** (Scheme 1). The phosphonate function was
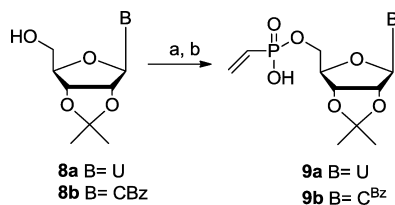
Scheme 1[a]

[a](a) CH_2=CHP(O)(OMe)OH, MeIm, TPSCl, DCM/MeCN; (b) 60% aq pyridine.

introduced by esterification of monomethyl vinylphosphonate[21,22] using triisopropylbenzensulfonylchloride (TPSCl) as a condensing agent (Scheme 1). Obtained methyl phosphonates were partially de-esterified by heating with 60% aqueous pyridine to remove the methyl ester group, affording nucleosidyl vinylphosphonates **9a−b**.

Next, esterification was performed with the appropriate alcohol using TPSCl as a condensing agent, yielding synthons **10a−h** (Scheme 2; Table 2).

Scheme 2[a]
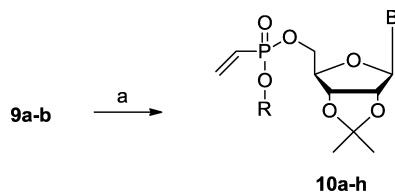
[a](a) ROH, MeIM, TPSCl, DCM/MeCN.

Table 2. Vinylphosphonates 10a−h

compd	B	R
10a	U	$PivSCH_2CH_2$
10b	U	CH_3CH_2
10c	U	$C_{14}H_{29}$
10d	U	$C_{16}H_{33}$
10e	U	$C_{18}H_{37}$
10f	U	$C_{20}H_{41}$
10g	U	$C_{16}H_{33}OCH_2CH_2CH_2$
10h	C^{Bz}	$C_{16}H_{33}OCH_2CH_2CH_2$

Finally, Michael addition of pyrrolidine derivatives **11a−d**[23,24] or piperidine derivatives **11e−f**[24,25] to vinylphosphonates **10a−d** was carried out, followed by deprotection, resulting in moderate to good yields of final lipophosphonoxins **12a−l** (Scheme 3, Tables 3 and 4). The deprotection consisted of the
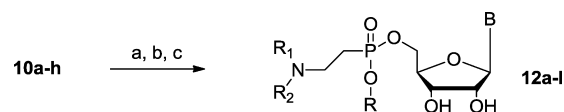
Scheme 3[a]

[a](a) R_1R_2NH (**11a−f**), nBuOH, 90 °C; (b) $MeNH_2/MeOH$ (B = C^{Bz}); (c) 0.2M HCl/MeOH.

removal of the nucleobase protecting group (in the case of cytosine derivative) with ethanolic methylamine and the subsequent cleavage of isopropylidene group with 0.2 M methanolic HCl. The final products were obtained by flash column chromatography on silica gel or using preparative reversed phase HPLC.

Antimicrobial Activity. The prepared compounds were tested against a panel of selected reference bacterial strains (Table 5). The minimal inhibitory concentration (MIC) values obtained by the standard microdilution method[26,27] were used to evaluate the antibacterial properties of the compounds.

The compound **12a**, consisting of the uridine NM, hexadecyloxypropyl HM, and (3R,4R)-3,4-dihydroxypyrrolidine IM, exhibited significant antibacterial properties against several Gram-positive bacteria, such as *Enterococcus faecalis* (12.50 μg/mL), *Bacillus subtilis* (6.25 μg/mL), and *Streptococcus agalactiae* (3.13 μg/mL), respectively (Table 5). The compound **12b**, wherein the uridine NM was replaced with cytidine, exhibited a slightly improved antibacterial activity: *E. faecalis* (6.25 μg/mL), *B. subtilis* (3.13 μg/mL), *S. agalactiae* (3.13 μg/mL), and *S. aureus* (25.00 μg/mL).

The replacement of the IM ((3R,4R)-3,4-dihydroxypyrrolidine) of **12a** with its enantiomeric (3S,4S)-3,4-dihydroxypyrrolidine (in the case of **12c**) did not change the activity. However, when (3R,4S,5S)-3,4-trihydroxypiperidine (in the case of **12d**) or (3R,5R)-3,4-dihydroxypiperidine (in the case of **12e**) were used as the IM, the antibacterial activity was almost abolished except for *S. agalactiae* (12.50 μg/mL).

The hexadecyloxypropyl HM of **12a** was replaced with either ethyl (in the case of **12g**), tetradecyl (in the case of **12h**), hexadecyl (in the case of **12i**), octadecyl (in the case of **12j**), or icosanyl (in the case of **12k**) ester group, respectively. The LPPO **12g** with ethyl ester HM did not exhibit any antibacterial activity. Compound **12k** exhibited the lowest activity; **12h** and **12j** exhibited activities comparable to their parent structure, **12a**. The LPPO **12i** with hexadecyl ester HM appeared to be

Table 3. Amines (Pyrrolidines and Piperidines) 11a–f

11a	11b	11c	11d	11e	11f
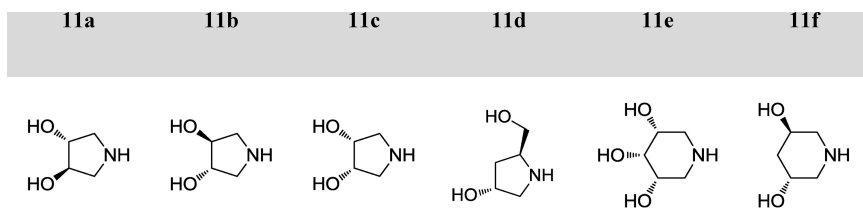
the most active compound of the tested series: *E. faecalis* (6.25 μg/mL), *B. subtilis* (3.13 μg/mL), *S. agalactiae* (1.56 μg/mL) and *S. aureus* (12.50−6.25 μg/mL). In the case of the LPPO **12f** with pivaloylthioethyl ester HM, no activity was observed.

None of the tested compounds exhibited MIC below 200 μg/mL against Gram-negative *Escherichia coli* or *Pseudomonas aeruginosa*. Possible explanations included (i) problems of these compounds with cell entry, (ii) their rapid degradation while in the cell, (iii) their rapid export from the cell, or (iv) the lack of molecular target(s) in Gram-negative bacteria. To better characterize these compounds, it would be useful to distinguish between (i) versus (ii−iv). To test the inhibitory potential of these compounds on a Gram-negative bacterium, we had to use permeabilized *E. coli* cells. Such cells have an enhanced ability to uptake molecules from their environment. Permeabilized *E. coli* cells were incubated with/without the tested compounds (see Experimental Section for details). If (i) were correct, at least some compound(s) would adversely affect the cell survival. If (ii), (iii), or (iv) were correct, no difference relative to the control would be observed.

Compounds **1**, **12a**, **12i**, and **12k** were tested on permeabilized *E. coli* cells. Compound **1** had no antibacterial effect on these cells. On the other hand, compounds **12a** and **12i** killed 90% of cells at 10 μM and **12k** at 25 μM (Table 6). These results suggest that the inefficiency of lipophosphonoxins against Gram-negative bacteria is likely due to their inability to cross the two plasmatic membranes of these species, and future modification may be attempted to allow their entry into the Gram-negative cell.

More importantly, these results imply that the HM may be required for the interaction of the compounds with their molecular target(s) because compound **1**, which lacks the HM, exhibited no activity. In other words, the HM may not be only an auxiliary module attached to the active molecule to create its prodrug form that is cleaved off upon the cell entry but an integral part of the active compound.

The most active compounds were further tested against clinically relevant multiresistant bacterial strains (Table 7). Compounds **12a**, **12b**, **12c**, **12i**, and **12l** showed significant antibacterial activities (6.25−3.13 μg/mL) against *Enterococcus feacium* VanA419/ana and *Staphylococcus epidermidis* 8700/B. Compound **12h** exhibited good activity against methicillin-resistant *S. aureus* (MRSA) 4591 (25.00 μg/mL), *Staphylococcus haemolyticus* 16568 (12.50 μg/mL), *E. faecium* VanA419/ana (6.25 μg/mL), and *S. epidermidis* 8700/B (6.25 μg/mL). Compound **12i** exhibited slightly stronger activity than **12h** against MRSA 4591 (12.50 μg/mL), *S. haemolyticus* 16568 (25.00−12.50 μg/mL), *E. faecium* VanA419/ana (3.13 μg/mL), and *S. epidermidis* 8700/B (3.13 μg/mL).

Viability, Cytotoxicity, and Apoptosis of Human Progenitor Cells. The effects of the newly synthesized lipophosphonoxins were tested on cell viability (metabolic activity), cytotoxicity (membrane integrity), and apoptosis

(caspase 3/7 activation), using erythroid progenitor cells derived from human umbilical cord blood. Cell viability was measured 48 h after exposure, while cytotoxicity and apoptosis were measured 4 h after exposure to the compounds.
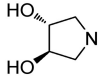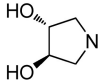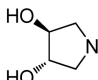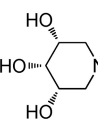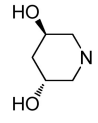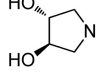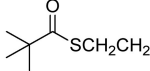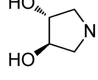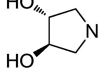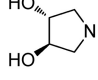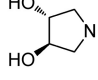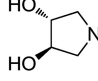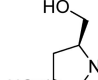
Compounds **12a**, **12b** and **12i**, shown to have the best antibacterial activity, had no detectable activity on normal primary cell viability and toxicity at the MIC concentrations (Figure 3). According to the cell viability results, these compounds showed to be toxic to these cells at concentrations that were well above their MIC values for most of the bacterial strains tested (Table 8). Finally, these compounds induced only a low level of apoptosis. Other tested compounds showed either higher toxicity to the primary cells or lower activity/selectivity against the selected bacterial strains (Supporting Information Figure 1), but this still does not exclude their potential antibacterial use, such as in topical applications.

Effect of the Diastereomeric Configuration at the Phosphorus Atom on Biological Activity. The compound **12i**, exhibiting the highest antibacterial activity, was separated into both diastereomers differing in the configuration at the phosphorus atom, yielding two pure diastereomers **12i-P1** and **12i-P2**. Figure 4 shows analytical HPLC records of the mixture and the two separated diastereomers. Diastereomer **12i-P1** with t_R = 8.20 min showed ^{31}P NMR shift at 31.27, while diastereomer **12i-P2** with t_R = 8.69 min showed ^{31}P NMR shift at 32.03.

Subsequently, the antibacterial activities of both diastereomers were evaluated and both diastereomers displayed almost the same MIC values, identical with MIC values of the original mixed compound **12i**. This suggests that the configuration at the phosphorus atom does not play an important role in the antibacterial activity. This is reminiscent of muraymycin analogues **6b** and **7b** (see Introduction) where the chirality at the atom of the lipophilic chain attachment did not significantly affect their antibacterial activity.[18] Nevertheless, in our case, the **12i-P1** diastereomer was slightly less toxic to erythroid progenitor cells (Figure 5).

Effect of LPPOs on Bacterial RNAP. An initial concern had been that LPPOs, due to their amphiphilic character, might function as nonspecific, detergent-like compounds. This concern was dispelled by the cytotoxicity tests: the used cell lines are highly sensitive to their environment and compounds acting in a detergent-like manner would severely compromise their viability, which was not the case. To further test whether LPPOs function in a nonspecific way, the effect of several LPPOs on the enzymatic activity of a key bacterial protein, RNA polymerase (RNAP), was evaluated (see Experimental Section for details). Multiple-round transcriptions with purified components were carried out in the absence or presence of high, 1 mM (∼700 μg/mL) concentration of selected LPPOs (**12a**, **12c**, **12d**, and **12e**). None of these compounds significantly inhibited the enzymatic activity of RNAP, while two control detergents, cetyltrimethylammonium bromide and

Table 4. Structures of Lipophosphonoxines 12a–l

Compound	R_1R_2N	B	R
12a		U	$C_{16}H_{33}OCH_2CH_2CH_2$
12b		C	$C_{16}H_{33}OCH_2CH_2CH_2$
12c		U	$C_{16}H_{33}OCH_2CH_2CH_2$
12d		U	$C_{16}H_{33}OCH_2CH_2CH_2$
12e		U	$C_{16}H_{33}OCH_2CH_2CH_2$
12f		U	SCH_2CH_2 (tert-butyl thioester)
12g		U	CH_3CH_2
12h		U	$C_{14}H_{29}$
12i		U	$C_{16}H_{33}$
12j		U	$C_{18}H_{37}$
12k		U	$C_{20}H_{41}$
12l		U	$C_{16}H_{33}$

cetylpyridinium bromide, completely abolished transcription at 0.2 mM (~80 μg/mL) concentration.

■ **CONCLUSIONS**

We describe here a novel molecular scaffold leading to structures exhibiting significant antibacterial activities. The compounds based on this scaffold were collectively termed lipophosphonoxins (LPPOs). The most active LPPOs dis-played good activities against a panel of Gram-positive bacteria strains at subcytotoxic concentrations. Importantly, the most active compounds also exhibited antibacterial activities against several multiresistant strains.

The molecular target(s) of LPPOs are unknown. On the basis of a gross structural resemblance (nucleobase, long alkyl chain), they may act in a similar way as, e.g., lipisidomycins or caprazamycins (Figure 1). In comparison with these com-

Table 5. Antibacterial Activity (against Reference Bacterial Strains)

compd			MIC μg/mL	
	E. faecalis CCM 4224	*S.aureus* CCM 4223	*B. subtilis*	*S.agalactiae*
12a[a]	12.50		6.25	3.13
12b[a]	6.25	25.00	3.13	3.13
12c[a]	12.50		6.25	6.25
12d[a]				12.50
12e[a]	200		100	6.25
12f[a]				
12g[a]				
12h[a]	12.50	25.00−12.50	6.25	6.25
12i[a]	6.25	12.50−6.25	3.13	1.56
12j[a]	6.25	25.00−12.50	12.50−6.25	3.13
12k[a]	100			6.25
12l[a]	6.25	100	3.13	3.13
CMP[b]			16	2
TET[c]			2	1

[a]In all cases MIC = MBC. [b]CMP = chloramphenicol. [c]TET = tetracycline.

Table 6. Effect of Selected Compounds on Permeabilized *E. coli*

compd [10 μM]	killing power (log reduction[a])	
1	(4.4 μg/mL)	0[b]
12a	(7.2 μg/mL)	1
12i	(6.6 μg/mL)	1
12k	(7.2 μg/mL)	0.7

[a]One log is 90% reduction in colony forming units. [b]This compound had no effect also at 1 mM concentration.

Table 7. Antibacterial Activity (against Multiresistant Bacterial Strains)[a]

	MIC μg/mL			
compd	*S. aureus* MRSA 4591	*S. haemolyticus* 16568	*E. faecium* VanA419/ana	*S. epidermidis* 8700/B
12a			6.25	3.13
12b			6.25	6.25
12c			6.25	6.25
12h	25.00	12.5	12.50	12.50
12i	12.50	25−12.5	3.13	3.13
12j	200		6.25	6.25
12l			6.25	6.25

[a]In all cases MIC = MBC; multiresistant bacterial strains isolated from clinical isolates of patients from Teaching Hospital Olomouc: MRSA (methicilin-resistant *S. aureus* 4591); *S. haemolyticus* (fluoroquinolone-resistant strain 16568); *E. faecium* (vancomycin-resistant strain VanA419/ana); *S. epidermidis* (methicilin-resistant strain 8700/B).

pounds, however, LPPOs are significantly easier to synthesize. In summary, LPPOs appear to be specific antibacterial compounds and the molecular basis of their antibacterial activity has yet to be elucidated experimentally. Experiments to this effect are under way in our laboratory.

The modular composition of the scaffold and its simple synthesis will allow further optimization of its structure to enhance its antibacterial efficiency while decreasing its cytotoxicity. We will also focus on modifications of lipophosphonoxins to enhance their efficiency against Gram-
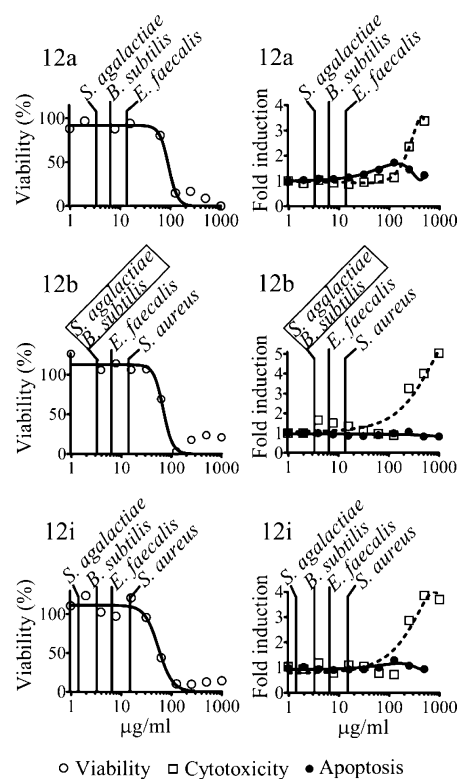
Figure 3. Cell viability, cytotoxicity, and apoptosis of erythroid progenitor cells after exposure to selected compounds (**12a**, **12b**, and **12i**). For comparison, the antibacterial activities (MIC values) of these compounds against selected bacterial species are indicated with vertical lines in the graphs (bacterial strains with the same MIC value are inside the boxes).

Table 8. Erythroid Progenitor Cells Viability

compd	IC$_{50}$ (μg/mL)	maximum safe concentration
12a	91.00	62.50
12b	67.00	31.25
12c	47.00	31.25
12d	149.00	62.50
12e	53.00	31.25
12f	>1000	>1000
12g	nd	nd
12h	58.00	31.25
12i	56.00	31.25
12j	36.00	15.60
12k	31.00	15.60
12l	116.00	62.50

negative bacteria. Results from these experiments as well as the research into the molecular mechanism of LPPOs will be reported in due course.

■ EXPERIMENTAL SECTION

Antibacterial Activity. Antimicrobial activity was assessed using the standard microdilution method determining the minimum inhibitory concentration (MIC) of tested samples leading to inhibition of bacterial growth.[26,27] Disposable microtitration plates were used for the tests. The samples were diluted in brain heart infusion broth (Himedia) to yield a concentration range between 200 and 1.56 μg/mL (in some cases, the lower concentration range was extended to 0.78 μg/mL). The plates were inoculated with a standard amount of the tested microbe; the inoculum density in each well was equal to 10^{5-6} CFU/ml. The MIC was read after 24/48 h of incubation at 37
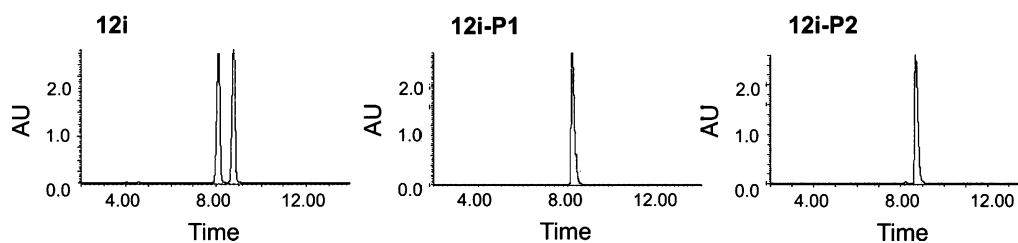
Figure 4. The analytical HPLC chromatograms of **12i**, **12i-P1**, and **12i-P2**. HPLC analysis was performed on Waters AutoPurification system with 2545 quarternary gradient module and 3100 single quadrupole mass detector using LUNA C18, column (Phenomenex, 100 mm × 4.6 mm, 3 μm) at flow rate 1 mL/min using gradient, A→B/15 min, (A, 50 mM NH_4HCO_3 in 50% aq CH_3CN; C, CH_3CN). AU, absorption units.
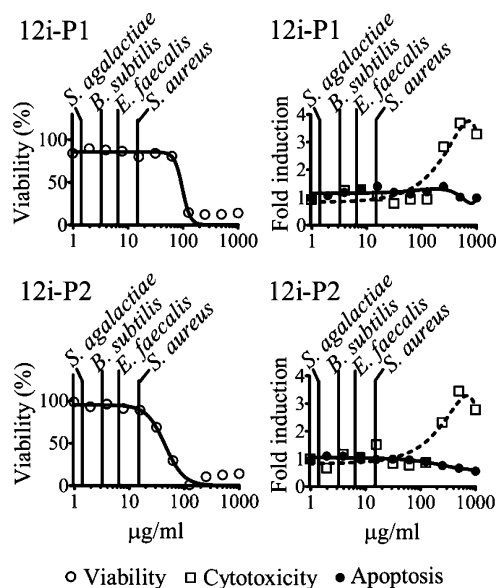
Figure 5. Cell viability, cytotoxicity, and apoptosis of erythroid progenitor cells after exposure to diastereomers **12i-P1** and **12i-P2**. Vertical lines in the graphs represent the MIC values for the respective bacterial strains.

°C as the minimum inhibitory concentration of the tested substance that inhibited the growth of the bacterial strains.

The minimum bactericidal concentration (MBC) is characterized as the minimum concentration of the sample required to achieve irreversible inhibition, i.e. killing the bacterium after a defined period of incubation. The MBC was examined by the inoculation method. With an applicator, 10 μL were transferred from microplate wells with defined concentrations of the tested sample and inoculated onto the surface of blood agar (Trios, Czech Republic). The MBC was determined as the lowest concentration that inhibited the visible growth of the used bacterium.

Standard reference bacterial strains (*E. faecalis* CCM 4224, *S. aureus* CCM 4223) from the Czech Collection of Microorganisms (CCM), Faculty of Science, Masaryk University Brno, and *S. agalactiae*, *B. subtilis*, methicilin-resistant *S. aureus* 4591, fluoroquinolone-resistant *S. haemolyticus* 16568, vancomycin-resistant *E. faecium* VanA419/ana, and methicilin-resistant *S. epidermidis* 8700/B strains obtained from the Teaching Hospital Olomouc were used. All tested microorganisms were stored in cryotubes (ITEST plus, Czech Republic) at −80 °C.

Antibacterial Activity against Competent *E. coli*. We mixed together 20 μL of *E. coli* (strain DH5α) competent cells (i.e., permeabilized, with an increased ability to uptake molecules from the outside),[28] pUC18 plasmid DNA (5 ng) (bearing amp^R as the selective marker after transformation) and a serially diluted tested compound/equal volume of "empty" buffer. The mixture was incubated for 30 min on ice followed by a heat shock performed at 42 °C for 90 s. The mixture was then allowed to sit on ice for 5 min. Subsequently, 1 mL of LB medium without antibiotics was added and the mixture was

incubated for 1 h at 37 °C by vigorous shaking. Then the mixture was plated on LB agarose plates containing ampicillin at 100 μg/mL and incubated at 37 °C overnight. The number of colonies obtained from transformation with a tested compound was compared to the number of colonies obtained after transformation without inhibitor (positive control).

Cell Viability, Cytotoxicity, And Apoptosis. Culture and expansion of normal human erythroid progenitor cells was described earlier.[29] Cells were plated at 25000 cells/well/20 μL in 384-well plates immediately before compound addition. Cell viability and cytotoxicity have a fluorescent readout, and cells were plated into black 384-well plates (Corning, Cat. no. 3571), while apoptosis has a luminescent readout and cells were plated into white 384-well plates (Corning, Cat. no. 3570). Compounds were prediluted in the appropriate culture media and 5 μL of five times concentrated solution of compounds were added to the cell supernatant. Cytotoxicity and apoptosis were measured 4 h after compound addition using the CytoTox-ONE homogeneous membrane integrity assay (Promega, Cat. no. G7892) and the Caspase-Glo 3/7 assay (Promega, Cat. no. G8091). Cell viability was measured using the CellTiter-Blue cell viability assay (Promega, Cat. no. G8082) 48 h after compound addition. All assays were measured using the EnVision plate reader (PerkinElmer). Data were analyzed using GraphPad Prism 5.0 statistical software, and the data were normalized to the values of untreated control cells that were set as 100%.

Tests on Purified RNA Polymerase. *Bacillus subtilis* RNAP and σ^A were purified, and the holoenzyme was reconstituted as described.[30] As the template for transcriptions, we used supercoiled plasmid DNA bearing a fragment containing the *B. subtilis* rrnB P1 promoter (pLK7).[31] Multiple-round transcriptions were carried out in 10 μL reactions containing 6nM RNAP, 4 ng/μL supercoiled plasmid template, 40 mM Tris−HCl pH 8.0, 10 mM $MgCl_2$, 1 mM DTT, 0.1 mg/mL BSA, and 150 mM KCl. ATP, CTP, and GTP were 200 μM each. UTP was 10 μM plus 2 μM [α-^{32}P]-UTP purchased from Institute of Isotopes Co., Ltd. The transcriptions were carried out in the absence or presence (1 mM) of the tested compound. As a control, cetyltrimethylammonium bromide and cetylpyridinium bromide were used (0.2 mM).

Each sample was preincubated at 30 °C for 5 min followed by initiation with RNAP. The reaction was stopped after 15 min at 30 °C by 10 μL of formamide loading buffer (95% formamide, 20 mM EDTA pH 8.0) and briefly vortexed. Samples were loaded onto 7 M UREA 7% polyacrylamide gels and separated by electrophoresis. The dried gels were scanned with Molecular Imager_ FX (BIO-RAD). The amounts of the 145-nt-long transcript that originated from the rrnB P1 promoter were quantitated with Quantity One (BioRad).

Chemistry. Unless stated otherwise, all used solvents were anhydrous. Dimethyl vinylphosphonate, tetradecanol, hexadecanol, octadecanol, and eicosanol were purchased from Sigma Aldrich (Czech Republic). Protected nucleosides were prepared according to standard procedures. Hexadecyloxypropanol was prepared according to Hostetler et al.,[19] pivaloylthioethanol was prepared according to Lefebvre et al.,[23] dihydroxypyrrolidines **11a−c** were prepared according to Rejman et al.,[23] piperidine derivatives **11d** and **11e** were prepared according to Rejman et al.[25] and Kovačková et al.[24] respectively. All reactions were performed under an inert atmosphere

of dry Ar or N$_2$. TLC was performed on silica gel precoated aluminum plates Silica gel/TLC-cards, UV 254 (Fluka), and compounds were detected by UV light (254 nm), by spraying with 1% ethanolic solution of ninhydrine to visualize amines, and by spraying with 1% solution of 4-(4-nitrobenzyl)pyridine in ethanol followed by heating and treating with gaseous ammonia (blue color, detection of alkylating agents, e.g. mesylderivatives, phosphonate esters). The purity of the final compounds was greater than 95%. Purity of prepared compounds was determined by LC-MS performed on Waters AutoPurification System with 2545 Quarternary Gradient Module and 3100 Single Quadrupole Mass Detector using LUNA C18, column (Phenomenex, 100 mm × 4.6 mm, 3 μm) at flow rate 1 mL/min. Typical conditions: mobile phase, A, 50 mM NH$_4$HCO$_3$; B, 50 mM NH$_4$HCO$_3$ in 50% aq CH$_3$CN; C, CH$_3$CN; A→B/10 min, B→C/10 min, C/5 min. Preparative RP HPLC was performed on LC5000 liquid chromatograph (INGOS-PIKRON, CR) using Luna C18 (2) column (250 mm × 21.2 mm, 5 μm) at flow rate of 10 mL/min at a gradient elution of methanol in 0.1 M TEAB pH 7.5 (A = 0.1 M TEAB; B = 0.1 M TEAB in 50% aq methanol; C = methanol) or without buffer. All final compounds were lyophilized from water. IR spectra were recorded on a FTIR spectrometer (Bruker Equinox 55, Germany). Mass spectra were recorded on LTQ Orbitrap XL (Thermo Fisher Scientific) using ESI ionization. NMR spectra were measured as DMSO-d_6 or D$_2$O solutions on Bruker AVANCE 400 (^{1}H at 400.0 MHz, ^{13}C at 100.6 MHz, ^{31}P at 162.0 MHz) and/or Bruker AVANCE 500 (^{1}H at 500.0 MHz, ^{13}C at 125.7 MHz, ^{31}P at 202.3 MHz) spectrometers. Chemical shifts (in ppm, δ scale) were referenced to the residual DMSO-d_6 signal (2.5 ppm for ^{1}H and 39.7 ppm for ^{13}C) or to 1,4-dioxane signal (3.75 ppm for ^{1}H and 69.3 ppm for ^{13}C) as internal standard in D$_2$O. ^{31}P NMR spectra were referenced to H$_3$PO$_4$ (0 ppm) as an external standard. Coupling constants (J) are given in Hz. Complete assignment of protons and carbons was done by analysis of correlated homonuclear H,H-COSY and heteronuclear H,C-HSQC and H,C-HMBC spectra. Relative configuration was checked using DPFGSE-NOE and 2D-ROESY techniques.

General Method A, Phosphonylation: Preparation of Compounds 9a−b. Dimethyl vinylphosphonate (0.53 mL, 1.5 mmol) was treated with 60% aqueous pyridine (10 mL/mmol) at 60 °C overnight to remove one methyl ester group. The reaction mixture was concentrated in vacuo and coevaporated with EtOH (2 × 50 mL/mmol). The residue was dissolved in the mixture of H$_2$O/EtOH 1:1 (10 mL/mmol) and passed through a column of Dowex 50 in H$^+$ form (10 mL/mmol). The resin was washed with additional mixture of H$_2$O/EtOH 1:1 (2 × 10 mL/mmol). The liquid was concentrated in vacuo. The obtained monomethyl vinylphosphonate was coevaporated with EtOH (2 × 10 mL/mmol) and toluene (2 × 10 mL/mmol). To the mixture of the monomethyl phosphonate, protected nucleoside (1 mmol) and methylimidazole (3 mmol) in DCM (10 mL/mmol), TPSCl (3 mmol) was added. The reaction mixture was stirred at rt overnight. The mixture was washed with a saturated aq NaHCO$_3$ (10−20 mL/mmol) followed by washing with 3% aq citric acid (10−20 mL/mmol) and dried over Na$_2$SO$_4$. Organic phase was concentrated in vacuo and monomethyl ester of nucleosidevinylphosphonic acid was obtained by flash chromatography on silica gel using linear gradient of ethanol in chloroform. The monomethyl ester intermediate in 60% aqueous pyridine (10 mL/mmol) was stirred at 60 °C overnight. The reaction mixture was concentrated in vacuo, coevaporated in EtOH (2 × 10 mL/mmol), and dissolved in the same solvent (10 mL/mmol). Dowex 50 in Et$_3$N form (10 mL/mmol) was added, and the suspension was stirred for 10 min. The resin was removed by filtration, and the filtrate was concentrated in vacuo.

General Method B, Esterification: Preparation of Compounds 10a−h. TPSCl (3 mmol) was added to the mixture of triethylamonium salt of nucleosidyl ester of vinylphosphonic acid (1 mmol), alcohol (2 mmol), and methylimidazole (3 mmol) in DCM (10 mL/mmol). The reaction mixture was stirred at rt overnight. The mixture was washed with saturated aq NaHCO$_3$ (10−20 mL/mmol), followed by washing with 3% aq citric acid (10−20 mL/mmol) and dried over Na$_2$SO$_4$. Organic phase was concentrated in vacuo and the

product of esterification was obtained by flash chromatography on silica gel using linear gradient of ethanol in chloroform.

General Method C, Michael Addition and Deprotection: Preparation of Compounds 12a−l. The mixture of alkyl nucleosidyl mixed ester of vinylphosphonic acid (1 mmol) and amine (1.5 mmol) in nBuOH (10 mL/mmol) was stirred at 100 °C overnight. The mixture was concentrated in vacuo, and the protected intermediate was obtained by flash chromatography on silica gel using linear gradient of solvent system H1 (ethyl acetate:acetone:ethanol:water 4:1:1:1) in ethyl acetate. In the case of N-4-Bz-Cyt, the intermediate was dissolved in 33% ethanolic methylamine, stirred at rt overnight, and concentrated in vacuo (this step is skipped in the case of uridine derivative). The intermediate was dissolved in 0.2 M methanolic HCl (10 mL/mmol) and stirred overnight. The reaction mixture was applied on a silica gel column. The final product was obtained by flash chromatography using linear gradient of solvent system H1 (ethyl acetate:acetone:ethanol:water 4:1:1:1) in ethyl acetate and lyophilized from water.

2, 3′-Isopropylideneuridin-5′-yl Vinylphosphonate (9a). The title compound was prepared according to general method A from 2′,3′-isopropylideneuridine (14 g, 50 mmol) in 48% yield (11.38 g, 23.93 mmol) as a yellowish thick oil. NMR of UrdPhN has shown free acid (not Et$_3$NH$^+$ salt). ^{1}H NMR (499.8 MHz, CD$_3$OD): 1.35, 1.54 (2 × q, 2 × 3H, ^4J = 0.5, (CH$_3$)$_2$C); 3.98 (dd, 2H, $J_{H,P}$ = 5.3, $J_{5',4'}$ = 3.4, H-5′); 4.35 (m, 1H, H-4′); 4.90 (m, 2H, H-2′,3′); 5.74 (d, 1H, $J_{5,6}$ = 8.1, H-5); 5.86 (ddd, 1H, $J_{H,P}$ = 46.0, J_{cis} = 12.3, J_{gem} = 3.1, CH$_{cis}$**H$_{trans}$**=CHP); 5.95 (d, 1H, $J_{1',2'}$ = 2.5, H-1′); 6.00 (ddd, 1H, $J_{H,P}$ = 22.8, J_{trans} = 18.7, J_{gem} = 3.1, **CH$_{cis}$**H$_{trans}$=CHP); 6.12 (ddd, 1H, $J_{H,P}$ = 19.7, J_{trans} = 18.7, J_{cis} = 12.3, =CHP); 7.86 (d, 1H, $J_{6,5}$ = 8.1, H-6). ^{13}C NMR (125.7 MHz, CD$_3$OD): 25.53, 27.55 ((**CH$_3$**)$_2$C); 65.31 (d, $J_{C,P}$ = 4.8, CH$_2$-5′); 82.49 (CH-3′); 85.67 (CH-2′); 86.56 (d, $J_{C,P}$ = 8.0, CH-4′); 93.40 (CH-1′); 102.98 (CH-5); 114.99 (**C**(CH$_3$)$_2$); 130.74 (**CH$_2$**=CHP); 132.70 (d, $J_{C,P}$ = 174.3, =CHP); 143.42 (CH-6); 152.16 (C-2); 166.15 (C-4). ^{31}P NMR (202.3 MHz, CD$_3$OD): 13.16. HR-ESI: C$_{14}$H$_{18}$O$_8$N$_2$P (M − H)$^-$ calcd 373.0806; found 373.0809

4 N-Benzoyl-2′,3′-isopropylidenecytidin-5′-yl Vinylphosphonate (9b). The title compound was prepared according to general method A from 4-N-benzoyl-2′,3′-isopropylidenecytidine (3.05 g, 7.87 mmol) in 52% yield (1.95 g, 4.1 mmol) as a yellowish thick oil. NMR 9b has shown Et$_3$NH$^+$ salt (not free acid). ^{1}H NMR (600.1 MHz, CD$_3$OD): 1.31 (t, 9H, J_{vic} = 7.3, CH$_3$CH$_2$N); 1.37, 1.57 (2 × q, 2 × 3H, ^4J = 0.7, (CH$_3$)$_2$C); 3.20 (q, 6H, J_{vic} = 7.3, CH$_3$CH$_2$N); 4.02 (ddd, 1H, J_{gem} = 11.5, $J_{H,P}$ = 6.0, $J_{5'b,4'}$ = 3.4, H-5′b); 4.06 (ddd, 1H, J_{gem} = 11.5, $J_{H,P}$ = 4.5, $J_{5'a,4'}$ = 3.0, H-5′a); 4.50 (m, 1H, H-4′); 4.91 (dd, 1H, $J_{3',2'}$ = 6.0, $J_{3',4'}$ = 2.2, H-3′); 4.93 (dd, 1H, $J_{2',3'}$ = 6.0, $J_{2',1'}$ = 2.3, H-2′); 5.86 (ddd, 1H, $J_{H,P}$ = 46.0, J_{cis} = 12.4, J_{gem} = 3.1, CH$_{cis}$**H$_{trans}$**=CHP); 6.00 (d, 1H, $J_{1',2'}$ = 2.3, H-1′); 6.01 (ddd, 1H, $J_{H,P}$ = 22.9, J_{trans} = 18.7, J_{gem} = 3.1, **CH$_{cis}$**H$_{trans}$=CHP); 6.11 (ddd, 1H, $J_{H,P}$ = 19.6, J_{trans} = 18.7, J_{cis} = 12.4, =CHP); 7.55 (m, 2H, H-m-Ph); 7.62 (bd, 1H, $J_{5,6}$ = 7.5, H-5) 7.64 (m, 1H, H-p-Ph); 7.98 (m, 2H, H-o-Ph); 8.35 (d, 1H, $J_{6,5}$ = 7.5, H-6). ^{13}C NMR (150.9 MHz, CD$_3$OD): 9.18 (**CH$_3$**CH$_2$N); 25.45, 27.47 ((**CH$_3$**)$_2$C); 47.73 (CH$_3$**CH$_2$**N); 65.09 (d, $J_{C,P}$ = 4.8, CH$_2$-5′); 82.47 (CH-3′); 87.16 (CH-2′); 87.91 (d, $J_{C,P}$ = 8.1, CH-4′); 95.59 (CH-1′); 98.54 (CH-5); 114.69 (**C**(CH$_3$)$_2$); 129.16 (CH-o-Ph); 129.82 (CH-m-Ph); 130.80 (**CH$_2$**=CHP); 132.71 (d, $J_{C,P}$ = 174.8, =CHP); 134.05 (CH-p-Ph); 134.78 (C-i-Ph); 147.24 (CH-6); 157.90 (C-2); 164.99 (C-4); 169.02 (CO). ^{31}P NMR (202.3 MHz, CD$_3$OD): 13.02. HR-ESI: C$_{21}$H$_{25}$O$_8$N$_3$P (M + H)$^+$ calcd 478.13738; found 478.13719.

2 Pivaloylthioethyl 2′,3′-Isopropylideneuridin-5′-yl Vinylphosphonate (10a). The title compound was prepared according to general method B from 9a (0.36 g, 1.2 mmol) and pivaloylthioethanol (0.39 g, 2.4 mmol) in 92% yield (0.57 g, 1.1 mmol) as a colorless oil. A mixture of diastereomers ~1:1. ^{1}H NMR (600.1 MHz, CDCl$_3$): 1.15 (m, 18H, (CH$_3$)$_3$C); 1.27, 1.28, 1.49 (3 × s, 12H, (CH$_3$)$_2$C); 3.05, 3.06 (2 × t, 2 × 2H, J_{vic} = 6.8, SCH$_2$CH$_2$O); 3.97−4.09 (m, 4H, SCH$_2$**CH$_2$**O); 4.17−4.25 (m, 4H, H-5′); 4.29 (m, 2H, H-4′); 4.80, 4.81 (2 × dd, 2 × 1H, $J_{3',2'}$ = 6.5, $J_{3',4'}$ = 3.7, H-3′); 4.88 (dd, 2H, $J_{2',3'}$ = 6.5, $J_{2',1'}$ = 2.3, H-2′); 5.655, 5.657 (2 × d, 2 × 1H, $J_{5,6}$ = 8.1, H-5); 5.70, 5.73 (2 × d, 2 × 1H, $J_{1',2'}$ = 2.3, H-1′); 5.99, 6.00 (2 × ddd, 2 ×

1H, $J_{H,P}$ = 23.1, J_{trans} = 18.5, J_{cis} = 12.7, =CHP); 6.12, 6.14 (2 × ddd, 2 × 1H, $J_{H,P}$ = 52.4, J_{cis} = 12.7, J_{gem} = 1.8, CH$_{cis}$**H**$_{trans}$=CHP); 6.28, 6.30 (2 × ddd, 2 × 1H, $J_{H,P}$ = 25.2, J_{trans} = 18.5, J_{gem} = 1.8, **CH**$_{cis}$H$_{trans}$=CHP); 7.34, 7.38 (2 × d, 2 × 1H, $J_{6,5}$ = 8.1, H-6); 10.34 (bs, 2H, NH). ^13C NMR (150.9 MHz, CDCl$_3$): 24.97, 24.99, 26.81, 26.82 ((**CH$_3$**)$_2$C); 27.00 ((**CH$_3$**)$_3$C); 28.43 (d, $J_{C,P}$ = 6.6, SCH$_2$CH$_2$O); 46.19 (**C**(CH$_3$)$_2$); 64.19, 64.21 (d, $J_{C,P}$ = 5.0, OCH$_2$CH$_2$S); 64.98, 65.06 (d, $J_{C,P}$ = 5.4, CH$_2$-5′); 80.39, 80.49 (CH-3′); 84.14, 84.22 (CH-2′); 85.16, 85.43 (d, $J_{C,P}$ = 6.9, CH-4′); 93.41, 93.82 (CH-1′); 102.25, 102.34 (CH-5); 114.16, 114.22 (**C**(CH$_3$)$_2$); 124.31, 124.36 (d, $J_{C,P}$ = 184.6, =CHP); 136.85 (**CH$_2$**=CHP); 141.69, 141.81 (CH-6); 150.03, 150.05 (C-2); 163.55, 163.57 (C-4); 205.41, 205.43 (CO). ^31P NMR (162.0 MHz, CDCl$_3$): 18.75, 18.88. HR-ESI: C$_{21}$H$_{32}$O$_9$N$_2$PS (M + H)$^+$ calcd 519.1561; found 519.1562.

Ethyl 2′,3′-Isopropylideneuridin-5′-yl Vinylphosphonate (10b). The title compound was prepared according to general method B from **9a** (1.86 g, 6.2 mmol) and ethanol (1 g, 30 mmol) in 80% yield (2 g, 4.97 mmol) as a colorless oil. A mixture of diastereomers ∼6:5. ^1H NMR (499.8 MHz, CDCl$_3$): 1.33, 1.34 (2 × td, 2 × 3H, J_{vic} = 7.1, $J_{H,P}$ = 0.3, **CH$_3$**CH$_2$O); 1.35, 1.57 (2 × s, 2 × 6H, (CH$_3$)$_2$C); 4.09–4.17 (m, 4H, CH$_3$**CH$_2$**O); 4.21–4.30 (m, 4H, H-5′); 4.34–4.39 (m, 2H, H-4′); 4.86, 4.87 (2 × dd, 2 × 1H, $J_{3′,2′}$ = 6.4, $J_{3′,4′}$ = 3.7, H-3′); 4.92 (dd, 2H, $J_{2′,3′}$ = 6.5, $J_{2′,1′}$ = 2.4, H-2′); 5.71, 5.73 (2 × d, 2 × 1H, $J_{5,6}$ = 8.1, H-5); 5.78, 5.805 (2 × d, 2 × 1H, $J_{1′,2′}$ = 2.4, H-1′); 6.05, 6.06 (2 × ddd, 2 × 1H, $J_{H,P}$ = 22.9, J_{trans} = 18.6, J_{cis} = 12.8, =CHP); 6.12, 6.14 (2 × ddd, 2 × 1H, $J_{H,P}$ = 51.6, J_{cis} = 12.8, J_{gem} = 2.0, CH$_{cis}$**H**$_{trans}$=CHP); 6.34, 6.35 (2 × ddd, 2 × 1H, $J_{H,P}$ = 24.7, J_{trans} = 18.6, J_{gem} = 2.0, **CH**$_{cis}$H$_{trans}$=CHP); 7.40, 7.44 (2 × d, 2 × 1H, $J_{6,5}$ = 8.1, H-6); 10.15 (bs, 2H, NH). ^13C NMR (125.7 MHz, CDCl$_3$): 16.18 (d, $J_{C,P}$ = 6.2, **CH$_3$**CH$_2$O); 25.10, 25.12, 26.95, 26.96 ((CH$_3$)$_2$C); 62.30 (d, $J_{C,P}$ = 5.5, CH$_3$**CH$_2$**O); 64.94, 64.99 (d, $J_{C,P}$ = 5.8, CH$_2$-5′); 80.54, 80.60 (CH-3′); 84.31, 84.39 (CH-2′); 85.32, 85.52 (d, $J_{C,P}$ = 7.1, CH-4′); 93.51, 93.78 (CH-1′); 102.36, 102.44 (CH-5); 114.34, 114.38 (**C**(CH$_3$)$_2$); 124.91, 124.95 (d, $J_{C,P}$ = 184.2, =CHP); 136.51, 136.53 (d, $J_{C,P}$ = 2.3, CH$_2$=CHP); 141.67, 141.73 (CH-6); 150.08, 150.11 (C-2); 163.58 (C-4). ^31P NMR (202.3 MHz, CDCl$_3$): 18.49, 18.66. HR-ESI: C$_{16}$H$_{24}$O$_8$N$_2$P (M + H)$^+$ calcd 403.12648; found 403.12632.

Tetradecyl 2′,3′-Isopropylideneuridin-5′-yl Vinylphosphonate (10c). The title compound was prepared according to general method B from **9a** (2.45 g, 5.15 mmol) and tetradecanol (2.2 g, 10.31 mmol) in 40% yield (1.17 g, 2.05 mmol) as a colorless thick oil. A mixture of diastereomers ∼6:5. ^1H NMR (499.8 MHz, CDCl$_3$): 0.88 (m, 6H, **CH$_3$**(CH$_2$)$_{13}$); 1.20–1.35 (m, 44H, CH$_3$(**CH$_2$**)$_{11}$CH$_2$CH$_2$O); 1.350, 1.354, 1.573, 1.576 (4 × q, 4 × 3H, ^4J = 0.7, (CH$_3$)$_2$C); 1.67 (m, 4H, CH$_3$(CH$_2$)$_{11}$**CH$_2$**CH$_2$O); 4.03, 4.04 (2 × dt, 2 × 2H, $J_{H,P}$ = 7.3, J_{vic} = 6.7, CH$_3$(CH$_2$)$_{11}$CH$_2$**CH$_2$**O); 4.19–4.29 (m, 4H, H-5′); 4.35–4.39 (m, 2H, H-4′); 4.85, 4.86 (2 × dd, 2 × 1H, $J_{3′,2′}$ = 6.4, $J_{3′,4′}$ = 3.6, H-3′); 4.88, 4.89 (2 × dd, 2 × 1H, $J_{2′,3′}$ = 6.4, $J_{2′,1′}$ = 2.3, H-2′); 5.71, 5.72 (2 × d, 2 × 1H, $J_{5,6}$ = 8.1, H-5); 5.77, 5.81 (2 × d, 2 × 1H, $J_{1′,2′}$ = 2.3, H-1′); 6.03, 6.04 (2 × ddd, 2 × 1H, $J_{H,P}$ = 22.9, J_{trans} = 18.6, J_{cis} = 12.7, =CHP); 6.16, 6.19 (2 × ddd, 2 × 1H, $J_{H,P}$ = 51.6, J_{cis} = 12.7, J_{gem} = 2.0, CH$_{cis}$**H**$_{trans}$=CHP); 6.33, 6.34 (2 × ddd, 2 × 1H, $J_{H,P}$ = 25.7, J_{trans} = 18.7, J_{gem} = 2.0, **CH**$_{cis}$H$_{trans}$=CHP); 7.38, 7.43 (2 × d, 2 × 1H, $J_{6,5}$ = 8.1, H-6); 9.34 (bs, 2H, NH). ^13C NMR (125.7 MHz, CDCl$_3$): 14.08 (**CH$_3$**(CH$_2$)$_{13}$); 22.64 (CH$_3$(**CH$_2$**)$_{11}$CH$_2$CH$_2$O); 25.23, 25.25 ((**CH$_3$**)$_2$C); 25.43 (CH$_3$(CH$_2$)$_{11}$**CH$_2$**CH$_2$O); 27.08, 27.09 ((CH$_3$)$_2$C); 29.10, 29.30, 29.46, 29.52, 29.59, 29.60, 29.62, 29.64 (CH$_3$(CH$_2$)$_{11}$CH$_2$CH$_2$O); 30.39 (d, $J_{C,P}$ = 6.2, CH$_3$(CH$_2$)$_{11}$**CH$_2$**CH$_2$O); 31.87 (CH$_3$(CH$_2$)$_{11}$CH$_2$**CH$_2$**O); 64.93, 65.01 (d, $J_{C,P}$ = 5.5, CH$_2$-5′); 66.47, 66.48 (d, $J_{C,P}$ = 5.7, CH$_3$(CH$_2$)$_{11}$CH$_2$**CH$_2$**O); 80.57, 80.66 (CH-3′); 84.45, 84.53 (CH-2′); 85.26, 85.55 (d, $J_{C,P}$ = 7.0, CH-4′); 93.43, 93.83 (CH-1′); 102.49, 102.58 (CH-5); 114.54, 114.59 (**C**(CH$_3$)$_2$); 124.97, 125.02 (d, $J_{C,P}$ = 184.3, =CHP); 136.60, 136.62 (**CH$_2$**=CHP); 141.47, 141.55 (CH-6); 149.96, 149.99 (C-2); 163.11 (C-4). ^31P NMR (202.3 MHz, CDCl$_3$): 18.59, 18.74. HR-ESI: C$_{28}$H$_{48}$O$_8$N$_2$P [M + H]$^+$ calcd 571.31428, found 571.31445, C$_{28}$H$_{47}$O$_8$N$_2$NaP [M + Na]$^+$ calcd 593.29622, found 593.29616.

Hexadecyl 2′,3′-Isopropylideneuridin-5′-yl Vinylphosphonate (10d). The title compound was prepared according to general

method B from **9a** (1.7 g, 6 mmol) and hexadecanol (2.9 g, 12 mmol) in 38% yield (1.38 g, 2.3 mmol) as a colorless thick oil. A mixture of diastereomers ∼6:5. ^1H NMR (499.8 MHz, CDCl$_3$): 0.88 (m, 6H, **CH$_3$**(CH$_2$)$_{15}$); 1.22–1.35 (m, 52H, CH$_3$(**CH$_2$**)$_{13}$CH$_2$CH$_2$O); 1.350, 1.354, 1.573, 1.577 (4 × q, 4 × 3H, ^4J = 0.7, (CH$_3$)$_2$C); 1.67 (m, 4H, CH$_3$(CH$_2$)$_{13}$**CH$_2$**CH$_2$O); 4.03, 4.04 (2 × dt, 2 × 2H, $J_{H,P}$ = 7.3, J_{vic} = 6.7, CH$_3$(CH$_2$)$_{13}$CH$_2$**CH$_2$**O); 4.19–4.30 (m, 4H, H-5′); 4.35–4.39 (m, 2H, H-4′); 4.85, 4.86 (2 × dd, 2 × 1H, $J_{3′,2′}$ = 6.4, $J_{3′,4′}$ = 3.6, H-3′); 4.878, 4.8984 (2 × dd, 2 × 1H, $J_{2′,3′}$ = 6.4, $J_{2′,1′}$ = 2.3, H-2′); 5.71, 5.72 (2 × dd, 2 × 1H, $J_{5,6}$ = 8.1, $J_{5,NH}$ = 2.2, H-5); 5.78, 5.81 (2 × d, 2 × 1H, $J_{1′,2′}$ = 2.3, H-1′); 6.03, 6.05 (2 × ddd, 2 × 1H, $J_{H,P}$ = 22.8, J_{trans} = 18.6, J_{cis} = 12.8, =CHP); 6.12, 6.13 (2 × ddd, 2 × 1H, $J_{H,P}$ = 51.7, J_{cis} = 12.8, J_{gem} = 2.0, CH$_{cis}$**H**$_{trans}$=CHP); 6.33, 6.34 (2 × ddd, 2 × 1H, $J_{H,P}$ = 24.8, J_{trans} = 18.6, J_{gem} = 2.0, **CH**$_{cis}$H$_{trans}$=CHP); 7.38, 7.43 (2 × d, 2 × 1H, $J_{6,5}$ = 8.1, H-6); 9.15, 9.18 (2 × bs, 2 × 2H, NH). ^13C NMR (125.7 MHz, CDCl$_3$): 14.08 (**CH$_3$**(CH$_2$)$_{15}$); 22.65 (CH$_3$(**CH$_2$**)$_{13}$CH$_2$CH$_2$O); 25.23, 25.26 ((**CH$_3$**)$_2$C); 25.43 (CH$_3$(CH$_2$)$_{13}$**CH$_2$**CH$_2$O); 27.08, 27.10 ((CH$_3$)$_2$C); 29.11, 29.32, 29.47, 29.53, 29.60, 29.61, 29.63, 29.65 (CH$_3$(CH$_2$)$_{13}$CH$_2$CH$_2$O); 30.40 (d, $J_{C,P}$ = 6.3, CH$_3$(CH$_2$)$_{13}$**CH$_2$**CH$_2$O); 31.88 (CH$_3$(CH$_2$)$_{13}$CH$_2$**CH$_2$**O); 64.93, 65.00 (d, $J_{C,P}$ = 5.5, CH$_2$-5′); 66.47, 66.48 (d, $J_{C,P}$ = 5.7, CH$_3$(CH$_2$)$_{13}$CH$_2$**CH$_2$**O); 80.57, 80.66 (CH-3′); 84.46, 84.54 (CH-2′); 85.25, 85.55 (d, $J_{C,P}$ = 7.1, CH-4′); 93.40, 93.80 (CH-1′); 102.49, 102.57 (CH-5); 114.55, 114.60 (**C**(CH$_3$)$_2$); 124.99, 125.04 (d, $J_{C,P}$ = 184.2, =CHP); 136.62, 136.66 (d, $J_{C,P}$ = 2.0, **CH$_2$**=CHP); 141.46, 141.55 (CH-6); 149.92, 149.95 (C-2); 163.05, 163.07 (C-4). ^31P NMR (202.3 MHz, CDCl$_3$): 18.59, 18.73. HR-ESI: C$_{30}$H$_{51}$O$_8$N$_2$PNa (M + Na)$^+$ calcd 621.32752; found 621.32778.

Octadecyl 2′,3′-Isopropylideneuridin-5′-yl Vinylphosphonate (10e). The title compound was prepared according to general method B from **9a** (2.18 g, 4.58 mmol) and octadecanol (2.48 g, 9.17 mmol) in 43% yield (1.23 g, 1.96 mmol) as a colorless thick oil. A mixture of diastereomers ∼6:5. ^1H NMR (499.8 MHz, CDCl$_3$): 0.88 (m, 6H, **CH$_3$**(CH$_2$)$_{17}$); 1.20–1.40 (m, 60H, CH$_3$(**CH$_2$**)$_{15}$CH$_2$CH$_2$O); 1.350, 1.354, 1.573, 1.576 (4 × q, 4 × 3H, ^4J = 0.7, (CH$_3$)$_2$C); 1.66 (m, 4H, CH$_3$(CH$_2$)$_{15}$**CH$_2$**CH$_2$O); 4.03, 4.04 (2 × dt, 2 × 2H, $J_{H,P}$ = 7.3, J_{vic} = 6.7, CH$_3$(CH$_2$)$_{15}$CH$_2$**CH$_2$**O); 4.19–4.29 (m, 4H, H-5′); 4.34–4.39 (m, 2H, H-4′); 4.85, 4.86 (2 × dd, 2 × 1H, $J_{3′,2′}$ = 6.4, $J_{3′,4′}$ = 3.7, H-3′); 4.88, 4.89 (2 × dd, 2 × 1H, $J_{2′,3′}$ = 6.4, $J_{2′,1′}$ = 2.3, H-2′); 5.71, 5.72 (2 × d, 2 × 1H, $J_{5,6}$ = 8.1, H-5); 5.77, 5.81 (2 × d, 2 × 1H, $J_{1′,2′}$ = 2.3, H-1′); 6.03, 6.04 (2 × ddd, 2 × 1H, $J_{H,P}$ = 22.9, J_{trans} = 18.6, J_{cis} = 12.7, =CHP); 6.16, 6.19 (2 × ddd, 2 × 1H, $J_{H,P}$ = 51.7, J_{cis} = 12.7, J_{gem} = 2.0, CH$_{cis}$**H**$_{trans}$=CHP); 6.33, 6.34 (2 × ddd, 2 × 1H, $J_{H,P}$ = 25.6, J_{trans} = 18.6, J_{gem} = 2.0, **CH**$_{cis}$H$_{trans}$=CHP); 7.38, 7.43 (2 × d, 2 × 1H, $J_{6,5}$ = 8.1, H-6); 9.37 (bs, 2H, NH). ^13C NMR (125.7 MHz, CDCl$_3$): 14.08 (**CH$_3$**(CH$_2$)$_{17}$); 22.64 (CH$_3$(**CH$_2$**)$_{15}$CH$_2$CH$_2$O); 25.22, 25.25 ((**CH$_3$**)$_2$C); 25.43 (CH$_3$(CH$_2$)$_{15}$**CH$_2$**CH$_2$O); 27.07, 27.09 ((CH$_3$)$_2$C); 29.10, 29.31, 29.46, 29.53, 29.60, 29.61, 29.63, 29.65 (CH$_3$(CH$_2$)$_{15}$CH$_2$CH$_2$O); 30.39 (d, $J_{C,P}$ = 6.2, CH$_3$(CH$_2$)$_{15}$**CH$_2$**CH$_2$O); 31.87 (CH$_3$(CH$_2$)$_{15}$CH$_2$**CH$_2$**O); 64.93, 65.01 (d, $J_{C,P}$ = 5.5, CH$_2$-5′); 66.46, 66.47 (d, $J_{C,P}$ = 5.7, CH$_3$(CH$_2$)$_{15}$CH$_2$**CH$_2$**O); 80.57, 80.66 (CH-3′); 84.45, 84.53 (CH-2′); 85.27, 85.56 (d, $J_{C,P}$ = 7.0, CH-4′); 93.44, 93.83 (CH-1′); 102.49, 102.58 (CH-5); 114.53, 114.58 (**C**(CH$_3$)$_2$); 124.97, 125.01 (d, $J_{C,P}$ = 184.2, =CHP); 136.62, 136.66 (d, $J_{C,P}$ = 2.0, **CH$_2$**=CHP); 141.47, 141.56 (CH-6); 149.97, 150.00 (C-2); 163.14, 163.16 (C-4). ^31P NMR (202.3 MHz, CDCl$_3$): 18.59, 18.74. HR-ESI: C$_{32}$H$_{56}$O$_8$N$_2$P [M + H]$^+$ calcd 627.37688, found 627.37738.

Icosanyl 2′,3′-Isopropylideneuridin-5′-yl Vinylphosphonate (10f). The title compound was prepared according to general method B from **9a** (2.35 g, 4.94 mmol) and icosanol (2.95 g, 9.9 mmol) in 34% yield (1.1 g, 1.68 mmol) as a colorless white wax. A mixture of diastereomers ∼6:5. ^1H NMR (499.8 MHz, CDCl$_3$): 0.88 (m, 6H, **CH$_3$**(CH$_2$)$_{19}$); 1.20–1.36 (m, 68H, CH$_3$(**CH$_2$**)$_{17}$CH$_2$CH$_2$O); 1.351, 1.354, 1.574, 1.577 (4 × q, 4 × 3H, ^4J = 0.7, (CH$_3$)$_2$C); 1.66 (m, 4H, CH$_3$(CH$_2$)$_{17}$**CH$_2$**CH$_2$O); 4.03, 4.04 (2 × dt, 2 × 2H, $J_{H,P}$ = 7.3, J_{vic} = 6.7, CH$_3$(CH$_2$)$_{17}$CH$_2$**CH$_2$**O); 4.19–4.29 (m, 4H, H-5′); 4.35–4.39 (m, 2H, H-4′); 4.84, 4.86 (2 × dd, 2 × 1H, $J_{3′,2′}$ = 6.4, $J_{3′,4′}$ = 3.4, H-3′); 4.87, 4.89 (2 × dd, 2 × 1H, $J_{2′,3′}$ = 6.4, $J_{2′,1′}$ = 2.3, H-2′); 5.706, 5.714 (2

× d, 2 × 1H, $J_{5,6}$ = 8.1, H-5); 5.77, 5.80 (2 × d, 2 × 1H, $J_{1',2'}$ = 2.3, H-1'); 6.03, 6.06 (2 × ddd, 2 × 1H, $J_{H,P}$ = 22.8, J_{trans} = 18.6, J_{cis} = 12.7, =CHP); 6.17, 6.19 (2 × ddd, 2 × 1H, $J_{H,P}$ = 51.7, J_{cis} = 12.7, J_{gem} = 2.0, CH$_{cis}$**H$_{trans}$**=CHP); 6.33, 6.34 (2 × ddd, 2 × 1H, $J_{H,P}$ = 25.6, J_{trans} = 18.6, J_{gem} = 2.0, **CH$_{cis}$**H$_{trans}$=CHP); 7.37, 7.43 (2 × d, 2 × 1H, $J_{6,5}$ = 8.1, H-6); 9.08 (bs, 2H, NH). ^{13}C NMR (125.7 MHz, CDCl$_3$): 14.10 (**CH$_3$**(CH$_2$)$_{19}$); 22.66 (CH$_3$(**CH$_2$**)$_{17}$CH$_2$CH$_2$O); 25.24, 25.26 ((**CH$_3$**)$_2$C); 25.44 (CH$_3$(**CH$_2$**)$_{17}$CH$_2$CH$_2$O); 27.09, 27.11 ((**CH$_3$**)$_2$C); 29.12, 29.33, 29.48, 29.55, 29.62, 29.65, 29.67 (CH$_3$(**CH$_2$**)$_{17}$CH$_2$CH$_2$O); 30.41 (d, $J_{C,P}$ = 6.3, CH$_3$(CH$_2$)$_{17}$**CH$_2$**CH$_2$O); 31.89 (CH$_3$(**CH$_2$**)$_{17}$CH$_2$CH$_2$O); 64.92, 64.99 (d, $J_{C,P}$ = 5.5, CH$_2$-5'); 66.48, 66.50 (d, $J_{C,P}$ = 5.7, CH$_3$(CH$_2$)$_{17}$**CH$_2$**CH$_2$O); 80.57, 80.66 (CH-3'); 84.47, 84.56 (CH-2'); 85.25, 85.54 (d, $J_{C,P}$ = 7.0, CH-4'); 93.44, 93.83 (CH-1'); 102.50, 102.59 (CH-5); 114.56, 114.62 (**C**(CH$_3$)$_2$); 124.98, 125.02 (d, $J_{C,P}$ = 184.2, =CHP); 136.65, 136.70 (d, $J_{C,P}$ = 1.9, **CH$_2$**=CHP); 141.41, 141.50 (CH-6); 149.90, 149.93 (C-2); 162.92, 162.95 (C-4). ^{31}P NMR (202.3 MHz, CDCl$_3$): 18.59, 18.74. HR-ESI: C$_{34}$H$_{60}$O$_8$N$_2$P [M + H] calcd 655.40818, found 655.40857; C$_{34}$H$_{59}$O$_8$N$_2$NaP [M + Na] calcd 677.39012, found 677.39032.

Hexadecyloxypropyl 2′,3′-Isopropylideneuridin-5′-yl Vinylphosphonate (10g). The title compound was prepared according to general method B from **9a** (1.8 g, 6.1 mmol) and hexadecyloxypropanol (1.45 g, 3.05 mmol) in 71% yield (1.42 g, 2.16 mmol) as a colorless white wax. A mixture of diastereomers ∼1:1. ^{1}H NMR (500.0 MHz, CDCl$_3$): 0.88 (m, 6H, **CH$_3$**(CH$_2$)$_{15}$); 1.23−1.33 (m, 52H, CH$_3$(**CH$_2$**)$_{13}$CH$_2$CH$_2$O); 1.348, 1.352 (2 × q, 2 × 3H, ^4J = 0.6, (CH$_3$)$_2$C); 1.54 (m, 4H, CH$_3$(CH$_2$)$_{13}$**CH$_2$**CH$_2$O); 1.57 (s, 6H, (CH$_3$)$_2$C); 1.92, 1.94 (2 × p, 2 × 2H, J_{vic} = 6.1, OCH$_2$**CH$_2$**CH$_2$OC$_{16}$H$_{33}$); 3.38, 3.39 (2 × t, 2 × 2H, J_{vic} = 6.7, CH$_3$(CH$_2$)$_{13}$CH$_2$**CH$_2$**); 3.48, 3.49 (2 × t, 2 × 2H, J_{vic} = 6.1, OCH$_2$CH$_2$**CH$_2$**OC$_{16}$H$_{33}$); 4.13, 4.15 (2 × td, 2 × 2H, J_{vic} = 6.1, $J_{H,P}$ = 4.8, O**CH$_2$**CH$_2$CH$_2$OC$_{16}$H$_{33}$); 4.20−4.30 (m, 4H, H-5′); 4.34−4.38 (m, 2H, H-4′); 4.85, 4.86 (2 × dd, 2 × 1H, $J_{3',2'}$ = 6.5, $J_{3',4'}$ = 3.6, H-3′); 4.92 (dd, 2H, $J_{2',3'}$ = 6.5, $J_{2',1'}$ = 2.3, H-2′); 5.700, 5.704 (2 × d, 2 × 1H, $J_{5,6}$ = 8.1 H-5); 5.74, 5.76 (2 × d, 2 × 1H, $J_{1',2'}$ = 2.3, H-1′); 6.03, 6.05 (2 × ddd, 2 × 1H, $J_{H,P}$ = 22.9, J_{trans} = 18.4, J_{cis} = 12.7, =CHP); 6.16, 6.18 (2 × ddd, 2 × 1H, $J_{H,P}$ = 51.8, J_{cis} = 12.7, J_{gem} = 1.9, CH$_{cis}$**H$_{trans}$**=CHP); 6.33, 6.35 (2 × ddd, 2 × 1H, $J_{H,P}$ = 25.5, J_{trans} = 18.4, J_{gem} = 1.9, **CH$_{cis}$**H$_{trans}$=CHP); 7.34, 7.39 (2 × d, 2 × 1H, $J_{6,5}$ = 8.1, H-6). ^{13}C NMR (125.7 MHz, CDCl$_3$): 14.07 (**CH$_3$**(CH$_2$)$_{15}$); 22.62 (CH$_3$(**CH$_2$**)$_{13}$CH$_2$CH$_2$O); 25.19, 25.21 ((**CH$_3$**)$_2$C); 26.08 (CH$_3$(**CH$_2$**)$_{14}$CH$_2$O); 27.04, 27.06 ((**CH$_3$**)$_2$C); 29.29, 29.45, 29.55, 29.57, 29.58, 29.63 (CH$_3$(**CH$_2$**)$_{14}$CH$_2$O); 30.66, 30.68 (d, $J_{C,P}$ = 6.4, OCH$_2$**CH$_2$**CH$_2$OC$_{16}$H$_{33}$); 31.85 (CH$_3$(**CH$_2$**)$_{13}$CH$_2$CH$_2$O); 63.56, 63.57 (d, $J_{C,P}$ = 5.5, O**CH$_2$**CH$_2$CH$_2$OC$_{16}$H$_{33}$); 64.92, 65.01 (d, $J_{C,P}$ = 5.5, CH$_2$-5′); 66.32, 66.36 (OCH$_2$CH$_2$**CH$_2$**OC$_{16}$H$_{33}$); 71.15, 71.16 (CH$_3$(**CH$_2$**)$_{14}$CH$_2$O); 80.60, 80.67 (CH-3′); 84.44, 84.53 (CH-2′); 85.38, 85.62 (d, $J_{C,P}$ = 7.1, CH-4′); 93.82, 94.12 (CH-1′); 102.57, 102.64 (CH-5); 114.42, 114.46 (**C**(CH$_3$)$_2$); 124.75, 124.80 (d, $J_{C,P}$ = 184.0, =CHP); 136.75, 136.77 (d, $J_{C,P}$ = 1.9, **CH$_2$**=CHP); 141.43, 141.48 (CH-6); 150.16 (C-2); 163.29, 163.32 (C-4). ^{31}P NMR (202.3 MHz, CDCl$_3$): 18.64, 18.80. HR-ESI: C$_{33}$H$_{58}$O$_9$N$_2$P (M + H)$^+$ calcd 657.3874; found 657.3876.

Hexadecyloxypropyl 4-N-Benzoyl-2′,3′-isopropylidenecytidin-5′-yl Vinylphosphonate (10h). The title compound was prepared according to general method B from **9b** (0.65 g, 1.36 mmol) and hexadecyloxypropanol (0.81 g, 2.7 mmol) in 78% yield (0.81 g, 1.06 mmol) as a white foam. A mixture of diastereomers ∼1:1. ^{1}H NMR (600.1 MHz, CD$_3$OD): 0.895 (m, 6H, **CH$_3$**(CH$_2$)$_{15}$); 1.24−1.35 (m, 52H, CH$_3$(**CH$_2$**)$_{13}$CH$_2$CH$_2$O); 1.368, 1.371 (2 × q, 2 × 3H, ^4J = 0.6, (CH$_3$)$_2$C); 1.51 (m, 4H, CH$_3$(CH$_2$)$_{13}$**CH$_2$**CH$_2$O); 1.57 (s, 6H, (CH$_3$)$_2$C); 1.89, 1.91 (2 × p, 2 × 2H, J_{vic} = 6.1, OCH$_2$**CH$_2$**CH$_2$OC$_{16}$H$_{33}$); 3.38, 3.39 (2 × t, 2 × 2H, J_{vic} = 6.7, CH$_3$(CH$_2$)$_{13}$CH$_2$**CH$_2$**); 3.47 (td, 2H, J_{vic} = 6.1, $J_{H,P}$ = 1.2, OCH$_2$CH$_2$**CH$_2$**OC$_{16}$H$_{33}$); 3.49 (t, 2H, J_{vic} = 6.1, OCH$_2$CH$_2$**CH$_2$**OC$_{16}$H$_{33}$); 4.09−4.16 (m, 4H, O**CH$_2$**CH$_2$CH$_2$OC$_{16}$H$_{33}$); 4.27−4.36 (m, 4H, H-5′); 4.48 (m, 2H, H-4′); 4.91 (dd, 2H, $J_{3',2'}$ = 6.2, $J_{3',4'}$ = 3.6, H-3′); 5.06, 507 (2 × dd, 2 × 1H, $J_{2',3'}$ = 6.2, $J_{2',1'}$ = 1.8, H-2′); 5.87, 5.88 (2 × d, 2 × 1H, $J_{1',2'}$ = 1.8,

H-1′); 6.145, 6.17 (2 × ddd, 2 × 1H, $J_{H,P}$ = 24.0, J_{trans} = 18.4, J_{cis} = 12.8, =CHP); 6.257, 6.261 (2 × ddd, 2 × 1H, $J_{H,P}$ = 52.0, J_{cis} = 12.8, J_{gem} = 2.1, CH$_{cis}$**H$_{trans}$**=CHP); 6.30, 6.31 (2 × ddd, 2 × 1H, $J_{H,P}$ = 26.0, J_{trans} = 18.4, J_{gem} = 2.1, **CH$_{cis}$**H$_{trans}$=CHP); 7.54 (m, 4H, H-m-Bz); 7.59 (d, 2H, $J_{5,6}$ = 7.7, H-5); 7.64 (m, 2H, H-p-Bz); 7.99 (m, 4H, H-o-Bz); 8.16, 8.17 (2 × d, 2 × 1H, $J_{6,5}$ = 7.7, H-5). ^{13}C NMR (150.9 MHz, CD$_3$OD): 14.48 (**CH$_3$**(CH$_2$)$_{15}$); 23.75 (CH$_3$(**CH$_2$**)$_{13}$CH$_2$CH$_2$O); 25.46, 25.48 ((**CH$_3$**)$_2$C); 27.27 (CH$_3$(**CH$_2$**)$_{14}$CH$_2$O); 27.43 ((**CH$_3$**)$_2$C); 30.49, 30.61, 30.78, 30.80, 30.81 (CH$_3$(**CH$_2$**)$_{14}$CH$_2$O); 31.70 (d, $J_{C,P}$ = 6.5, OCH$_2$**CH$_2$**CH$_2$OC$_{16}$H$_{33}$); 33.09 (CH$_3$(**CH$_2$**)$_{13}$CH$_2$CH$_2$O); 64.96, 64.98 (d, $J_{C,P}$ = 5.7, O**CH$_2$**CH$_2$CH$_2$OC$_{16}$H$_{33}$); 66.97, 67.04 (d, $J_{C,P}$ = 5.6, CH$_2$-5′); 67.42, 67.43 (OCH$_2$CH$_2$**CH$_2$**OC$_{16}$H$_{33}$); 72.10 (CH$_3$(**CH$_2$**)$_{14}$CH$_2$O); 82.64, 82.635, 82.644 (CH-3′); 86.57, 86.58 (CH-2′); 88.23, 88.30 (d, $J_{C,P}$ = 7.2, CH-4′); 97.60, 97.71 (CH-1′); 98.51, 98.54 (CH-5); 115.10, 115.11 (**C**(CH$_3$)$_2$); 125.63, 125.67 (d, $J_{C,P}$ = 183.9, =CHP); 129.25 (CH-o-Bz); 129.83 (CH-m-Bz); 134.14 (CH-p-Bz); 134.70 (C-i-Bz); 138.01, 138.04 (d, $J_{C,P}$ = 1.9, **CH$_2$**=CHP); 148.26, 148.34 (CH-6); 157.58, 157.60 (C-2); 165.58 (C-4); 169.19 (CO-Bz). ^{31}P NMR (202.3 MHz, CD$_3$OD): 19.62, 19.72. HR-EI: C$_{40}$H$_{62}$N$_3$O$_9$P (M + H)$^+$ calcd 759.4224; found 759.4225.

Hexadecyloxypropyl Uridin-5′-yl 2-([3R,4R]-3,4-Dihydroxypyrrolidin-1-N-yl)ethylphosphonate (12a). The mixture of dihydroxypyrrolidine **11a** (0.12 g, 1.18 mmol) and phosphonate **10g** (0.4 g, 0.61 mmol) in nBuOH (15 mL) was stirred at 105 °C overnight. The solvent was removed, and the isopropylidene intermediate was obtained by flash chromatography on silica gel using linear gradient of H1 in ethyl acetate. This compound was without further characterization dissolved in 0.5 M methanolic HCl (30 mL), and the mixture was stirred at rt for 4 h. The desired product was obtained after evaporation of solvent in 34% overall yield (152 mg, 0.205 mmol) as a white amorphous solid. A mixture of diastereomers ∼6:5. ^{1}H NMR (499.8 MHz, CD$_3$OD): 0.90 (m, 6H, **CH$_3$**(CH$_2$)$_{15}$); 1.25−1.38 (m, 52H, CH$_3$(**CH$_2$**)$_{13}$CH$_2$CH$_2$O); 1.55 (m, 4H, CH$_3$(CH$_2$)$_{13}$**CH$_2$**CH$_2$O); 1.93 (m, 4H, OCH$_2$**CH$_2$**CH$_2$OC$_{16}$H$_{33}$); 2.12−2.25 (m, 4H, CH$_2$P); 2.71 (dd, 4H, J_{gem} = 10.6, J_{vic} = 3.0, H-2b,5b-pyrr); 2.86−3.00 (m, 4H, CH$_2$N); 3.116, 3.118 (2 × dd, 2 × 2H, J_{gem} = 10.6, J_{vic} = 5.0, H-2a,5a-pyrr); 3.42, 3.43 (2 × t, 2 × 2H, J_{vic} = 6.6, CH$_3$(CH$_2$)$_{13}$CH$_2$**CH$_2$**); 3.515, 3.522 (2 × t, 2 × 2H, J_{vic} = 6.1, OCH$_2$CH$_2$**CH$_2$**OC$_{16}$H$_{33}$); 4.08 (m, 4H, O**CH$_2$**CH$_2$CH$_2$OC$_{16}$H$_{33}$); 4.11−4.21 (m, 8H, H-3′,4′, H-3,4-pyrr); 4.216, 4.218 (2 × dd, 2 × 1H, $J_{2',3'}$ = 5.1, $J_{2',1'}$ = 4.1, H-2′); 4.26 (ddd, 1H, J_{gem} = 11.6, $J_{H,P}$ = 6.8, $J_{5'b,4'}$ = 4.5, H-5′b); 4.30−4.34 (m, 2H, H-5′); 4.36 (ddd, 1H, J_{gem} = 11.6, $J_{H,P}$ = 6.6, $J_{5'a,4'}$ = 2.9, H-5′a); 5.751, 5.753 (2 × d, 2 × 1H, $J_{5,6}$ = 8.1, H-5); 5.845 (d, 2H, $J_{1',2'}$ = 4.1, H-1′); 7.70, 7.73 (2 × d, 2 × 1H, $J_{6,5}$ = 8.1, H-6). ^{13}C NMR (125.7 MHz, CD$_3$OD): 14.47 (**CH$_3$**(CH$_2$)$_{15}$); 23.73 (CH$_3$(**CH$_2$**)$_{14}$CH$_2$O); 24.75, 24.81 (d, $J_{C,P}$ = 139.6, CH$_2$P); 27.28, 30.47, 30.63, 30.76, 30.79 (CH$_3$(**CH$_2$**)$_{14}$CH$_2$O); 31.75, 31.78 (d, $J_{C,P}$ = 6.2, OCH$_2$**CH$_2$**CH$_2$OC$_{16}$H$_{33}$); 33.06 (CH$_3$(**CH$_2$**)$_{14}$CH$_2$O); 50.81, 50.85 (CH$_2$N); 60.95, 60.98 (CH$_2$-2,5-pyrr); 64.86, 64.93 (d, $J_{C,P}$ = 6.7, O**CH$_2$**CH$_2$CH$_2$OC$_{16}$H$_{33}$); 66.52, 66.54 (d, $J_{C,P}$ = 6.2, CH$_2$-5′); 67.49, 67.53 (OCH$_2$CH$_2$**CH$_2$**OC$_{16}$H$_{33}$); 70.79, 70.86 (CH-3′); 72.14 (CH$_3$(**CH$_2$**)$_{14}$CH$_2$O); 74.87, 74.93 (CH-2′); 78.12, 78.19 (CH-3,4-pyrr); 83.57, 83.58 (d, $J_{C,P}$ = 6.6, CH-4′); 91.75, 91.85 (CH-1′); 103.02 (CH-5); 142.58, 142.64 (CH-6); 152.18, 152.20 (C-2); 165.99 (C-4). ^{31}P NMR (202.3 MHz, CD$_3$OD): 31.37, 31.64. HR-ESI: C$_{34}$H$_{63}$O$_{11}$N$_3$P (M + H)$^+$ calcd 720.41947; found 720.41939.

Hexadecyloxypropyl Cytidin-5′-yl 2-([3R,4R]-3,4-Dihydroxypyrrolidin-1-N-yl)ethylphosphonate (12b). The mixture of dihydroxypyrrolidine **11a** (0.05 g, 0.49 mmol) and benzoylcytosine vinylphosphonate **10h** (0.34 g, 0.45 mmol) in nBuOH (10 mL) was stirred at 100 °C for 12 h. The solvent was removed and the protected intermediate was purified by flash chromatography on silica gel using linear gradient of H1 in ethyl acetate. White foam obtained after evaporation of solvents was without further characterization (only LC-MS confirmation) dissolved in 8 M ethanolic methylamine (10 mL) and left aside at rt overnight. The mixture was concentrated in vacuo, coevaporated with ethanol (2 × 20 mL), dissolved in 0.2 M methanolic HCl (10 mL), and the reaction mixture was left aside at rt overnight. After concentration in vacuo (note: temperature in the

J

dx.doi.org/10.1021/jm2009343 | J. Med. Chem. XXXX, XXX, XXX−XXX

bath did not exceed 40 °C) and coevaporation with ethanol (3 × 20 mL), the final product was obtained by preparative HPLC in 27% overall yield (90.6 mg, 120 μM) as a white amorphous solid. A mixture of diastereomers ∼8:7. ^{1}H NMR (600.1 MHz, CD$_3$OD): 0.90 (m, 6H, **CH$_3$**(CH$_2$)$_{15}$); 1.25−1.38 (m, 52H, CH$_3$(**CH$_2$**)$_{13}$CH$_2$CH$_2$O); 1.55 (m, 4H, CH$_3$(CH$_2$)$_{13}$**CH$_2$**CH$_2$O); 1.93 (m, 4H, OCH$_2$**CH$_2$**CH$_2$OC$_{16}$H$_{33}$); 2.10−2.18 (m, 4H, CH$_2$P); 2.56 (bm, 4H, H-2b,5b-pyrr); 2.75−2.87 (bm, 4H, CH$_2$N); 3.00 (bm, 4H, H-2a,5a-pyrr); 3.41, 3.43 (2 × t, 2 × 2H, J_{vic} = 6.7, CH$_3$(CH$_2$)$_{13}$CH$_2$**CH$_2$**O); 3.51, 3.53 (2 × t, 2 × 2H, J_{vic} = 6.0, OCH$_2$CH$_2$**CH$_2$**OC$_{16}$H$_{33}$); 4.04 (m, 4H, H-3,4-pyrr); 4.08−4.23 (m, 10H, H-2′,3′,4′-pyrr, O**CH$_2$**CH$_2$CH$_2$OC$_{16}$H$_{33}$); 4.25−4.42 (m, 4H, H-5′); 5.83, 5.84 (d, 2H, $J_{1′,2′}$ = 3.0, H-1′); 5.93, 5.94 (2 × d, 2 × 1H, $J_{5,6}$ = 7.6, H-5); 7.77, 7.79 (2 × d, 2 × 1H, $J_{6,5}$ = 7.6, H-6). ^{13}C NMR (150.9 MHz, CD$_3$OD): 14.47 (**CH$_3$**(CH$_2$)$_{15}$); 23.75 (CH$_3$(**CH$_2$**)$_{14}$CH$_2$O); 25.09, 25.14 (d, $J_{C,P}$ = 139.1, CH$_2$P); 27.29, 27.30, 30.49, 30.64, 30.77, 30.80 (CH$_3$(**CH$_2$**)$_{14}$CH$_2$O); 31.76, 31.79 (d, $J_{C,P}$ = 6.3, OCH$_2$**CH$_2$**CH$_2$OC$_{16}$H$_{33}$); 33.08 (CH$_3$(**CH$_2$**)$_{14}$CH$_2$O); 50.55 (CH$_2$N); 60.99, 61.02 (CH$_2$-2,5-pyrr); 64.71, 64.79 (d, $J_{C,P}$ = 6.6, OCH$_2$**CH$_2$**CH$_2$OC$_{16}$H$_{33}$); 66.24, 66.31 (d, $J_{C,P}$ = 6.4, CH$_2$-5′); 67.51, 67.55 (OCH$_2$CH$_2$**CH$_2$**OC$_{16}$H$_{33}$); 70.52, 70.55 (CH-3′); 72.15 (CH$_3$(CH$_2$)$_{14}$**CH$_2$**O); 75.68, 75.70 (CH-2′); 78.61, 78.66 (CH-3,4-pyrr); 83.13, 83.16 (d, $J_{C,P}$ = 6.6, CH-4′); 92.89, 92.90 (CH-1′); 96.17, 96.18 (C-5); 142.56, 142.64 (CH-6); 158.26, 158.27 (C-2); 167.646, 167.653 (C-4). ^{31}P NMR (202.3 MHz, CD$_3$OD): 32.67, 32.99. HR-ESI: C$_{34}$H$_{64}$O$_{10}$N$_4$P (M + H)$^+$ calcd 719.4355; found 719.4357.

Hexadecyloxypropyl Uridin-5′-yl 2-([3S,4S]-3,4-Dihydroxy-pyrrolidin-1-N-yl)ethylphosphonate (12c). The mixture of dihydroxypyrrolidine **11b** (0.26 g, 2.56 mmol) and phosphonate **10g** (0.84 g, 1.28 mmol) in nBuOH (30 mL) was stirred at 105 °C overnight. The solvent was removed, and the isopropylidene intermediate was obtained by flash chromatography on silica gel using linear gradient of H1 in ethyl acetate. This compound was without further characterization dissolved in 0.5 M methanolic HCl (40 mL), and the mixture was stirred at rt for 4 h. After concentration in vacuo (note: temperature in the bath did not exceeded 40 °C) and coevaporation with ethanol (3 × 20 mL) the desired product was obtained by flash chromatography on silica gel using linear gradient of H1 in ethyl acetate in 36% overall yield (344 mg, 0.46 mmol) as a white amorphous solid. A mixture of diastereomers ∼6:5. ^{1}H NMR (499.8 MHz, CD$_3$OD): 0.90 (m, 6H, **CH$_3$**(CH$_2$)$_{15}$); 1.25−1.39 (m, 52H, CH$_3$(**CH$_2$**)$_{13}$CH$_2$CH$_2$O); 1.55 (m, 4H, CH$_3$(CH$_2$)$_{13}$**CH$_2$**CH$_2$O); 1.95 (m, 4H, OCH$_2$**CH$_2$**CH$_2$OC$_{16}$H$_{33}$); 2.37−2.52 (m, 4H, CH$_2$P); 3.16 (bm, 2H, H-2b,5b-pyrr); 3.42 (t, 2H, J_{vic} = 6.7, CH$_3$(CH$_2$)$_{13}$CH$_2$**CH$_2$**O); 3.425 (bm, 2H, H-2b,5b-pyrr); 3.43 (t, 2H, J_{vic} = 6.7, CH$_3$(CH$_2$)$_{13}$CH$_2$**CH$_2$**O); 3.515 (m, 4H, CH$_2$N); 3.52, 3.53 (2 × t, 2 × 2H, J_{vic} = 6.1, OCH$_2$CH$_2$**CH$_2$**OC$_{16}$H$_{33}$); 3.59, 3.92 (2 × bm, 2 × 2H, H-2a,5a-pyrr); 4.14 (m, 2H, H-4′); 4.16 (m, 2H, H-3′); 4.18−4.27 (m, 10H, H-2′, O**CH$_2$**CH$_2$CH$_2$OC$_{16}$H$_{33}$, H-3,4-pyrr); 4.31 (ddd, 1H, J_{gem} = 11.5, $J_{H,P}$ = 7.6, $J_{5′b,4′}$ = 5.4, H-5′b); 4.36 (m, 2H, H-5′); 4.40 (ddd, 1H, J_{gem} = 11.5, $J_{H,P}$ = 7.3, $J_{5′a,4′}$ = 2.9, H-5′a); 5.742, 5.746 (2 × d, 2 × 1H, $J_{5,6}$ = 8.1, H-5); 5.78, 5.80 (2 × d, 2 × 1H, $J_{1′,2′}$ = 3.9, H-1′); 7.68, 7.70 (2 × d, 2 × 1H, $J_{6,5}$ = 8.1, H-6). ^{13}C NMR (125.7 MHz, CD$_3$OD): 14.45 (**CH$_3$**(CH$_2$)$_{15}$); 23.32 (d, $J_{C,P}$ = 142.0, CH$_2$P); 23.74 (CH$_3$(**CH$_2$**)$_{14}$CH$_2$O); 27.29, 30.48, 30.64, 30.76, 30.79 (CH$_3$(**CH$_2$**)$_{14}$CH$_2$O); 31.70, 31.72 (d, $J_{C,P}$ = 6.1, OCH$_2$**CH$_2$**CH$_2$OC$_{16}$H$_{33}$); 33.07 (CH$_3$(**CH$_2$**)$_{14}$CH$_2$O); 52.18, 52.22 (CH$_2$N); 60.67, 60.75, 60.98, 61.01 (CH$_2$-2,5-pyrr); 65.33, 65.58 (d, $J_{C,P}$ = 6.7, OCH$_2$**CH$_2$**CH$_2$OC$_{16}$H$_{33}$); 67.16 (d, $J_{C,P}$ = 6.5, CH$_2$-5′); 67.44 (OCH$_2$CH$_2$**CH$_2$**OC$_{16}$H$_{33}$); 67.45 (d, $J_{C,P}$ = 4.3, CH$_2$-5′); 67.47 (OCH$_2$CH$_2$**CH$_2$**OC$_{16}$H$_{33}$); 70.77 (CH-3′); 72.16 (CH$_3$(CH$_2$)$_{14}$**CH$_2$**O); 74.55, 74.60 (CH-2′); 75.67, 75.68, 76.04 (CH-3,4-pyrr); 83.29 (d, $J_{C,P}$ = 6.2, CH-4′); 83.40 (d, $J_{C,P}$ = 5.8, CH-4′); 92.83, 92.85 (CH-1′); 103.03, 103.10 (CH-5); 143.12, 143.19 (CH-6); 152.13, 152.14 (C-2); 166.00 (C-4). ^{31}P NMR (202.3 MHz, CD$_3$OD): 26.79, 27.26.

Hexadecyloxypropyl Uridin-5′-yl 2-([3R,4S,5S]-3,4-Trihydroxypiperidin-1-N-yl)ethylphosphonate (12d). The mixture of trihydroxypiperidine **11e** (0.04 g, 0.33 mmol) and phosphonate **10g** (0.1 g, 0.16 mmol) in nBuOH (5 mL) was stirred at 105 °C overnight.

The solvent was removed and the isopropylidene intermediate was obtained by flash chromatography on silica gel using linear gradient of ethanol in chloroform. This compound was without characterization dissolved in 0.5 M methanolic HCl (20 mL), and the mixture was stirred at rt for 2 h. After concentration in vacuo (note: temperature in the bath did not exceeded 40 °C) and coevaporation with ethanol (3 × 20 mL), the desired product was obtained by flash chromatography on silica gel using linear gradient of H1 in ethyl acetate in 68% overall yield (80 mg, 0.11 mmol) as a white amorphous solid. A mixture of diastereomers ∼7:3. ^{1}H NMR (499.8 MHz, CD$_3$OD): 0.90 (m, 6H, **CH$_3$**(CH$_2$)$_{15}$); 1.25−1.38 (m, 52H, CH$_3$(**CH$_2$**)$_{13}$CH$_2$CH$_2$O); 1.55 (m, 4H, CH$_3$(CH$_2$)$_{13}$**CH$_2$**CH$_2$O); 1.93 (m, 4H, OCH$_2$**CH$_2$**CH$_2$OC$_{16}$H$_{33}$); 2.10−2.18 (m, 4H, CH$_2$P); 2.43, 2.54 (2 × bm, 2 × 4H, H-2,6-pip); 2.75 (m, 4H, CH$_2$N); 3.42, 3.43 (2 × t, 2 × 2H, J_{vic} = 6.6, CH$_3$(CH$_2$)$_{13}$CH$_2$**CH$_2$**O); 3.52, 3.53 (2 × t, 2 × 2H, J_{vic} = 6.1, OCH$_2$CH$_2$**CH$_2$**OC$_{16}$H$_{33}$); 3.68 (bm, 4H, H-3,5-pip); 3.81 (bm, 2H, H-4-pip); 4.11−4.22 (m, 10H, H-2′,3′,4′, O**CH$_2$**CH$_2$CH$_2$OC$_{16}$H$_{33}$); 4.23−4.38 (m, 4H, H-5′); 5.746, 5.749 (2 × d, 2 × 1H, $J_{5,6}$ = 8.1, H-5); 5.84 (d, 2H, $J_{1′,2′}$ = 4.1, H-1′); 7.71, 7.73 (2 × d, 2 × 1H, $J_{6,5}$ = 8.1, H-6). ^{13}C NMR (125.7 MHz, CD$_3$OD): 14.45 (**CH$_3$**(CH$_2$)$_{15}$); 23.55, 23.65 (d, $J_{C,P}$ = 138.5, CH$_2$P); 23.75 (CH$_3$(**CH$_2$**)$_{14}$CH$_2$O); 27.30, 30.49, 30.63, 30.77, 30.80 (CH$_3$(**CH$_2$**)$_{14}$CH$_2$O); 31.79, 31.82 (d, $J_{C,P}$ = 6.2, OCH$_2$**CH$_2$**CH$_2$OC$_{16}$H$_{33}$); 33.08 (CH$_3$(**CH$_2$**)$_{14}$CH$_2$O); 51.75 (CH$_2$N); 54.40 (CH$_2$-2,6-pip); 64.72, 64.78 (d, $J_{C,P}$ = 6.5, OCH$_2$**CH$_2$**CH$_2$OC$_{16}$H$_{33}$); 66.37 (d, $J_{C,P}$ = 6.3, CH$_2$-5′); 67.51, 67.55 (OCH$_2$CH$_2$**CH$_2$**OC$_{16}$H$_{33}$); 69.67 (CH-3,5-pip); 70.81, 70.83 (CH-3′); 71.83 (CH-4-pip); 72.17 (CH$_3$(CH$_2$)$_{14}$**CH$_2$**O); 74.97, 75.01 (CH-2′); 83.59, 83.63 (d, $J_{C,P}$ = 6.7, CH-4′); 91.84, 91.92 (CH-1′); 103.00 (CH-5); 142.56, 142.60 (CH-6); 152.18, 152.19 (C-2); 166.05 (C-4). ^{31}P NMR (202.3 MHz, CD$_3$OD): 32.91, 33.23. HR-ESI: C$_{35}$H$_{65}$O$_{11}$N$_3$P (M + H)$^+$ calcd 734.4347; found 734.4351.

Hexadecyloxypropyl Uridin-5′-yl 2-([3R,5R]-3,4-Dihydroxy-piperidin-1-N-yl)ethylphosphonate (12e). The mixture of dihydroxypiperidine **11e** (0.05 g, 0.42 mmol) and phosphonate **10g** (0.25 g, 0.38 mmol) in nBuOH (5 mL) was stirred at 105 °C overnight. The solvent was removed, and the isopropylidene intermediate was obtained by flash chromatography on silica gel using linear gradient of ethanol in chloroform. This compound was without characterization dissolved in 0.5 M methanolic HCl (40 mL), and the mixture was stirred at rt for 3 h. After concentration in vacuo (note: temperature in the bath did not exceeded 40 °C) and coevaporation with ethanol (3 × 20 mL), the desired product was obtained by chromatography on silica gel using linear gradient of H1 in ethyl acetate in 76% overall yield (230 mg, 0.29 mmol) as a white amorphous solid. A mixture of diastereomers ∼6:4. ^{1}H NMR (600.1 MHz, CD$_3$OD): 0.90 (m, 6H, **CH$_3$**(CH$_2$)$_{15}$); 1.25−1.38 (m, 52H, CH$_3$(**CH$_2$**)$_{13}$CH$_2$CH$_2$O); 1.55 (m, 4H, CH$_3$(CH$_2$)$_{13}$**CH$_2$**CH$_2$O); 1.70 (bm, 4H, H-4-pip); 1.93 (m, 4H, OCH$_2$**CH$_2$**CH$_2$OC$_{16}$H$_{33}$); 2.12−2.19 (m, 4H, CH$_2$P); 2.36, 2.57 (2 × m, 2 × 4H, H-2,6-pip); 2.66−2.76 (m, 4H, CH$_2$N); 3.42, 3.43 (2 × t, 2 × 2H, J_{vic} = 6.6, CH$_3$(CH$_2$)$_{13}$CH$_2$**CH$_2$**O); 3.51, 3.53 (2 × t, 2 × 2H, J_{vic} = 6.1, OCH$_2$CH$_2$**CH$_2$**OC$_{16}$H$_{33}$); 4.01 (m, 4H, H-3,5-pip); 4.12−4.24 (m, 10H, H-2′,3′,4′, O**CH$_2$**CH$_2$CH$_2$OC$_{16}$H$_{33}$); 4.24−4.40 (m, 4H, H-5′); 5.751, 5.754 (2 × d, 2 × 1H, $J_{5,6}$ = 8.1, H-5); 5.854, 5.856 (2 × d, 2 × 1H, $J_{1′,2′}$ = 4.1, H-1′); 7.71, 7.74 (2 × d, 2 × 1H, $J_{6,5}$ = 8.1, H-6). ^{13}C NMR (150.9 MHz, CD$_3$OD): 14.49 (**CH$_3$**(CH$_2$)$_{15}$); 23.49, 23.53 (d, $J_{C,P}$ = 138.4, CH$_2$P); 23.75 (CH$_3$(**CH$_2$**)$_{14}$CH$_2$O); 27.29, 27.30, 30.49, 30.65, 30.78, 30.81 (CH$_3$(**CH$_2$**)$_{14}$CH$_2$O); 31.76, 31.83 (d, $J_{C,P}$ = 6.3, OCH$_2$**CH$_2$**CH$_2$OC$_{16}$H$_{33}$); 33.08 (CH$_3$(**CH$_2$**)$_{14}$CH$_2$O); 40.63, 40.65 (CH$_2$-4-pip); 52.02, 52.04 (d, $J_{C,P}$ = 2.0, CH$_2$N); 60.07, 60.10 (CH$_2$-2,6-pip); 64.63, 64.75 (d, $J_{C,P}$ = 6.6, OCH$_2$**CH$_2$**CH$_2$OC$_{16}$H$_{33}$); 65.58 (CH-3,5-pip); 66.27, 66.52 (d, $J_{C,P}$ = 6.2, CH$_2$-5′); 67.51, 67.54 (OCH$_2$CH$_2$**CH$_2$**OC$_{16}$H$_{33}$); 70.77, 70.84 (CH-3′); 72.13, 72.15 (CH$_3$(CH$_2$)$_{14}$**CH$_2$**O); 74.99, 75.05 (CH-2′); 83.59, 83.60 (d, $J_{C,P}$ = 6.6, CH-4′); 91.65, 91.66 (CH-1′); 102.99 (CH-5); 142.45, 142.51 (CH-6); 152.16, 152.18 (C-2); 165.99 (C-4). ^{31}P NMR (202.3 MHz, CD$_3$OD): 33.22, 33.53. HR-ESI: C$_{35}$H$_{65}$O$_{10}$N$_3$P (M + H)$^+$ calcd 718.4402; found 718.4402.

2 Pivaloylthioethyl Uridin-5′-yl 2-([3R,4R]-3,4-Dihydroxypyr-rolidin-1-N-yl)ethylphosphonate (12f). The mixture of dihydrox-

ypyrrolidine **11a** (0.25 g, 2.4 mmol) and phosphonate **10a** (0.57 g, 1.1 mmol) in *n*BuOH (12 mL) was stirred at 100 °C for 12 h. The solvent was removed, and the product was obtained by flash chromatography on silica gel using linear gradient of H1 in ethyl acetate in 85% yield (0.58 g, 0.93 mmol) as white foam (HR-ESI: $C_{25}H_{39}O_{11}N_3PS$ (M − H)$^-$ calcd 620.2048; found 620.2049). The solution of this intermediate (0.58 g, mmol) in 0.2 M methanolic HCl (50 mL) was stirred at rt overnight. The mixture was concentrated in vacuo, and the product was obtained by preparative reverse phase HPLC in 26% overall yield (0.177 g, 0.29 mmol) as a white amorphous solid. A mixture of diastereomers ∼5:3. ^{1}H NMR (499.8 MHz, CD$_3$OD): 1.23, 1.24 (2 × s, 2 × 9H, (CH$_3$)$_3$C); 2.46 (m, 4H, CH$_2$P); 3.12−3.24 (m, 4H, SC**H$_2$**CH$_2$O); 3.38 (bm, 4H, H-2b,5b-pyrr); 3.51 (m, 4H, CH$_2$N); 3.66 (bm, 4H, H-2a,5a-pyrr); 4.11−4.22 (m, 8H, H-3′,4′, OC**H$_2$**CH$_2$S); 4.26 (m, 6H, H-2′, H-3,4-pyrr); 4.34 (ddd, 1H, J_{gem} = 11.6, $J_{H,P}$ = 8.0, $J_{5'b,4'}$ = 5.4, H-5′b); 4.36−4.40 (m, 2H, H-5′); 4.41 (ddd, 1H, J_{gem} = 11.6, $J_{H,P}$ = 7.7, $J_{5'a,4'}$ = 2.8, H-5′a); 5.746, 5.750 (2 × d, 2 × 1H, $J_{5,6}$ = 8.1, H-5); 5.797, 5.800 (2 × d, 2 × 1H, $J_{1'2'}$ = 4.0, H-1′); 7.68, 7.70 (2 × d, 2 × 1H, $J_{6,5}$ = 8.1, H-6). ^{13}C NMR (125.7 MHz, CD$_3$OD): 23.43, 23.49 (d, $J_{C,P}$ = 142.2, CH$_2$P); 27.66 ((**CH$_3$**)$_3$C); 29.52, 29.58 (d, $J_{C,P}$ = 6.6, S**CH$_2$**CH$_2$O); 47.56 (**C**(CH$_3$)$_3$); 52.13, 52.17 (CH$_2$N); 60.86, 60.89 (CH$_2$-2,5-pyrr); 66.20, 66.34 (d, $J_{C,P}$ = 6.6, OCH$_2$CH$_2$S); 67.40 (d, $J_{C,P}$ = 6.8, CH$_2$-5′); 67.50 (d, $J_{C,P}$ = 6.4, CH$_2$-5′); 70.77 (CH-3′); 74.54, 74.58 (CH-2′); 75.90 (CH-3,4-pyrr); 83.29, 83.34 (d, $J_{C,P}$ = 6.0, CH-4′); 92.65, 92.82 (CH-1′); 103.10, 103.12 (CH-5); 143.11, 143.14 (CH-6); 152.17 (C-2); 166.01 (C-4); 207.15 (COS). ^{31}P NMR (202.3 MHz, CD$_3$OD): 26.92, 27.39. HR-ESI: $C_{22}H_{37}O_{11}N_3PS$ (M + H)$^+$ calcd 582.18809; found 582.18811.

Ethyl Uridin-5′-yl 2-([3*R*,4*R*]-3,4-Dihydroxypyrrolidin-1-*N*-yl)ethylphosphonate (12g). The mixture of dihydroxypyrrolidine **11a** (0.24 g, 2.3 mmol) and phosphonate **10b** (0.6 g, 1.5 mmol) in *n*BuOH (12 mL) was stirred at 100 °C for 12 h. The solvent was removed, and the intermediate was obtained by flash chromatography on silica gel using linear gradient of H1 in ethyl acetate. The intermediate (0.76 g, 1.5 mmol) was dissolved in 0.5 M methanolic HCl (100 mL), and the mixture was stirred at rt overnight. The mixture was concentrated in vacuo, coevaporated with diethylether (3 × 50 mL) and ethylacetate (2 × 50 mL), and the product was obtained by crystallization from a mixture of ethanol and diethylether (1:1) in 77% yield (0.58 g, 1.16 mmol) as a white solid. Characterized by NMR as hydrochloride, a mixture of diastereomers ∼1:1. ^{1}H NMR (600.1 MHz, DMSO-*d$_6$*): 1.235, 1.242 (2 × s, 2 × 3H, J_{vic} = 7.0, CH$_3$CH$_2$); 2.38 (m, 4H, CH$_2$P); 3.07 (bd, 2H, J_{gem} = 12.1, H-2b or 5b-pyrr); 3.30 (bm, 6H, CH$_2$N, H-2b or 5b-pyrr); 3.42, 3.67 (2 × bm, 2 × 2H, H-2a,5a-pyrr); 3.95, 3.97 (2 × t, 2 × 1H, $J_{3',2'}$ = $J_{3',4'}$ = 4.9, H-3′); 3.98 (m, 2H, H-4′); 4.05 (m, 4H, CH$_3$C**H$_2$**); 4.07 (m, 2H, H-2′); 4.09 (m, 4H, H-3,4-pyrr); 4.13, 4.20 (2 × m, 4H, H-5′); 5.38, 5.55 (2 × bs, 2 × 2H, OH-2′,3′); 5.67, 5.68 (2 × dd, 2 × 1H, $J_{5,6}$ = 8.1, $J_{5,NH}$ = 2.6, H-5); 5.76 (d, 2H, $J_{1'2'}$ = 5.2, H-1′); 5.83 (bs, 4H, OH-3,4-pyrr); 7.64, 7.66 (2 × d, 2 × 1H, $J_{6,5}$ = 8.1, H-6); 10.61 (bs, 2H, NH-pyrr); 11.39 (s, 2H, NH-3). ^{13}C NMR (150.9 MHz, DMSO-*d$_6$*): 16.49 (d, $J_{C,P}$ = 5.1, **CH$_3$**CH$_2$); 22.05, 22.10 (d, $J_{C,P}$ = 139.2, CH$_2$P); 50.90 (CH$_2$N); 58.89, 58.95, 59.07 (CH$_2$-2,5-pyrr); 66.37, 66.44 (d, $J_{C,P}$ = 6.2, **CH$_2$**CH$_3$); 65.51, 65.56 (d, $J_{C,P}$ = 6.5, CH$_2$-5′); 69.67, 69.73 (CH-3′); 72.81, 72.85 (CH-2′); 74.41, 74.57 (CH-3,4-pyrr); 82.23 (d, $J_{C,P}$ = 5.2, CH-4′); 88.84, 88.94 (CH-1′); 102.36, 102.37 (CH-5); 141.21, 141.23 (CH-6); 150.95, 150.97 (C-2); 163.44 (C-4). ^{31}P NMR (202.3 MHz, DMSO-*d$_6$*): 27.31, 27.58. HR-ESI: $C_{17}H_{29}O_{10}N_3P$ (M + H)$^+$ calcd 466.1585; found 466.1585.

Tetradecyl Uridin-5′-yl 2-([3*R*,4*R*]-3,4-Dihydroxypyrrolidin-1-*N*-yl)ethylphosphonate (12h). The mixture of dihydroxypyrrolidine **11a** (0.42 g, 4.1 mmol) and phosphonate **10c** (1.17 g, 2.05 mmol) in *n*BuOH (30 mL) was stirred at 100 °C overnight. The solvent was removed, and the isopropylidene intermediate was obtained by flash chromatography on silica gel using linear gradient of H1 in ethyl acetate. This compound was without further characterization dissolved in 0.5 M methanolic HCl (50 mL), and the mixture was stirred at rt for 4 h. The reaction mixture was concentrated in vacuo and coevaporated with ethanol (3 × 40 mL). The desired product was obtained by flash chromatography on silica

gel using linear gradient of H1 in ethyl acetate in 66% overall yield (862 mg, 1.36 mmol) as a white amorphous solid. A mixture of two diastereomers ∼6:5. ^{1}H NMR (600.1 MHz, CD$_3$OD): 0.90 (m, 6H, CH$_3$(CH$_2$)$_{13}$); 1.25−1.43 (m, 44H, CH$_3$(CH$_2$)$_{11}$CH$_2$CH$_2$O); 1.68 (m, 4H, CH$_3$(CH$_2$)$_{11}$**CH$_2$**CH$_2$O); 2.06−2.19 (m, 4H, CH$_2$P); 2.56 (m, 4H, H-2b,5b-pyrr); 2.74−2.88 (m, 4H, CH$_2$N); 3.00 (m, 4H, H-2a,5a-pyrr); 4.04 (m, 4H, H-3,4-pyrr); 4.06−4.13 (m, 4H, CH$_3$(CH$_2$)$_{11}$CH$_2$**CH$_2$**O); 4.13−4.16 (m, 4H, H-3′,4′); 4.200, 4.202 (2 × dd, 2 × 1H, $J_{2',3'}$ = 5.0, $J_{2',1'}$ = 4.0, H-2′); 4.24 (ddd, 1H, J_{gem} = 11.6, $J_{H,P}$ = 6.7, $J_{5'b,4'}$ = 4.3, H-5′b); 4.29 (ddd, 1H, J_{gem} = 11.6, $J_{H,P}$ = 7.2, $J_{5'b,4'}$ = 2.4, H-5′b); 4.31 (ddd, 1H, J_{gem} = 11.6, $J_{H,P}$ = 5.0, $J_{5'a,4'}$ = 2.6, H-5′a); 4.35 (ddd, 1H, J_{gem} = 11.6, $J_{H,P}$ = 6.6, $J_{5'a,4'}$ = 2.8, H-5′a); 5.736, 5.745 (2 × d, 2 × 1H, $J_{5,6}$ = 8.1, H-5); 5.85, 5.86 (2 × d, 2 × 1H, $J_{1'2'}$ = 4.0, H-1′); 7.71, 7.74 (2 × d, 2 × 1H, $J_{6,5}$ = 8.1, H-6). ^{13}C NMR (150.9 MHz, CD$_3$OD): 14.46 (**CH$_3$**(CH$_2$)$_{13}$); 23.75 (CH$_3$(CH$_2$)$_{11}$CH$_2$CH$_2$O); 25.11 (d, $J_{C,P}$ = 139.5, CH$_2$P); 25.16 (d, $J_{C,P}$ = 139.0, CH$_2$P); 26.65, 30.27, 30.28, 30.50, 30.68, 30.71, 30.72, 30.78, 30.80, 30.82 (CH$_3$(**CH$_2$**)$_{11}$CH$_2$CH$_2$O); 31.55, 31.57 (d, $J_{C,P}$ = 6.0, CH$_3$(CH$_2$)$_{11}$**CH$_2$**CH$_2$O); 33.09 (CH$_3$(**CH$_2$**)$_{11}$CH$_2$CH$_2$O); 50.57, 50.60 (d, $J_{C,P}$ = 1.0, CH$_2$N); 61.01, 61.03 (CH$_2$-2,5-pyrr); 66.36, 66.42 (d, $J_{C,P}$ = 6.3, CH$_2$-5′); 66.60, 67.63 (d, $J_{C,P}$ = 6.8, CH$_3$(CH$_2$)$_{11}$CH$_2$**CH$_2$**O); 70.81, 70.88 (CH-3′); 74.95, 75.01 (CH-2′); 78.60, 78.65 (CH-3,4-pyrr); 83.63, 83.64 (d, $J_{C,P}$ = 6.6, CH-4′); 91.57, 91.75 (CH-1′); 102.95, 102.98 (CH-5); 142.56, 142.57 (CH-6); 152.18, 152.22 (C-2); 166.03 (C-4). ^{31}P NMR (202.3 MHz, CD$_3$OD): 32.08, 32.38. HR-ESI: $C_{29}H_{53}O_{10}N_3P$ (M + H)$^+$ calcd 634.34631, found 634.34635.

Hexadecyl Uridin-5′-yl 2-([3*R*,4*R*]-3,4-Dihydroxypyrrolidin-1-*N*-yl)ethylphosphonate (12i). The mixture of dihydroxypyrrolidine **11a** (0.36 g, 3.45 mmol) and phosphonate **10d** (1.38 g, 2.3 mmol) in *n*BuOH (20 mL) was stirred at 100 °C overnight. The solvent was removed and isopropylidene intermediate was obtained by flash chromatography on silica gel using linear gradient of H1 in ethyl acetate. This compound was without further characterization dissolved in 0.5 M methanolic HCl (50 mL), and the mixture was stirred at rt for 4 h. The reaction mixture was concentrated in vacuo and coevaporated with ethanol (3 × 40 mL). The desired product was obtained by flash chromatography on silica gel using linear gradient of H1 in ethyl acetate in 39% overall yield (590 mg, 0.89 mmol) as a white amorphous solid. A mixture of two diastereomers ∼1:1. ^{1}H NMR (600.1 MHz, CD$_3$OD): 0.90 (m, 6H, CH$_3$(CH$_2$)$_{15}$); 1.24−1.43 (m, 52H, CH$_3$(CH$_2$)$_{13}$CH$_2$CH$_2$O); 1.68 (m, 4H, CH$_3$(CH$_2$)$_{13}$**CH$_2$**CH$_2$O); 2.06−2.18 (m, 4H, CH$_2$P); 2.55 (m, 4H, H-2b,5b-pyrr); 2.73−2.86 (m, 4H, CH$_2$N); 2.99 (m, 4H, H-2a,5a-pyrr); 4.04 (m, 4H, H-3,4-pyrr); 4.05−4.12 (m, 4H, CH$_3$(CH$_2$)$_{13}$CH$_2$**CH$_2$**O); 4.12−4.16 (m, 4H, H-3′,4′); 4.198, 4.200 (2 × dd, 2 × 1H, $J_{2',3'}$ = 5.1, $J_{2',1'}$ = 4.1, H-2′); 4.24 (ddd, 1H, J_{gem} = 11.6, $J_{H,P}$ = 6.5, $J_{5'b,4'}$ = 4.2, H-5′b); 4.28 (ddd, 1H, J_{gem} = 11.6, $J_{H,P}$ = 7.2, $J_{5'b,4'}$ = 2.4, H-5′b); 4.30 (ddd, 1H, J_{gem} = 11.6, $J_{H,P}$ = 5.2, $J_{5'a,4'}$ = 2.7, H-5′a); 4.34 (ddd, 1H, J_{gem} = 11.6, $J_{H,P}$ = 6.6, $J_{5'a,4'}$ = 2.8, H-5′a); 5.73, 5.74 (2 × d, 2 × 1H, $J_{5,6}$ = 8.1, H-5); 5.85, 5.86 (2 × d, 2 × 1H, $J_{1'2'}$ = 4.1, H-1′); 7.71, 7.74 (2 × d, 2 × 1H, $J_{6,5}$ = 8.1, H-6). ^{13}C NMR (150.9 MHz, CD$_3$OD): 14.46 (**CH$_3$**(CH$_2$)$_{15}$); 23.75 (CH$_3$(CH$_2$)$_{13}$CH$_2$CH$_2$O); 25.14, 25.19 (d, $J_{C,P}$ = 139.3, CH$_2$P); 26.65, 30.27, 30.28, 30.50, 30.68, 30.69, 30.72, 30.73, 30.78, 30.81 (CH$_3$(**CH$_2$**)$_{13}$CH$_2$CH$_2$O); 31.55, 31.57 (d, $J_{C,P}$ = 6.0, CH$_3$(CH$_2$)$_{13}$**CH$_2$**CH$_2$O); 33.09 (CH$_3$(**CH$_2$**)$_{13}$CH$_2$CH$_2$O); 50.55, 50.59 (d, $J_{C,P}$ = 1.0, CH$_2$N); 61.02, 61.05 (CH$_2$-2,5-pyrr); 66.34, 66.42 (d, $J_{C,P}$ = 6.3, CH$_2$-5′); 66.60, 67.63 (d, $J_{C,P}$ = 6.8, CH$_3$(CH$_2$)$_{13}$CH$_2$**CH$_2$**O); 70.81, 70.89 (CH-3′); 74.96, 75.02 (CH-2′); 78.65, 78.69 (CH-3,4-pyrr); 83.64, 83.66 (d, $J_{C,P}$ = 6.6, CH-4′); 91.58, 91.76 (CH-1′); 102.94, 102.98 (CH-5); 142.57, 142.58 (CH-6); 152.18, 152.22 (C-2); 166.04 (C-4). ^{31}P NMR (202.3 MHz, CD$_3$OD): 32.33, 32.63. HR-ESI: $C_{31}H_{57}O_{10}N_3P$ (M + H)$^+$ calcd 662.37761, found 662.37759.

Hexadecyl Uridin-5′-yl 2-([3*R*,4*R*]-3,4-Dihydroxypyrrolidin-1-*N*-yl)ethylphosphonate (12i-P1). The title compound was obtained by preparative HPLC from **12i** using Waters AutoPurification system with 2545 quarternary gradient module and 3100 single quadrupole mass detector using LUNA C18, column (Phenomenex,

250 mm × 21.2 mm, 5 μm) at flow rate 10 mL/min using gradient: A, 50 mM NH$_4$HCO$_3$ in 50% aq CH$_3$CN; C, CH$_3$CN; A→A/10 min, A→B/50 min. ^{1}H NMR (600.1 MHz, CD$_3$OD): 0.90 (t, 3H, J_{vic} = 7.2, **CH$_3$**(CH$_2$)$_{15}$); 1.26−1.41 (m, 26H, CH$_3$(**CH$_2$**)$_{13}$CH$_2$CH$_2$O); 1.69 (m, 2H, CH$_3$(CH$_2$)$_{13}$**CH$_2$**CH$_2$O); 2.20 (m, 2H, CH$_2$P); 2.80 (bdd, 2H, J_{gem} = 10.5, J_{vic} = 1.9, H-2b,5b-pyrr); 3.00 (bm, 2H, CH$_2$N); 3.19 (bdd, 2H, J_{gem} = 10.9, J_{vic} = 4.5, H-2a,5a-pyrr); 4.05−4.16 (m, 6H, H-3′,4′, H-3,4-pyrr, CH$_3$(CH$_2$)$_{13}$CH$_2$**CH$_2$**O); 4.21 (dd, 1H, $J_{2',3'}$ = 5.1, $J_{2',1'}$ = 4.2, H-2′); 4.26 (ddd, 1H, J_{gem} = 11.3, $J_{H,P}$ = 7.0, $J_{5'b,4'}$ = 4.7, H-5′b); 4.36 (ddd, 1H, J_{gem} = 11.3, $J_{H,P}$ = 6.7, $J_{5'a,4'}$ = 2.6, H-5′a); 5.74 (d, 1H, $J_{5,6}$ = 8.1, H-5); 5.83 (d, 1H, $J_{1',2'}$ = 4.2, H-1′); 7.73 (d, 1H, $J_{6,5}$ = 8.1, H-6). ^{13}C NMR (150.9 MHz, CD$_3$OD): 14.46 (**CH$_3$**(CH$_2$)$_{15}$); 23.76 (CH$_3$(**CH$_2$**)$_{13}$CH$_2$CH$_2$O); 24.66 (d, $J_{C,P}$ = 140.2, CH$_2$P); 26.64, 30.29, 30.50, 30.69, 30.74, 30.78, 30.79, 30.82 (CH$_3$(**CH$_2$**)$_{13}$CH$_2$CH$_2$O); 31.54 (d, $J_{C,P}$ = 6.0, CH$_3$(CH$_2$)$_{13}$**CH$_2$**CH$_2$O); 33.09 (CH$_3$(**CH$_2$**)$_{13}$CH$_2$CH$_2$O); 51.04 (CH$_2$N); 60.99 (CH$_2$-2,5-pyrr); 66.66 (d, $J_{C,P}$ = 6.4, CH$_2$-5′); 67.84 (d, $J_{C,P}$ = 6.8, CH$_3$(CH$_2$)$_{13}$CH$_2$**CH$_2$**O); 70.86 (CH-3′); 74.84 (CH-2′); 77.87 (CH-3,4-pyrr); 83.55 (d, $J_{C,P}$ = 6.4, CH-4′); 91.96 (CH-1′); 102.98 (CH-5); 142.74 (CH-6); 152.19 (C-2); 166.03 (C-4). ^{31}P NMR (202.3 MHz, CD$_3$OD): 31.27.

Hexadecyl Uridin-5′-yl 2-([3R,4R]-3,4-Dihydroxypyrrolidin-1-N-yl)ethylphosphonate (12i-P2). The title compound was obtained by preparative HPLC from **12i** using Waters AutoPurification system with 2545 quarternary gradient module and 3100 single quadrupole mass detector using LUNA C18, column (Phenomenex, 250 mm × 21.2 mm, 5 μm) at flow rate 10 mL/min using gradient: A, 50 mM NH$_4$HCO$_3$ in 50% aq CH$_3$CN; C, CH$_3$CN; A→A/10 min, A→B/50 min. ^{1}H NMR (600.1 MHz, CD$_3$OD): 0.90 (t, 3H, J_{vic} = 7.2, **CH$_3$**(CH$_2$)$_{15}$); 1.26−1.43 (m, 26H, CH$_3$(**CH$_2$**)$_{13}$CH$_2$CH$_2$O); 1.69 (m, 2H, CH$_3$(CH$_2$)$_{13}$**CH$_2$**CH$_2$O); 2.18 (m, 2H, CH$_2$P); 2.72 (bd, 2H, J_{gem} = 10.5, H-2b,5b-pyrr); 2.94 (bm, 2H, CH$_2$N); 3.13 (bdd, 2H, J_{gem} = 10.5, J_{vic} = 5.0, H-2a,5a-pyrr); 4.05−4.15 (m, 6H, H-3′,4′, H-3,4-pyrr, CH$_3$(CH$_2$)$_{13}$CH$_2$**CH$_2$**O); 4.21 (dd, 1H, $J_{2',3'}$ = 5.0, $J_{2',1'}$ = 4.1, H-2′); 4.27−4.34 (m, 2H, H-5′); 5.73 (d, 1H, $J_{5,6}$ = 8.1, H-5); 5.84 (d, 1H, $J_{1',2'}$ = 4.1, H-1′); 7.70 (d, 1H, $J_{6,5}$ = 8.1, H-6). ^{13}C NMR (150.9 MHz, CD$_3$OD): 14.46 (**CH$_3$**(CH$_2$)$_{15}$); 23.76 (CH$_3$(**CH$_2$**)$_{13}$CH$_2$CH$_2$O); 24.78 (d, $J_{C,P}$ = 139.8, CH$_2$P); 26.64, 30.28, 30.50, 30.68, 30.69, 30.73, 30.79, 30.81, 30.82 (CH$_3$(**CH$_2$**)$_{13}$CH$_2$CH$_2$O); 31.56 (d, $J_{C,P}$ = 6.0, CH$_3$(CH$_2$)$_{13}$**CH$_2$**CH$_2$O); 33.10 (CH$_3$(**CH$_2$**)$_{13}$CH$_2$CH$_2$O); 50.94 (CH$_2$N); 60.99 (CH$_2$-2,5-pyrr); 66.59 (d, $J_{C,P}$ = 6.1, CH$_2$-5′); 67.71 (d, $J_{C,P}$ = 6.8, CH$_3$(CH$_2$)$_{13}$CH$_2$**CH$_2$**O); 70.81 (CH-3′); 74.93 (CH-2′); 78.06 (CH-3,4-pyrr); 83.59 (d, $J_{C,P}$ = 6.6, CH-4′); 92.02 (CH-1′); 102.96 (CH-5); 142.69 (CH-6); 152.17 (C-2); 166.04 (C-4). ^{31}P NMR (202.3 MHz, CD$_3$OD): 32.03.

Octadecyl Uridin-5′-yl 2-([3R,4R]-3,4-Dihydroxypyrrolidin-1-N-yl)ethylphosphonate (12j). The mixture of dihydroxypyrrolidine **11a** (0.3 g, 2.94 mmol) and phosphonate **10e** (1.23 g, 1.96 mmol) in nBuOH (20 mL) was stirred at 100 °C overnight. The solvent was removed, and the isopropylidene intermediate was obtained by flash chromatography on silica gel using linear gradient of H1 in ethyl acetate. This compound was without further characterization dissolved in 0.5 M methanolic HCl (50 mL), and the mixture was stirred at rt for 4 h. The reaction mixture was concentrated in vacuo and coevaporated with ethanol (3 × 40 mL). The desired product was obtained by flash chromatography on silica gel using linear gradient of H1 in ethyl acetate in 68% overall yield (920 mg, 1.33 mmol) as a white amorphous solid. A mixture of two diastereomers ~6:5. ^{1}H NMR (600.1 MHz, CD$_3$OD): 0.90 (m, 6H, **CH$_3$**(CH$_2$)$_{17}$); 1.25−1.43 (m, 60H, CH$_3$(**CH$_2$**)$_{15}$CH$_2$CH$_2$O); 1.68 (m, 4H, CH$_3$(CH$_2$)$_{15}$**CH$_2$**CH$_2$O); 2.06−2.19 (m, 4H, CH$_2$P); 2.55 (m, 4H, H-2b,5b-pyrr); 2.73−2.86 (m, 4H, CH$_2$N); 2.99 (m, 4H, H-2a,5a-pyrr); 4.04 (m, 4H, H-3,4-pyrr); 4.05−4.13 (m, 4H, CH$_3$(CH$_2$)$_{15}$CH$_2$**CH$_2$**O); 4.13−4.16 (m, 4H, H-3′,4′); 4.199, 4.201 (2 × dd, 2 × 1H, $J_{2',3'}$ = 4.8, $J_{2',1'}$ = 4.2, H-2′); 4.24 (ddd, 1H, J_{gem} = 11.6, $J_{H,P}$ = 6.7, $J_{5'b,4'}$ = 4.2, H-5′b); 4.28 (ddd, 1H, J_{gem} = 11.6, $J_{H,P}$ = 7.4, $J_{5'b,4'}$ = 2.5, H-5′b); 4.30 (ddd, 1H, J_{gem} = 11.6, $J_{H,P}$ = 5.2, $J_{5'a,4'}$ = 2.7, H-5′a); 4.34 (ddd, 1H, J_{gem} = 11.6, $J_{H,P}$ = 6.5, $J_{5'a,4'}$ = 2.7, H-5′a); 5.735, 5.745 (2 × d, 2 × 1H, $J_{5,6}$ = 8.1, H-5); 5.85, 5.86 (2 × d, 2 × 1H, $J_{1',2'}$ = 4.2, H-1′); 7.71, 7.74 (2 × d, 2 × 1H, $J_{6,5}$ = 8.1, H-6). ^{13}C NMR (150.9 MHz,

(150.9 MHz, CD$_3$OD): 14.47 (**CH$_3$**(CH$_2$)$_{17}$); 23.75 (CH$_3$(**CH$_2$**)$_{15}$CH$_2$CH$_2$O); 25.13, 25.17 (d, $J_{C,P}$ = 139.3, CH$_2$P); 26.65, 30.28, 30.29, 30.49, 30.68, 30.69, 30.72, 30.73, 30.78, 30.79, 30.80 (CH$_3$(**CH$_2$**)$_{15}$CH$_2$CH$_2$O); 31.55, 31.57 (d, $J_{C,P}$ = 6.0, CH$_3$(CH$_2$)$_{15}$**CH$_2$**CH$_2$O); 33.09 (CH$_3$(**CH$_2$**)$_{15}$CH$_2$CH$_2$O); 50.55, 50.57 (d, $J_{C,P}$ = 1.1, CH$_2$N); 61.01, 61.04 (CH$_2$-2,5-pyrr); 66.34, 66.42 (d, $J_{C,P}$ = 6.3, CH$_2$-5′); 66.60, 67.62 (d, $J_{C,P}$ = 6.8, CH$_3$(CH$_2$)$_{15}$CH$_2$**CH$_2$**O); 70.80, 70.88 (CH-3′); 74.96, 75.02 (CH-2′); 78.63, 78.68 (CH-3,4-pyrr); 83.63, 83.65 (d, $J_{C,P}$ = 6.7, CH-4′); 91.56, 91.74 (CH-1′); 102.95, 102.98 (CH-5); 142.55, 142.57 (CH-6); 152.18, 152.22 (C-2); 166.03 (C-4). ^{31}P NMR (202.3 MHz, CD$_3$OD): 32.12, 32.43. HR-ESI: C$_{33}$H$_{61}$O$_{10}$N$_3$P (M + H)$^+$ calcd 690.40891, found 690.40891.

Icosanyl Uridin-5′-yl 2-([3R,4R]-3,4-Dihydroxypyrrolidin-1-N-yl)ethylphosphonate (12k). The mixture of dihydroxypyrrolidine **11a** (0.26 g, 2.52 mmol) and phosphonate **10f** (1.1 g, 1.68 mmol) in nBuOH (17 mL) was stirred at 100 °C overnight. The solvent was removed, and the isopropylidene intermediate was obtained by flash chromatography on silica gel using linear gradient of H1 in ethyl acetate. This compound was without further characterization dissolved in 0.5 M methanolic HCl (50 mL), and the mixture was stirred at rt for 4 h. The reaction mixture was concentrated in vacuo and coevaporated with ethanol (3 × 40 mL). The desired product was obtained by flash chromatography on silica gel using linear gradient of H1 in ethyl acetate in 70% overall yield (840 mg, 1.17 mmol) as a white amorphous solid. A mixture of two diastereomers ~6:5. ^{1}H NMR (600.1 MHz, CD$_3$OD): 0.90 (m, 6H, **CH$_3$**(CH$_2$)$_{19}$); 1.25−1.43 (m, 68H, CH$_3$(**CH$_2$**)$_{17}$CH$_2$CH$_2$O); 1.69 (m, 4H, CH$_3$(CH$_2$)$_{17}$**CH$_2$**CH$_2$O); 2.06−2.23 (m, 4H, CH$_2$P); 2.68 (dd, 4H, J_{gem} = 10.6, J_{vic} = 2.9, H-2b,5b-pyrr); 2.84−2.97 (m, 4H, CH$_2$N); 3.10 (dd, 4H, J_{gem} = 10.6, J_{vic} = 5.0, H-2a,5a-pyrr); 4.07 (m, 4H, H-3,4-pyrr); 4.08−4.13 (m, 4H, CH$_3$(CH$_2$)$_{17}$CH$_2$**CH$_2$**O); 4.13−4.16 (m, 4H, H-3′,4′); 4.207, 4.210 (2 × dd, 2 × 1H, $J_{2',3'}$ = 5.0, $J_{2',1'}$ = 4.2, H-2′); 4.25 (ddd, 1H, J_{gem} = 11.6, $J_{H,P}$ = 6.8, $J_{5'b,4'}$ = 4.4, H-5′b); 4.31 (m, 2H, H-5′); 4.35 (ddd, 1H, J_{gem} = 11.6, $J_{H,P}$ = 6.6, $J_{5'a,4'}$ = 2.7, H-5′a); 5.735, 5.743 (2 × d, 2 × 1H, $J_{5,6}$ = 8.1, H-5); 5.84, 5.85 (2 × d, 2 × 1H, $J_{1',2'}$ = 4.2, H-1′); 7.71, 7.74 (2 × d, 2 × 1H, $J_{6,5}$ = 8.1, H-6). ^{13}C NMR (150.9 MHz, CD$_3$OD): 14.46 (**CH$_3$**(CH$_2$)$_{19}$); 23.75 (CH$_3$(**CH$_2$**)$_{17}$CH$_2$CH$_2$O); 24.85, 24.91 (d, $J_{C,P}$ = 139.8, CH$_2$P); 26.64, 30.28, 30.29, 30.49, 30.69, 30.73, 30.74, 30.77, 30.79, 30.80 (CH$_3$(**CH$_2$**)$_{17}$CH$_2$CH$_2$O); 31.55, 31.57 (d, $J_{C,P}$ = 6.0, CH$_3$(CH$_2$)$_{17}$**CH$_2$**CH$_2$O); 33.09 (CH$_3$(**CH$_2$**)$_{17}$CH$_2$CH$_2$O); 50.81, 50.86 (CH$_2$N); 60.98, 61.02 (CH$_2$-2,5-pyrr); 66.52, 66.54 (d, $J_{C,P}$ = 6.1, CH$_2$-5′); 67.69, 67.73 (d, $J_{C,P}$ = 7.1, CH$_3$(CH$_2$)$_{17}$CH$_2$**CH$_2$**O); 70.80, 70.87 (CH-3′); 74.90, 74.95 (CH-2′); 78.19, 78.26 (CH-3,4-pyrr); 83.60 (d, $J_{C,P}$ = 6.5, CH-4′); 91.75, 91.93 (CH-1′); 102.97, 102.99 (CH-5); 142.65 (CH-6); 152.17, 152.20 (C-2); 166.03 (C-4). ^{31}P NMR (202.3 MHz, CD$_3$OD): 31.29, 31.57. HR-ESI: C$_{35}$H$_{65}$O$_{10}$N$_3$P (M + H)$^+$ calcd 718.44021, found 718.44030.

Hexadecyl Uridin-5′-yl 2-([3R,5S]-3-Hydroxy-5-(hydroxymethyl)pyrrolidin-1-N-yl)ethylphosphonate (12l). The mixture of dihydroxypyrrolidine **11d** (0.12 g, 1.0 mmol) and phosphonate **10d** (0.3 g, 0.5 mmol) in nBuOH (5 mL) was stirred at 95 °C overnight. The solvent was removed, and the isopropylidene intermediate was obtained by flash chromatography on silica gel using linear gradient of H1 in ethyl acetate. This compound was without further characterization dissolved in 0.5 M methanolic HCl (50 mL) and the mixture was stirred at rt for 4 h. The reaction mixture was concentrated in vacuo and coevaporated with ethanol (3 × 40 mL). The desired product was obtained by flash chromatography on silica gel using linear gradient of H1 in ethyl acetate in 60% overall yield (200 mg, 0.3 mmol) as a white amorphous solid. A mixture of diastereomers ~6:5. ^{1}H NMR (500.0 MHz, CD$_3$OD): 0.90 (m, 6H, **CH$_3$**(CH$_2$)$_{15}$); 1.24−1.43 (m, 52H, CH$_3$(**CH$_2$**)$_{13}$CH$_2$CH$_2$O); 1.70 (m, 4H, CH$_3$(CH$_2$)$_{13}$**CH$_2$**CH$_2$O); 2.03, 2.17 (2 × m, 2 × 1H, H-4-pyrr); 2.44−2.58 (m, 4H, CH$_2$P); 3.30 (m, 2H, H-2b-pyrr); 3.53 (m, 2H, CH$_a$**H$_b$**N); 3.70 (m, 2H, H-2a-pyrr); 3.73 (m, 2H, CH$_a$**H$_b$**OH); 3.78 (m, 2H, **CH$_a$H$_b$**N); 3.93 (m, 2H, **CH$_a$**H$_b$OH); 3.96 (m, 2H, H-5-pyrr); 4.07−4.18 (m, 8H, H-3′,4′, CH$_3$(CH$_2$)$_{13}$CH$_2$**CH$_2$**O); 4.24 (m, 2H, H-2′); 4.28−4.42 (m, 4H, H-5′); 4.53 (m, 2H, H-3-pyrr); 5.75 (d,

M

dx.doi.org/10.1021/jm2009343 | J. Med. Chem. XXXX, XXX, XXX−XXX

2H, $J_{5,6}$ = 8.1, H-5); 5.81, 5.83 (2 × d, 2 × 1H, $J_{1',2'}$ = 4.0, H-1'); 7.69, 7.71 (2 × d, 2 × 1H, $J_{6,5}$ = 8.1, H-6). ^{13}C NMR (125.7 MHz, CD$_3$OD): 14.44 (**CH$_3$**(CH$_2$)$_{15}$); 23.17, 23.22 (d, $J_{C,P}$ = 140.5, CH$_2$P); 23.73 (CH$_3$(**CH$_2$**)$_{13}$CH$_2$CH$_2$O); 26.59, 30.28, 30.29, 30.47, 30.66, 30.73, 30.76, 30.79 (CH$_3$(**CH$_2$**)$_{13}$CH$_2$CH$_2$O); 31.51 (d, $J_{C,P}$ = 5.9, CH$_3$(CH$_2$)$_{13}$**CH$_2$**CH$_2$O); 33.07 (CH$_3$(CH$_2$)$_{13}$CH$_2$**CH$_2$**O); 37.35 (CH$_2$-3); 52.72, 52.76 (CH$_2$N); 60.82 (CH$_2$OH); 62.25, 62.28 (CH$_2$-2-pyrr); 67.18, 67.38 (d, $J_{C,P}$ = 6.3, CH$_2$-5'); 68.14, 68.37 (d, $J_{C,P}$ = 6.8, CH$_3$(CH$_2$)$_{13}$CH$_2$**CH$_2$**O); 70.14 (CH-3-pyrr); 70.40, 70.49 (CH-5-pyrr); 70.75, 70.79 (CH-3'); 74.66, 74.71 (CH-2'); 83.39, 83.45 (d, $J_{C,P}$ = 6.4, CH-4'); 92.40, 92.46 (CH-1'); 103.08, 103.12 (CH-5); 142.94, 142.97 (CH-6); 152.17, 152.19 (C-2); 166.00 (C-4). ^{31}P NMR (162.0 MHz, CD$_3$OD): 27.81, 28.26. HR-ESI: C$_{32}$H$_{59}$O$_{10}$N$_3$P (M + H)$^+$ calcd 676.39326, found 676.39306.

ASSOCIATED CONTENT

Ⓢ Supporting Information

Cell viability, cytotoxicity and apoptosis of erythroid progenitor cells after exposure to selected compounds and IR data of synthesized compounds. This material is available free of charge via the Internet at http://pubs.acs.org.

AUTHOR INFORMATION

Corresponding Author

*E-mail: rejman@uochb.cas.cz, Phone: (+420220183371) (D.R.); E-mail: krasny@biomed.cas.cz , Phone: (+420241063208) (L.K.).

ACKNOWLEDGMENTS

ABBREVIATIONS USED

C, cytosine; C^{Bz}, 4-N-benzoylcytosine; CPZ, caprazamycin; CWS, cyst wall synthase; ED$_{50}$, effective dose; HM, hydrophobic module; HPLC, high performance liquid chromatography; IM, an iminosugar module; LM, linker module; LPM, liposidomycin; LPPO, lipophosphonoxin; MBC, minimum bactericidal concentration; MIC, minimum inhibitory concentration; NM, nucleoside module; [poly(GalNAc)], poly β-1−3-linked N-acetylgalactosamine; SATE, pivaloylthioethyl; TPSCl, triisopropylbenzensulfonylchloride; U, uracil; UDP-GalNAc, uridinediphosphate-N-acetyl-alpha-D-galactosamine

REFERENCES

(1) Winn, M.; Goss, R. J. M.; Kimurab, K.; Bugg, T. D. H. Antimicrobial nucleoside antibiotics targeting cell wall assembly: recent advances in structure−function studies and nucleoside biosynthesis. *Nat. Prod. Rep.* **2010**, 27, 279−304.

(2) Davies, D.; Davies, J. Origins and Evolution of Antibiotic Resistance. *Microbiol. Mol. Biol. Rev.* **2010**, 74 (3), 417−433.

(3) Kesselheim, A. S.; Outterson, K. Fighting Antibiotic Resistance: Marrying New Financial Incentives To Meeting Public Health Goals. *Health Aff.* **2010**, 29, 1689−1696.

(4) Suk, D. H.; Rejman, D.; Dykstra, Ch.; Pohl, R.; Pankiewicz, K. W.; Patterson, S. E. Phosphonoxins: rational design and discovery of a potent nucleotide anti-Giardia agent. *Bioorg. Med. Chem. Lett.* **2007**, 17 (10), 2811−2816.

(5) Isono, K.; Asahi, K.; Suzuki, S. Studies on polyoxins, antifungal antibiotics. XII. The structure of polyoxins. *J. Am. Chem. Soc.* **1969**, 91, 7490−7505.

(6) Isono, K.; Nagatsu, J.; Kawashima, Y.; Suzuki, S. Studies on polyoxins, antifungal antibiotics. Part I. Isolation and characterization of polyoxins A and B. *Agric. Biol. Chem.* **1965**, 29, 848−854.

(7) Endo, A.; Kakiki, K.; Misato, J. Mechanism of action of the antifungal agent polyoxin D. *J. Bacteriol.* **1970**, 104, 189−196.

(8) Ohta, N.; Kakiki, K.; Misato, T. Studies on the mode of action of polyoxin D. Part 11. Effect of polyoxin D on the synthesis of fungal cell wall chitin. *Agric. Biol. Chem.* **1970**, 34, 1224−1234.

(9) Igarashi, M.; Nakagawa, N.; Doi, N.; Hattori, S.; Naganawa, H.; Hamada, M. Caprazamycin B, a novel anti-tuberculosis antibiotic, from *Streptomyces* sp. *J. Antibiot.* **2003**, 56, 580−583.

(10) Igarashi, M.; Takahashi, Y.; Shitara, T.; Nakamura, H.; Naganawa, H.; Miyake, T.; Akamatsu, Y. Caprazamycins, novel liponucleoside antibiotics, from *Streptomyces* sp.: II. structure elucidation of caprazamycins. *J. Antibiot.* **2005**, 58, 327−337.

(11) Kimura, K.; Miyata, N.; Kawanishi, G.; Kamio, Y.; Izaki, K.; Isono, K. Liposidomycin C inhibits phospho-N-acetylmuramylpentapeptide transferase in peptidoglycan synthesis of *Escherichia coli* Y-10. *Agric. Biol. Chem.* **1989**, 53, 1811−1815.

(12) McDonald, L. A.; Barbieri, L. R.; Carter, G. T.; Lenoy, E.; Lotvin, J.; Petersen, P. J.; Siegel, M. M.; Singh, G.; Williamson, R. T. Structures of the muraymycins, novel peptidoglycan biosynthesis inhibitors. *J. Am. Chem. Soc.* **2002**, 124, 10260−10261.

(13) Bugg, T. D. H.; Lloyd, A. J.; Roper, D. I. Phospho-MurNAcpentapeptide translocase (MraY) as a target for antibacterial agents and antibacterial proteins. *Infect. Dis. Drug Targets* **2006**, 6, 85−106.

(14) Kimura, K.; Bugg, T. D. H. Recent advances in antimicrobial nucleoside antibiotics targeting cell wall biosynthesis. *Nat. Prod. Rep.* **2003**, 20, 252−273.

(15) Bouhss, A.; Mengin-Lecreulx, D.; Le Beller, D.; Van Heijenoort, J. Topological analysis of the MraY protein catalyzing the first membrane step of peptidoglycan synthesis. *Mol. Microbiol.* **1999**, 34, 576−585.

(16) Bouhss, A.; Trunkfield, A. E.; Bugg, T. D.; Mengin-Lecreulx, D. The biosynthesis of peptidoglycan lipid-linked intermediates. *FEMS Microbiol. Rev.* **2008**, 32, 208−33.

(17) Al-Dabbagh, B.; Henry, X.; El Ghachi, M.; Auger, G.; Blanot, D.; Parquet, C.; Mengin-Lecreulx, D.; Bouhss, A. Active site mapping of MraY, a member of the polyprenyl-phosphate N-acetylhexosamine 1-phosphate transferase superfamily, catalyzing the first membrane step of peptidoglycan biosynthesis. *Biochemistry* **2008**, 47, 8919−8928.

(18) Tanino, T.; Ichikawa, S.; Al-Dabbagh, B.; Bouhss, A.; Oyama, H.; Matsuda, A. Synthesis and Biological Evaluation of Muraymycin Analogues Active against Anti-Drug-Resistant Bacteria. *Med. Chem. Lett.* **2010**, 1, 258−262.

(19) Hostetler, K. Y.; Beadle, J. R.; Hornbuckle, W. E.; Bellezza, C. A.; Ilia, A.; Tochkov, I. A.; Cote, P. J.; Gerin, J. L.; Korba, B. E.; Tennant, B. C. Antiviral Activities of Oral 1-O-Hexadecylpropanediol-3-phosphoacyclovir and Acyclovir in Woodchucks with Chronic Woodchuck Hepatitis Virus Infection. *Antimicrob. Agents Chemother.* **2000**, 44 (7), 1964−1969.

(20) Lefebvre, I.; Perigaud, C.; Pompon, A.; Aubertin, A.-M.; Girardet, J.-L.; Kirn, A.; Gosselin, G.; Imbach, J. L. Mononucleoside phosphotriester derivatives with S-acyl-2-thioethyl bioreversible phosphate-protecting groups: intracellular delivery of 3'-azido-2',3'-dideoxythymidine 5'-monophosphate. *J. Med. Chem.* **1995**, 38, 3941−3950.

(21) Boutevin, B.; Hervaud, Y.; Jeanmarie, T.; Boulahna, A.; Elasri, M. Monodealkylation Des Esters Phosphoniques Synthese De Monosels Et De Monoacides Phosphoniques. *Phosphorus Sulfur* **2001**, 174, 1−14.

(22) Gao, F.; Yan, X.; Auclair, K. Synthesis of a Phosphonate-Linked Aminoglycoside−Coenzyme A Bisubstrate and Use in Mechanistic Studies of an Enzyme Involved in Aminoglycoside Resistance. *Chem.—Eur. J.* **2009**, 15 (9), 2064−2070.

(23) Rejman, D.; Kočalka, P.; Buděšínský, M.; Pohl, R.; Rosenberg, I. Synthesis of diastereomeric 3-hydroxy-4-pyrrolidinyl derivatives of nucleobases. *Tetrahedron* **2007**, *63* (5), 1243−1253.

(24) Kovačková, S.; Dračínský, M.; Rejman, D. The Synthesis of Piperidine Nucleoside Analogs—A Comparison of Several Methods To Access The Introduction of Nucleobase. *Tetrahedron* **2011**, *67* (7), 1485−1500.

(25) Rejman, D.; Pohl, R.; Dračínský, M. The Synthesis and Conformation of Dihydroxypiperidinyl Derivates of Nucleobases as Novel Iminosugar Nucleoside Analogs. *Eur. J. Org. Chem.* **2011**, *11*, 2172−2187.

(26) *Performance Standards for Antimicrobial Susceptibility Testing; 19th Informational Supplement*; Clinical and Laboratory Standards Institute: Wayne, PA, 2009; Vol. *29*, issue 3, pp M100−S19.

(27) *Methods for Dilution Antimicrobial Susceptibility Tests for Bacteria That Grow Aerobically; Approved Standard*, 8th ed.; Clinical and Laboratory Standards Institute: Wayne, PA, 2009; Vol. *29*, issue 2, pp M07−A8.

(28) Hanahan, D. Studies on transformation of *Escherichia coli* with plasmids. *J. Mol. Biol.* **1983**, *166* (4), 557−80.

(29) Panzenböck, B.; Bartůněk, P.; Mapara, M. Y.; Zenke, M. Growth and differentiation of human stem cell factor/erythropoietin-dependent erythroid progenitor cells in vitro. *Blood* **1998**, *92* (10), 3658−68.

(30) Krásný, L.; Tišerová, H.; Jonák, J.; Rejman, D.; Šanderová, H. The identity of the transcription +1 position is crucial for changes in gene expression in response to amino acid starvation in *Bacillus subtilis*. *Mol. Microbiol.* **2008**, *69*, 42−54.

(31) Sojka, L; Kouba, T; Barvík, I; Šanderová, H; Maderová, Z; Jonák, J; Krásný, L. Rapid changes in gene expression: DNA determinants of promoter regulation by the concentration of the transcription initiating NTP in *Bacillus subtilis*. *Nucleic Acids Res.* **2011**, *39* (11), 4598−611.

ORIGINAL PAPER

The plant alkaloid and anti-leukemia drug homoharringtonine sensitizes resistant human colorectal carcinoma cells to TRAIL-induced apoptosis via multiple mechanisms

Lenka Beranova · Antonio R. Pombinho · Jarmila Spegarova · Michal Koc ·
Magdalena Klanova · Jan Molinsky · Pavel Klener · Petr Bartunek ·
Ladislav Andera

Abstract TNF-related apoptosis-inducing ligand (TRAIL) is a pro-apoptotic ligand from the TNF-alpha family that is under consideration, along with agonistic anti-TRAIL receptor antibodies, as a potential anti-tumor agent. However, most primary human tumors are resistant to mono-therapy with TRAIL apoptogens, and thus the potential applicability of TRAIL in anti-tumor therapy ultimately depends on its rational combination with drugs targeting these resistances. In our high-throughput screening for novel agents/drugs that could sensitize TRAIL-resistant colorectal cancer cells to TRAIL-induced apoptosis, we found homo-harringtonine (HHT), a cephalotaxus alkaloid and tested anti-leukemia drug, to be a very effective, low nanomolar enhancer of TRAIL-mediated apoptosis/growth suppression of these resistant cells. Co-treatment of TRAIL-resistant RKO or HT-29 cells with HHT and TRAIL led to the effective induction of apoptosis and the complete elimination of the treated cells. HHT suppressed the expression of the anti-apoptotic proteins Mcl-1 and cFLIP and enhanced the TRAIL-triggered activation of JNK and p38 kinases. The shRNA-mediated down-regulation of cFLIP or Mcl-1 in HT-29 or RKO cells variably enhanced their TRAIL-induced apoptosis but it did not markedly sensitize them to TRAIL-mediated growth suppression. However, with the notable exception of RKO/sh cFLIP cells, the downregulation of cFLIP or Mcl-1 significantly lowered the effective concentration of HHT in HHT + TRAIL co-treatment. Combined HHT + TRAIL therapy also led to the strong suppression of HT-29 tumors implanted into immunodeficient mice. Thus, HHT represents a very efficient enhancer of TRAIL-induced apoptosis with potential application in TRAIL-based, anti-cancer combination therapy.

Keywords Harringtonine · Apoptosis · Death receptor · cFLIP · Mcl-1

L. Beranova and A.R. Pombinho contributed equally to this study.

L. Beranova · J. Spegarova · M. Koc · L. Andera (✉)
Department of Cell Signaling & Apoptosis, Institute of
Molecular Genetics, Academy of Sciences of the Czech
Republic, Vídeňská 1083, 14220 Praha 4, Czech Republic
e-mail: andera@img.cas.cz

A. R. Pombinho · P. Bartunek (✉)
Center for Chemical Genetics, CZ-OPENSCREEN, Institute
of Molecular Genetics, Academy of Sciences of the Czech
Republic, Vídeňská 1083, 14220 Praha 4, Czech Republic
e-mail: bartunek@img.cas.cz

M. Klanova · J. Molinsky · P. Klener
Department of Pathophysiology, 1st Medical Faculty,
Charles University in Prague, Prague, Czech Republic

Introduction

New natural and rationally designed drugs are being developed and tested in the never-ending battle against cancer [1–5]. Among these agents is the pro-apoptotic ligand TNF-related apoptosis-inducing ligand (TRAIL), which can, along with agonistic anti-TRAIL receptor antibodies, selectively induce the apoptosis of cancer cells. These TRAIL-related apoptogens are currently being evaluated in phase I/II clinical trials (recently reviewed in [6–8]). TRAIL binding to its pro-apoptotic receptors TRAIL-R1/DR4 or TRAIL-R2/DR5 leads to the rapid formation of the intra-cellular multiprotein death-inducing signaling complex (DISC), which, in addition to the ligand/receptor cluster, is

composed of the adapter protein FADD, the initiator pro-caspases-8/-10 and the caspases-8/-10 antagonist cFLIP [9, 10]. In addition to these core DISC components, other proteins such as PEA-15/PED, DDX-3, TRADD, DJ-1 or MADD can, in a cell- and conditionally-specific manner, associate with the TRAIL receptosome and negatively affect either DISC formation or caspase-8 processing [11–15].

Though TRAIL induces the apoptosis of a number of cultured cancer cells [16, 17], many primary cancer cells are resistant to TRAIL, either intrinsically and/or through anti-apoptotic signals from the tumor microenvironment. Among these protective signals are the activation of the PI3K/Akt pathway, the increased expression of anti-apoptotic proteins such as cFLIP, Mcl-1, Bcl-XL or XIAP and the suppressed expression/modification of pro-apoptotic molecules (caspases, Bid, pro-apoptotic TRAIL receptors) [8, 18]. Moreover, the TRAIL-induced activation of NF-κB signaling can enhance the survival and proliferation of these resistant cancer cells [19]. For these reasons, "smart" therapy combining TRAIL apoptogens with current tested anti-tumor drugs seems to be a preferred choice. Indeed, many drugs such as DNA damaging agents, histone deacetylase or proteasome inhibitors, Bcl-2 and IAP antagonists, natural products as well as therapeutic antibodies can synergize with TRAIL, effectively eliminating resistant cancer cells of various origin [20–22]. The sensitizing mechanisms, though not fully understood, include the increased expression of TRAIL receptors or initiator/effector caspases, the production of reactive oxygen species (ROS), the downregulation of anti-apoptotic proteins (cFLIP, Mcl-1), the suppression of anti-apoptotic signaling (NF-κB or PI3K inhibitors) and the stabilization of pro-apoptotic proteins such as active caspases or tBid (recently reviewed in [20]).

Currently, many natural products such as wogonin, nimbolide and others have emerged as potent sensitizers of resistant cancer cells to TRAIL-induced apoptosis [23–25]. Using a high-throughput screening (HTS) approach, we uncovered homoharringtonine (HHT), an alkaloid originally isolated from Cephalotaxus harringtonia, and found it to be one of the most potent sensitizers of resistant colorectal cancer cells to TRAIL-induced apoptosis. HHT has been used in traditional Chinese medicine for the treatment of diverse malignancies. Recently, its semisynthetic variant Omacetaxine mepesuccinate (marketed under the name Omapro) has been considered as an alternative therapeutic option in the treatment of imatinib-resistant chronic myeloid leukemias [26, 27]. HHT can inhibit proteosynthesis, which in affected cells leads to the proteolytic degradation of short-lived anti-apoptotic proteins such as Mcl-1, cFLIP, survivin and others [28]. HHT also suppresses the growth of non-leukemia cancer cells [29, 30], and in our model of TRAIL-resistant RKO or HT-29 colorectal cancer cells,

HHT treatment led to the downregulation of Mcl-1 and cFLIP expression. However, the shRNA-mediated downregulation of either Mcl-1 or cFLIP expression in these cells did not fully sensitize them to TRAIL-induced growth suppression. HHT also very robustly cooperated with TRAIL in the growth suppression of HT-29 tumors in immunodeficient mice. Thus, HHT in combination with TRAIL or with agonistic anti-TRAIL receptor antibodies could represent an interesting option in anticancer therapy.

Materials and methods

Cell cultures and chemicals

The human colon carcinoma cell lines RKO and HT-29 and normal colon epithelial cells CCD 841 were purchased from ATCC. RKO and HT-29 cells were maintained in DMEM + 10 % FCS at 37 °C and 5 % CO_2. CCD 841 cells were cultivated in collagen-coated dishes in the recommended medium (ATCC, CRL-1790) supplemented with 10 % FCS. All chemicals used were purchased from Sigma-Aldrich unless stated otherwise.

High-throughput screening

HT-29 cells were plated in 384-well plates (Corning) at a density of 2,500 cells/25 μl/well using a Multidrop Combi dispenser (Thermo Scientific) and cultivated overnight. Then, library compounds were added using pintool (V&P Scientific) coupled to a JANUS Automated Workstation (PerkinElmer) to a final concentration of 1 μM in the absence or in combination with 100 ng/ml of recombinant TRAIL (Killer TRAIL, ENZO LS). The compound library included the Library of Pharmacologically Active Compounds (LOPAC1280, Sigma-Aldrich), the Prestwick Chemical Library (Illkirch, France) and the NIH Clinical Trial Collection (NIH, USA). In total 2,448 various unique compounds were used in the course of HTS screening. The cells were cultivated for 48 h, and then their viability was determined by the CellTiter-Blue assay (Promega) and an EnVision microplate reader (PerkinElmer).

Analysis of cell proliferation/survival and activation of effector caspases

The long-term survival of treated cells was determined by the WST-1 (Roche) and CellTiter-Blue (Promega) assays using a 96- or 384-well format, respectively, according to the manufacturers' recommendations. The real-time kinetic xCELLigence-based cell survival assay was performed according to the manufacturer's recommendations. Briefly,

3,000–5,000 cells were plated in triplicate into individual wells of an E-plate (Roche), placed into the monitoring unit in a CO_2 incubator and monitored for growth. When the cells reached approximately 40–50 % confluency, HHT and/or TRAIL were added and the on-line monitoring continued for an additional 60–70 h. The activity of the effector caspases-3/7 was quantified by the Caspase-Glo 3/7 assay (Promega) in 384-well plates, according to the manufacturer's instructions.

DISC precipitation

Cells grown to 80 % confluence in 140 mm cell culture dishes were pretreated with 50 nM HHT for 3 h, then the medium was replaced with ice-cold medium and the cells were incubated on ice for 10 min. Where applicable, biotin-labeled TRAIL (bio-TRAIL) was added to a final concentration of 1 μg/ml for 20 min. After this pre-incubation, the cold medium containing bio-TRAIL was replaced with warm medium at 37 °C (without bio-TRAIL), and the cells were incubated at 37 °C for 0–40 min. At selected time points, the culture dishes were placed on ice, and the cultivation medium was replaced with 20 ml of ice-cold phosphate-buffered saline (PBS). After washing with ice-cold PBS, the cells were scraped and centrifuged ($800 \times g$, 4 °C, 5 min). The cell pellets were lysed in ice-cold lysis buffer (1 % NP-40, 20 mM Tris–Cl pH 7.5, 150 mM NaCl, 10 mM NaF, 10 mM EDTA, 1 mM Na_3VO_4, 10 % glycerol) supplemented with protease inhibitors (complete protease inhibitor cocktail, Roche) on ice for 30 min, and the lysates were then centrifuged ($15,000 \times g$, 4 °C, 30 min). The cleared lysates were diluted to the same protein concentration (usually 3 mg/ml) and incubated with streptavidin agarose beads (Thermo Scientific) at 4 °C for 2 h. After five washes with 10 volumes of the lysis buffer, the DISC precipitates were directly eluted with $2\times$ SDS sample buffer (95 °C, 5 min) and analyzed by Western blotting.

Cell lysis and western blotting

Cells were washed with ice-cold PBS, scraped, centrifuged, and the cell pellets lysed in ice-cold lysis buffer (1 % Triton X-100, 25 mM Tris–HCl pH 7.4, 150 mM NaCl, 10 mM NaF, 1 mM EDTA, 1 mM Na_3VO_4) supplemented with protease inhibitors (Complete, Roche) on ice for 30 min. The lysates were centrifuged ($15,000 \times g$, 4 °C, 30 min), and the amount of total protein in the supernatants was quantified by the BCA assay (Pierce). The supernatants were diluted 1:1 with $2\times$ SDS sample buffer, heated to 95 °C for 5 min and analyzed by Western blotting (usually 50 μg of total protein was loaded per well). The antibodies against following proteins were used: Bcl-XL (2764), Bid (2002), caspase-9 (9502), FADD (2782), IκBα (8414), P-IκBα

(2859), NF-κB/p65 (4764), P-NF-κB/p65 (3033), SAPK/JNK (9252), P-SAPK/JNK Thr183/Tyr185 (9251), p-38 MAPK (9212) and P-p38MAPK (9211) from Cell Signaling; Mcl-1 (559027) and Caspase-8 (559932) from BD Biosciences; β-actin (SC-1615) and Bak (SC-832) from Santa Cruz Biotechnology; cFLIP (ALX-804-428) and Bim (ALX-804-351) from Enzo Life Science; caspase-10 (M059-3) from MBL and DR5 (SAB3500427) from Sigma-Aldrich.

Flow cytometry analysis of apoptosis and receptor expression

For the Annexin V-FITC assay of apoptotic cells, the cell cultures (typically 1.5×10^5 cells in each well of a 24-well plate) were harvested by trypsinization, washed once with PBS and once with ice-cold Annexin binding buffer. Then, Annexin V-FITC (Apronex Biotechnologies) was added to a final concentration of 2 μg/ml and the samples incubated on ice for 20 min. After adding Hoechst 33258 to a final concentration of 0.5 μg/ml, the samples were analyzed by flow cytometry on a LSRII (BD Biosciences).

For flow cytometry analysis of death receptor expression, cells were harvested by trypsinization and incubated in a blocking buffer (PBS + 0.2 % gelatin and 0.1 % sodium azide—PBS-GA) containing 20 % heat-inactivated human serum for 10 min. Then, the samples were incubated on ice for 30 min with antibodies against DR4, DR5 (10-403, 11-461, EXBIO) or FAS/CD95 (DX2, R&D System Inc.) diluted in PBS-GA to a final concentration of 2–5 μg/ml. The cells were then washed twice with ice-cold PBS-GA and incubated with phycoerythrin-conjugated goat anti-mouse IgG1 (Southern Biotech, diluted in PBS-GA to 4 μg/ml) on ice for 30 min. After two final washes, the cells were resuspended in PBS-GA containing 0.5 μg/ml Hoechst 33258, and the cell surface expression of receptors on living cells (Hoechst 33258-negative) was analyzed by flow cytometry on a LSRII.

Preparation of RKO and HT-29 cells with the downregulated expression of cFLIP or Mcl-1 and RKO cells with transiently suppressed expression of p53

HEK293T cells were transfected with the lentivirus packaging plasmids pMD2G, psPAX (Addgene) and pLKO.1 carrying shRNA against cFLIP (4 shRNA), Mcl-1 (5 shRNA) (all from Open Biosystems/Hermo Scientific). Two days later the lentiviral particles were purified from the supernatant using PEG/it Virus Precipitation Solution (SBI, LV810A-1). RKO and HT-29 cells were transduced at MOI 5 and selected in medium containing puromycin (3 μg/ml) for 4 days. Cells displaying the effective (80–90 %) downregulation of cFLIP (TRCN0000007229—shFLIP1, TRCN0000007230—shFLIP2) or Mcl-1 (TRCN0000005515—shMcl-1-2,

TRCN0000005517—shMcl-1-4, TRCN0000005518—shMcl-1-5) expression were used for further experiments. For Mcl-1, the effective downregulation of its expression was achieved by co-transduction of the target cells with shMcl-1-5+2 (=shMcl-1 5/2) or shMcl-1-5+4 (=shMcl-1 5/4) expressing lentiviruses.

Expression of p53 in RKO cells was downregulated by their Lipofectamine RNAiMax-mediated transfection with p53 On-TARGET siGENOME (Thermo Scientific/Dharmacon) according to the manufacture's recommendations. Two days post-transfection, the p53 downregulation was confirmed by Western blotting and cells were used within the following day for experiments.

Subcutaneous xenograft studies

Female immunodeficient NOD.Cg-*Prkdc*^{scid} *Il2rg*^{tm1Wjl}/SzJ mice (Jackson Laboratory) were maintained in individually ventilated cages. HT-29 cells were harvested, suspended in PBS, and injected (10^7 cells/mouse) subcutaneously into the left dorsal flank of 8–12-week-old mice. When tumors reached 800–1,000 mm^3, the animals were randomized into four groups and treated. The control group was injected with vehicle (PBS) intraperitoneally. HHT (1.3 or 2.6 mg/kg; 26 or 52 μg/mouse) and TRAIL (25 mg/kg; 500 μg/mouse) were administered intraperitoneally in a volume of 300 μl. The animals were treated with these agents and their combination on days 1, 3 and 5; when the tumors in the control group reached 2.5–3 cm in diameter, the animals were sacrificed and the tumors weighed.

Statistical analysis

Data are presented as mean ± SD (standard deviation) for the given numer of independent experiments. Student's unpaired t test or one-way ANOVA for multiple comparisons were used to determine significant differences between the experimental groups. Values of *$p < 0.05$ were considered significant, **$p < 0.01$ very significant and ***$p < 0.001$ extremely significant.

Results

Homoharringtonine enhances the TRAIL-induced apoptosis and growth suppression of TRAIL-resistant colorectal cancer cells but not normal colon epithelial cells

TRAIL-induced apoptosis/growth suppression of primary tumors is rather inefficient. The new emerging concept based on TRAIL-related apoptogens encompasses tailored selection of TRAIL-induced apoptosis enhancing agents combined with molecular targeting (e.g., to EGFR via anti-EGFRcs Fv-TRAIL fusion protein) [31, 32]. We were interested in identifying novel TRAIL sensitizers, and thus we screened several chemical libraries for compounds that would significantly enhance TRAIL-mediated growth suppression of resistant colon carcinoma cells (HT-29). Compounds that showed to be at least two times more efficient in decreasing the viability of HT-29 cells in the presence of TRAIL were considered as primary hits. These hits were validated in dose–response for their ability to enhance TRAIL-mediated apoptosis (Suppl. Fig. 1). Among the positive hits were previously identified sensitizers such as camptothecin and thapsigargin [33, 34] Other validated hits were emetine and its analog cephaeline, the inhibitors of protein synthesis anisomycin, the alcohol dehydrogenase inhibitor disulfiram and HHT. HHT was by far the most potent TRAIL sensitizer and the only compound showing activity at low nanomolar concentrations.

Homoharringtonine consistently and strongly sensitized not only HT-29, but also other TRAIL-resistant carcinoma cell lines such as RKO and SW620 to TRAIL-induced apoptosis (Fig. 1a and data not shown). In contrast, the normal colon epithelial cell line CCD 841 and normal human fibroblasts remained resistant to combined HHT + TRAIL treatment (Fig. 1a and data not shown). HHT also synergized with TRAIL in enhancing the TRAIL-induced activation of effector caspases (Fig. 1b, c). For RKO cells the saturation in caspase-3/7 activity was reached at 35 ng/ml and for HT-29 at 76 ng/ml of recombinant TRAIL (LC50 = 7 and 15 ng/ml, respectively) with a constant 100 nM HHT (Fig. 1b). Vice versa, titrating HHT under a constant LC50 concentration of TRAIL revealed that the saturating concentration of HHT required for the activation of effector caspases is 50–60 nM with a LC at 15 nM (Fig. 1c). More efficient activation of caspases is necessary but might not be sufficient for the reliable elimination of cancer cells. Thus, by various approaches, we analyzed the long-term survival of resistant cancer cells treated with HHT, TRAIL and their combination. Both xCELLigence- and WST-1-based survival assays confirmed that only the combined effect of 50 nM HHT and TRAIL could lead to the effective long-term elimination of cancer cells (Fig. 2 and Suppl. Fig. 2a, c). In agreement with the Annexin-FITC staining, combined HHT + TRAIL treatment of normal colon epithelial cells with sub-lethal and lethal combinations of HHT + TRAIL did not markedly change their viability (Fig. 2 and Suppl. Fig. 2b).

Homoharringtonine modifies TRAIL-induced proximal signaling in colorectal cancer cells and the expression of some apoptosis-regulating proteins

For the efficient induction of TRAIL-induced apoptosis, the essential requirements are (a) the presence and
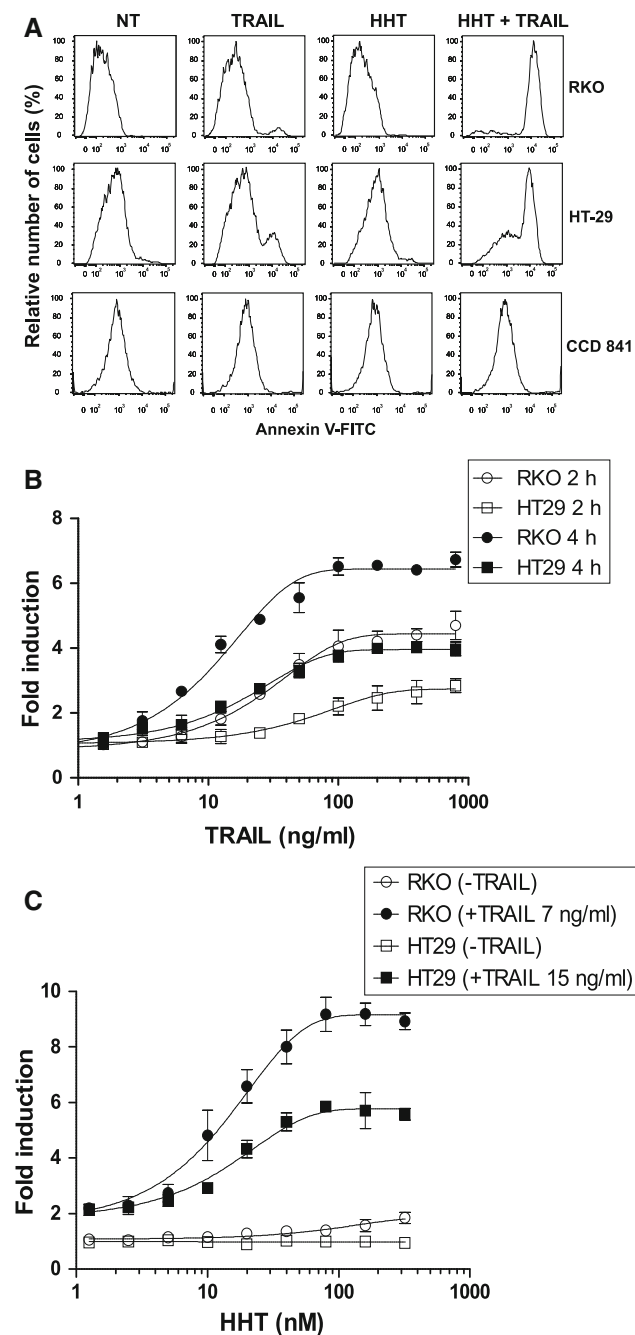
Fig. 1 Homoharringtonine enhances TRAIL-induced pro-apoptotic signaling in resistant colorectal cancer cells. HT-29 or RKO cells were treated with TRAIL, HHT or their combination and assayed for the manifestation of apoptosis by Annexin V-FITC staining and the activity of caspase-3. **a** Cells were incubated with 50 nM HHT, 20 ng/ml TRAIL or their combination for 5 h, stained with Annexin-V-FITC and analyzed by flow cytometry. **b** The concentration-dependent activation of caspase-3 in cells co-treated with 100 nM HHT and TRAIL for 2 and 4 h was quantified by the Caspase 3/7 GLO assay. **c** Titration of HHT at a fixed concentration of TRAIL (7 ng/ml for RKO and 15 ng/ml for HT-29 cells) quantified by the caspase 3/7 GLO assay. The experiments were run in triplicate in 384-well plates and were repeated three times. Means and standard deviations are shown

accessibility of pro-apoptotic TRAIL receptors and (b) the efficient formation of the DISC platform leading to rapid self-processing and the activation of caspase-8. However, short or long-term treatment (4 or 15 h) of RKO or HT-29 cells with 50 nM HHT did not significantly affect the cell surface expression of TRAIL receptors (we even noticed a small but reproducible decrease in TRAIL-R2/DR5 expression in RKO cells; Suppl. Fig. 3 and Fig. 3—lower staining of DR5 in the cell lysates).

Next, we aimed to assess the efficacy of DISC formation and the processing of the initiator caspases. In RKO cells, TRAIL engagement led to the rapid formation of the DISC and the processing of both initiator caspases-8 and -10 (Fig. 3a, left side of the left panel). In RKO cells pre-treated with HHT for 3 h, TRAIL addition resulted in a lesser quantity of DISC proteins in the precipitates (Fig. 3a, right side of the left panel); however, the processing of the initiator caspases and cFLIP cleavage in the DISC were not significantly affected. A decrease of both DR5 and also cFLIP levels (both L and S forms) in HHT-pretreated RKO cells was also observable in the cell-free lysates used for DISC precipitation in response to TRAIL addition (Fig. 3a, right panel). Similarly in HT-29 cells we also observed a drop in cFLIP levels in precipitated DISC complexes and no observable differences in the efficacy of activation of the initiator caspases (data not shown).

In addition to the activation of caspases, TRAIL-induced proximal signaling also feeds into MAP kinase and NF-κB pathways. TRAIL-treatment of RKO cells resulted in the strong but transient activation of NF-κB signaling (phosphorylation of IκB and p65/RelA, transient degradation of IκB, Fig. 3b). IκB phosphorylation and degradation were evident at 30 and 60 min post-TRAIL treatment respectively, also in cells co-treated with TRAIL + HHT. However, after co-treatment, in contrast to TRAIL-only-treated cells, there was no recovery of IκB expression at 2 h post-treatment (p.t.), and we even observed the stronger phosphorylation of p65/RelA at this time point. HHT alone did not have any effect on canonical NF-κB signaling (Fig. 3b, upper panels). Treatment with either HHT or TRAIL alone also activated the JNK signaling pathway and induced JNK1/2 phosphorylation as early as 30–60 min p.t. (Fig. 3b, middle panels). Interestingly, there was a strong synergism in JNK1/2 phosphorylation in RKO cells co-treated with HHT + TRAIL. Similarly, the TRAIL-induced phosphorylation of p38 MAP kinase was significantly enhanced at 60 min post-treatment in cells co-treated with TRAIL + HHT (Fig. 3b, lower panels). Published reports have connected the increased activation of JNK and p38 kinases with the apoptosis-sensitizing effects of HHT [35, 36], and these authors used MAP kinase inhibitors for the suppression of HHT-mediated apoptosis. However, neither the JNK inhibitor SP600125 nor the p38 inhibitor SB202190 had any effect
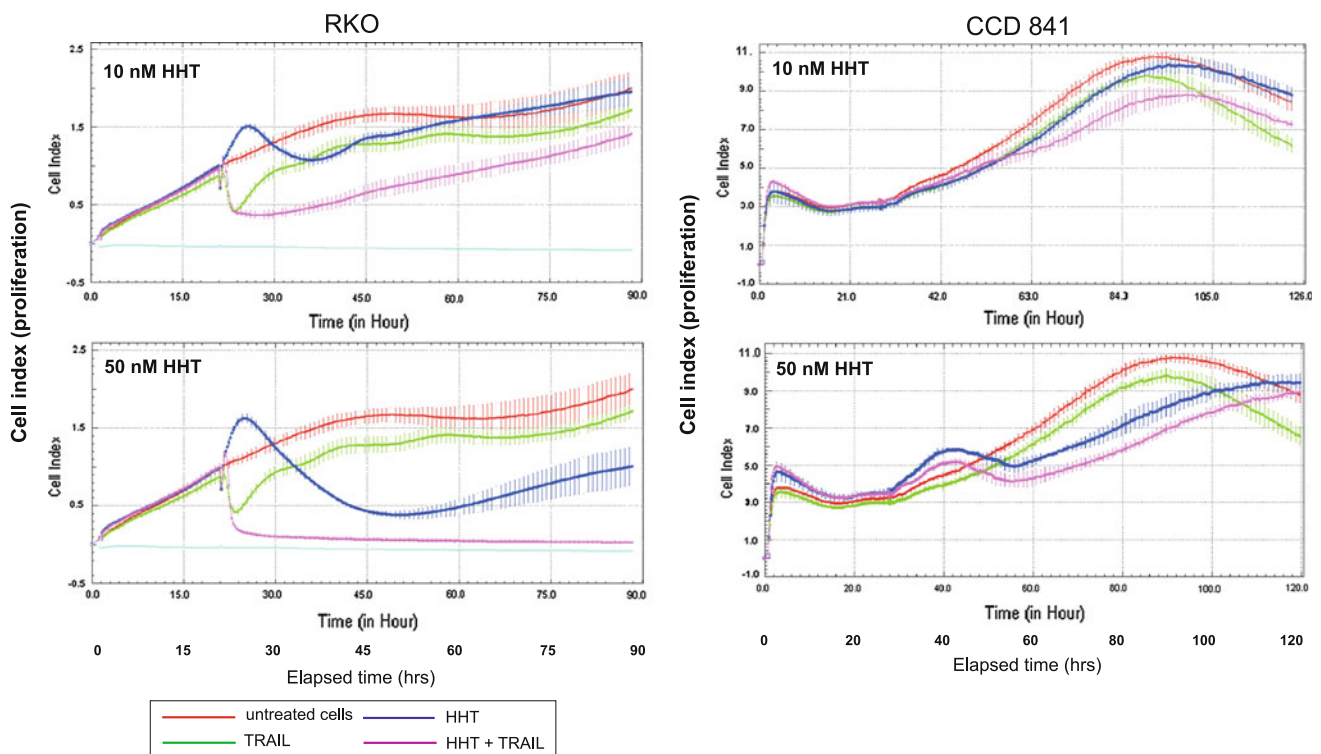
Fig. 2 HHT collaborates with TRAIL in the growth suppression of resistant cancer cells. 5,000 cfu of cancer RKO or normal CCD 841 cells were seeded in triplicate into a 96-well E-plate and treated with 100 ng/ml TRAIL, 10 or 50 nM HHT or their combination in the xCELLigence RTCA analyzer (Roche). The cell index representing cell proliferation was measured every 15 min. The data represent one out of four experiments with similar outcomes

(positive or negative) on the HHT-induced sensitization of either RKO or HT-29 cells to TRAIL-induced apoptosis (data not shown), indicating none or minor role of these kinases in the HHT-mediated sensitization of these cells to TRAIL. In contrast to MAP/stress kinases inhibitors blocking NF-κB signaling with IKKα inhibitors Bay 11-7082 surprisingly resulted in blunting the HHT-mediated sensitization of RKO cells to TRAIL-induced apoptosis (Suppl. Fig. 4 and not shown). Especially at higher 20 μM concentration that effectively suppressed IκB phosphorylation, Bay 11-7082 reproducibly attenuated TRAIL-triggered externalization of phosphatidyl choline (Suppl. Fig. 4a) and activation of caspases (Suppl. Fig. 4b). However, this concentration was also significantly toxic for RKO cells as documented by over 25 % dead, Hoechst-positive cells after their 5 h treatment with Bay 11-7082 alone or in combination with HHT/TRAIL (Suppl. Fig. 4A, right panel). Likely also for Bay's toxic side effects, long-term survival of Bay 11-7082/HHT/TRAIL-treated cells was very low and similarly as for HHT + TRAIL-treated cells virtually no cells survived this combined treatment.

The significant down-regulation of cFLIP expression in HHT + TRAIL-treated cells (see Fig. 3a) as well as published data on HHT as a translation inhibitor [37] prompted

us to assess the effect of HHT on the stability of apoptosis-regulating proteins. Western blots of RKO or HT-29 lysates of cells treated with 50 nM HHT for up to 6 h documented a significant, time-dependent decrease of both cFLIP-L and, even more strongly, of cFLIP-S levels starting between 1 and 2 h p.t. We did not see any effect of HHT on the cellular levels of Bak, Bax, Bcl-XL, Bim or XIAP (Fig. 4a and data not shown), but the stability of the short-lived protein Mcl-1 was strongly affected by HHT treatment and its levels dramatically dropped within 2–4 h post-treatment (Fig. 4a). Kinetics of caspase processing and cleavage of some of their substrate was then analyzed in HHT + TRAIL-treated RKO cells. The cells were either treated with 50 nM HHT and 100 ng/ml TRAIL alone for up to 4 h or they were co-treated for the same time periods. In contrast to HHT- or TRAIL-only treated cells, cells co-treated with the combination of HHT + TRAIL efficiently within the first 2 h processed both initiator caspases- and 10. After the second hour of the treatment also caspase-8 substrate tBid and mitochondrial-activated caspase-9 were fully or strongly processed/activated only in HHT + TRAIL-treated cells (Fig. 4b). In addition the combined treatment even accelerated HHT-mediated downregulation of cFLIP-S or Mcl-1.

Fig. 3 Homoharringtonine affects TRAIL-induced proximal signaling in RKO cells. **a** Precipitation of TRAIL receptor DISC from Biot-TRAIL- and Biot-TRAIL + HHT-treated RKO cells (Biot-TRAIL was used at a concentration of 1 µg/ml and HHT at 50 nM). The precipitated proteins and cell lysates were analyzed by Western blotting using the indicated antibodies. **b** RKO cells were treated with HHT, TRAIL or their combination for up to 120 min, and the expression and phosphorylation status of the proteins shown were determined by Western blotting. The data represent typical blots from two (**a**) or three (**b**) independent experiments
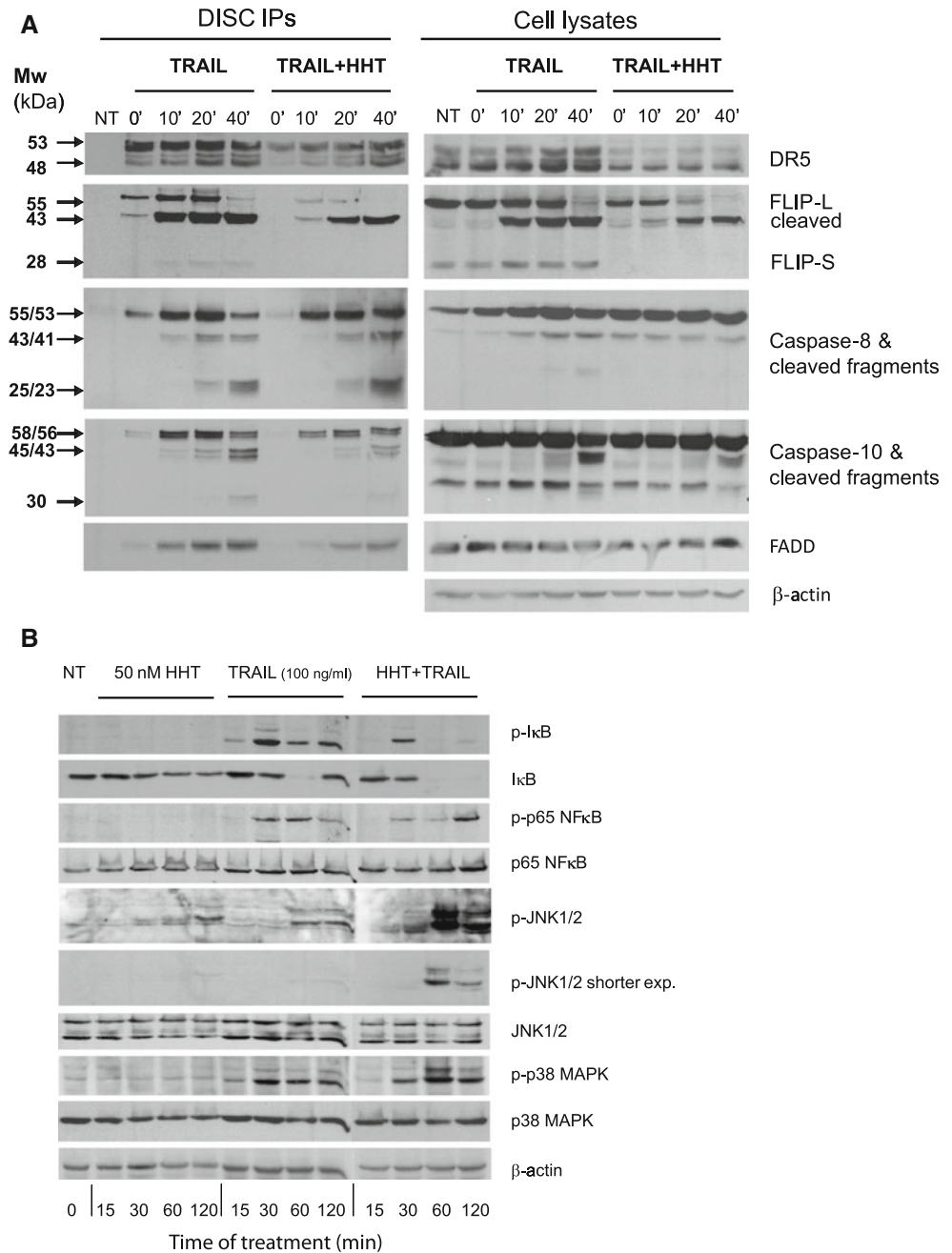
Downregulation of cFLIP or Mcl-1 enhances TRAIL-induced apoptosis but is not sufficient for TRAIL-mediated growth suppression of resistant cells

As HHT treatment of TRAIL-resistant cells led to a time-dependent downregulation of cFLIP and Mcl-1, two major inhibitors of TRAIL-induced apoptosis, we aimed to assess the individual contribution of these proteins to the TRAIL-resistant phenotype of RKO and HT-29 cells. Using two different shRNA-expressing lentiviruses for each gene, we established both RKO and HT-29 cells with the downregulated expression of either cFLIP or Mcl-1. In both cell lines we achieved at least an 80–90 % decrease in the expression of either cFLIP or Mcl-1 (Fig. 5a). The downregulation of Mcl-1 enhanced TRAIL-induced pro-apoptotic signaling in both cell lines (Fig. 5b and Suppl. Fig. 5a, b, right graphs). However, to our surprise downregulating cFLIP augmented TRAIL-induced apoptosis only in HT-29 cells, but it had no or even an inhibitory effect on the TRAIL-induced apoptosis of RKO cells. Similarly, using a sub-optimal, 25 nM concentration of HHT enhanced the TRAIL-induced apoptosis of both RKO and HT-29 cells with the downregulated expression of Mcl-1 and of HT-29 cells with the downregulated expression
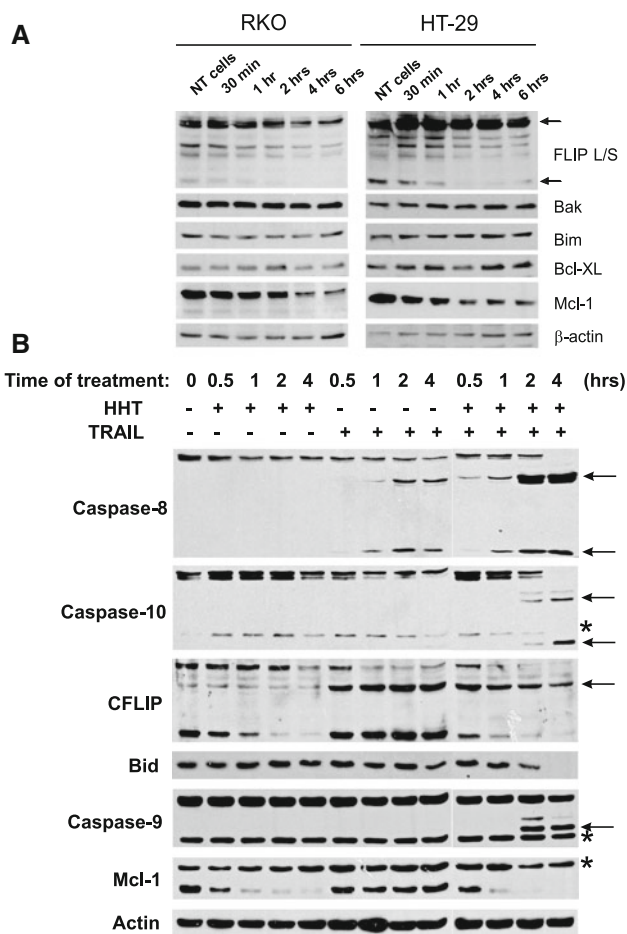
Fig. 4 Homoharringtonine suppresses the expression of some anti-apoptotic proteins and enhances processing of caspases in TRAIL-resistant cancer cells. **a** RKO or HT-29 cells were treated with 50 nM HHT for up to 6 h, and the expression of selected apoptosis-regulating proteins was analyzed by Western blotting. Representative Western blots from three independent experiments are shown. *Arrows* point to cFLIP-L and cFLIP-S, respectively. **b** RKO cells were treated with HHT (50 nM), TRAIL (100 ng/ml) and their combination in time-dependent manner and the expression/processing of selected, TRAIL-mediated apoptosis-related caspases and proteins was analyzed by Western blotting. *Arrows* indicate processed caspases and cleaved cFLIP-L, and *asterisk* then non-specifically stained proteins

of FLIP, but such treatment led to much lower pro-apoptotic responses in RKO cells with the downregulated expression of cFLIP (Fig. 5b and Suppl. Fig. 5).

The results of viability/proliferation assays of these cells with suppressed cFLIP or Mcl-1 expression followed a quite similar pattern. Both CellTiter-Blue and xCELLigence viability tests showed that despite the significant increase of apoptosis in TRAIL-treated cells with the downregulated expression of Mcl-1 or cFLIP (only for HT-29), knocking-down either of these anti-apoptotic proteins had only a marginal effect on the long-term survival of TRAIL-treated cells (Suppl. Fig. 5, left panels and Suppl. Fig. 6). However, especially the suppressed expression of

Mcl-1 markedly boosted the HHT-mediated sensitization of both RKO and HT-29 cells to TRAIL-induced apoptosis, as documented by more than a twofold lower viability in comparison to control cells in the CellTiter-Blue assay (Suppl. Fig. 5) and virtually no survival of treated cells in the xCELLigence test (compare none and shMcl-1; Suppl. Fig. 6). Strangely, RKO cells with the downregulated expression of cFLIP virtually became resistant to the sensitizing effect of HHT and TRAIL + HHT (Suppl. Fig. 5, left panels and Suppl. Fig. 6). These cells basically reflected just the anti-proliferative effects of HHT itself.

RKO cells in contrast to HT-29 contain wt p53 and thus it might be possible that p53 presence/activity could make RKO cells even more vulnerable to the combined effect of HHT + TRAIL. But this premise was not fulfilled, as RKO cells with by siGENOME downregulated expression of p53 responded to either TRAIL alone or TRAIL + HHT with no difference in the efficacy or kinetics of their apoptosis (data not shown).

The combined action of homoharringtonine and TRAIL efficiently suppressed the growth of TRAIL-resistant cancer cells in vivo

To validate our in vitro findings documenting the very strong sensitizing impact of HHT on the TRAIL-induced apoptosis/growth suppression of resistant cancer cells, we used an in vivo model with HT-29 cells subcutaneously xenotransplanted into immunodeficient NOD/SCID mice. A cohort of 36 mice was injected with 10^7 cells, and when the resulting tumors reached approximately 1 cm³, the mice were divided into six groups and treated three times (every second day) with intraperitoneal injections of TRAIL (25 mg/kg), HHT (1.3 mg/kg) or a combination of TRAIL with HHT. Within 18 days of tumor growth, the tumor mass in untreated mice increased approximately 3.5-fold; both individual treatments had only a marginal inhibitory effect on tumor growth, but the tumors in animals co-treated with HHT + TRAIL ceased growing, and the animals did not suffer any adverse effects (Fig. 6). All mice in the HHT + TRAIL-treated cohort survived the treatment until their sacrifice at the end of the experiment.

Discussion

Primary tumors only weakly react to mono-therapy with TRAIL apoptogens, and even binary or ternary combinations of TRAIL with sensitizing agents were only partly effective in a number of phase I/II trials. Thus, if TRAIL apoptogens are still to be considered as potential anti-tumor drugs, tailored combination treatment that would overcome

Fig. 5 Downregulation of Mcl-1 or cFLIP predominantly leads to the increased sensitivity of resistant cancer cells to TRAIL-induced apoptosis. RKO or HT-29 cells were transduced with cFLIP- or Mcl-1-expressing lentiviruses and analyzed for their sensitivity to TRAIL- or HHT + TRAIL-induced apoptosis. a Western blots of mixed populations of RKO and HT-29 cells stably transduced with the pLKO1 lentivirus (none) and two different cFLIP or Mcl-1 shRNAs. Asterisk at Mcl-1 signal indicates non-specific staining. b The activation of TRAIL-induced apoptosis in these cells treated for 5 h with the indicated reagents was analyzed by Annexin-V-FITC staining and flow cytometry. The data represent means and standard deviations of three independent experiments from shFLIP and shMcl-1 expressing RKO cells
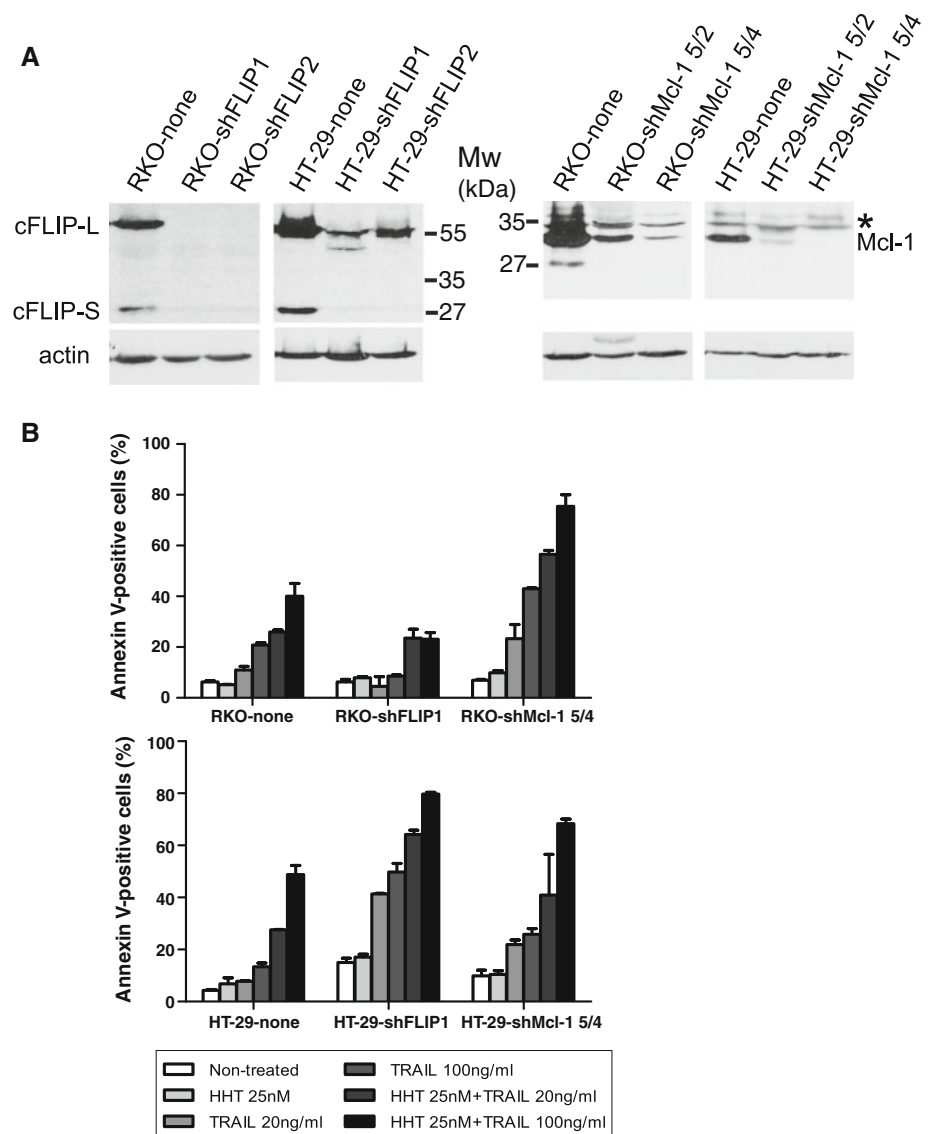
the acquired resistance of cancer cells and have few, or better, no side effects would be an optimal therapeutic option [31].

Here we show that HHT, an inhibitor of translation and a tested anti-leukemia drug, efficiently sensitizes resistant cancer cells to their TRAIL-mediated elimination both in vitro and in vivo and, within the therapeutic window, is not harmful to normal cells or the organism. In agreement with the published data we also found that in our model of TRAIL-resistant colorectal cancer cell lines, HHT caused, in a time- and concentration-dependent manner, a fairly rapid (within 2–4 h) drop in the cellular levels of two important regulators of TRAIL-induced apoptosis—the anti-apoptotic proteins Mcl-1 and cFLIP [38, 39]. Also as expected, the shRNA-mediated downregulation of either of these proteins significantly enhanced TRAIL-induced apoptosis but surprisingly had only a marginal effect on

TRAIL-mediated growth suppression. However, shRNA treatment lowered the effective sensitizing concentration of HHT by at least two-fold.

In contrast to HT-29 cells, downregulation in RKO cells provided quite ambiguous results. While the downregulation of Mcl-1 strongly boosted both TRAIL-induced apoptosis and HHT-mediated sensitization, cells with downregulated cFLIP expression became more resistant not only to TRAIL, but also to their HHT-mediated sensitization to TRAIL-induced apoptosis. This was quite an unexpected finding as the downregulation of cFLIP in various cancer cell lines has generally been connected with the strong enhancement of TRAIL- or FasL-induced apoptosis [40–42]. However, cFLIP-L, in sharp contrast to cFLIP-S or -R, is likely not just a competitive inhibitor of caspase-8 activation, but also, due to its high affinity for caspase-8, either a platform in a cytoplasmic caspase-8-activating complex
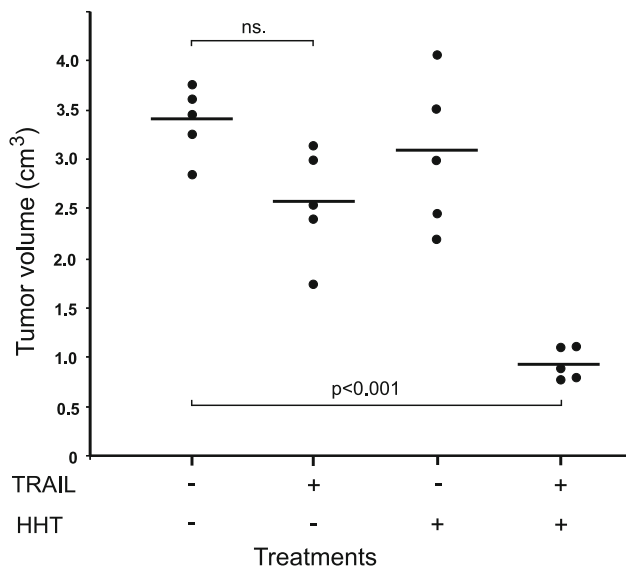
Fig. 6 Homoharringtonine assists TRAIL in suppressing the growth of colon cancer cells in immunodeficient mice. HT-29 cells (10^6 cfu) were subcutaneously injected into a cohort of NOD/SCID mice, and when the tumors reached approximately 1 cm^3 in size, these mice (at least five per group) received three intraperitoneal injections (every second day) of TRAIL (25 mg/kg), HHT (1.3 mg/kg) or their combination (25 mg/kg TRAIL plus 1.3 mg/kg HHT). At day 10 post-treatment the mice were sacrificed, and the size of their tumors was determined. The average volumes and standard deviations are shown with *marked* statistical significance

[43] or even an enhancer of caspase-8 processing in the DISC at low (sub) stochiometric concentrations [44, 45]. RKO cells express significantly less cFLIP than HT-29 cells, and thus shRNA-mediated downregulation basically eliminated cFLIP expression in these cells. This apparently made RKO cells more resistant even to the combined effects of HHT + TRAIL, indicating a positive role for low levels cFLIP-L in the fine tuning of TRAIL-induced apoptotic signaling in these cells. This finding might be in apparent contradiction with the HHT-mediated downregulation of cFLIP in RKO cells. However, in HHT-treated RKO cells the more unstable cFLIP-S is rapidly downregulated, but the decrease in cFLIP-L levels is only modest, and cFLIP-L is still detectable in the DISC precipitates (and lysates) of HHT + TRAIL-treated RKO cells.

Intracellular levels of Mcl-1 were many times shown as important decision nodes for various apoptotic stimuli including e.g. BH3 analog ABT-737 [46], and Mcl-1 expression alone or together with cFLIP was targeted and suppressed by a number of existing and novel drugs such as roscovitine, quercetin or aspirin plus sorafenib, enhancing thus (not exclusively) TRAIL-induced apoptosis of cancer cells [47–49]. Multikinase inhibitor sorafenib or ectopic expression of cMyc blocked TRAIL-induced, NF-κB-mediated expression of Mcl-1 and thus sensitized TRAIL-resistant cells to TRAIL-induced apoptosis [50]. In contrast

to this generally accepted anti-apoptotic role of NF-κB signaling we found out that blocking NF-κB signaling by BAY 11-7082, a well-known inhibitor of IKKα also attenuated sensitizing effect of HHT and suppressed TRAIL-induced apoptosis of RKO cell. This unexpected finding is however supported by recent publication from Simone Fulda's group. In this communication the authors for the first time document that in glioblastoma cell lines, blocking NF-κB signaling pathway by overexpression of dominant-negative non-phosphorylated IκB also suppressed TRAIL-induced apoptosis likely via for yet unknown reasons less efficient caspase-8 processing in DISC [51].

Being a potent inhibitor of translation, HHT could be potentially harmful to normal cells in combination with TRAIL, similarly as another anti-cancer drug and proteasome inhibitor, bortezomib (Velcade) [52]. On the other hand, bortezomib has proven to be a very efficient enhancer of the TRAIL-induced apoptosis of therapy-resistant glioblastoma or melanoma cells and Lex-atumumab-resistant BJAB cells [53–55] and within the therapeutic window also safe to normal cells. Similarly, combining HHT with TRAIL was not only effective in vitro, but also suppressed the growth of xenotransplanted TRAIL-resistant HT-29 cells in immunodeficient mice, thus proving its efficacy and safety within the therapeutic window. As an already tested drug in cancer treatment, HHT could, after thorough testing, represent a potentially interesting option for sensitizing TRAIL-resistant cancer cells to apoptosis.

Conflict of interest The authors declare that they have no conflict of interest.

References

1. Venugopal B, Evans TR (2011) Developing histone deacetylase inhibitors as anti-cancer therapeutics. Curr Med Chem 18:1658–1671
2. Schumacher M, Kelkel M, Dicato M, Diederich M (2011) A survey of marine natural compounds and their derivatives with anti-cancer activity reported in 2010. Molecules 16:5629–5646
3. Scheinberg DA, Villa CH, Escorcia FE, McDevitt MR (2010) Conscripts of the infinite armada: systemic cancer therapy using nanomaterials. Nat Rev Clin Oncol 7:266–276
4. Biasutto L, Dong LF, Zoratti M, Neuzil J (2010) Mitochondrially targeted anti-cancer agents. Mitochondrion 10:670–681

5. Deckert PM (2009) Current constructs and targets in clinical development for antibody-based cancer therapy. Curr Drug Targets 10:158–175

6. Yerbes R, Palacios C, Lopez-Rivas A (2011) The therapeutic potential of TRAIL receptor signalling in cancer cells. Clin Transl Oncol 13:839–847

7. Bernardi S, Secchiero P, Zauli G (2012) State of art and recent developments of anti-cancer strategies based on TRAIL. Recent Pat Anticancer Drug Discov 7:207–217

8. Abdulghani J, El-Deiry WS (2010) TRAIL receptor signaling and therapeutics. Expert Opin Ther Targets 14:1091–1108

9. Pennarun B, Meijer A, de Vries EG, Kleibeuker JH, Kruyt F, de Jong S (2010) Playing the DISC: turning on TRAIL death receptor-mediated apoptosis in cancer. Biochim Biophys Acta 1805:123–140

10. Gonzalvez F, Ashkenazi A (2010) New insights into apoptosis signaling by Apo2L/TRAIL. Oncogene 29:4752–4765

11. Fu K, Ren H, Wang Y, Fei E, Wang H, Wang G (2011) DJ-1 inhibits TRAIL-induced apoptosis by blocking pro-caspase-8 recruitment to FADD. Oncogene 31:1311–1322

12. Cao X, Pobezinskaya YL, Morgan MJ, Liu ZG (2011) The role of TRADD in TRAIL-induced apoptosis and signaling. Faseb J 25:1353–1358

13. Sun M, Song L, Li Y, Zhou T, Jope RS (2008) Identification of an antiapoptotic protein complex at death receptors. Cell Death Differ 15:1887–1900

14. Mulherkar N, Prasad KV, Prabhakar BS (2007) MADD/DENN splice variant of the IG20 gene is a negative regulator of caspase-8 activation. Knockdown enhances TRAIL-induced apoptosis of cancer cells. J Biol Chem 282:11715–11721

15. Xiao C, Yang BF, Asadi N, Beguinot F, Hao C (2002) Tumor necrosis factor-related apoptosis-inducing ligand-induced death-inducing signaling complex and its modulation by c-FLIP and PED/PEA-15 in glioma cells. J Biol Chem 277:25020–25025

16. Castro Alves C, Terziyska N, Grunert M et al (2012) Leukemia-initiating cells of patient-derived acute lymphoblastic leukemia xenografts are sensitive towards TRAIL. Blood 119(18): 4224–4227

17. Piggott L, Omidvar N, Perez SM, Eberl M, Clarkson RW (2011) Suppression of apoptosis inhibitor c-FLIP selectively eliminates breast cancer stem cell activity in response to the anti-cancer agent, TRAIL. Breast Cancer Res 13:R88

18. Zhang L, Fang B (2005) Mechanisms of resistance to TRAIL-induced apoptosis in cancer. Cancer Gene Ther 12:228–237

19. Ehrhardt H, Fulda S, Schmid I, Hiscott J, Debatin KM, Jeremias I (2003) TRAIL induced survival and proliferation in cancer cells resistant towards TRAIL-induced apoptosis mediated by NF-kappaB. Oncogene 22:3842–3852

20. Amm HM, Oliver PG, Lee CH, Li Y, Buchsbaum DJ (2011) Combined modality therapy with TRAIL or agonistic death receptor antibodies. Cancer Biol Ther 11:431–449

21. Fulda S (2012) Histone deacetylase (HDAC) inhibitors and regulation of TRAIL-induced apoptosis. Exp Cell Res 318(11): 1208–1212

22. Sayers TJ (2011) Targeting the extrinsic apoptosis signaling pathway for cancer therapy. Cancer Immunol Immunother 60: 1173–1180

23. Ding J, Polier G, Kohler R, Giaisi M, Krammer PH, Li-Weber M (2012) Wogonin and related natural flavones overcome tumor necrosis factor-related apoptosis-inducing ligand (TRAIL) protein resistance of tumors by down-regulation of c-FLIP protein and up-regulation of TRAIL receptor 2 expression. J Biol Chem 287:641–649

24. Gupta SC, Reuter S, Phromnoi K et al (2011) Nimbolide sensitizes human colon cancer cells to TRAIL through reactive oxygen species- and ERK-dependent up-regulation of death receptors, p53, and Bax. J Biol Chem 286:1134–1146

25. Whitson EL, Sun H, Thomas CL et al (2012) Synergistic TRAIL sensitizers from barleria alluaudii and diospyros maritima. J Nat Prod 75:394–399

26. Kim TD, Frick M, le Coutre P (2011) Omacetaxine mepesuccinate for the treatment of leukemia. Expert Opin Pharmacother 12:2381–2392

27. Klag T, Hartel N, Erben P et al (2012) Omacetaxine mepesuccinate prevents cytokine-dependent resistance to nilotinib in vitro: potential role of the common beta-subunit c of cytokine receptors. Leukemia 26:1321–1328

28. Meng H, Yang C, Jin J, Zhou Y, Qian W (2008) Homoharringtonine inhibits the AKT pathway and induces in vitro and in vivo cytotoxicity in human multiple myeloma cells. Leuk Lymphoma 49:1954–1962

29. Eckelbarger JD, Wilmot JT, Epperson MT et al (2008) Synthesis of antiproliferative Cephalotaxus esters and their evaluation against several human hematopoietic and solid tumor cell lines: uncovering differential susceptibilities to multidrug resistance. Chemistry 14:4293–4306

30. Efferth T, Sauerbrey A, Halatsch ME, Ross DD, Gebhart E (2003) Molecular modes of action of cephalotaxine and homoharringtonine from the coniferous tree Cephalotaxus hainanensis in human tumor cell lines. Naunyn Schmiedebergs Arch Pharmacol 367:56–67

31. Dimberg LY, Anderson CK, Camidge R, Behbakht K, Thorburn A, Ford HL (2012) On the TRAIL to successful cancer therapy? Predicting and counteracting resistance against TRAIL-based therapeutics. Oncogene. doi:10.1038/onc.2012.164

32. Siegemund M, Pollak N, Seifert O et al (2012) Superior antitumoral activity of dimerized targeted single-chain TRAIL fusion proteins under retention of tumor selectivity. Cell Death Dis 3:e295

33. Frese S, Schuller A, Frese-Schaper M, Gugger M, Schmid RA (2009) Cytotoxic effects of camptothecin and cisplatin combined with tumor necrosis factor-related apoptosis-inducing ligand (Apo2L/TRAIL) in a model of primary culture of non-small cell lung cancer. Anticancer Res 29:2905–2911

34. Chen LH, Jiang CC, Kiejda KA et al (2007) Thapsigargin sensitizes human melanoma cells to TRAIL-induced apoptosis by up-regulation of TRAIL-R2 through the unfolded protein response. Carcinogenesis 28:2328–2336

35. Chen R, Guo L, Chen Y, Jiang Y, Wierda WG, Plunkett W (2011) Homoharringtonine reduced Mcl-1 expression and induced apoptosis in chronic lymphocytic leukemia. Blood 117: 156–164

36. Sah NK, Munshi A, Kurland JF, McDonnell TJ, Su B, Meyn RE (2003) Translation inhibitors sensitize prostate cancer cells to apoptosis induced by tumor necrosis factor-related apoptosis-inducing ligand (TRAIL) by activating c-Jun N-terminal kinase. J Biol Chem 278:20593–20602

37. Kantarjian HM, Talpaz M, Santini V, Murgo A, Cheson B, O'Brien SM (2001) Homoharringtonine: history, current research, and future direction. Cancer 92:1591–1605

38. Kim SH, Ricci MS, El-Deiry WS (2008) Mcl-1: a gateway to TRAIL sensitization. Cancer Res 68:2062–2064

39. Bagnoli M, Canevari S, Mezzanzanica D (2011) Cellular FLICE-inhibitory protein (c-FLIP) signalling: a key regulator of receptor-mediated apoptosis in physiologic context and in cancer. Int J Biochem Cell Biol 42:210–213

40. Sharp DA, Lawrence DA, Ashkenazi A (2005) Selective knockdown of the long variant of cellular FLICE inhibitory protein augments death receptor-mediated caspase-8 activation and apoptosis. J Biol Chem 280:19401–19409

41. Haag C, Stadel D, Zhou S et al (2011) Identification of c-FLIP(L) and c-FLIP(S) as critical regulators of death receptor-induced apoptosis in pancreatic cancer cells. Gut 60:225–237

42. Thome M, Schneider P, Hofmann K et al (1997) Viral FLICE-inhibitory proteins (FLIPs) prevent apoptosis induced by death receptors. Nature 386:517–521

43. Pop C, Oberst A, Drag M et al (2011) FLIP(L) induces caspase 8 activity in the absence of interdomain caspase 8 cleavage and alters substrate specificity. Biochem J 433:447–457

44. Fricker N, Beaudouin J, Richter P, Eils R, Krammer PH, Lavrik IN (2011) Model-based dissection of CD95 signaling dynamics reveals both a pro- and antiapoptotic role of c-FLIPL. J Cell Biol 190:377–389

45. Micheau O, Thome M, Schneider P et al (2002) The long form of FLIP is an activator of caspase-8 at the Fas death-inducing signaling complex. J Biol Chem 277:45162–45171

46. Tromp JM, Geest CR, Breij EC et al (2012) Tipping the Noxa/Mcl-1 balance overcomes ABT-737 resistance in chronic lymphocytic leukemia. Clin Cancer Res 18:487–498

47. Jacquemin G, Granci V, Gallouet AS et al (2012) Quercetin-mediated Mcl-1 and survivin downregulation restores TRAIL-induced apoptosis in non-Hodgkin's lymphoma B cells. Haematologica 97:38–46

48. Leitch AE, Riley NA, Sheldrake TA et al (2010) The cyclin-dependent kinase inhibitor R-roscovitine down-regulates Mcl-1 to override pro-inflammatory signalling and drive neutrophil apoptosis. Eur J Immunol 40:1127–1138

49. Pennarun B, Kleibeuker JH, Boersma-van Ek W et al (2012) Targeting FLIP and Mcl-1 using a combination of aspirin and sorafenib sensitizes colon cancer cells to TRAIL. J Pathol 229(3):410–421

50. Ricci MS, Kim SH, Ogi K et al (2007) Reduction of TRAIL-induced Mcl-1 and cIAP2 by c-Myc or sorafenib sensitizes resistant human cancer cells to TRAIL-induced death. Cancer Cell 12:66–80

51. Jennewein C, Karl S, Baumann B, Micheau O, Debatin KM, Fulda S (2012) Identification of a novel pro-apoptotic role of NF-kappaB in the regulation of TRAIL- and CD95-mediated apoptosis of glioblastoma cells. Oncogene 31:1468–1474

52. Koschny R, Ganten TM, Sykora J et al (2007) TRAIL/bortezomib cotreatment is potentially hepatotoxic but induces cancer-specific apoptosis within a therapeutic window. Hepatology 45:649–658

53. Lecis D, Drago C, Manzoni L et al (2010) Novel SMAC-mimetics synergistically stimulate melanoma cell death in combination with TRAIL and bortezomib. Br J Cancer 102:1707–1716

54. Menke C, Bin L, Thorburn J, Behbakht K, Ford HL, Thorburn A (2011) Distinct TRAIL resistance mechanisms can be overcome by proteasome inhibition but not generally by synergizing agents. Cancer Res 71:1883–1892

55. Unterkircher T, Cristofanon S, Vellanki SH et al (2011) Bortezomib primes glioblastoma, including glioblastoma stem cells, for TRAIL by increasing tBid stability and mitochondrial apoptosis. Clin Cancer Res 17:4019–4030

(54) **Lipophosphonoxins, method of their preparation and use**

Lipophosphonoxine, Verfahren zur Herstellung und Verwendung

Lipophosphonoxines, leur procédé de préparation et d'utilisation

(73) Proprietors:
• Ustav organicke chemie a biochemie AV CR, v.v.i.
166 10 Praha 6 (CZ)
• Mikrobiologicky ustav AV CR, v.v.i.
142 20 Praha 4 - Krc (CZ)
• Ustav molekularni genetiky AV CR, v.v.i.
142 20 Praha 4 (CZ)
• Trios, spol. s r.o.
14900 Praha 4 (CZ)

(72) Inventors:
• Rejman, Dominik
17000 Praha 7 (CZ)
• Pohl, Radek
25264 Uholicky (CZ)
• Bartunek, Petr
11000 Praha 1 (CZ)

• Ribeiro Pombinho, Antonio Jose
Golfeiras, Mirandela (PT)
• Krasny, Libor
25263 Roztoky u Prahy (CZ)
• Latal, Tomas
78314 Hlusovice (CZ)

(74) Representative: **Gabrielova, Marta et al**
Inventia s.r.o.
Na Belidle 3
150 00 Praha 5 (CZ)

(56) References cited:
• SUK ET AL: "Phosphonoxins: Rational design
and discovery of a potent nucleotide anti-Giardia
agent", BIOORGANIC & MEDICINAL CHEMISTRY
LETTERS, PERGAMON, ELSEVIER SCIENCE,
GB, vol. 17, no. 10, 27 April 2007 (2007-04-27),
pages 2811-2816, XP022049593, ISSN:
0960-894X, DOI: 10.1016/J.BMCL.2007.02.063
• DOMINIK REJMAN ET AL: "Lipophosphonoxins:
New Modular Molecular Structures with
Significant Antibacterial Properties", JOURNAL
OF MEDICINAL CHEMISTRY, vol. 54, no. 22, 24
November 2011 (2011-11-24), pages 7884-7898,
XP55036669, ISSN: 0022-2623, DOI:
10.1021/jm2009343

EP 2 527 351 B1

Description

<u>Field of the Invention</u>

[0001]   The invention relates to novel compounds with antibacterial properties, methods of synthesis thereof, and utilisation thereof *in vitro* and *in vivo*.

<u>Background Art</u>

[0002]   The advantages offered by antibiotics in the treatment of infectious diseases are endangered due to the increase in the number of antibiotic-resistant bacterial strains. This reduces the efficiency of antibiotic treatments and poses a serious health and economical problem. Currently, the need for novel antibiotics is becoming increasingly apparent (Davies D., Davies J., Microbiol. Mol. Biol. Rev. 2010, 74(3), 417; Kesselheim A. S., Outterson K., Health Aff. 2010, 29, 1689).

[0003]   An effective inhibitor of *Giardia* trophozoite growth termed phosphonoxin (1) (Figure 1) with an activity that rivaled existing therapeutics was recently reported. Phosphonoxin was designed as a transient-state inhibitor of a glycosyl transferase - cyst wall synthase (CWS). CWS catalyzes synthesis of the chitin-like poly β-1-3-linked *N*-acetylgalactosamine [poly(GalNAc)] that comprises about 63% of the giardia cyst wall. Although phosphonoxin did not specifically inhibit cyst formation, it potently inhibited vegetative growth. (Suk D. H., Rejman D. et al., Bioorg. Med. Chem. Letters 2007, 17(10), 2811). The molecule of phosphonoxin display certain structural similarity to several types of nucleoside antibiotics: (i) polyoxins **3**, (ii) muraymycins **4**, and (iii) caprazamycins **5**.

[0004]   The polyoxins are a new group of antifungal antibiotics isolated from *Streptomyces cacaoi* that inhibit the growth of a number of mycelial fungi by interfering with chitin synthesis. (Isono, K., Asahi K., Suzuki S., J. Am. Chem. Soc. 1969, 91, 7490; Isono K. et al., Agricultural Biol. Chem. 1965, 29, 848; Endo A., Kakiki K., Misato J., J. Bacteriol. 1970, 104, 189; Ohta N., Kakiki K., Misato, T., Agric. Biol. Chem. 1970, 34, 1224). Polyoxin D shares a gross structural similarity with uridine diphospho-*N*-acetyl-D-glucosamine (UDP-GlcNAc 2) in agreement with its role as a competitive inhibitor.

[0005]   The muraymycins, isolated from a culture broth of *Streptomyces* species are members of a class of naturally occurring 6'-*N*-alkyl-5'-β-*O*-aminorybosyl-*C*-glycyluridine antibiotics. The muraymycins bearing lipophylic side chain exhibit excelent activity against gram-positive bacteria. The muraymycins inhibit the formation of lipid II and peptidoglycan and are believed to be inhibitors of phosphor-MurNAc-pentapeptide translocase (MraY), which is responsible for the formation of lipid I in the peptidoglycan biosynthesis pathway. (Bugg T. D. H., Lloyd A. J., Roper D. I., Infect. Dis. Drug Targets 2006, 6, 85. Kimura K., Bugg T. D. H., Nat. Prod. Rep. 2003, 20, 252; Bouhss A. et al., J. Mol. Microbiol. 1999, 34, 576; Bouhss A., et al., FEMS Microbiol. Rev. 2008, 32, 208. Bouhss, A. et al., FEMS Microbiol. Rev. 2008, 32, 208). Tanino recently described the synthesis of lipophilic muraymycin analog **6** exhibiting a significant activity against methicillin-resistant *Staphylococcus aureus* (MRSA) and vancomycin-resistant *Enterococci* (VRE). (Tanino T. et al., Med. Chem. Lett. 2010, 1, 258).

[0006]   The caprazamycins (CPZs) (**5**) were isolated from the culture broth of the actinomycete strain *Streptomyces* spp. MK730-62F2 in 2003 (Igarashi M. et al., J. Antibiot. 2003, 56, 580; Igarashi M. et al., J. Antibiot. 2005, 58, 327) and represent the most recent members of the class of naturally occurring 6'-*N*-alkyl-5'-β-*O*-aminoribosyl-*C*-glycyluridine antibiotics that include the liposidomycins (7) (LPMs). The CPZs have shown excellent antimycobacterial activity *in vitro* not only against drug-susceptible (MIC = 3.13 μg/mL) but also multidrug-resistant *Mycobacterium tuberculosis* strains (MIC = 3.13 μg/mL) and exhibit no significant toxicity in mice. The biological target of the 6'-*N*-alkyl-5'-β-*O*-aminoribosyl-*C*-glycyluridine class of antibiotics is believed to be MraY translocase (IC$_{50}$= 0.05 μg/mL for LPMs). (Kimura K. et al., Agric. Biol. Chem. 1989, 53, 1811)

1 Phosphonoxin   2 UDP-GlcNAc   3 Polyoxins

4 (-)-Muramycin 2D

5 Caprazamycins

6

7 Liposidomycins
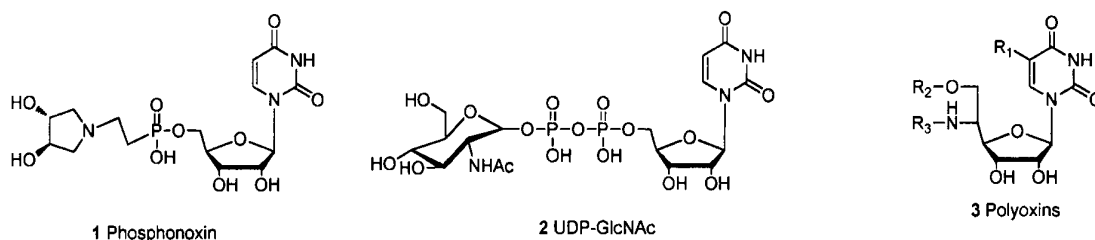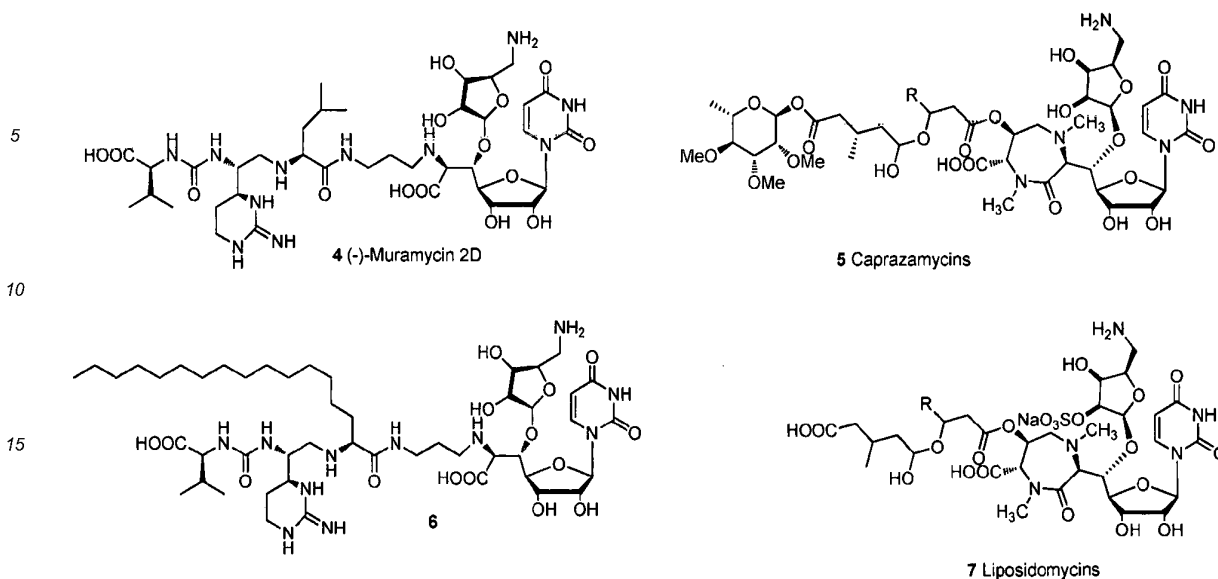
Disclosure of the Invention

[0007] This invention provides novel compound of general formula I that exhibit significant antibacterial activity, in particular against gram-positive bacteria. The advantages of these compounds include simple synthesis and modular structure allowing for further optimization of their biological properties.

[0008] An object of this invention are lipophosphonoxins of general formula I

$$(I)$$
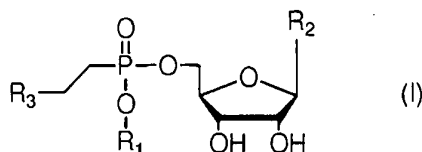
wherein R_1 is $(C_8\text{-}C_{22})$alkyl or hexadecyloxypropyl, tetradecyloxypropyl, tetradecyloxyethyl, or hexadecyloxyethyl, and

R_2 is uracil, thymin or cytosin,

R_3 is selected from the group comprising compounds of general formula II and III:
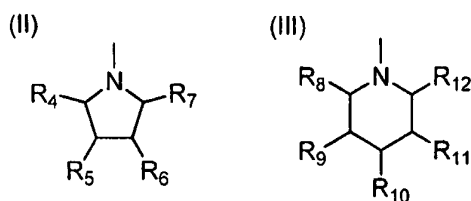
where R_4 is H or CH_2OH, R_5 is H or OH, R_6 is H or OH, R_7 is H or CH_2OH, R_8 is H or CH_2OH, R_9 is H or OH, R_{10} is H or OH, R_{11} is H or OH, R_{12} is H or CH_2OH,

diastereomers and mixtures of diastereomers thereof, and

their pharmaceutically acceptable salts and hydrates.

[0009] Compounds of formula I contain several chiral centers (particularly on the phosphorus atom and in the R_3 group). The presence of a chiral center allows a compound to exist as one of two possible optical isomers ((R)- or (S)-enantiomer), or as a racemic mixture of both. In this case, where several chiral centers are present, diastereoisomers and mixtures of diastereoisomers are obtained, which are all covered by general formula I and included in the scope of this invention.

[0010] Another object of this invention is the synthesis of the novel lipophosphonoxins. The starting material for the

synthesis of the final compounds arc nucleoside vinylphosphonic acids of general formula 11 (Scheme 2). These compounds are prepared by esterification of methyl vinylphosphonate 9 (Gao, Feng et al.; Chemistry-A European Journal, 2009, 15, 9, 2064 — 2070) that is prepared according to literature procedures. The synthesis according to this invention is novel, simpler than the previously described procedures and affords good yields.

In the first step A), the comercially available dimethyl vinylphosphonate **VIII** (see Scheme 1) is heated overnight in 40% - 70% aqueous pyridine at 50 - 80 °C.

VIII   **IX**
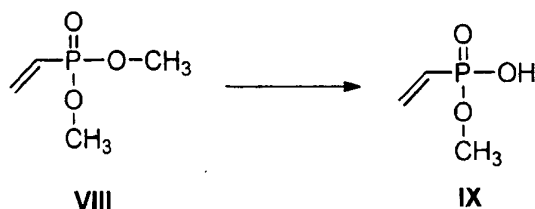
Scheme 1

[0011] The obtained methyl vinylphosphonate **IX** is allowed to react in the second reaction step B with nucleoside **X** possessing free 5'-hydroxyl group and protected in the positions 2'and 3'with a group selected from 2',3'-isopropylidene, 2',3'-bis(dimethoxytrityl), 2',3'-dibenzoyl, and 2',3'-diacetyl.

[0012] The esterification is carried out using triisopropylbenzenesulfonylchloride (TPSCl) under N-methylimidazole catalysis in a solvent selected from the group comprising acetonitrile, dioxane, tetrahydrofuran (THF), dichloroethane, chloroform and dichloromethane. The obtained methyl ester is purified by chromatography on silica gel using linear gradient of ethanol in chloroform. The methyl ester group is subsequently removed by heating with 40% - 70% aqueous pyridine at 50 - 80 °C overnight (Scheme 2). The obtained vinylphosphonic acid **XI** is purified by chromatography on silica gel using linear gradient of mixture H1 (ethyl acetate:acetone:ethanol:water, volume ratios 4:1:1:1) in ethyl acetate.

X   **XI**
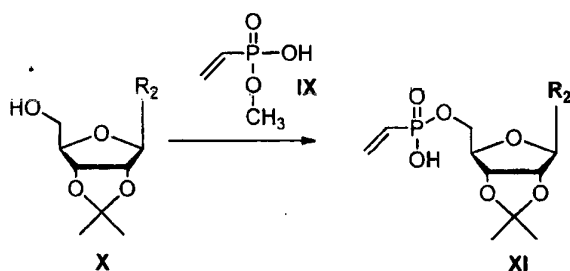
Scheme 2

[0013] In the next step C), the vinylphosphonic acids **XI** are esterified with alcohol using TPSCl as a condensing agent under N-methylimidazole catalysis in a solvent selected from the group comprising acetonitrile, dioxane, tetrahydrofuran (THF), dichloroethane, chloroform and dichloromethane (Scheme 3). The obtained vinylphosphonate **XII** is purified by chromatography on silica gel using linear gradient of ethanol in chloroform.

XI   **XII**
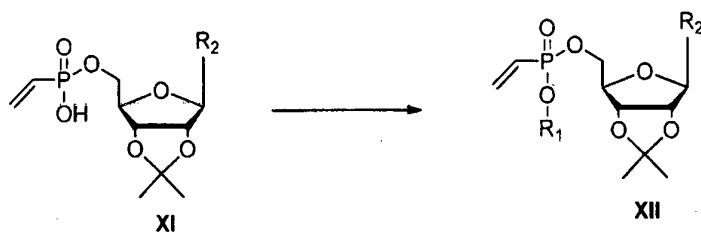
Scheme 3

[0014] The final step D) consists in Michael addition of secondary amine to the vinyl moiety of intermediate **XII**. The reaction is accomplished by heating in a solvent selected from the group comprising acetonitrile, dioxane, THF, dichloroethane, chloroform, ethanol, propanol, isopropanol and n-butanol at 80 - 120 °C for 4 to 12 hours. Subsequently, the protecting groups are removed from the nucleoside moiety. The final product is isolated by chromatography on silica gel using linear gradient of mixture H1 (as described above) in ethyl acetate. If required, the final product is re-purified by preparative HPLC on reverse phase.

Scheme 4
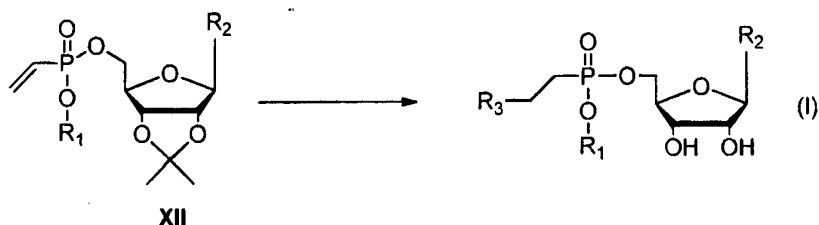
[0015] It is an aspect of the method of preparation of lipophosphonoxins of general formula I or their diastereomers or mixtures of such diastereomers, that heating overnight with aqueous pyridine in steps A) and/or B) is preferably carried out at 60 °C and the concentration of the aqueous pyridine solution is preferably 60 vol. %.

[0016] In another preferred embodiment, the Michael addition in the step D is carried out in n-butanol at 105 °C; more preferably, the reaction is perfomed overnight.

[0017] In one aspect of the present invention, the esterification in the steps B and/or C is carried out preferably in dichloromethane.

[0018] In another preferred embodiment of the method of the preparation of lipophosphonoxins of general formula I or their diastereomers and mixtures of such diastereomers, in the step D), the nucleoside protecting groups are removed by ethanolic methylamine or aqueous ammonia: if 2',3'-protected ribonucleoside is used, the protecting group is preferably removed by treatment with 0.5 mol.l^{-1} hydrochloride in methanol overnight at room temperature.

[0019] Another object of the present invention are the lipophoshonoxins of general formula I or their diastereomers or pharmaceutically acceptable salts and hydrates thereof and/or mixtures of such compounds for use as medicaments.

[0020] Yet another object of the present invention are the lipophoshonoxins of general formula I or their diastereomers or pharmaceutically acceptable salts and hydrates thereof and/or mixtures of such compounds for use as antibacterial medicaments.

[0021] Another object of the present invention is an antibacterial medicament containing as the active ingredient at least one lipophoshonoxin of general formula I or their diastereomers or pharmaceutically acceptable salts and hydrates thereof and/or mixture of such compounds.

[0022] Finally, an object of the invention is the use of lipophoshonoxins of general formula I or their diastereomers or pharmaceutically acceptable salts and hydrates thereof and/or mixtures of such compounds as active components of disinfectants and/or selective growth media for *in vitro* cultivations.

[0023] The compounds according to this invention possess antibacterial activity particularly against bacterial strains *Enterococcus faecalis, Bacterium subtilis, Streptococcus agalactiae, Staphylococcus aureus, Staphylococcus haemolyticus, Enterococcus faecium, Staphylococcus epidermidis,* including strains resistant to current antibiotics.

[0024] The compounds according to this invention simultaneously exhibited none or very low effect on the viability of normal human erythroid progenitor cells cultivated *in vitro* in the range of concentrations sufficient for antibacterial activity. The same applies to cytotoxicity induced by these compounds.

[0025] The modular structure as well as the simple synthetic procedure consisting in connecting single modules allows for large structural variations of the compounds according to this invention that can lead to the modulation of their biological activity.

Brief Description of the Figures

[0026]

Figures 1A-I depict the cell viability determined by the commercially available CellTiter-Blue® Cell Viability Assay (Promega, catalogue. no. G8082). The x-axis represents concentration of the tested compound in μg/ml in logarithmic scale, the y-axis represents cell viability in % of control. 1A: compound from the example 9, 1B: compound from the example 10, 1C: compound from the example 11, 1D: compound from the example 12, 1E: compound from the example 13, 1F: compound from the example 14, 1G: compound from the example 15, 1H: compound from the

example 16, 1I: compound from the example 17. For comparison, the antibacterial activities (MIC values) of these compounds against selected bacterial species are indicated with vertical lines in the charts.

Figures 2A-E depict the cytotoxicity determined by the commercially available CytoTox-ONE™ Homogeneous Membrane Integrity Assay (Promega, catalogue no. G7892). The x-axis represents concentration of the tested compound in μg/ml in logarithmic scale, the y-axis represents normalized cytotoxicity described by a dimensionless number. 2A: compound from the example 9, 2B: compound from the example 14, 2C: compound from the example 15, 2D: compound from the example 16, 2E: compound from the example 17. For comparison, the antibacterial activities (MIC values) of these compounds against selected bacterial species are indicated with vertical lines in the charts.

Examples

Abbreviations:

[0027]

DCM   dichloromethane

TPSCl   triisopropyl benzenesulfonylchloride

IR   infrared spectrum

HR-ESI   high resolution mass spectroscopy, using electrospray ionisation

HR-EI   high resolution mass spectroscopy, using electron impact ionisation

n-BuOH   n-butanol

DMTr   dimethoxytrityl

THF   tetrahydrofuran

EC_{50} half maximal effective concentration

IC_{50} half maximal inhibitory concentration

A) Preparation of the novel compounds

Example 1

2',3'-isopropylideneuridin-5'-yl-vinylphosphonate

[0028] To the mixture of the monomethyl phosphonate (9,15 g, 75 mmol), 2',3'-isopropylideneuridine (14 g, 50 mmol) and methylimidazole (5,9 ml, 150 mmol) in DCM (500 ml), TPSCl (45,43 g, 150 mmol) is added. The reaction mixture is stirred at room temperature (rt) overnight, then washed with a saturated aq $NaHCO_3$ (2 x 500 ml) followed by washing with 3% aq citric acid (2 x 500 ml) and dried over Na_2SO_4. Organic phase is concentrated *in vacuo* and monomethyl ester of nucleosidevinylphosphonic acid is obtained by flash chromatography on silica gel using linear gradient of ethanol in chloroform. The monomethyl ester intermediate in 40-70%, preferably in 60% (vol. %) aqueous pyridine (500 ml) is stirred at 50-80 °C, preferably at 60 °C overnight. The reaction mixture is concentrated *in vacuo,* co-evaporated in EtOH (2 x 300 ml), and dissolved in the same solvent (500 ml). Dowex 50 in Et_3N form (200 mll) is added and the suspension is stirred for 10 min. The resin is removed by filtration, and the filtrate is concentrated *in vacuo.* The title product is obtained by flash chromatography on silica gel using linear gradient of solvent mixture H1 (ethyl acetate:acetone:ethanol: water, volume ratios 4:1:1:1) in ethyl acetate in 48% yield (11.38 g, 23.93 mmol) as a yellowish foam.
[0029]   ^{1}H NMR (499.8 MHz, CD_3OD): 1.35, 1.54 (2 × q, 2 × 3H, [4]J = 0.5, $(CH_3)_2C$); 3.98 (dd, 2H, $J_{H,P}$ = 5.3, $J_{5',4'}$ = 3.4, H-5'); 4.35 (m, 1H, H-4'); 4.90 (m, 2H, H-2',3'); 5.74 (d, 1H, $J_{5,6}$ = 8.1, H-5); 5.86 (ddd, 1H, $J_{H,P}$ = 46.0, J_{cis} = 12.3, J_{gem} = 3.1, $CH_{cis}\mathbf{H_{trans}}$=CHP); 5.95 (d, 1H, $J_{1',2'}$ = 2.5, H-1'); 6.00 (ddd, 1H, $J_{H,P}$ = 22.8, J_{trans} = 18.7, J_{gem} = 3.1, $CH_{\mathbf{cis}}H_{\mathbf{trans}}$=CHP); 6.12 (ddd, 1H, $J_{H,P}$ = 19.7, J_{trans} = 18.7, J_{cis} = 12.3, =CHP); 7.86 (d, 1H, $J_{6,5}$ = 8.1, H-6).
[0030]   ^{13}C NMR (125.7 MHz, CD_3OD): 25.53, 27.55 $((CH_3)_2C)$; 65.31 (d, $J_{C,P}$ = 4.8, CH_2-5'); 82.49 (CH-3'); 85.67

(CH-2'); 86.56 (d, $J_{C,P}$ = 8.0, CH-4'); 93.40 (CH-1'); 102.98 (CH-5); 114.99 (C(CH$_3$)$_2$); 130.74 (CH$_2$=CHP); 132.70 (d, $J_{C,P}$ = 174.3, =CHP); 143.42 (CH-6); 152.16 (C-2); 166.15 (C-4).

[0031] ^{31}P NMR (202.3 MHz, CD$_3$OD): 13.16.

[0032] IR v_{max}(KBr) 3200 (w, br), 2977 (m), 2939 (m), 2803-2100 (s-vw), 1715 (s, sh), 1695 (vs), 1630 (w, sh), 1612 (w, sh), 1469 (m), 1434 (m), 1398 (m), 1384 (m), 1373 (m, sh), 1273 (m), 1214 (s), 1115 (m, sh), 1070 (s, br), 1037 (s), 1018 (m, sh), 995 (w), 765 (w), 517 (w) cm^{-1}.

[0033] HR-ESI C$_{14}$H$_{18}$O$_8$N$_2$P (M-H)$^-$ calcd 373.0806; found 373.0809

Example 2

2',3'-Isopropylideneuridin-5'-yl tetradecyl vinylphosphonate

[0034]
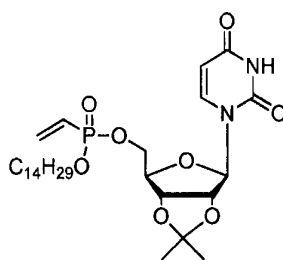
[0035] TPSCl (4.68 g, 15.45 mmol) is added to the mixture of vinylphosphonic acid from the example 1 (1.93 g, 5.15 mmol), tetradekanol (2.2 g, 10.31 mmol), and N-methylimidazole (1.22 ml, 15.45 mmol) in DCM (50 ml). The reaction mixture is stirred overnight at rt, then extracted/washed with saturated solution of NaHCO$_3$ (2 x 100 ml), 3% aqueous citric acid (2 x 100 ml) and dried over Na$_2$SO$_4$. The organic phase is concentrated *in vacuo* and the product is obtained by flash chromatography on silica gel using linear gradient of ethanol in chloroform in 40% yield (1.17 g, 2.05 mmol) in the form of yellowish viscous oil.

A mixture of diastereoisomers ~ 6:5

[0036] ^{1}H NMR (499.8 MHz, CDCl$_3$): 0.88 (m, 6H, **CH$_3$**(CH$_2$)$_{13}$); 1.20-1.35 (m, 44H, CH$_3$(**CH$_2$**)$_{11}$CH$_2$CH$_2$O); 1.350, 1.354, 1.573, 1.576 (4 × q, 4 × 3H, ^4J = 0.7, (CH$_3$)$_2$C); 1.67 (m, 4H, CH$_3$(CH$_2$)$_{11}$**CH$_2$**CH$_2$O); 4.03, 4.04 (2 × dt, 2 × 2H, $J_{H,P}$ = 7.3, J_{vic} = 6.7, CH$_3$(CH$_2$)$_{11}$**CH$_2$**CH$_2$O); 4.19-4.29 (m, 4H, H-5'); 4.35-4.39 (m, 2H, H-4'); 4.85, 4.86 (2 × dd, 2 × 1H, $J_{3',2'}$ = 6.4, $J_{3',4'}$ = 3.6, H-3'); 4.88, 4.89 (2 × dd, 2 × 1H, $J_{2',3'}$ = 6.4, $J_{2',1'}$ = 2.3, H-2'); 5.71, 5.72 (2 × d, 2 × 1H, $J_{5,6}$ = 8.1, H-5); 5.77, 5.81 (2 × d, 2 × 1H, $J_{1',2'}$ = 2.3, H-1'); 6.03, 6.04 (2 × ddd, 2 × 1H, $J_{H,P}$ = 22.9, J_{trans} = 18.6, J_{cis} = 12.7, =CHP); 6.16, 6.19 (2 × ddd, 2 × 1H, $J_{H,P}$ = 51.6, J_{cis} = 12.7, J_{gem} = 2.0, CH$_{cis}$**H$_{trans}$**=CHP); 6.33, 6.34 (2 × ddd, 2 × 1H, $J_{H,P}$ = 25.7, J_{trans} = 18.7, J_{gem} = 2.0, **CH$_{cis}$**H$_{trans}$=CHP); 7.38, 7.43 (2 × d, 2 × 1H, $J_{6,5}$ = 8.1, H-6); 9.34 (bs, 2H, NH). ^{13}C NMR (125.7 MHz, CDCl$_3$): 14.08 (CH$_3$(CH$_2$)$_{13}$); 22.64 (CH$_3$(CH$_2$)$_{11}$CH$_2$CH$_2$O); 25.23, 25.25 ((CH$_3$)$_2$C); 25.43 (CH$_3$(CH$_2$)$_{11}$CH$_2$CH$_2$O); 27.08, 27.09 ((CH$_3$)$_2$C); 29.10, 29.30, 29.46, 29.52, 29.59, 29.60, 29.62, 29.64 (CH$_3$(CH$_2$)$_{11}$CH$_2$CH$_2$O); 30.39 (d, $J_{C,P}$ = 6.2, CH$_3$(CH$_2$)$_{11}$CH$_2$CH$_2$O); 31.87 (CH$_3$(CH$_2$)$_{11}$CH$_2$CH$_2$O); 64.93, 65.01 (d, $J_{C,P}$ = 5.5, CH$_2$-5'); 66.47, 66.48 (d, $J_{C,P}$ = 5.7, CH$_3$(CH$_2$)$_{11}$CH$_2$CH$_2$O); 80.57, 80.66 (CH-3'); 84.45, 84.53 (CH-2'); 85.26, 85.55 (d, $J_{C,P}$ = 7.0, CH-4'); 93.43, 93.83 (CH-1'); 102.49, 102.58 (CH-5); 114.54, 114.59 (C(CH$_3$)$_2$); 124.97, 125.02 (d, $J_{C,P}$ = 184.3, =CHP); 136.60, 136.62 (CH$_2$=CHP); 141.47, 141.55 (CH-6); 149.96, 149.99 (C-2); 163.11 (C-4).

^{31}P NMR (202.3 MHz, CDCl$_3$): 18.59, 18.74.

IR v_{max}(CHCl$_3$) 3390 (w), 3170 (w, br), 2957 (s), 2928 (vs), 2856 (s), 1715 (vs), 1695 (vs), 1634 (m), 1616 (m), 1457 (s), 1421 (m), 1399 (m), 1384 (s), 1378 (s), 1240 (vs, br), 1121 (s), 1109 (s), 1070 (vs), 1011 (vs), 988 (s), 973 (s, sh), 860 (s), 544 (m), 512 (m) cm^{-1}.

HR-ESI C$_{28}$H$_{48}$O$_8$N$_2$P [M+H]$^+$ calcd 571.31428, found 571.31445, C$_{28}$H$_{47}$O$_8$N$_2$NaP [M+Na]$^+$ calcd 593.29622, found 593.29616.

Example 3

Hexadecyl-2',3'-isopropylideneuridin-5'-yl-vinylphosphonate

[0037]
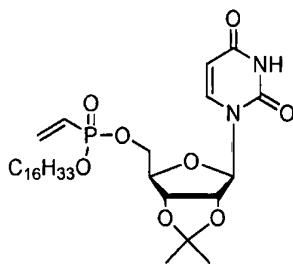
[0038] TPSCl (4.12 g, 13.62 mmol) is added to the mixture of vinylphosphonic acid from the example 1 (1.7 g, 4.54 mmol), hexadecanol (2.9 g, 12 mmol), and 1-methylimidazole (1.08 ml, 13.62 mmol) in DCM (50 ml). The reaction mixture is stirred overnight at rt, then extracted/washed with saturated solution of $NaHCO_3$ (2 x 100 ml), 3% aqueous citric acid (2 x 100 ml) and dried over Na_2SO_4. The organic phase is concentrated *in vacuo* and the product is obtained by flash chromatography on silica gel using linear gradient of ethanol in chloroform in 50% yield (1.38 g, 2.3 mmol) in the form of colorless viscous oil.

A mixture of diastereoisomers ~ 6:5

[0039] ^{1}**H NMR** (499.8 MHz, $CDCl_3$): 0.88 (m, 6H, **CH$_3$**(CH$_2$)$_{15}$); 1.22-1.35 (m, 52H, CH$_3$(**CH$_2$**)$_{13}$CH$_2$CH$_2$O); 1.350, 1.354, 1.573, 1.577 (4 × q, 4 × 3H, ^4J = 0.7, (CH$_3$)$_2$C); 1.67 (m, 4H, CH$_3$(CH$_2$)$_{13}$**CH$_2$**CH$_2$O); 4.03, 4.04 (2 × dt, 2 × 2H, $J_{H,P}$ = 7.3, J_{vic} = 6.7, CH$_3$(CH$_2$)$_{13}$CH$_2$**CH$_2$**O); 4.19-4.30 (m, 4H, H-5'); 4.35-4.39 (m, 2H, H-4'); 4.85, 4.86 (2 × dd, 2 × 1H, $J_{3',2'}$ = 6.4, $J_{3',4'}$ = 3.6, H-3'); 4.878, 4.8984 (2 × dd, 2 × 1H, $J_{2',3'}$ = 6.4, $J_{2',1'}$ = 2.3, H-2'); 5.71, 5.72 (2 × dd, 2 × 1H, $J_{5,6}$ = 8.1, $J_{5,NH}$ = 2.2, H-5); 5.78, 5.81 (2 × d, 2 × 1H, $J_{1',2'}$ = 2.3, H-1'); 6.03, 6.05 (2 × ddd, 2 × 1H, $J_{H,P}$ = 22.8, J_{trans} = 18.6, J_{cis} = 12.8, =CHP); 6.12, 6.13 (2 × ddd, 2 × 1H, $J_{H,P}$ = 51.7, J_{cis} = 12.8, J_{gem} = 2.0, CH$_{cis}$**H$_{trans}$**=CHP); 6.33, 6.34 (2 × ddd, 2 × 1H, $J_{H,P}$ = 24.8, J_{trans} = 18.6, J_{gem} = 2.0, **CH$_{cis}$**H$_{trans}$=CHP); 7.38, 7.43 (2 × d, 2 × 1H, $J_{6,5}$ = 8.1, H-6); 9.15, 9.18 (2 × bs, 2 × 2H, NH).

[0040] ^{13}**C NMR** (125.7 MHz, $CDCl_3$): 14.08 (CH$_3$(CH$_2$)$_{15}$); 22.65 (CH$_3$(CH$_2$)$_{13}$CH$_2$CH$_2$O); 25.23, 25.26 ((CH$_3$)$_2$C); 25.43 (CH$_3$(CH$_2$)$_{13}$CH,CH$_2$O); 27.08, 27.10 ((CH$_3$)$_2$C); 29.11, 29.32, 29.47, 29.53, 29.60, 29.61, 29.63, 29.65 (CH$_3$(CH$_2$)$_{13}$CH$_2$CH$_2$O); 30.40 (d, $J_{C,P}$ = 6.3, CH$_3$(CH$_2$)$_{13}$CH$_2$CH$_2$O); 31.88 (CH$_3$(CH$_2$)$_{13}$CH$_2$CH$_2$O); 64.93, 65.00 (d, $J_{C,P}$ = 5.5, CH$_2$-5'); 66.47, 66.48 (d, $J_{C,P}$ = 5.7, CH$_3$(CH$_2$)$_{13}$CH$_2$CH$_2$O); 80.57, 80.66 (CH-3'); 84.46, 84.54 (CH-2'); 85.25, 85.55 (d, $J_{C,P}$ = 7.1, CH-4'); 93.40, 93.80 (CH-1'); 102.49, 102.57 (CH-5); 114.55, 114.60 (C(CH$_3$)$_2$); 124.99, 125.04 (d, $J_{C,P}$ 184.2, =CHP); 136.62, 136.66 (d, $J_{C,P}$ = 2.0, CH$_2$=CHP); 141.46, 141.55 (CH-6); 149.92, 149.95 (C-2); 163.05, 163.07 (C-4).

[0041] ^{31}**P NMR** (202.3 MHz, $CDCl_3$): 18.59, 18.73.

[0042] **HR-ESI** $C_{30}H_{51}O_8N_2PNa$ (M+Na)$^+$ calcd 621.32752; found 621.32778

Example 4

2',3'-Isopropylidenuridin-5'-yl octadecyl vinylphosphonate

[0043]
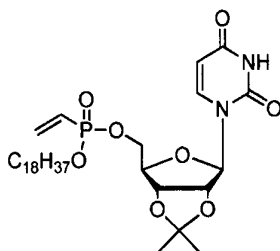
[0044] TPSCl (4.16 g, 13.74 mmol) is added to the mixture of vinylphosphonic acid from the example 1 (1.7 g, 4.54 mmol), octadecanol (2.48 g, 9.17 mmol), and 1-methylimidazole (1.08 ml, 13.74 mmol) in DCM (50 ml). The reaction mixture is stirred overnight at rt, then extracted/washed with saturated solution of $NaHCO_3$ (2 x 100 ml), 3% aqueous citric acid (2 x 100 ml) and dried over Na_2SO_4. The rganic phase is concentrated *in vacuo* and the product is obtained

by flash chromatography on silica gel using linear gradient of ethanol in chloroform in 43% yield (1,23 g, 1,96 mmol) in the form of colorless viscous oil.

A mixture of diastereoisomers ~ 6:5

[0045] ^{1}**H NMR** (499.8 MHz, CDCl$_3$): 0.88 (m, 6H, **CH$_3$**(CH$_2$)$_{17}$); 1.20-1.40 (m, 60H, CH$_3$(**CH$_2$**)$_{15}$CH$_2$CH$_2$O); 1.350, 1.354, 1.573, 1.576 (4 × q, 4 × 3H, ^4J = 0.7, (CH$_3$)$_2$C); 1.66 (m, 4H, CH$_3$(CH$_2$)$_{15}$**CH$_2$**CH$_2$O); 4.03, 4.04 (2 × dt, 2 × 2H, $J_{H,P}$ = 7.3, J_{vic} = 6.7, CH$_3$(CH$_2$)$_{15}$CH$_2$**CH$_2$**O); 4.19-4.29 (m, 4H, H-5'); 4.34-4.39 (m, 2H, H-4'); 4.85, 4.86 (2 × dd, 2 × 1H, $J_{3',2'}$ = 6.4, $J_{3',4'}$ = 3.7, H-3'); 4.88, 4.89 (2 × dd, 2 × 1H, $J_{2',3'}$ = 6.4, $J_{2',1'}$ = 2.3, H-2'); 5.71, 5.72 (2 × d, 2 × 1H, $J_{5,6}$ = 8.1, H-5); 5.77, 5.81 (2 × d, 2 × 1H, $J_{1',2'}$ = 2.3, H-1'); 6.03, 6.04 (2 × ddd, 2 × 1H, $J_{H,P}$ = 22.9, J_{trans} = 18.6, J_{cis} = 12.7, =CHP); 6.16, 6.19 (2 × ddd, 2 × 1H, $J_{H,P}$ = 51.7, J_{cis} = 12.7, J_{gem} = 2.0, CH$_{cis}$**H$_{trans}$**=CHP); 6.33, 6.34 (2 × ddd, 2 × 1H, $J_{H,P}$ = 25.6, J_{trans} = 18.6, J_{gem} = 2.0, **CH$_{cis}$**H$_{trans}$=CHP); 7.38, 7.43 (2 × d, 2 × 1H, $J_{6,5}$ = 8.1, H-6); 9.37 (bs, 2H, NH).
[0046] ^{13}**C NMR** (125.7 MHz, CDCl$_3$): 14.08 (CH$_3$(CH$_2$)$_{17}$); 22.64 (CH$_3$(CH$_2$)$_{15}$CH$_2$CH$_2$O); 25.22, 25.25 ((CH$_3$)$_2$C); 25.43 (CH$_3$(CH$_2$)$_{15}$CH$_2$CH$_2$O); 27.07, 27.09 ((CH$_3$)$_2$C); 29.10, 29.31, 29.46, 29.53, 29.60, 29.61, 29.63, 29.65 (CH$_3$(CH$_2$)$_{15}$CH$_2$CH$_2$O); 30.39 (d, $J_{C,P}$ = 6.2, CH$_3$(CH$_2$)$_{15}$CH$_2$CH$_2$O); 31.87 (CH$_3$(CH$_2$)$_{15}$CH$_2$CH$_2$O); 64.93, 65.01 (d, $J_{C,P}$ = 5.5, CH$_2$-5'); 66.46, 66.47 (d, $J_{C,P}$ = 5.7, CH$_3$(CH$_2$)$_{15}$CH$_2$CH$_2$O); 80.57, 80.66 (CH-3'); 84.45, 84.53 (CH-2'); 85.27, 85.56 (d, $J_{C,P}$ = 7.0, CH-4'); 93.44, 93.83 (CH-1'); 102.49, 102.58 (CH-5); 114.53, 114.58 (C(CH$_3$)$_2$); 124.97, 125.01 (d, $J_{C,P}$ = 184.2, =CHP); 136.62, 136.66 (d, $J_{C,P}$ = 2.0, CH$_2$=CHP); 141.47, 141.56 (CH-6); 149.97, 150.00 (C-2); 163.14, 163.16 (C-4).
[0047] ^{31}**P NMR** (202.3 MHz, CDCl$_3$): 18.59, 18.74.
[0048] **IR** v_{max}(CHCl$_3$) 3390 (w), 3170 (w, br), 2928 (vs), 2855 (vs), 1716 (vs), 1695 (vs), 1634 (m), 1615 (w), 1457 (s), 1420 (m), 1399 (m), 1385 (s), 1378 (s), 1246 (s, br), 1121 (s), 1110 (s), 1071 (s), 1010 (s), 988 (s), 974 (s, sh), 860 (m), 544 (w), 512 (w) cm^{-1}.
[0049] **HR**-ESI C$_{32}$H$_{56}$O$_8$N$_2$P [M+H]$^+$ calcd 627.37688, found 627.37738.

Example 5

Icosanyl 2',3'-isopropylideneuridin-5'-yl vinylphosphonate

[0050]
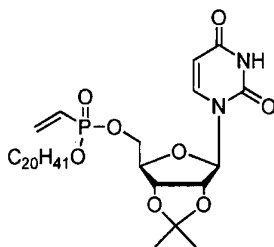
[0051] TPSCl (4.49 g, 14.82 mmol) is added to the mixture of vinylphosphonic acid from the example 1 (2.35 g, 4.94 mmol), icosanol (2,95 g, 9,9 mmol), and 1-methylimidazole (1.17 ml, 14.82 mmol) in DCM (50 ml). The reaction mixture is stirred overnight at rt, then extracted/washed with saturated solution of NaHCO$_3$ (2 x 100 ml), 3% aqueous citric acid (2 x 100 ml) and dried over Na$_2$SO$_4$. The organic phase is concentrated *in vacuo* and the product is obtained by flash chromatography on silica gel using linear gradient of ethanol in chloroform in 34% yield (1,1 g, 1,68 mmol) in the form of colorless wax.

A mixture of diastereoisomers ~ 6:5

[0052] ^{1}**H NMR** (499.8 MHz, CDCl$_3$): 0.88 (m, 6H, **CH$_3$**(CH$_2$)$_{19}$); 1.20-1.36 (m, 68H, CH$_3$(**CH$_2$**)$_{17}$CH$_2$CH$_2$O); 1.351, 1.354, 1.574, 1.577 (4 × q, 4 × 3H, ^4J = 0.7, (CH$_3$)$_2$C); 1.66 (m, 4H, CH$_3$(CH$_2$)$_{17}$**CH$_2$**CH$_2$O); 4.03, 4.04 (2 × dt, 2 × 2H, $J_{H,P}$ = 7.3, J_{vic} = 6.7, CH$_3$(CH$_2$)$_{17}$CH$_2$**CH$_2$**O); 4.19-4.29 (m, 4H, H-5'); 4.35-4.39 (m, 2H, H-4'); 4.84, 4.86 (2 × dd, 2 × 1H, $J_{3',2'}$ = 6.4, $J_{3',4'}$ = 3.4, H-3'); 4.87, 4.89 (2 × dd, 2 × 1H, $J_{2',3'}$ = 6.4, $J_{2',1'}$ = 2.3, H-2'); 5.706, 5.714 (2 × d, 2 × 1H, $J_{5,6}$ = 8.1, H-5); 5.77, 5.80 (2 × d, 2 × 1H, $J_{1',2'}$ = 2.3, H-1'); 6.03, 6.06 (2 × ddd, 2 × 1H, $J_{H,P}$ = 22.8, J_{trans} = 18.6, J_{cis} = 12.7, =CHP); 6.17, 6.19 (2 × ddd, 2 × 1H, $J_{H,P}$ = 51.7, J_{cis} = 12.7, J_{gem} = 2.0, CH$_{cis}$**H$_{trans}$**=CHP); 6.33, 6.34 (2 × ddd, 2 × 1H, $J_{H,P}$ = 25.6, J_{trans} = 18.6, J_{gem} = 2.0, **CH$_{cis}$**H$_{trans}$=CHP); 7.37, 7.43 (2 × d, 2 × 1H, $J_{6,5}$ = 8.1, H-6); 9.08 (bs, 2H, NH).

[0053] ^{13}C NMR (125.7 MHz, CDCl$_3$): 14.10 (CH$_3$(CH$_2$)$_{19}$); 22.66 (CH$_3$(CH$_2$)$_{17}$CH$_2$CH$_2$O); 25.24, 25.26 ((CH$_3$)$_2$C); 25.44 (CH$_3$(CH$_2$)$_{17}$CH$_2$CH$_2$O); 27.09, 27.11 ((CH$_3$)$_2$C); 29.12, 29.33, 29.48, 29.55, 29.62, 29.65, 29.67 (CH$_3$(CH$_2$)$_{17}$CH$_2$CH$_2$O); 30.41 (d, $J_{C,P}$ = 6.3, CH$_3$(CH$_2$)$_{17}$CH$_2$CH$_2$O); 31.89 (CH$_3$(CH$_2$)$_{17}$CH$_2$CH$_2$O); 64.92, 64.99 (d, $J_{C,P}$ = 5.5, CH$_2$-5'); 66.48, 66.50 (d, $J_{C,P}$ = 5.7, CH$_3$(CH$_2$)$_{17}$CH$_2$CH$_2$O); 80.57, 80.66 (CH-3'); 84.47, 84.56 (CH-2'); 85.25, 85.54 (d, $J_{C,P}$ = 7.0, CH-4'); 93.44, 93.83 (CH-1'); 102.50, 102.59 (CH-5); 114.56, 114.62 (C(CH$_3$)$_2$); 124.98, 125.02 (d, $J_{C,P}$ = 184.2, =CHP); 136.65, 136.70 (d, $J_{C,P}$ = 1.9, CH$_2$=CHP); 141.41, 141.50 (CH-6); 149.90, 149.93 (C-2); 162.92, 162.95 (C-4).

[0054] ^{31}P NMR (202.3 MHz, CDCl$_3$): 18.59, 18.74.

[0055] IR ν_{max}(CHCl$_3$) 3389 (w), 3167 (w, vbr), 2928 (vs), 2855 (s), 1715 (vs), 1695 (vs), 1634 (m), 1615 (w), 1457 (s), 1420 (w), 1399 (m), 1384 (s), 1378 (s), 1249 (s, sh), 1122 (m), 1110 (s), 1078 (s), 1011 (s), 989 (s), 975 (s, sh), 860 (m), 544 (w), 512 (w) cm^{-1}.

[0056] HR-ESI C$_{34}$H$_{60}$O$_8$N$_2$P [M+H] calcd 655.40818, found 655.40857, C$_{34}$H$_{59}$O$_8$N$_2$NaP [M+Na] calcd 677.39012, found 677.39032.

Example 6

Hexadecyloxypropyl 2',3'-isopropylideneuridin-5'-yl vinyphosphonate

[0057]
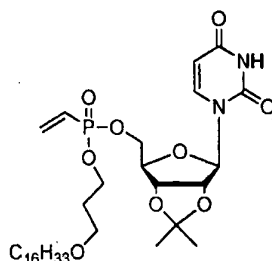
[0058] TPSCI (5.54 g, 18.3 mmol) is added to the mixture of vinylphosphonic acid from the example 1 (1.8 g, 6.1 mmol), hexadecyloxypropanol (1.45 g, 3.05 mmol), and 1-methylimidazole (1.45 ml, 18.3 mmol) in DCM (60 ml). The reaction mixture is stirred overnight at rt, then extracted/washed with saturated solution of NaHCO$_3$ (2 x 100 ml), 3% aqueous citric acid (2 x 100 ml) and dried over Na$_2$SO$_4$. The organic phase is concentrated *in vacuo* and the product is obtained by flash chromatography on silica gel using linear gradient of ethanol in chloroform in 71% yield (1.42 g, 2.16 mmol) in the form of colorless wax.

A mixture of diastereoisomers ~ 1:1

^{1}**H NMR** (500.0 MHz, CDCl$_3$): 0.88 (m, 6H, CH$_3$(CH$_2$)$_{15}$); 1.23-1.33 (m, 52H, CH$_3$(CH$_2$)$_{13}$CH$_2$CH$_2$O); 1.348, 1.352 (2 × q, 2 × 3H, ^4J= 0.6, (CH$_3$)$_2$C); 1.54 (m, 4H, CH$_3$(CH$_2$)$_{13}$CH$_2$CH$_2$O); 1.57 (s, 6H, (CH$_3$)$_2$C); 1.92, 1.94 (2 × p, 2 × 2H, J_{vic} = 6.1, OCH$_2$**CH$_2$**CH$_2$OC$_{16}$H$_{33}$); 3.38, 3.39 (2 × t, 2 × 2H, J_{vic} = 6.7, CH$_3$(CH$_2$)$_{13}$**CH$_2$**CH$_2$O); 3.48, 3.49 (2 × t, 2 × 2H, J_{vic} = 6.1, OCH$_2$CH$_2$CH$_2$OC$_{16}$H$_{33}$); 4.13, 4.15 (2 × td, 2 × 2H, J_{vic} = 6.1, $J_{H,P}$ = 4.8, O**CH$_2$**CH$_2$CH$_2$OC$_{16}$H$_{33}$); 4.20-4.30 (m, 4H, H-5'); 4.34-4.38 (m, 2H, H-4'); 4.85, 4.86 (2 × dd, 2 × 1H, $J_{3',2'}$ = 6.5, $J_{3',4'}$ = 3.6, H-3'); 4.92 (dd, 2H, $J_{2',3'}$ = 6.5, $J_{2',1'}$ = 2.3, H-2'); 5.700, 5.704 (2 × d, 2 × 1H, $J_{5,6}$ = 8.1 H-5); 5.74, 5.76 (2 × d, 2 × 1H, $J_{1',2'}$ = 2.3, H-1'); 6.03, 6.05 (2 × ddd, 2 × 1H, $J_{H,P}$ = 22.9, J_{trans} = 18.4, J_{cis} = 12.7, =CHP); 6.16, 6.18 (2 × ddd, 2 × 1H, $J_{H,P}$ = 51.8, J_{cis} = 12.7, J_{gem} = 1.9, CH$_{cis}$**H$_{trans}$**=CHP); 6.33, 6.35 (2 × ddd, 2 × 1H, $J_{H,P}$ = 25.5, J_{trans} = 18.4, J_{gem} = 1.9, **CH$_{cis}$**H$_{trans}$=CHP); 7.34, 7.39 (2 × d, 2 × 1H, $J_{6,5}$ = 8.1, H-6).

^{13}**C NMR** (125.7 MHz, CDCl$_3$): 14.07 (CH$_3$(CH$_2$)$_{15}$); 22.62 (CH$_3$(CH$_2$)$_{13}$CH$_2$CH$_2$O); 25.19, 25.21 ((CH$_3$)$_2$C); 26.08 (CH$_3$(CH$_2$)$_{14}$CH$_2$O); 27.04, 27.06 ((CH$_3$)$_2$C); 29.29, 29.45, 29.55, 29.57, 29.58, 29.63 (CH$_3$(CH$_2$)$_{14}$CH$_2$O); 30.66, 30.68 (d, $J_{C,P}$ = 6.4, OCH$_2$CH$_2$CH$_2$OC$_{16}$H$_{33}$); 31.85 (CH$_3$(CH$_2$)$_{13}$CH$_2$CH$_2$O); 63.56 63.57 (d, $J_{C,P}$ = 5.5, OCH$_2$CH$_2$CH$_2$OC$_{16}$H$_{33}$); 64.92, 65.01 (d, $J_{C,P}$ = 5.5, CH$_2$-5'); 66.32, 66.36 (OCH$_2$CH$_2$CH$_2$OC$_{16}$H$_{33}$); 71.15, 71.16 (CH$_3$(CH$_2$)$_{14}$CH$_2$O); 80.60, 80.67 (CH-3'); 84.44, 84.53 (CH-2'); 85.38, 85.62 (d, $J_{C,P}$ = 7.1, CH-4'); 93.82, 94.12 (CH-1'); 102.57, 102.64 (CH-5); 114.42, 114.46 (C(CH$_3$)$_2$); 124.75, 124.80 (d, $J_{C,P}$ = 184.0, =CHP); 136.75, 136.77 (d, $J_{C,P}$ = 1.9, CH$_2$=CHP); 141.43, 141.48 (CH-6); 150.16 (C-2); 163.29, 163.32 (C-4).

^{31}**P NMR** (202.3 MHz, CDCl$_3$): 18.64, 18.80.

IR ν_{max}(KBr) 2925 (vs), 2854 (s), 1709 9vs, sh), 1696 (vs), 1630 (w), 1459 (m), 1421 (m), 1400 (w, sh), 1381 (m), 1270 (m, sh), 1250 (m, sh), 1109 (s), 1078 (s), 1028 (s), 1012 (s), 972 (m, sh), 859 (m), 762 (w), 548 (w), 514 (w) cm^{-1}.

HR-ESI C$_{33}$H$_{58}$O$_9$N$_2$P (M+H)$^+$ calcd 657.3874; found 657.3876

Example 7

4-*N*-Benzoyl-2',3'-isopropylidenecytidin-5'-yl-vinylphosphonate

[0059]
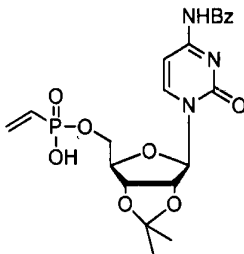
[0060] TPSCl (7.15 g, 23.61 mmol) is added to the mixture of monomethyl vinylphosphonate (1.95 g, 16 mmol), 4-*N*-benzoyl-2',3'-isopropylidenecytidine (3.05g, 7.87 mmol), and 1-methylimmidazole (1.9 ml, 23.61 mmol) in DCM (80 ml). The reaction mixture is stirred overnight at rt, then extracted/washed with saturated solution of $NaHCO_3$ (2 x 100 ml), 3% aqueous citric acid (2 x 100 ml) and dried over Na_2SO_4. Organic phase is concentrated *in vacuo* and monomethyl intermediate obtained by flash chromatography on silica gel using linear gradient of ethanol in chloroform is without detailed characterisation stirred in 40-70%, preferably in 60% (vol. %) aqueous pyridine (100 ml) at 50-80 °C, preferably at 60 °C, overnight. The reaction mixture is concentrated *in vacuo,* co-evaporated in EtOH (2 x 100 ml), and dissolved in the same solvent (100 ml). Dowex 50 in Et_3N form (80 ml) is added and the suspension is stirred for 10 min. The resin is removed by filtration, and the filtrate is concentrated *in vacuo.* The title product is obtained by flash chromatography on silica gel using linear gradient of solvent mixture H1 (ethyl acetate:acetone:ethanol: water, volume ratios 4:1:1:1) in ethyl acetate in 52% yield (1.95 g, 4.1 mmol) as a beige foam. NMR of 9b has shown Et_3NH^+ salt (not free acid):

^{1}H NMR (600.1 MHz, CD_3OD): 1.31 (t, 9H, J_{vic} = 7.3, **CH3**CH2N); 1.37, 1.57 (2 × q, 2 × 3H, [4]J = 0.7, $(CH_3)_2$C); 3.20 (q, 6H, J_{vic} = 7.3, CH3**CH2**N); 4.02 (ddd, 1H, J_{gem} = 11.5, $J_{H,P}$ = 6.0, $J_{5'b,4'}$ = 3.4, H-5'b); 4.06 (ddd, 1H, J_{gem} = 11.5, $J_{H,P}$ = 4.5, $J_{5'a,4'}$ = 3.0, H-5'a); 4.50 (m, 1H, H-4'); 4.91 (dd, 1H, $J_{3',2'}$ = 6.0, $J_{3',4'}$ = 2.2, H-3'); 4.93 (dd, 1H, $J_{2',3'}$ = 6.0, $J_{2',1'}$ = 2.3, H-2'); 5.86 (ddd, 1H, $J_{H,P}$ = 46.0, J_{cis} = 12.4, J_{gem} = 3.1, CH**cis**H**trans**=CHP); 6.00 (d, 1H, $J_{1',2'}$ = 2.3, H-1'); 6.01 (ddd, 1H, $J_{H,P}$ = 22.9, J_{trans} = 18.7, J_{gem} = 3.1, CH**cis**H**trans**=CHP); 6.11 (ddd, 1H, $J_{H,P}$ = 19.6, J_{trans} = 18.7, J_{cis} = 12.4, =CHP); 7.55 (m, 2H, H-*m*-Ph); 7.62 (bd, 1H, $J_{5,6}$ = 7.5, H-5) 7.64 (m, 1H, H-*p*-Ph); 7.98 (m, 2H, H-*o*-Ph); 8.35 (d, 1H, $J_{6,5}$ = 7.5, H-6).

^{13}C NMR (150.9 MHz, CD_3OD): 9.18 (CH_3CH_2N); 25.45, 27.47 $((CH_3)_2C)$; 47.73 (CH_3CH_2N); 65.09 (d, $J_{C,P}$ = 4.8, CH_2-5'); 82.47 (CH-3'); 87.16 (CH-2'); 87.91 (d, $J_{C,P}$ = 8.1, CH-4'); 95.59 (CH-1'); 98.54 (CH-5); 114.69 $(C(CH_3)_2)$; 129.16 (CH-*o*-Ph); 129.82 (CH-*m*-Ph); 130.80 (CH_2=CHP); 132.71 (d, $J_{C,P}$ = 174.8, =CHP); 134.05 (CH-*p*-Ph); 134.78 (C-*i*-Ph); 147.24 (CH-6); 157.90 (C-2); 164.99 (C-4); 169.02 (CO).

^{31}P NMR (202.3 MHz, CD_3OD): 13.02.

HR-ESI $C_{21}H_{23}O_8N_3P$ (M-H)$^+$ calcd 476.1223; found 476.1221.

Example 8

4-*N*-Benzoyl-2',3'-isopropylidenecytidin-5'-yl hexadecyloxypropyl vinylphosphonate

[0061]
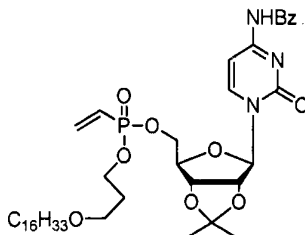
[0062] TPSCl (1.24 g, 4.08 mmol) is added to the mixture of vinylphosphonic acid from the example 7 (0.65 g, 1.36

mmol), hexadecyloxypropanol (0.81 g, 2.7 mmol), and 1-methylimidazole (1.45 ml, 18.3 mmol) in DCM (60 ml). The reaction mixture is stirred overnight at rt, then extracted/washed with saturated solution of $NaHCO_3$ (2 x 100 ml), 3% aqueous citric acid (2 x 100 ml) and dried over Na_2SO_4. Organic phase is concentrated *in vacuo* and product is obtained by flash chromatography on silica gel using linear gradient of ethanol in chloroform in 78% yield (0.81 g, 1.06 mmol) in the form of colorless wax.

A mixture of diastereoisomers ~ 1:1

[0063] **^{1}H NMR** (600.1 MHz, CD_3OD): 0.895 (m, 6H, $CH_3(CH_2)_{15}$); 1.24-1.35 (m, 52H, $CH_3(CH_2)_{13}CH_2CH_2O$); 1.368, 1.371 (2 × q, 2 × 3H, ^4J = 0.6, $(CH_3)_2C$); 1.51 (m, 4H, $CH_3(CH_2)_{13}CH_2CH_2O$); 1.57 (s, 6H, $(CH_3)_2C$); 1.89, 1.91 (2 × p, 2 × 2H, J_{vic} = 6.1, $OCH_2CH_2CH_2OC_{16}H_{33}$); 3.38, 3.39 (2 × t, 2 × 2H, J_{vic} = 6.7, $CH_3(CH_2)_{13}CH_2CH_2O$); 3.47 (td, 2H, J_{vic} = 6.1, $J_{H,P}$ = 1.2, $OCH_2CH_2CH_2OC_{16}H_{33}$); 3.49 (t, 2H, J_{vic} = 6.1, $OCH_2CH_2CH_2OC_{16}H_{33}$); 4.09-4.16 (m, 4H, $OCH_2CH_2CH_2OC_{16}H_{33}$); 4.27-4.36 (m, 4H, H-5'); 4.48 (m, 2H, H-4'); 4.91 (dd, 2H, $J_{3',2'}$ = 6.2, $J_{3',4'}$ = 3.6, H-3'); 5.06, 507 (2 × dd, 2 × 1H, $J_{2',3'}$ = 6.2, $J_{2',1'}$ = 1.8, H-2'); 5.87, 5.88 (2 × d, 2 × 1H, $J_{1',2'}$ = 1.8, H-1'); 6.145, 6.17 (2 × ddd, 2 × 1H, $J_{H,P}$ = 24.0, J_{trans} = 18.4, J_{cis} = 12.8, =CHP); 6.257, 6.261 (2 × ddd, 2 × 1H, $J_{H,P}$ = 52.0, J_{cis} = 12.8, J_{gem} = 2.1, $CH_{cis}H_{trans}$=CHP); 6.30, 6.31 (2 × ddd, 2 × 1H, $J_{H,P}$ = 26.0, J_{trans} = 18.4, J_{gem} = 2.1, $CH_{cis}H_{trans}$=CHP); 7.54 (m, 4H, H-m-Bz); 7.59 (d, 2H, $J_{5,6}$ = 7.7, H-5); 7.64 (m, 2H, H-p-Bz); 7.99 (m, 4H, H-o-Bz); 8.16, 8.17 (2 × d, 2 × 1H, $J_{6,5}$ = 7.7, H-5).
[0064] **^{13}C NMR** (150.9 MHz, CD_3OD): 14.48 ($CH_3(CH_2)_{15}$); 23.75 ($CH_3(CH_2)_{13}CH_2CH_2O$); 25.46, 25.48 ($(CH_3)_2C$); 27.27 ($CH_3(CH_2)_{14}CH_2O$); 27.43 ($(CH_3)_2C$); 30.49, 30.61, 30.78, 30.80, 30.81 ($CH_3(CH_2)_{14}CH_2O$); 31.70 (d, $J_{C,P}$ = 6.5, $OCH_2CH_2CH_2OC_{16}H_{33}$); 33.09 ($CH_3(CH_2)_{13}CH_2CH_2O$); 64.96, 64.98 (d, $J_{C,P}$ = 5.7, $OCH_2CH_2CH_2OC_{16}H_{33}$); 66.97, 67.04 (d, $J_{C,P}$ = 5.6, CH_2-5'); 67.42, 67.43 ($OCH_2CH_2CH_2OC_{16}H_{33}$); 72.10 ($CH_3(CH_2)_{14}CH_2O$); 82.64, 82.635, 82.644 (CH-3'); 86.57, 86.58 (CH-2'); 88.23, 88.30 (d, $J_{C,P}$ = 7.2, CH-4'); 97.60, 97.71 (CH-1'); 98.51, 98.54 (CH-5); 115.10, 115.11 ($C(CH_3)_2$); 125.63, 125.67 (d, $J_{C,P}$ = 183.9, =CHP); 129.25 (CH-o-Bz); 129.83 (CH-m-Bz); 134.14 (CH-p-Bz); 134.70 (C-i-Bz); 138.01, 138.04 (d, $J_{C,P}$ = 1.9, CH_2=CHP); 148.26, 148.34 (CH-6); 157.58, 157.60 (C-2); 165.58 (C-4); 169.19 (CO-Bz).
[0065] **^{31}P NMR** (202.3 MHz, CD_3OD): 19.62, 19.72.
IR v_{max}($CHCl_3$) 3406 (w), 2928 (s), 2856 (m), 1703 (m), 1670 (s), 1628 (m), 1603 (w), 1554 (m), 1582 (w), 1497 (m, sh), 1480 (vs), 1455 (w, sh), 1400 (m), 1385 (m), 1377 (m), 1301 (m), 1248 (s, sh), 1186 (w), 1158 (m), 1121 (m), 1110 (m), 1078 (s), 1070 (s), 1028 (m), 1003 (m, sh), 989 (m), 909 (w), 865 (w), 842 (vw), 708 (w), 687 (w), 512 (w) cm^{-1}.
HR-EI $C_{40}H_{62}N_3O_9P$ (M+H)$^+$ calcd 759.4224; found 759.4225

Example 9

Hexadecyloxypropyl uridin-5'-yl 2-([3R,4R]-3,4-dihydroxypyrrolidin-1-N-yl)ethyl-phosphonate

[0066]
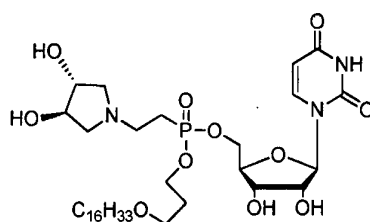
[0067] The mixture of (3R,4R)-3,4-dihydroxypyrrolidine (0.12 g, 1.18 mmol) and vinylphosphonate from the example 6 (0.4 g, 0.61 mmol) in n-BuOH (15 ml) is stirred at 105 °C overnight. The solvent is removed and the isopropylidene intermediate is obtained by flash chromatography on silica gel using linear gradient of H1 in ethyl acetate. This compound is dissolved in 0.5 M methanolic HCl (30 ml) and the mixture is stirred at rt for 4 h. The final product is obtained by flash chromatography on silica gel using linear gradient of H1 in ethyl acetate in in 34% overall yield (152 mg, 0.205 mmol) and lyophilized from water. A mixture of diastereoisomers ~ 6:5
^{1}H NMR (499.8 MHz, CD_3OD): 0.90 (m, 6H, $CH_3(CH_2)_{15}$); 1.25-1.38 (m, 52H, $CH_3(CH_2)_{13}CH_2CH_2$-O); 1.55 (m, 4H, $CH_3(CH_2)_{13}CH_2CH_2O$); 1.93 (m, 4H, $OCH_2CH_2CH_2OC_{16}H_{33}$); 2.12-2.25 (m, 4H, CH_2P); 2.71 (dd, 4H, J_{gem} = 10.6, J_{vic} = 3.0, H-2b,5b-pyrr); 2.86-3.00 (m, 4H, CH_2N); 3.116, 3.118 (2 × dd, 2 × 2H, J_{gem} = 10.6, J_{vic} = 5.0, H-2a,5a-pyrr); 3.42, 3.43 (2 × t, 2 × 2H, J_{vic} = 6.6, $CH_3(CH_2)_{13}CH_2CH_2O$); 3.515, 3.522 (2 × t, 2 × 2H, J_{vic} = 6.1, $OCH_2CH_2CH_2OC_{16}H_{33}$); 4.08 (m, 4H, $OCH_2CH_2CH_2OC_{16}H_{33}$); 4.11-4.21 (m, 8H, H-3',4', H-3,4-pyrr); 4.216, 4.218 (2 × dd, 2 × 1H, $J_{2',3'}$ = 5.1,

$J_{2',1'}$ = 4.1, H-2'); 4.26 (ddd, 1H, J_{gem} = 11.6, $J_{H,P}$ = 6.8, $J_{5'b,4'}$= 4.5, H-5'b); 4.30-4.34 (m, 2H, H-5'); 4.36 (ddd, 1H, J_{gem} = 11.6, $J_{H,P}$ = 6.6, $J_{5'a,4'}$ = 2.9, H-5'a); 5.751, 5.753 (2 × d, 2 × 1H, $J_{5,6}$ = 8.1, H-5); 5.845 (d, 2H, $J_{1',2'}$= 4.1, H-1'); 7.70, 7.73 (2 × d, 2 × 1H, $J_{6,5}$ = 8.1, H-6).

^{13}C NMR (125.7 MHz, CD$_3$OD): 14.47 (CH$_3$(CH$_2$)$_{15}$); 23.73 (CH$_3$(CH$_2$)$_{14}$CH$_2$O); 24.75, 24.81 (d, $J_{C,P}$ = 139.6, CH$_2$P); 27.28, 30.47, 30.63, 30.76, 30.79 (CH$_3$(CH$_2$)$_{14}$CH$_2$O); 31.75, 31.78 (d, $J_{C,P}$ = 6.2, OCH$_2$CH$_2$CH$_2$OC$_{16}$H$_{33}$); 33.06 (CH$_3$(CH$_2$)$_{14}$CH$_2$O); 50.81, 50.85 (CH$_2$N); 60.95, 60.98 (CH$_2$-2,5-pyrr); 64.86, 64.93 (d, $J_{C,P}$ = 6.7, OCH$_2$CH$_2$CH$_2$OC$_{16}$H$_{33}$); 66.52, 66.54 (d, $J_{C,P}$ = 6.2, CH$_2$-5'); 67.49, 67.53 (OCH$_2$CH$_2$CH$_2$OC$_{16}$H$_{33}$); 70.79, 70.86 (CH-3'); 72.14 (CH$_3$(CH$_2$)$_{14}$CH$_2$O); 74.87, 74.93 (CH-2'); 78.12, 78.19 (CH-3,4-pyrr); 83.57, 83.58 (d, $J_{C,P}$ = 6.6, CH-4'); 91.75, 91.85 (CH-1'); 103.02 (CH-5); 142.58, 142.64 (CH-6); 152.18, 152.20 (C-2); 165.99 (C-4).

^{31}P NMR (202.3 MHz, CD$_3$OD): 31.37, 31.64.

IR v_{max}(KBr) 3405 (s, vbr), 3063 (w), 2960 (m, sh), 2925 (vs), 2854 (s), 2810 (w, sh), 1696 (vs), 1629 (w, sh), 1466 (m), 1460 (m, sh), 1418 (w), 1384 (m), 1266 (m), 1223 (m), 1111 (s), 1075 (m, sh), 1046 (s, br), 998 (m), 821 (w), 765 (w), 721 (w) cm^{-1}.

HR-ESI C$_{34}$H$_{63}$O$_{11}$N$_3$P (M+H)$^+$ calcd 720.41947; found 720.41939.

Example 10

Hexadecyloxypropyl cytidin-5'-yl 2-([3R,4R]-3,4-dihydroxypyrrolidin-1-N-yl)ethyl-phosphonate

[0068]
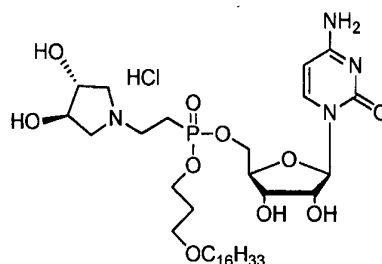
[0069]   The mixture of (3R,4R)-3,4-dihydroxypyrrolidine (0.05 g, 0.49 mmol) and benzoylcytosine vinylphosphonate from example 9 (0.34 g, 0.45 mmol) in n-BuOH (10 ml) is stirred at 100 °C overnight. The solvent is removed and the protected intermediate is purified by flash chromatography on silica gel using linear gradient of H1 in ethyl acetate. White foam obtained after evaporation of solvents is without further characterization (only LC-MS confirmation) dissolved in 8M ethanolic methylamine (10 ml) and stirred at rt overnight. The mixture is concentrated *in vacuo*, co-evaporated with ethanol (2x 20 ml), dissolved in 0.2M methanolic HCl (10 ml), and the reaction mixture is stirred at rt for 4 hours. After concentration *in vacuo* the final product is obtained by preparative HPLC in 27% overall yield (90.6 mg, 120 μM) after lyofilisation from water.

A mixture of diastereoisomers ~ 8:7

^{1}H NMR (600.1 MHz, CD$_3$OD): 0.90 (m, 6H, CH$_3$(CH$_2$)$_{15}$); 1.25-1.38 (m, 52H, CH$_3$(CH$_2$)$_{13}$CH$_2$CH$_2$-O); 1.55 (m, 4H, CH$_3$(CH$_2$)$_{13}$CH$_2$CH$_2$O); 1.93 (m, 4H, OCH$_2$CH$_2$CH$_2$OC$_{16}$H$_{33}$); 2.10-2.18 (m, 4H, CH$_2$P); 2.56 (bm, 4H, H-2b,5b-pyrr); 2.75-2.87 (bm, 4H, CH$_2$N); 3.00 (bm, 4H, H-2a,5a-pyrr); 3.41, 3.43 (2 × t, 2 × 2H, J_{vic} = 6.7, CH$_3$(CH$_2$)$_{13}$CH$_2$CH$_2$O); 3.51, 3.53 (2 × t, 2 × 2H, J_{vic} = 6.0, OCH$_2$CH$_2$CH$_2$OC$_{16}$H$_{33}$); 4.04 (m, 4H, H-3,4-pyrr); 4.08-4.23 (m, 10H, H-2',3',4'-pyrr, OCH$_2$CH$_2$CH$_2$OC$_{16}$H$_{33}$); 4.25-4.42 (m, 4H, H-5'); 5.83, 5.84 (d, 2H, $J_{1',2'}$ = 3.0, H-1'); 5.93, 5.94 (2 × d, 2 × 1H, $J_{5,6}$ = 7.6, H-5); 7.77, 7.79 (2 × d, 2 × 1H, $J_{6,5}$ = 7.6, H-6).

^{13}C NMR (150.9 MHz, CD$_3$OD): 14.47 (CH$_3$(CH$_2$)$_{15}$); 23.75 (CH$_3$(CH$_2$)$_{14}$CH$_2$O); 25.09, 25.14 (d, $J_{C,P}$ = 139.1, CH$_2$P); 27.29, 27.30, 30.49, 30.64, 30.77, 30.80 (CH$_3$(CH$_2$)$_{14}$CH$_2$O); 31.76, 31.79 (d, $J_{C,P}$ = 6.3, OCH$_2$CH$_2$CH$_2$OC$_{16}$H$_{33}$); 33.08 (CH$_3$(CH$_2$)$_{14}$CH$_2$O); 50.55 (CH$_2$N); 60.99, 61.02 (CH$_2$-2,5-pyrr); 64.71, 64.79 (d, $J_{C,P}$ = 6.6, OCH$_2$CH$_2$CH$_2$OC$_{16}$H$_{33}$); 66.24, 66.31 (d, $J_{C,P}$ = 6.4, CH$_2$-5'); 67.51, 67.55 (OCH$_2$CH$_2$CH$_2$OC$_{16}$H$_{33}$); 70.52, 70.55 (CH-3'); 72.15 (CH$_3$(CH$_2$)$_{14}$CH$_2$O); 75.68, 75.70 (CH-2'); 78.61, 78.66 (CH-3,4-pyrr); 83.13, 83.16 (d, $J_{C,P}$ = 6.6, CH-4'); 92.89, 92.90 (CH-1'); 96.17, 96.18 (C-5); 142.56, 142.64 (CH-6); 158.26, 158.27 (C-2); 167.646, 167.653 (C-4).

^{31}P NMR (202.3 MHz, CD$_3$OD): 32.67, 32.99.

IR v_{max}(CHCl$_3$) 3341 (m, vbr), 3220 (m, vbr), 2927 (vs), 2855 (s), 1649 (vs), 1609 (m, sh), 1578 (w), 1527 (m), 1494 (m), 1407 (m), 1468 (m), 1459 (m, sh), 1380 (m), 1287 (m), 1240 (m), 1110 (s), 1077 (m), 1046 (s), 1030 (s, sh), 996 (m) cm^{-1}.

HR-ESI $C_{34}H_{64}O_{10}N_4P$ (M+H)$^+$ calcd 719.4355; found 719.4357
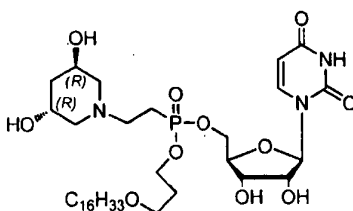
Example 11

5 **Hexadecyloxypropyl uridin-5'-yl 2-([3R,5R]-3,4-dihydroxypiperidin-1-N-yl)ethyl-phosphonate**

[0070]
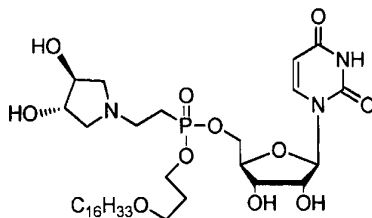
[0071] The mixture of (3S,4S)-3,4-dihydroxypyrrolidine (0.26 g, 2.56 mmol) and vinylphosphonate from example 7
20 (0.84 g, 1.28 mmol) in n-BuOH (30 ml) is stirred at 105 °C overnight. The solvent is removed and the isopropylidene intermediate is obtained by flash chromatography on silica gel using linear gradient of solvent mixture H1 in ethyl acetate. Obtained compound is dissolved in 0.5 M methanolic HCl (40 ml) and the mixture is stirred at rt for 4 h. The final product is obtained by chromatography on silica gel using linear gradient of H1 in ethyl acetate in 36% overall yield (344 mg, 0.46 mmol) and is lyophilized from water.

25 A mixture of diastereoisomers ~ 6:5

^{1}H NMR (499.8 MHz, CD$_3$OD): 0.90 (m, 6H, CH$_3$(CH$_2$)$_{15}$); 1.25-1.39 (m, 52H, CH$_3$(CH$_2$)$_{13}$CH$_2$CH$_2$-O); 1.55 (m, 4H, CH$_3$(CH$_2$)$_{13}$**CH$_2$**CH$_2$O); 1.95 (m, 4H, OCH$_2$**CH$_2$**CH$_2$OC$_{16}$H$_{33}$); 2.37-2.52 (m, 4H, CH$_2$P); 3.16 (bm, 2H, H-2b,5b-pyrr); 3.42 (t, 2H, J_{vic} = 6.7, CH$_3$(CH$_2$)$_{13}$CH$_2$**CH$_2$**O); 3.425 (bm, 2H, H-2b,5b-pyrr); 3.43 (t, 2H, J_{vic} = 6.7, CH$_3$(CH$_2$)$_{13}$CH$_2$**CH$_2$**O); 3.515 (m, 4H, CH$_2$N); 3.52, 3.53 (2 × t, 2 × 2H, J_{vic} = 6.1, OCH$_2$CH$_2$**CH$_2$**OC$_{16}$H$_{33}$); 3.59, 3.92 (2 × bm, 2 × 2H, H-2a,
30 5a-pyrr); 4.14 (m, 2H, H-4'); 4.16 (m, 2H, H-3'); 4.18-4.27 (m, 10H, H-2', O**CH$_2$**CH$_2$CH$_2$OC$_{16}$H$_{33}$, H-3,4-pyrr); 4.31 (ddd, 1H, J_{gem} = 11.5, $J_{H,P}$ = 7.6, $J_{5'b,4'}$ = 5.4, H-5'b); 4.36 (m, 2H, H-5'); 4.40 (ddd, 1H, J_{gem} = 11.5, $J_{H,P}$ = 7.3, $J_{5'a,4'}$ = 2.9, H-5'a); 5.742, 5.746 (2 × d, 2 × 1H, $J_{5,6}$ = 8.1, H-5); 5.78, 5.80 (2 × d, 2 × 1H, $J_{1',2'}$ = 3.9, H-1'); 7.68, 7.70 (2 × d, 2 × 1H, $J_{6,5}$ = 8.1, H-6).

^{13}C NMR (125.7 MHz, CD$_3$OD): 14.45 (CH$_3$(CH$_2$)$_{15}$); 23.32 (d, $J_{C,P}$ = 142.0, CH$_2$P); 23.74 (CH$_3$(CH$_2$)$_{14}$CH$_2$O); 27.29,
35 30.48, 30.64, 30.76, 30.79 (CH$_3$(CH$_2$)$_{14}$CH$_2$O); 31.70, 31.72 (d, $J_{C,P}$ = 6.1, OCH$_2$CH$_2$CH$_2$OC$_{16}$H$_{33}$); 33.07 (CH$_3$(CH$_2$)$_{14}$CH$_2$O); 52.18, 52.22 (CH$_2$N); 60.67, 60.75, 60.98, 61.01 (CH$_2$-2,5-pyrr); 65.33, 65.58 (d, $J_{C,P}$ = 6.7, OCH$_2$CH$_2$CH$_2$OC$_{16}$H$_{33}$); 67.16 (d, $J_{C,P}$ = 6.5, CH$_2$-5'); 67.44 (OCH$_2$CH$_2$**CH$_2$**OC$_{16}$H$_{33}$); 67.45 (d, $J_{C,P}$ = 4.3, CH$_2$-5'); 67.47 (OCH$_2$CH$_2$CH$_2$OC$_{16}$H$_{33}$); 70.77 (CH-3'); 72.16 (CH$_3$(CH$_2$)$_{14}$**CH$_2$**O); 74.55, 74.60 (CH-2'); 75.67, 75.68, 76.04 (CH-3,4-pyrr); 83.29 (d, $J_{C,P}$ = 6.2, CH-4'); 83.40 (d, $J_{C,P}$ = 5.8, CH-4'); 92.83, 92.85 (CH-1'); 103.03, 103.10 (CH-5);
40 143.12, 143.19 (CH-6); 152.13, 152.14 (C-2); 166.00 (C-4).

^{31}P NMR (202.3 MHz, CD$_3$OD): 26.79, 27.26.

IR ν_{max}(KBr) 3405 (s, vbr), 2694 (w, vbr), 2596 (w, vbr), 2925 (vs), 2854 (s), 1714 (s, sh), 1694 (vs), 1630 (m, sh), 1466 (m), 1458 (m, sh), 1418 (w), 1415 (w), 1385 (m), 1269 (m), 1229 (m, br), 1107 (s), 1053 (m, sh), 1030 (s, br), 1002 (s), 819 (w), 765 (vw), 721 (vw) cm^{-1}.

45 **HR-ESI** $C_{34}H_{63}O_{11}N_3P$ (M+H)$^+$ calcd 720.4195; found 720.4194

Example 12

Hexadecyloxypropyl uridin-5'-yl 2-([3R,4S,5S]-3,4-trihydroxypiperidin-1-N-yl)ethyl-phosphonate

50 [0072]
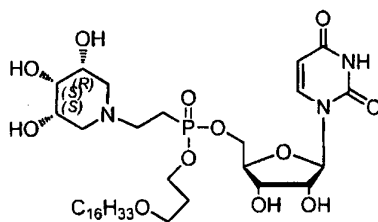
[0073]   The mixture of (3R,4S,5S)-3,4,5-trihydroxypiperidine (0.04 g, 0.33 mmol) and vinylphosphonate from the example 7 (0.1 g, 0.16 mmol) in n-BuOH (5 ml) is stirred at 105 °C overnight. The solvent is removed and the isopropylidene intermediate is obtained by flash chromatography on silica gel using linear gradient of H1 in ethyl acetate. This compound is dissolved in 0.5 M methanolic HCl (20 ml) and the mixture is stirred at rt for 4 h. The final product is obtained by flash chromatography on silica gel using linear gradient of H1 in ethyl acetate in 68% overall yield (80 mg, 0.11 mmol) and is lyophilized from water.

A mixture of diastereoisomers ~ 7:3

1H NMR (499.8 MHz, CD_3OD): 0.90 (m, 6H, $CH_3(CH_2)_{15}$); 1.25-1.38 (m, 52H, $CH_3(CH_2)_{13}CH_2CH_2$-O); 1.55 (m, 4H, $CH_3(CH_2)_{13}CH_2CH_2O$); 1.93 (m, 4H, $OCH_2CH_2CH_2OC_{16}H_{33}$); 2.10-2.18 (m, 4H, CH_2P); 2.43, 2.54 (2 × bm, 2 × 4H, H-2,6-pip); 2.75 (m, 4H, CH_2N); 3.42, 3.43 (2 × t, 2 × 2H, J_{vic} = 6.6, $CH_3(CH_2)_{13}CH_2CH_2O$); 3.52, 3.53 (2 × t, 2 × 2H, J_{vic} = 6.1, $OCH_2CH_2CH_2OC_{16}H_{33}$); 3.68 (bm, 4H, H-3,5-pip); 3.81 (bm, 2H, H-4-pip); 4.11-4.22 (m, 10H, H-2',3',4', $OCH_2CH_2CH_2OC_{16}H_{33}$); 4.23-4.38 (m, 4H, H-5'); 5.746, 5.749 (2 × d, 2 × 1H, $J_{5,6}$ = 8.1, H-5); 5.84 (d, 2H, $J_{1',2'}$ = 4.1, H-1'); 7.71, 7.73 (2 × d, 2 × 1H, $J_{6,5}$ = 8.1, H-6).

13C NMR (125.7 MHz, CD_3OD): 14.45 ($CH_3(CH_2)_{15}$); 23.55, 23.65 (d, $J_{C,P}$ = 138.5, CH_2P); 23.75 ($CH_3(CH_2)_{14}CH_2O$); 27.30, 30.49, 30.63, 30.77, 30.80 ($CH_3(CH_2)_{14}CH_2O$); 31.79, 31.82 (d, $J_{C,P}$ = 6.2, $OCH_2CH_2CH_2OC_{16}H_{33}$); 33.08 ($CH_3(CH_2)_{14}CH_2O$); 51.75 ($CH_2N$); 54.40 ($CH_2$-2,6-pip); 64.72, 64.78 (d, $J_{C,P}$ = 6.5, $OCH_2CH_2CH_2OC_{16}H_{33}$); 66.37 (d, $J_{C,P}$ = 6.3, CH_2-5'); 67.51, 67.55 ($OCH_2CH_2CH_2OC_{16}H_{33}$); 69.67 (CH-3,5-pip); 70.81, 70.83 (CH-3'); 71.83 (CH-4-pip); 72.17 ($CH_3(CH_2)_{14}CH_2O$); 74.97, 75.01 (CH-2'); 83.59, 83.63 (d, $J_{C,P}$ = 6.7, CH-4'); 91.84, 91.92 (CH-1'); 103.00 (CH-5); 142.56, 142.60 (CH-6); 152.18, 152.19 (C-2); 166.05 (C-4).

31P NMR (202.3 MHz, CD_3OD): 32.91, 33.23.

IR v_{max}(KBr) 3423 (vs, br), 2924 (s), 2854 (m), 1687 (s), 1632 (m), 1466 (m), 1406 (w), 1380 (w), 1264 (m), 1229 (m), 1116 (m), 1072 (m, sh), 1048 (m), 1029 (m), 996 (m, sh), 766 (vw) cm^{-1}. **HR-ESI** $C_{35}H_{65}O_{11}N_3P$ (M+H)$^+$ calcd 734.4347; found 734.4351

Example 13

Hexadecyloxypropyl uridin-5'-yl 2-([3R,5R]-3,4-dihydroxypiperidin-1-N-yl)ethylphosphonate

[0074]

[0075]   The mixture of (3R,5R)-3,5-dihydroxypiperidine (0.05 g, 0.42 mmol) and vinylphosphonate from the example 7 (0.25 g, 0.38 mmol) in n-BuOH (5 ml) is stirred at 105 °C overnight. The solvent is removed and the isopropylidene intermediate is obtained by flash chromatography on silica gel using linear gradient of H1 in ethyl acetate. Obtained compound is dissolved in 0.5 M methanolic HCl (20 ml) and the mixture is stirred at rt for 4 h. The final product is obtained by chromatography on silica gel using linear gradient of H1 in ethyl acetate in 76% overall yield (230 mg, 0.29 mmol) as a white amorphous solid.

A mixture of diastereoisomers ~ 6:4

1H NMR (600.1 MHz, CD_3OD): 0.90 (m, 6H, $CH_3(CH_2)_{15}$); 1.25-1.38 (m, 52H, $CH_3(CH_2)_{13}CH_2CH_2$-O); 1.55 (m, 4H,

$CH_3(CH_2)_{13}CH_2CH_2O$); 1.70 (bm, 4H, H-4-pip); 1.93 (m, 4H, $OCH_2CH_2CH_2OC_{16}H_{33}$); 2.12-2.19 (m, 4H, CH_2P); 2.36, 2.57 (2 × m, 2 × 4H, H-2,6-pip); 2.66-2.76 (m, 4H, CH_2N); 3.42, 3.43 (2 × t, 2 × 2H, J_{vic} = 6.6, $CH_3(CH_2)_{13}CH_2CH_2O$); 3.51, 3.53 (2 × t, 2 × 2H, J_{vic} = 6.1, $OCH_2CH_2CH_2OC_{16}H_{33}$); 4.01 (m, 4H, H-3,5-pip); 4.12-4.24 (m, 10H, H-2',3',4', $OCH_2CH_2CH_2OC_{16}H_{33}$); 4.24-4.40 (m, 4H, H-5'); 5.751, 5.754 (2 × d, 2 × 1H, $J_{5,6}$ = 8.1, H-5); 5.854, 5.856 (2 × 1H, $J_{1',2'}$ =4.1, H-1'); 7.71, 7.74 (2 × d, 2 × 1H, $J_{6,5}$ = 8.1, H-6).

13C NMR (150.9 MHz, CD_3OD): 14.49 ($CH_3(CH_2)_{15}$); 23.49, 23.53 (d, $J_{C,P}$ = 138.4, CH_2P); 23.75 ($CH_3(CH_2)_{14}CH_2O$); 27.29, 27.30, 30.49, 30.65, 30.78, 30.81 ($CH_3(CH_2)_{14}CH_2O$); 31.76, 31.83 (d, $J_{C,P}$ = 6.3, $OCH_2CH_2CH_2OC_{16}H_{33}$); 33.08 ($CH_3(CH_2)_{14}CH_2O$); 40.63, 40.65 ($CH_2$-4-pip); 52.02, 52.04 (d, $J_{C,P}$ = 2.0, CH_2N); 60.07, 60.10 (CH_2-2,6-pip); 64.63, 64.75 (d, $J_{C,P}$ = 6.6, $OCH_2CH_2CH_2OC_{16}H_{33}$); 65.58 ($CH$-3,5-pip); 66.27, 66.52 (d, $J_{C,P}$ = 6.2, CH_2-5'); 67.51, 67.54 ($OCH_2CH_2CH_2OC_{16}H_{33}$); 70.77, 70.84 ($CH$-3'); 72.13, 72.15 ($CH_3(CH_2)_{14}CH_2O$); 74.99, 75.05 ($CH$-2'); 83.59, 83.60 (d, $J_{C,P}$ = 6.6, CH-4'); 91.65, 91.66 (CH-1'); 102.99 (CH-5); 142.45, 142.51 (CH-6); 152.16, 152.18 (C-2); 165.99 (C-4).

31P NMR (202.3 MHz, CD_3OD): 33.22, 33.53.

IR v_{max}(KBr) 3431 (vs, br), 2924 (m), 2853 (w), 1710 (m, sh), 1693 (m), 1631 (m), 1468 (w), 1414 (vw), 1380 (w), 1265 (w, br), 1230 (w, br, sh), 1113 (m), 1060 (m, br), 1032 (m), 1006 (m), 764 (vw) cm⁻¹.

HR-ESI $C_{35}H_{65}O_{10}N_3P$ (M+H)⁺ calcd 718.4402; found 718.4402

Example 14

Icosanyl uridin-5'-yl 2-([3R,4R]-3,4-dihydroxypyrrolidin-1-N-yl)ethylphosphonate

[0076]
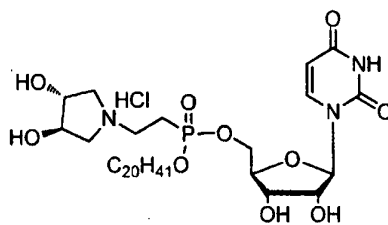
[0077] The mixture of (3R,4R)-3,4-dihydroxypyrrolidine (0.26 g, 2.52 mmol) and vinylphosphonate from the example 6 (1.1 g, 1.68 mmol) in n-BuOH (17 ml) is stirred at 100 °C overnight. The solvent is removed and the isopropylidene intermediate is obtained by flash chromatography on silica gel using linear gradient of H1 in ethyl acetate. This compound is dissolved in 0.5 M methanolic HCl (50 ml), and the mixture is stirred at rt for 4 h. The final product is obtained by flash chromatography on silica gel using linear gradient of H1 in ethyl acetate in 70% overall yield (840 mg, 1.17 mmol) and lyophilized from water.

A mixture of two diastereoisomers ~ 6:5

1H NMR (600.1 MHz, CD_3OD): 0.90 (m, 6H, $CH_3(CH_2)_{19}$); 1.25-1.43 (m, 68H, $CH_3(CH_2)_{17}CH_2CH_2$-O); 1.69 (m, 4H, $CH_3(CH_2)_{17}CH_2CH_2O$); 2.06-2.23 (m, 4H, CH_2P); 2.68 (dd, 4H, J_{gem} = 10.6, J_{vic} = 2.9, H-2b,5b-pyrr); 2.84-2.97 (m, 4H, CH_2N); 3.10 (dd, 4H, J_{gem} = 10.6, J_{vic} = 5.0, H-2a,5a-pyrr); 4.07 (m, 4H, H-3,4-pyrr); 4.08-4.13 (m, 4H, $CH_3(CH_2)_{17}CH_2CH_2$-O); 4.13-4.16 (m, 4H, H-3',4'); 4.207, 4.210 (2 × dd, 2 × 1H, $J_{2',3'}$ = 5.0, $J_{2',1'}$ = 4.2, H-2'); 4.25 (ddd, 1H, J_{gem} = 11.6, $J_{H,P}$ = 6.8, $J_{5'b,4'}$ = 4.4, H-5'b); 4.31 (m, 2H, H-5'); 4.35 (ddd, 1H, J_{gem} = 11.6, $J_{H,P}$ = 6.6, $J_{5'a,4'}$ = 2.7, H-5'a); 5.735, 5.743 (2 × d, 2 × 1H, $J_{5,6}$ = 8.1, H-5); 5.84, 5.85 (2 × d, 2 × 1H, $J_{1',2'}$ = 4.2, H-1'); 7.71, 7.74 (2 × d, 2 × 1H, $J_{6,5}$ = 8.1, H-6).

13C NMR (150.9 MHz, CD_3OD): 14.46 ($CH_3(CH_2)_{19}$); 23.75 ($CH_3(CH_2)_{17}CH_2CH_2O$); 24.85, 24.91 (d, $J_{C,P}$ = 139.8, CH_2P); 26.64, 30.28, 30.29, 30.49, 30.69, 30.73, 30.74, 30.77, 30.79, 30.80 ($CH_3(CH_2)_{17}CH_2CH_2O$); 31.55, 31.57 (d, $J_{C,P}$ = 6.0, $CH_3(CH_2)_{17}CH_2CH_2O$); 33.09 ($CH_3(CH_2)_{17}CH_2CH_2O$); 50.81, 50.86 (CH_2N); 60.98, 61.02 (CH_2-2,5-pyrr); 66.52, 66.54 (d, $J_{C,P}$ = 6.1, CH_2-5'); 67.69, 67.73 (d, $J_{C,P}$ = 7.1, $CH_3(CH_2)_{17}CH_2CH_2O$); 70.80, 70.87 (CH-3'); 74.90, 74.95 (CH-2'); 78.19, 78.26 (CH-3,4-pyrr); 83.60 (d, $J_{C,P}$ = 6.5, CH-4'); 91.75, 91.93 (CH-1'); 102.97, 102.99 (CH-5); 142.65 (CH-6); 152.17, 152.20 (C-2); 166.03 (C-4).

31P NMR (202.3 MHz, CD_3OD): 31.29, 31.57.

IR v_{max}(KBr) 3354 (m, vbr), 3063 (m), 2927 (vs), 2855 (s), 1694 (vs), 1630 (w, sh), 1467 (m), 1457 (m, sh), 1388 (m), 1267 (m), 1240 (m, sh), 1108 (m), 1075 (m), 1037 (s, br), 999 (s) cm⁻¹.

HR-ESI $C_{35}H_{65}O_{10}N_3P$ (M+H)⁺ calcd 718.44021, found 718.44030.

Example 15

Octadecyl uridin-5'-yl 2-([3*R*,4*R*]-3,4-dihydroxypyrrolidin-1-N-yl)ethylphosphonate

[0078]
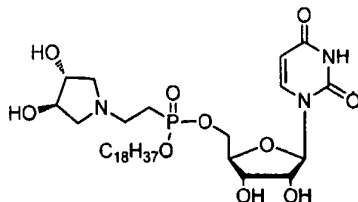
[0079] The mixture of (3R,4R)-3,4-dihydroxypyrrolidine (0.3 g, 2.94 mmol) and vinylphosphonate from the example 5 (1.23 g, 1.96 mmol) in n-BuOH (20 ml) is stirred at 100 °C overnight. The solvent is removed and the isopropylidene intermediate is obtained by flash chromatography on silica gel using linear gradient of H1 in ethyl acetate. Obtained compound is dissolved in 0.5 M methanolic HCl (50 ml), and the mixture is stirred at rt for 4 h. The final product is obtained by flash chromatography on silica gel using linear gradient of H1 in ethyl acetate in 68% overall yield (920 mg, 1.33 mmol) and lyophilized from water.

A mixture of two diastereoisomers ~ 6:5

^{1}**H NMR** (600.1 MHz, CD$_3$OD): 0.90 (m, 6H, CH$_3$(CH$_2$)$_{17}$); 1.25-1.43 (m, 60H, CH$_3$(CH$_2$)$_{15}$CH$_2$CH$_2$-O); 1.68 (m, 4H, CH$_3$(CH$_2$)$_{15}$CH$_2$CH$_2$O); 2.06-2.19 (m, 4H, CH$_2$P); 2.55 (m, 4H, H-2b,5b-pyrr); 2.73-2.86 (m, 4H, CH$_2$N); 2.99 (m, 4H, H-2a,5a-pyrr); 4.04 (m, 4H, H-3,4-pyrr); 4.05-4.13 (m, 4H, CH$_3$(CH$_2$)$_{15}$CH$_2$CH$_2$O); 4.13-4.16 (m, 4H, H-3',4'); 4.199, 4.201 (2 × dd, 2 × 1H, $J_{2',3'}$= 4.8, $J_{2',1'}$ = 4.2, H-2'); 4.24 (ddd, 1H, J_{gem} = 11.6, $J_{H,P}$ = 6.7, $J_{5'b,4'}$ = 4.2, H-5'b); 4.28 (ddd, 1H, J_{gem} = 11.6, $J_{H,P}$ = 7.4, $J_{5'b,4'}$= 2.5, H-5'b); 4.30 (ddd, 1H, J_{gem} = 11.6, $J_{H,P}$ = 5.2, $J_{5'a,4'}$ = 2.7, H-5'a); 4.34 (ddd, 1H, J_{gem} = 11.6, $J_{H,P}$ = 6.5, $J_{5'a,4'}$ = 2.7, H-5'a); 5.735, 5.745 (2 × d, 2 × 1H, $J_{5,6}$ = 8.1, H-5); 5.85, 5.86 (2 × d, 2 × 1H, $J_{1',2'}$ = 4.2, H-1'); 7.71, 7.74 (2 × d, 2 × 1H, $J_{6,5}$ = 8.1, H-6).

^{13}**C NMR** (150.9 MHz, CD$_3$OD): 14.47 (CH$_3$(CH$_2$)$_{17}$); 23.75 (CH$_3$(CH$_2$)$_{15}$CH$_2$CH$_2$O); 25.13, 25.17 (d, $J_{C,P}$ = 139.3, CH$_2$P); 26.65, 30.28, 30.29, 30.49, 30.68, 30.69, 30.72, 30.73, 30.78, 30.79, 30.80 (CH$_3$(CH$_2$)$_{15}$CH$_2$CH$_2$O); 31.55, 31.57 (d, $J_{C,P}$ = 6.0, CH$_3$(CH$_2$)$_{15}$CH$_2$CH$_2$O); 33.09 (CH$_3$(CH$_2$)$_{15}$CH$_2$CH$_2$O); 50.55, 50.57 (d, $J_{C,P}$ = 1.1, CH$_2$N); 61.01, 61.04 (CH$_2$-2,5-pyrr); 66.34, 66.42 (d, $J_{C,P}$ = 6.3, CH$_2$-5'); 66.60, 67.62 (d, $J_{C,P}$ = 6.8, CH$_3$(CH$_2$)$_{15}$CH$_2$CH$_2$O); 70.80, 70.88 (CH-3'); 74.96, 75.02 (CH-2'); 78.63, 78.68 (CH-3,4-pyrr); 83.63, 83.65 (d, $J_{C,P}$ = 6.7, CH-4'); 91.56, 91.74 (CH-1'); 102.95, 102.98 (CH-5); 142.55, 142.57 (CH-6); 152.18, 152.22 (C-2); 166.03 (C-4).

^{31}**P NMR** (202.3 MHz, CD$_3$OD): 32.12, 32.43.

IR v_{max}(CHCl$_3$) 3374 (m, vbr), 3063 (m), 2927 (vs), 2855 (s), 1694 (vs), 1630 (m, sh), 1467 (s), 1457 (s, sh), 1388 (m), 1267 (s), 1239 (m, sh), 1109 (s), 1074 (s), 1040 (s, br), 997 (s) cm^{-1}.

**HR-ESI** C$_{33}$H$_{61}$O$_{10}$N$_3$P (M+H)$^+$ calcd 690.40891, found 690.40891.

Example 16

Hexadecyl uridin-5'-yl 2-([3*R*,4*R*]-3,4-dihydroxypyrrolidin-1-N-yl)ethylphosphonate

[0080]
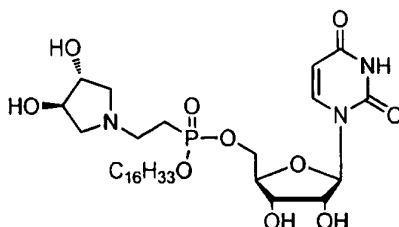
[0081] The mixture of (3R,4R)-3,4-dihydroxypyrrolidine (0.36 g, 3.45 mmol) and vinylphosphonate from the example 4 (1.38 g, 2.3 mmol) in n-BuOH (20 ml) is stirred at 100 °C overnight. The solvent is removed and isopropylidene

intermediate is obtained by flash chromatography on silica gel using linear gradient of H1 in ethyl acetate. Obtained compound is dissolved in 0.5 M methanolic HCl (50 ml), and the mixture is stirred at rt for 4 h. The final product is obtained by flash chromatography on silica gel using linear gradient of H1 in ethyl acetate in 38% overall yield (566 mg, 0.86 mmol) and is lyophilized from water.

A mixture of two diastereoisomers ~ 1:1

^{1}H NMR (600.1 MHz, CD$_3$OD): 0.90 (m, 6H, CH_3(CH$_2$)$_{15}$); 1.24-1.43 (m, 52H, CH$_3$(CH$_2$)$_{13}$CH$_2$CH$_2$-O); 1.68 (m, 4H, CH$_3$(CH$_2$)$_{13}$CH$_2$CH$_2$O); 2.06-2.18 (m, 4H, CH$_2$P); 2.55 (m, 4H, H-2b,5b-pyrr); 2.73-2.86 (m, 4H, CH$_2$N); 2.99 (m, 4H, H-2a,5a-pyrr); 4.04 (m, 4H, H-3,4-pyrr); 4.05-4.12 (m, 4H, CH$_3$(CH$_2$)$_{13}$CH$_2$CH$_2$O); 4.12-4.16 (m, 4H, H-3',4'); 4.198, 4.200 (2 × dd, 2 × 1H, $J_{2',3'}$ = 5.1, $J_{2',1'}$ = 4.1, H-2'); 4.24 (ddd, 1H, J_{gem} = 11.6, $J_{H,P}$ = 6.5, $J_{5'b,4'}$ = 4.2, H-5'b); 4.28 (ddd, 1H, J_{gem} = 11.6, $J_{H,P}$ = 7.2, $J_{5'b,4'}$ = 2.4, H-5'b); 4.30 (ddd, 1H, J_{gem} = 11.6, $J_{H,P}$ = 5.2, $J_{5'a,4'}$ = 2.7, H-5'a); 4.34 (ddd, 1H, J_{gem} = 11.6, $J_{H,P}$ = 6.6, $J_{5'a,4'}$ = 2.8, H-5'a); 5.73, 5.74 (2 × d, 2 × 1H, $J_{5,6}$ = 8.1, H-5); 5.85, 5.86 (2 × d, 2 × 1H, $J_{1',2'}$ = 4.1, H-1'); 7.71, 7.74 (2 × d, 2 × 1H, $J_{6,5}$ = 8.1, H-6).

^{13}C NMR (150.9 MHz, CD$_3$OD): 14.46 (CH$_3$(CH$_2$)$_{15}$); 23.75 (CH$_3$(CH$_2$)$_{13}$CH$_2$CH$_2$O); 25.14, 25.19 (d, $J_{C,P}$ = 139.3, CH$_2$P); 26.65, 30.27, 30.28, 30.50, 30.68, 30.69, 30.72, 30.73, 30.78, 30.81 (CH$_3$(CH$_2$)$_{13}$CH$_2$CH$_2$O); 31.55, 31.57 (d, $J_{C,P}$ = 6.0, CH$_3$(CH$_2$)$_{13}$CH$_2$CH$_2$O); 33.09 (CH$_3$(CH$_2$)$_{13}$CH$_2$CH$_2$O); 50.55, 50.59 (d, $J_{C,P}$ = 1.0, CH$_2$N); 61.02, 61.05 (CH$_2$-2,5-pyrr); 66.34, 66.42 (d, $J_{C,P}$ = 6.3, CH$_2$-5'); 66.60, 67.63 (d, $J_{C,P}$ = 6.8, CH$_3$(CH$_2$)$_{13}$CH$_2$CH$_2$O); 70.81, 70.89 (CH-3'); 74.96, 75.02 (CH-2'); 78.65, 78.69 (CH-3,4-pyrr); 83.64, 83.66 (d, $J_{C,P}$ = 6.6, CH-4'); 91.58, 91.76 (CH-1'); 102.94, 102.98 (CH-5); 142.57, 142.58 (CH-6); 152.18, 152.22 (C-2); 166.04 (C-4).

^{31}P NMR (202.3 MHz, CD$_3$OD): 32.33, 32.63.

IR ν_{max}(CHCl$_3$) 3376 (m, br), 3062 (w), 2927 (vs), 2855 (s), 1693 (vs), 1632 (w, sh), 1466 (m), 1459 (m, sh), 1388 (m), 1267 (s), 1237 (m, sh), 1109 (s), 1074 (s), 1039 (s, br), 997 (s) cm^{-1}.

HR-ESI C$_{31}$H$_{57}$O$_{10}$N$_3$P (M+H)$^+$ calcd 662.37761, found 662.37759.

Example 17

Tetradecyl uridin-5'-yl 2-([3R,4R]-3,4-dihydroxypyrrolidin-l-N-yl)ethylphosphonate

[0082]
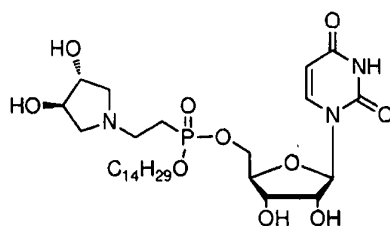
[0083] The mixture of (3R,4R)-3,4-dihydroxypyrrolidine (0.42 g, 4.10 mmol) and vinylphosphonate from the example 2 (1.17 g, 2.05 mmol) in n-BuOH (20 ml) is stirred at 100 °C overnight. The solvent is removed and the isopropylidene intermediate is obtained by flash chromatography on silica gel using linear gradient of H1 in ethyl acetate. This compound is dissolved in 0.5 M methanolic HCl (50 ml), and the mixture is stirred at rt for 4 h. The final product is obtained by flash chromatography on silica gel using linear gradient of H1 in ethyl acetate in 66% overall yield (862 mg, 1.36 mmol) and is lyophilized from water.

A mixture of two diastereoisomers ~ 6:5

^{1}H NMR (600.1 MHz, CD$_3$OD): 0.90 (m, 6H, CH$_3$(CH$_2$)$_{13}$); 1.25-1.43 (m, 44H, CH$_3$(CH$_2$)$_{11}$CH$_2$CH$_2$-O); 1.68 (m, 4H, CH$_3$(CH$_2$)$_{11}$CH$_2$CH$_2$O); 2.06-2.19 (m, 4H, CH$_2$P); 2.56 (m, 4H, H-2b,5b-pyrr); 2.74-2.88 (m, 4H, CH$_2$N); 3.00 (m, 4H, H-2a,5a-pyrr); 4.04 (m, 4H, H-3,4-pyrr); 4.06-4.13 (m, 4H, CH$_3$(CH$_2$)$_{11}$CH$_2$CH$_2$O); 4.13-4.16 (m, 4H, H-3',4'); 4.200, 4.202 (2 × dd, 2 × 1H, $J_{2',3'}$ = 5.0, $J_{2',1'}$ = 4.0, H-2'); 4.24 (ddd, 1H, J_{gem} = 11.6, $J_{H,P}$ = 6.7, $J_{5'b,4'}$ = 4.3, H-5'b); 4.29 (ddd, 1H, J_{gem} = 11.6, $J_{H,P}$ = 7.2, $J_{5'b,4'}$ = 2.4, H-5'b); 4.31 (ddd, 1H, J_{gem} = 11.6, $J_{H,P}$ = 5.0, $J_{5'a,4'}$ = 2.6, H-5'a); 4.35 (ddd, 1H, J_{gem} = 11.6, $J_{H,P}$ = 6.6, $J_{5'a,4'}$ = 2.8, H-5'a); 5.736, 5.745 (2 × d, 2 × 1H, $J_{5,6}$ = 8.1, H-5); 5.85, 5.86 (2 × d, 2 × 1H, $J_{1',2'}$ = 4.0, H-1'); 7.71, 7.74 (2 × d, 2 × 1H, $J_{6,5}$ = 8.1, H-6).

^{13}C NMR (150.9 MHz, CD$_3$OD): 14.46 (CH$_3$(CH$_2$)$_{13}$); 23.75 (CH$_3$(CH$_Z$)$_{11}$CH$_2$CH$_2$O); 25.11 (d, $J_{C,P}$ = 139.5, CH$_2$P); 25.16 (d, $J_{C,P}$ = 139.0, CH$_2$P); 26.65, 30.27, 30.28, 30.50, 30.68, 30.71, 30.72, 30.78, 30.80, 30.82 (CH$_3$(CH$_2$)$_{11}$CH$_2$CH$_2$O); 31.55, 31.57 (d, $J_{C,P}$ = 6.0, CH$_3$(CH$_2$)$_{11}$CH$_2$CH$_2$O); 33.09 (CH$_3$(CH$_2$)$_{11}$CH$_2$CH$_2$O); 50.57, 50.60 (d, $J_{C,P}$ = 1.0, CH$_2$N); 61.01, 61.03 (CH$_2$-2,5-pyrr); 66.36, 66.42 (d, $J_{C,P}$ = 6.3, CH$_2$-5'); 66.60, 67.63 (d, $J_{C,P}$ = 6.8, CH$_3$(CH$_2$)$_{11}$CH$_2$CH$_2$O); 70.81, 70.88 (CH-3'); 74.95, 75.01 (CH-2'); 78.60, 78.65 (CH-3,4-pyrr); 83.63, 83.64 (d, $J_{C,P}$ = 6.6,

CH-4'); 91.57, 91.75 (CH-1'); 102.95, 102.98 (CH-5); 142.56, 142.57 (CH-6); 152.18, 152.22 (C-2); 166.03 (C-4). ^{31}P NMR (202.3 MHz, CD$_3$OD): 32.08, 32.38.

IR v_{max}(CHCl$_3$) 3374 (m, vbr), 3063 (w), 2927 (vs), 2855 (s), 1694 (vs), 1630 (w, sh), 1467 (m), 1459 (m, sh), 1388 (m), 1267 (m), 1238 (m, sh), 1109 (m), 1074 (m), 1040 (s, br), 997 (s) cm^{-1}.

HR-ESI C$_{29}$H$_{53}$O$_{10}$N$_3$P (M+H)$^+$ calcd 634.34631, found 634.34635.

B) Antibacterial activity

[0084] Antimicrobial activity is assessed using the standard microdilution method determining the minimum inhibitory concentration (MIC) of the tested samples leading to inhibition of bacterial growth. Disposable microtitration plates are used for the tests. The samples were diluted in brain heart infusion broth (Himedia, Laboraties Pvt. Ltd., Č eská republika) and Mueller-Hinton broth (HiMedia Laboraties, see above) to yield a concentration range between 200 μg/ml and 1.5625 μg/ml. The plates are inoculated with a standard amount of the tested microbe - the inoculum density in each well is equal to 10$^{5-6}$ CFU/ml. The MIC is read after 24/48 hours of incubation at 37°C as the minimum inhibitory concentration of the tested substance that inhibits the growth of the bacterial strains. The minimum bactericidal concentration (MBC) is characterized as the minimum concentration of the sample required to achieve irreversible inhibition, i.e. killing the bacterium after a defined period of incubation. The MBC is examined by the inoculation method. With an applicator, 10 μL are transferred from microplate wells with defined concentrations of the tested sample and inoculated onto the surface of blood agar (Trios, Czech Republic). The MBC is determined as the lowest concentration that inhibited the visible growth of the used bacterium.

[0085] Standard reference bacterial strains *(E. faecalis* CCM 4224, *S. aureus* CCM 4223) from the Czech Collection of Microorganisms (CCM), Faculty of Science, Masaryk University Brno, *S. agalactiae, B. subtilis,* methicilin-resistant *S. aureus* 4591, fluoroquinolone-resistant *S. haemolyticus* 16568, vancomycin-resistant *E. faecium* VanA419/ana and methicilin-resistant *S. epidermidis* 8700/B strains obtained from the Teaching Hospital Olomouc were used. All tested microorganisms were stored in cryotubes (ITEST plus, Czech Republic) at -80°C.

Table 1

Minimum inhibitory concentration of selected novel lipophosphonoxines against a panel of reference bacterial strains				
	MIC μg/ml			
Compound prepared in example	*E. faecalis* CCM 4224	*S. aureus* CCM 4223	*B. subtilis*	*S. agalactiae*
9	12,5	-	6,25	3,125
10	6,25	25	3,125	3,125
11	12,5	-	6,25	6,25
12	-	-	-	12,5
13	-	-	-	6,25
14	-	-	-	6,25
15	6,25	25-12,5	12,5-6,25	3,125
16	6.25	12,5-6,25	3,125	1,5625
17	12,5	25-12.5	6,25	6,25

Table 2

Minimum inhibitory concentration of selected novel lipophosphonoxines against a panel of resistant bacterial strains

(continued)

Compound prepared in example	MIC µg/ml			
	S. aureus MRSA 4591	S. haemolyticus 16568	E. faecium VanA 419/ana	S. epidermidis 8700/B
9	-	-	6,25	3,125
10	-	-	6,25	6,25
11	-	-	6,25	6,25
15	-	-	6,25	6,25
16	12,5	25-12,5	3,125	3,125
17	25	12,5	12,5	12,5

[0086] Multiresistant bacterial strains isolated from clinical isolates of patients from Teaching Hospital Olomouc: MRSA - (methicilin-resistant *S. aureus* 4591); *S. haemolyticus* (fluoroquinolone-resistant strain 16568); *E. faecium* (vancomycin-resistant strain VanA419/ana); *S. epidermidis* (methicilin-resistant strain 8700/B).

[0087] In all cases the minimum inhibitory concentration (MIC, the concentration of tested compound at which the growth of 100 % of the tested bacteria was inhibited) is equal to minimum bactericidal concentration (MBC, the concentration of tested compound at which 100% of the tested bacteria is killed). The value of MBC is determined by revaccination of bacteria tested for MIC into an inhibitor free medium and monitoring the potential growth.

Methods of determination of cell viability and cytotoxicity:

[0088] Human immature erythroid progenitors isolated from umbilical cord blood are cultivated in the StemSpan serum-free medium (StemCell Technologies) in the presence of the stem cell factor (SCF, 100 ng/ml), erythropoietin (EPO, 33.34 nkat/ml) and dexamethasone (1 µmol.l^{-1}) (Panzenbock et al. 1998). Cells are plated at 25000 cells/well/20 µl in 384-well plates immediately before addition of lipophosphonoxine compound from particular examples. After 48 hours of incubation at 37 °C in 5% CO_2 viability is determined by using the commercial CellTiter-Blue® Cell Viability Assay (Promega, Cat.# G8082). The assay is based on the ability of living cells to convert a redox dye (resazurin) into a fluorescent end product (resorufin). Non-viable cells rapidly lose metabolic capacity and thus do not generate a fluorescent signal. The homogeneous assay procedure involves adding the single reagent directly to cells cultured in serum-supplemented medium. After an incubation step, data are recorded.

[0089] Cytotoxicity is determined after 4 hours at 37 °C in 5% CO_2 using commercial CytoTox-ONE™ Homogeneous Membrane Integrity Assay (Promega, Cat.# G7892), a fluorometric method for estimating the number of non-viable cells present in multiwell plates. The CytoTox-ONE™ Assay measures the release of lactate dehydrogenase (LDH) from the cells with a damaged membrane. LDH released into the culture medium is measured with a 10-minute coupled enzymatic assay that results in the conversion of resazurin into a fluorescent resorufin product. The amount of fluorescence produced is proportional to the number of lysed cells.

[0090] The fluorescence intensity is measured using the EnVision plate reader (PerkinElmer). Data are analyzed using GraphPad Prism 5.0 statistical software.

Table 3

Maximum safety concentration of selected novel lipophosphonoxins based on viability of normal erythroid progenitor cells using commercial test CellTiter Blue (Promega Corp., Madison, USA):		
Compound prepared in example	[Max. safety concentration] µg/ml	IC_{50} µg/ml
9	62	93
10	31	46
11	31	40
12	62	141
13	15	45

(continued)

Compound prepared in example	[Max. safety concentration] μg/ml	IC$_{50}$ μg/ml
14	15	29
15	31	38
16	31	44
17	31	47

Table 4

Cytotoxicity of selected newly prepared lipophosphonoxins:		
Compound prepard in example	[Max. safety concentration] μg/ml	EC$_{50}$ μg/ml
9	125	436
14	125	185
15	62	170
16	62	237
17	125	302

[0091] Cytotoxicity of tested compounds against normal human erythroid progenitor cells was determined using commercial test CytoToxOne (Promega Corp., Madison, USA)

Industrial Applicability

[0092] Lipophosphonoxins according to this invention can be used as antibacterial agents in pharmaceutical preparations destined for the treatment of bacterial infections, components of disinfectants and/or selective growth media.

Claims

1. Lipophosphonoxins of general formula I,

(I)
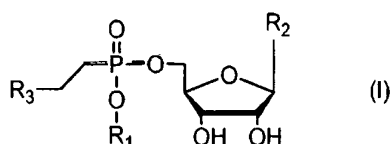
wherein R$_1$ is selected from a group comprising (C$_8$-C$_{22}$)alkyl, hexadecyloxypropyl, tetradecyloxypropyl, tetradecyloxyethyl, hexadecyloxyethyl,
R$_2$ is selected from a group comprising uracil, thymin, cytosin,
R$_3$ is selected from the group comprising compounds of general formula II and III:

(II)

(III)
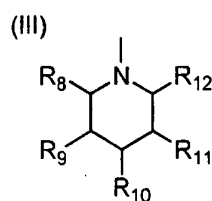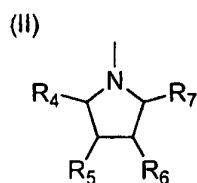
wherein R_4 is H or CH_2OH, R_5 is H or OH, R_6 is H or OH, R_7 is H or CH_2OH, R_8 is H or CH_2OH, R_9 is H or OH, R_{10} is H or OH, R_{11} is H or OH, R_{12} is H or CH_2OH,
diastereomers and mixtures of diaslereomers thereof, and
their pharmaceutically acceptable salts and hydrates.

2. A method of preparation of lipophosphonoxins of general formula I according to claim 1 or diastereomers and mixtures od diastereomers thereof, **characterized in that** it contains steps A-D, in which

A) dimethyl vinylphosphonate is heated overnight with 40% to 70% (v/v) aqueous pyridine at a temperature from 50 to 80 °C affording methyl vinylphosphonate **IX**

IX
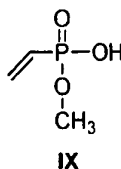
B) the obtained methyl vinylphosphonate is esterified with nucleoside **X,** protected in positions 2'and 3' with a protecting group selected from 2'.3'-isopropylidene, 2',3'-bis(diniethoxytrityl), 2',3'-dibenzoyl, or 2',3'-diacetyl, and possessing free 5'-hydroxyl group

X ,
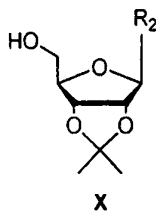
in the presence of triisopropylbenzenesulfonylchloride and under catalysis by *N*-methylimidazole in a solvent selected from the group comprising acetonitrile, dioxane, tetrahydrofuran, dichloroethane, chloroform and dichloromethane; the obtained methylester is isolated by chromatography on silica gel using linear gradient of ethanol in chloroform, and subsequently, the methyl ester group is removed by heating overnight with 40% to 70% (v/v) aqueous pyridine at a temperature from 50 to 80 °C affording vinylphosphonic acid **XI**

XI
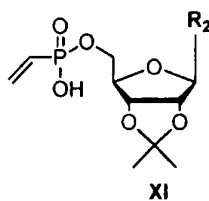
which is isolated by chromatography on silica gel using linear gradient of mixture of ethyl acetate:acetone: ethanol:water in volume ratios 4:1:1:1, in ethyl acetate;
C) the vinylphosphonic acid **XI** is esterified by alcohol using triisopropylbenzenesulfonylchloride as condensing agent and under catalysis by *N*-methylimidazole in a solvent selected from the group comprising acetonitrile, dioxane, tetrahydrofuran, dichloroethane, chloroform and dichloromethane, and the thereby obtained vinylphosphonate **XII**

XII ,
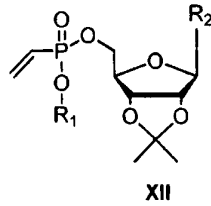
is separated by chromatography on silica gel using linear gradient of ethanol in chloroform;

D) Michael addition of secondary amine to the vinyl function of the vinylphosphonate **XII** is performed by heating in an organic solvent selected from the group comprising acetonitrile, dioxane, tetrahydrofuran, dichloroechane, chloroforme, etanol, propanol, isopropanol a n-butanol at temperature from 80 to 120 °C for 4 to 12 hours, followed by removal of the protecting groups on nucleoside; the product is subsequently isolated by chromatography on silica gel using linear gradient of mixture of ethyl acetate:acetone:ethanol:water in volume ratios 4:1:1:1, in ethyl acetate; or it is re-purified by reverse phase high performance liquid chromatography.

3. The method of preparation according to claim 2, **characterized in that** heating overnight with aqueous pyridine in step A) and/or B) is carried out at 60 °C and the concentration of the pyridine solution is 60% (v/v).

4. The method of preparation according to claim 2, **characterized in that** Michael addition in the step D is carried out in n-butanol at 105 °C. preferably overnight.

5. The method of preparation according to claim 2, **characterized in that** esterification in the steps B and/or C is preferably carried out in dichloromethane.

6. The method of preparation according to claim 2, **characterized in that** in the step D), the nucleoside protecting groups selected from 2',3'-bis(dimethoxytrityl), 2',3'-dibenzoyl and 2',3'-diacetyl are removed by ethanolic methylamine or aqueous ammonia.

7. The method of preparation according to claim 2, **characterized in that** in the step D), the 2',3'-isopropylidene protecting group is removed by treatment with 0,5 mol.1^{-1} hydrochloride in methanol at room temperature overnight.

8. The lipophoshonoxins of general formula I or their diastereomers or pharmaceutically acceptable salts and hydrates thereof and/or mixtures of such compounds according to claim 1 for use as medicaments.

9. Lipophoshonoxins of general formula I or their diastereomers or pharmaceutically acceptable salts and hydrates thereof and/or mixtures of such compounds according to claim 1 for use as antibacterial medicaments.

10. Lipophoshonoxins of general formula I or their diastereomers or pharmaceutically acceptable salts and hydrates thereof and/or mixtures of such compounds according to claim 1 for use as an active component of disinfectants and/or selective growth media for *in vitro* cultivations.

11. Antibacterial medicament, disinfectant and/or selective growth medium containing as an active ingredient at least one lipophoshonoxin of general formula I or their diastereomers and mixtures of such diastereomers or pharmaceutically acceptable salts and hydrates thereof and/or mixtures of such compounds according to claim 1.

Patentansprüche

1. Lipophosphonoxine der allgemeinen Formel I,

(I)
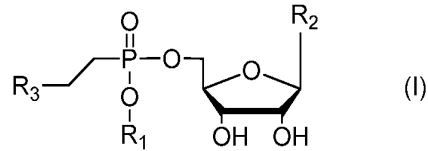
worin der Substituent R_1 aus einer Gruppe umfassend (C_8-C_{22})Alkyl, Hexadecyloxypropyl, Tetradecyloxypropyl, Tetradecyloxyethyl, Hexadecyloxyethyl ausgewählt ist,

R_2 aus einer Gruppe umfassend Uracil, Thymin, Cytosin ausgewählt ist,

R_3 aus einer Gruppe ausgewählt ist, welche die Verbindungen der allgemeinen Formeln II und III umfasst:

(II)   (III)
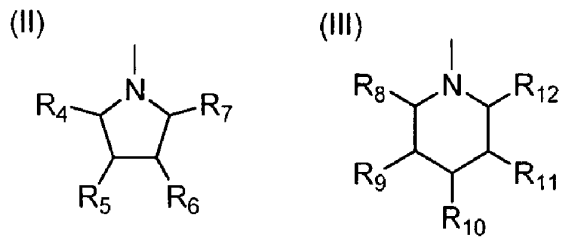
worin R_4 H oder CH_2OH ist, R_5 H oder OH ist, R_6 H oder OH ist, R_7 H oder CH_2OH ist, R_8 H oder CH_2OH ist, R_9 H oder OH ist, R_{10} H oder OH ist, R_{11} H oder OH ist, R_{12} H oder CH_2OH ist, deren Diastereomere und Diastereomer-Gemische, und deren pharmazeutisch annehmbare Salze und Hydrate.

2. Verfahren zur Herstellung von Lipophosphonoxinen der allgemeinen Formel I nach dem Anspruch 1 oder deren Diastereomeren und Gemischen deren Diastereomere, **dadurch gekennzeichnet, dass** es die Schritte A-D umfasst, wobei

A) Dimethylvinylphosphonat über Nacht mit 40% bis 70% (Vol.-%) wässriges Pyridin bei einer Temperatur von 50 bis 80°C unter Entstehung von Methylvinylphosphonat **IX** erwärmt wird

IX
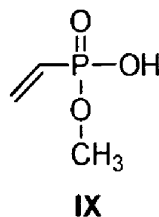
B) gewonnenes Methylvinylphosphonat esterifiziert mit dem Nukleosid **X**, geschützt in den Lagen 2' und 3' durch eine Schutzgruppe, ausgewählt aus 2',3'-Isopropyliden, 2',3'-Bis(Dimethoxytrityl), 2',3'-Dibenzoyl oder 2',3'-Diacetyl, besitzend eine freie 5'-HydroxylGruppe

X ,
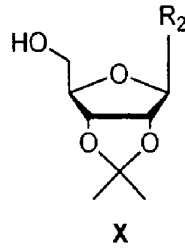
in Anwesenheit von Triisopropylbenzensulfonylchlorid und unter Katalyse durch N-Methylimidazol im Lösungs-mittel, ausgewäht aus einer Gruppe, umfassend Acetonitril, Dioxan, Tetrahydrofuran, Dichlorethan, Chloroform und Dichlormethan; gewonnenes Methylester wird vermittels Chromatographie auf Silikagel unter Verwendung von linearem Ethanolgradient im Chloroform isoliert, und nachfolgend wird die Methylester-Gruppe durch das Erwärmen über Nacht mit 40% bis 70% (Vol.-%) wässriges Pyridin bei einer Temperatur von 50 bis 80°C unter Entstehung von Vinylphosphonsäure **XI** beseitigt
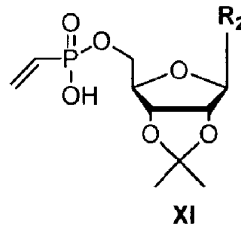
XI ,

die vermittels Chromatographie auf Silikagel unter Verwendung von linearem Gradient des Gemisches von Ethylacetat:Aceton:Ethanol:Wasser im Vol.-Verhältnis 4:1:1:1, im Ethylacetat isoliert wird;
C) die Vinylphosphonsäure **XI** wird esterifiziert mit dem Alkohol mit Hilfe von Triisopropylbenzensulfonylchlorid als Kondensationsmittel und unter Katalyse durch N-Methylimidazol im Lösungsmittel, ausgewählt aus einer Gruppe, umfassend Acetonitril, Dioxan, Tetrahydrofuran, Dichlorethan, Chloroform und Dichlormethan, und das entstandene Vinylphosphonat **XII**
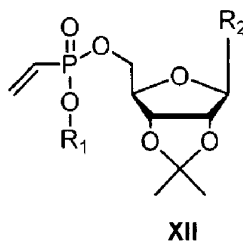
XII ,

wird vermittels Chromatographie auf Silikagel unter Verwendung von linearem Ethanolgradient im Chloroform abgetrennt;
D) Michael-Addition von Sekundäramin auf die Vinylfunktion des Vinylphosphonats **XII** durch das Erwärmen wird durchgeführt im organischen Lösungsmittel, ausgewählt aus einer Gruppe, umfassend Acetonitril, Dioxan, Tetrahydrofuran, Dichlorethan, Chloroform, Ethanol, Propanol, Isopropanol und n-Butanol, bei einer Temperatur 80 bis 120 °C für 4 bis 12 Stunden, gefolgt durch die Beseitigung der Schutzgruppen auf Nukleosid; das Produkt wird weiter vermittels Chromatographie auf Silikagel unter Verwendung von linearem Gradient des Gemisches Ethylacetat:Aceton:Ethanol:Wasser im Vol.-Verhältnis 4:1:1:1 im Ethylacetat isoliert; oder es wird mit Hilfe einer hocheffektiven Chromatographie auf der Reverse-Phase nachgereinigt.

3. Verfahren zur Herstellung nach dem Anspruch 2, **dadurch gekennzeichnet, dass** das Erwärmen über Nacht mit wässrigem Pyridin im Schritt A) und/oder B) bei der Temperatur von 60°C und Konzentration der Pyridin-Lösung

60% (Vol.-%) durchgeführt wird.

4. Verfahren zur Herstellung nach dem Anspruch 2, **dadurch gekennzeichnet, dass** die Michael-Addition im Schritt D in n-Butanol bei 105°C, insbesondere über Nacht, durchgeführt wird.

5. Verfahren zur Herstellung nach dem Anspruch 2, **gekennzeichnet dadurch, dass** die Esterifikation in den Schritten B und/oder C insbesondere im Dichlormethan durchgeführt wird.

6. Verfahren zur Herstellung nach dem Anspruch 2, **dadurch gekennzeichnet, dass** die Schutzgruppen von Nukleosid, ausgewählt aus 2',3'-Bis(Dimethoxytrityl), 2',3'-Dibenzoyl und 2',3'-Diacetyl, im Schritt D durch eine ethanolische Methylamin-Lösung oder wässriges Ammoniak beseitigt werden.

7. Verfahren zur Herstellung nach dem Anspruch 2, **gekennzeichnet dadurch, dass** die 2',3'-Isopropyliden-Schutzgruppe im Schritt D durch das Einwirken von 0,5 mol.l^{-1} Chlorwasserstoff im Methanol bei Raumtemperatur über Nacht beseitigt wird.

8. Lipophosphonoxine der allgemeinen Formel I oder deren Diastereomere oder pharmazeutisch annehmbare Salze und Hydrate, und/oder Gemische derartiger Verbindungen nach dem Anspruch 1 zur Verwendung als Arzneimittel.

9. Lipophosphonoxine der allgemeinen Formel I oder deren Diastereomere oder pharmazeutisch annehmbare Salze und Hydrate, und/oder Gemische derartiger Verbindungen nach dem Anspruch 1 zur Verwendung als antibakterielles Arzneimittel.

10. Lipophosphonoxine der allgemeinen Formel I oder deren Diastereomere oder pharmazeutisch annehmbare Salze und Hydrate, und/oder Gemische derartiger Verbindungen nach dem Anspruch 1 zur Verwendung als Wirkkomponenten von Desinfektionsmitteln und/oder selektiven Kultivierungsmedien für in vitro-Kultivierungen.

11. Antibakterielles Arzneimittel, Desinfektionsmittel und/oder selektives Kultivierungsmedium, enthaltend als Wirkkomponente mindestens ein Lipophosphonoxin der allgemeinen Formel I oder dessen Diastereomere oder pharamazeutische annehmbare Salze und Hydrate, und/oder Gemische derartiger Verbindungen nach dem Anspruch 1.

Revendications

1. Lipophosphonoxines selon la formule générale I,
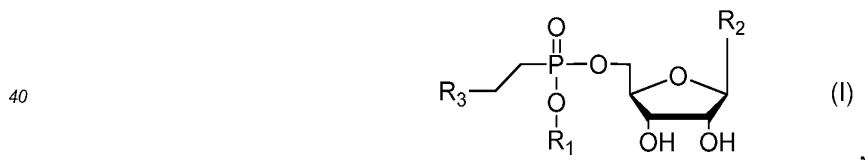
dans laquelle R$_1$ est sélectionné parmi un groupe comprenant (C$_8$-C$_{22}$) alkyle, hexadécyl-oxypropyle, tétradécyl-oxypropyle, tétradécyl-oxyéthyle, hexadécyl-oxyéthyle,
R$_2$ est sélectionné parmi un groupe comprenant l'uracile, thymine, cytosine,
R$_3$ est sélectionné parmi un groupe comprenant des composés de formules générales II et III :

(II) (III)
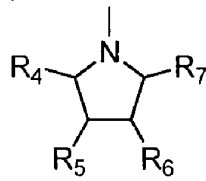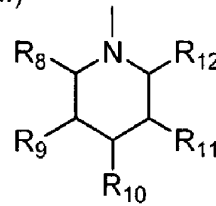
dans lesquelles R_4 représente H ou CH_2OH, R_5 représente H ou OH, R_6 représente H ou OH, R_7 représente H ou CH_2OH, R_8 représente H ou CH_2OH, R_9 représente H ou OH, R_{10} représente H ou OH, R_{11} représente H ou OH, R_{12} représente H ou CH_2OH,
leurs diastéréomères et mélanges de leurs diastéréomères et leurs sels et hydrates pharmaceutiquement acceptables.

2. Procédé de préparation de lipophosphonoxines de formule générale I selon la revendication 1 ou de leurs diasté-réomères et des mélanges de leurs diastéréomères, **caractérisé en ce qu**'il comprend les étapes A-D au cours desquelles

A) le diméthyl vinylphosphonate se réchauffe pendant la nuit avec la pyridine aqueuse de 40% à 70% (% de volume) à la température de 50 à 80 °C pour obtenir le méthyl vinylphosphanate **IX**

IX
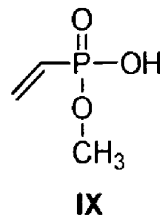
B) le méthyl vinylphosphanate obtenu estérifie avec le nucléoside **X,** protégé dans les positions 2'et 3' par un groupe protecteur, sélectionné parmi les 2',3'-isopropylidène, 2',3'-bis(diméthoxytrityle), 2',3'-dibenzoyle ou 2', 3'-diacétyle, ayant un groupe 5'-hydroxyde libre

X ,
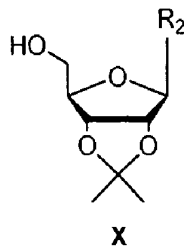
en présence du triisopropylbenzenesulfonyl chloride et sous catalyse par N-méthylimidazole dans un solvant, choisi parmi un groupe comprenant un acétonitrile, dioxane, tétrahydrofurane, dichloroéthane, chloroforme et dichlorométhane; l'ester méthylique obtenu est isolé par chromatographie sur un gel de silice en utilisant un gradient linéaire d'éthanol en chloroforme et consécutivement le groupe d'ester méthylique est éliminé par réchauffement pendant la nuit avec de la pyridine aqueuse de 40% à 70% (% de volume) à la température de 50 à 80 °C pour obtenir l'acide vinylphosphonique **XI**

XI ,
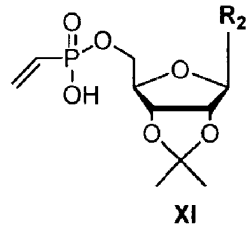
lequel est isolé par chromatographie sur un gel de silice en utilisant un gradient linéaire du mélange acétate d'éthyle : acétone : éthanol : eau en rapport des volumes 4:1:1:1, dans l'acétate d'éthyle ;

C) l'acide vinylphosphonique **XI** estérifie avec l'alcool à l'aide du triisopropylbenzensulfonyl chloride en tant qu'agent condensateur et sous catalyse par N-méthylimidazole dans un solvant, sélectionné parmi un groupe comprenant l'acétonitrile, le dioxane, le tétrahydrofurane, le dichloroéthane, le chloroforme et le dichlorométhane et le vinylphosphonate **XII** obtenu

XII ,
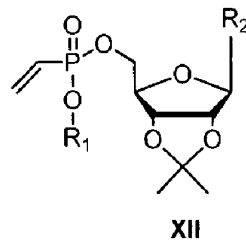
est séparé par chromatographie sur un gel de silice en utilisant un gradient d'éthanol en chloroforme ;

D) l'addition de Michael de l'amine secondaire sur la fonction vinyle du vinylphosphonate **XII** est effectuée par réchauffement dans un solvant organique sélectionné parmi un groupe comprenant l'acétonitrile, le dioxane, le tétrahydrofurane, le dichloroéthane, le chloroforme, l'éthanol, le propanol, l'isopropanol et le n-butanol à la température de 80 à 120 °C pendant une période de 4 à 12 heures, suivi de l'élimination du groupe protecteur sur le nucléoside; le produit est ensuite isolé par chromatographie sur un gel de silice en utilisant un gradient linéaire du mélange acétate d'éthyle: acétone: éthanol: eau en rapport des volumes 4:1:1:1 dans l'acétate d'éthyle; ou il est purifié à l'aide d'une chromatographie très efficace à la phase réversible.

3. Procédé de préparation selon la revendication 2, **caractérisé par** le réchauffement pendant la nuit avec la pyridine aqueuse à l'étape A) et/ou B) à la température de 60 °C et à la concentration de la solution de pyridine de 60 % (% de volume).

4. Procédé de préparation selon la revendication 2, **caractérisé en ce que** l'addition de Michael à l'étape D est effectuée dans le n-butanol à la température de 105 °C, de préférence pendant la nuit.

5. Procédé de préparation selon la revendication 2, **caractérisé en ce que** l'estérification aux étapes B et/ou C est de préférence effectuée dans le dichlorométhane.

6. Procédé de préparation selon la revendication 2, **caractérisé en ce que** les groupes protecteurs du nucléoside sélectionné parmi 2',3'-bis(diméthoxytrityle), 2',3'-dibenzoyle et 2',3'-diacétyle à l'étape D, sont éliminés par une solution éthanolique de méthylamine ou par l'ammoniaque aqueux.

7. Procédé de préparation selon la revendication 2, **caractérisé en ce que** le groupe protecteur 2',3'-isopropylidène à l'étape D est éliminé par un traitement avec 0.5 mol.l^{-1} d'acide chlorhydrique dans le méthanol à la température ambiante du laboratoire pendant la nuit.

8. Lipophosphonoxines de formule générale I ou leurs diastéréomères ou leurs sels et hydrates pharmaceutiquement acceptables, et/ou mélanges de tels composés, selon la revendication 1, pour utilisation en tant que médicament.

9. Lipophosphonoxines de formule générale I ou leurs diastéréomères ou leurs sels et hydrates pharmaceutiquement acceptables, et/ou mélanges de tels composés, selon la revendication 1, pour utilisation en tant que médicament antibactérien.

10. Lipophosphonoxines de formule générale I ou leurs diastéréomères ou leurs sels et hydrates pharmaceutiquement acceptables, et/ou mélanges de tels composés, selon la revendication 1, pour utilisation en tant qu'agent actif des produits désinfectants et/ou des milieus sélectifs de croissance pour les cultures *in vitro.*

11. Médicament antibactérien, produit désinfectant et/ou milieu sélectif de croissance contenant en tant qu'agent actif au moins un lipophosphonoxine de formule générale I, ou ses diastéréomères et mélanges de ses diastéréomères ou ses sels et hydrates pharmaceutiquement acceptables, et/ou mélanges de tels composés, selon la revendication 1.
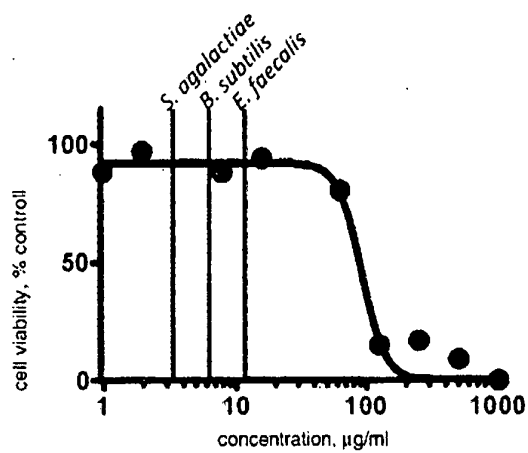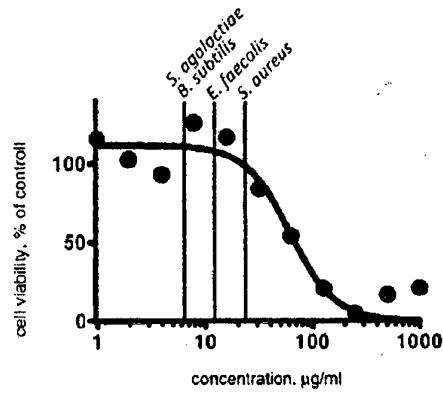
Fig. 1A
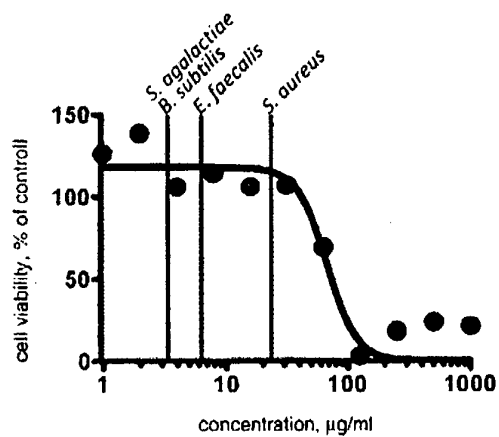
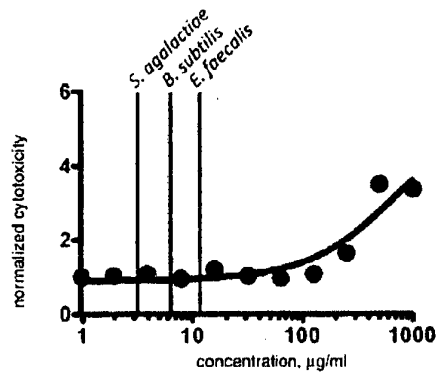

Fig. 1B
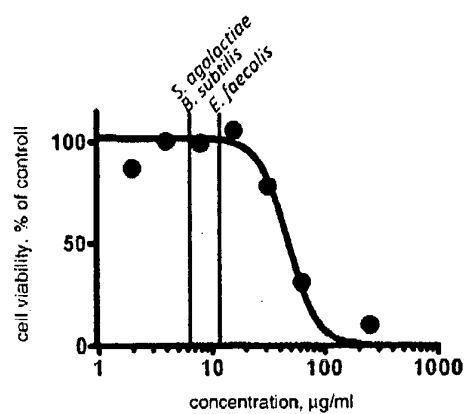
Fig. 1C
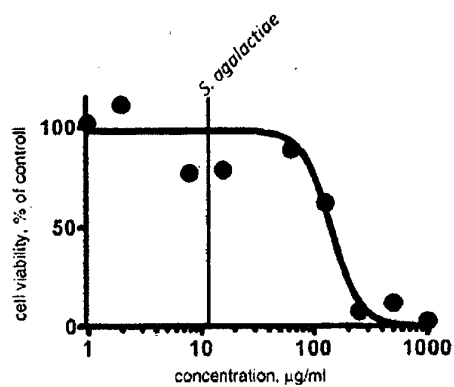
Fig. 1D
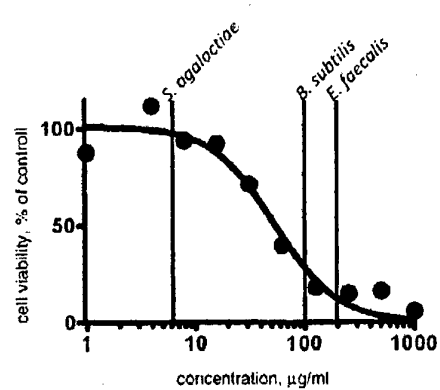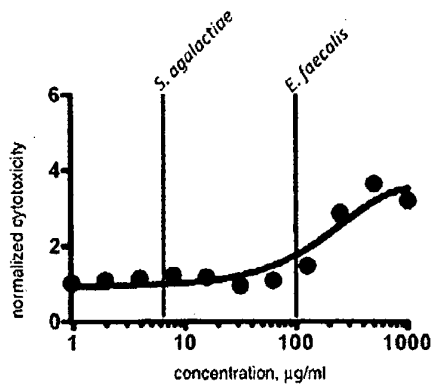

Fig. 1E
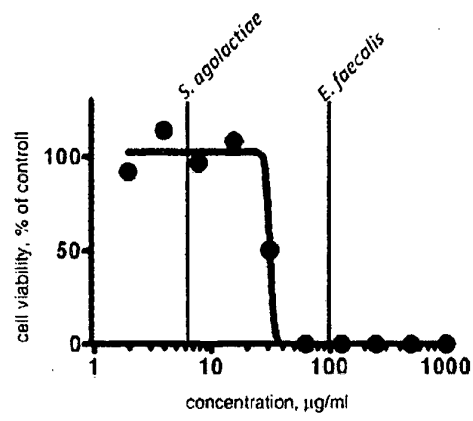
Fig.1F

Fig.1G

Fig.1H

Fig. 1I
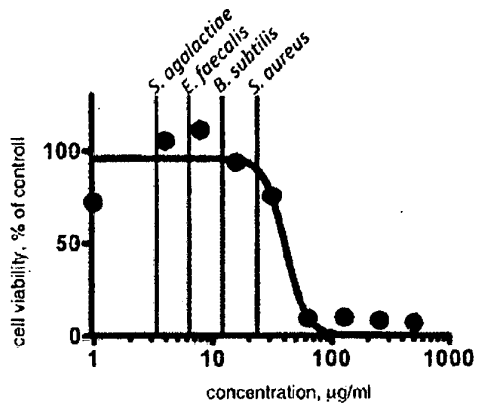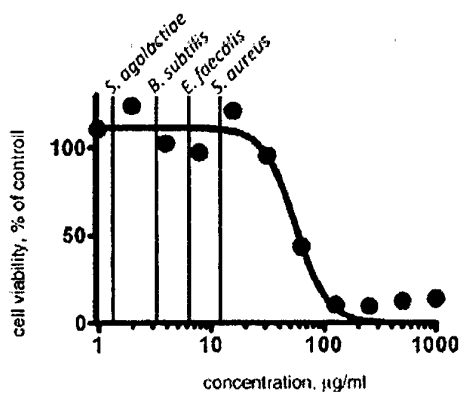
Fig. 2A

Fig. 2B
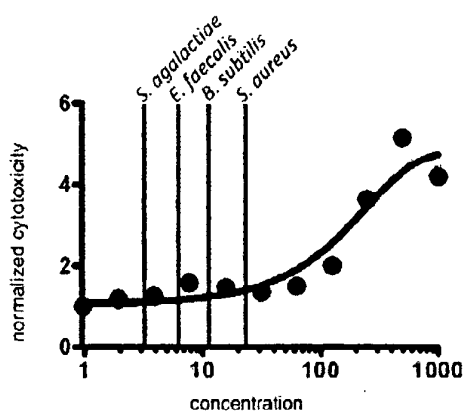
Fig. 2C
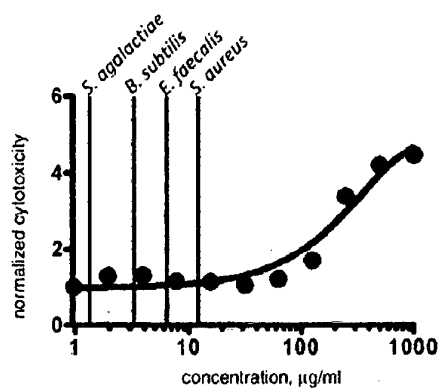
Fig. 2D
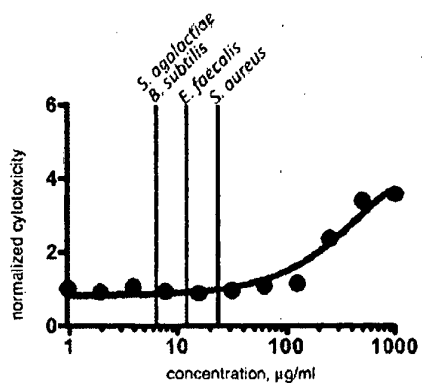
Fig. 2E

REFERENCES CITED IN THE DESCRIPTION

Non-patent literature cited in the description

- **DAVIES D. ; DAVIES J.** *Microbiol. Mol. Biol. Rev.,* 2010, vol. 74 (3), 417 **[0002]**
- **KESSELHEIM A. S. ; OUTTERSON K.** *Health Aff.,* 2010, vol. 29, 1689 **[0002]**
- **SUK D. H. ; REJMAN D. et al.** *Bioorg. Med. Chem. Letters,* 2007, vol. 17 (10), 2811 **[0003]**
- **ISONO, K. ; ASAHI K. ; SUZUKI S.** *J. Am. Chem. Soc.,* 1969, vol. 91, 7490 **[0004]**
- **ISONO K. et al.** *Agricultural Biol. Chem.,* 1965, vol. 29, 848 **[0004]**
- **ENDO A. ; KAKIKI K. ; MISATO J.** *J. Bacteriol.,* 1970, vol. 104, 189 **[0004]**
- **OHTA N. ; KAKIKI K. ; MISATO, T.** *Agric. Biol. Chem.,* 1970, vol. 34, 1224 **[0004]**
- **BUGG T. D. H. ; LLOYD A. J. ; ROPER D. I.** *Infect. Dis. Drug Targets,* 2006, vol. 6, 85 **[0005]**
- **KIMURA K. ; BUGG T. D. H.** *Nat. Prod. Rep.,* 2003, vol. 20, 252 **[0005]**
- **BOUHSS A. et al.** *J. Mol. Microbiol.,* 1999, vol. 34, 576 **[0005]**
- **BOUHSS A. et al.** *FEMS Microbiol. Rev.,* 2008, vol. 32, 208 **[0005]**
- **BOUHSS, A et al.** *FEMS Microbiol. Rev.,* 2008, vol. 32, 208 **[0005]**
- **TANINO T. et al.** *Med. Chem. Lett.,* 2010, vol. 1, 258 **[0005]**
- **IGARASHI M. et al.** *J. Antibiot.,* 2003, vol. 56, 580 **[0006]**
- **IGARASHI M. et al.** *J. Antibiot.,* 2005, vol. 58, 327 **[0006]**
- **KIMURA K. et al.** *Agric. Biol. Chem.,* 1989, vol. 53, 1811 **[0006]**
- **GAO, FENG et al.** *Chemistry-A European Journal,* 2009, vol. 15 (9), 2064-2070 **[0010]**